EXPERIMENTAL AND NUMERICAL STUDY OF LOCAL SCOUR AROUND SIDE-BY-SIDE BRIDGE PIERS UNDER ICE-COVERED CONDITIONS

By

Mohammad Reza Namaee

B.Sc., Islamic Azad University of Karaj, Iran, 2008

M.Sc., Khajeh Nasir Toosi University of Technology, Tehran, Iran, 2011

DISSERTATION SUBMITTED IN PARTIAL FULFILLMENT OF THE REQUIREMENTS
FOR THE DEGREE OF DOCTOR OF PHILOSOPHY IN
NATURAL RESOURCES AND ENVIRONMENTAL STUIDES

UNIVERSITY OF NORTHERN BRITISH COLUMBIA

April 2019

ABSTRACT

Local scour around piers and abutments is one of the main causes of the collapse of many bridges constructed inside rivers. Many researchers have conducted various studies to predict the maximum depth of a scour hole around bridge piers and abutments. However, most of them have been done in small-scale laboratory flumes and specifically for the open channel condition. Besides, most of the existing research on bridge piers uses uniform sediment which is not an appropriate representative of natural river systems. This can result in excessively conservative design values for scour in low risk or non-critical hydrologic conditions. The most severe cases of bridge pier scouring occur in cold regions when the surface of water turns into ice in which, an additional boundary layer is being added to the water surface, which leads to significant changes in the flow field and scour pattern around bridge piers. Ice cover also causes the maximum flow velocity to move closer to the channel bed. A precise prediction of maximum scour depth at piers under ice cover flow conditions is crucial for the safe design of the bridge foundation, because underestimation may result in bridge failure and over-estimation will lead to unnecessary construction cost. However, there is a dire paucity of information regarding local scour prediction under ice-covered flow conditions compared to the open channel condition. In the current study, a set of flume experiments was completed investigating local scour around four pairs of circular bridge piers with 60 mm, 90 mm, 110 mm and 170 mm in diameter with non-uniform bed under open channel, smooth and rough ice cover conditions. In order to simulate the ice cover condition, artificial smooth and rough ice covers were created to investigate the impacts of ice cover roughness on the scour geometry around the circular bridge piers. To represent non-uniform sediment condition, three different bed materials with average particle size (D_{50}) of 0.47 mm, 0.50 mm, 0.58 mm were used. In this study, regardless of flume cover and sediment grain size, the

maximum scour depths were observed to be at the upstream face of the pier nearly perpendicular to the approach flow and was maximized for the finest grain size under rough ice-cover condition. Further, the smaller the pier size and the greater the spacing distance between the bridge piers, the weaker the horseshoe vortices around the bridge piers and, thus, the shallower the scour holes around them. Results showed that, regardless of flow cover, the maximum scour depth decreases with an increase in the grain size of armor layer. Under the same flow condition, both scour volume and scour areas of a scour hole in the fine sand bed are larger comparing to those in the channel bed with coarser sands. The vertical velocity distribution which is a representative of the strength of downfall velocity was the greatest under rough ice cover. Under nearly the same flow conditions, the maximum value of turbulence kinetic energy and turbulent intensity occurred at the largest diameter pier. Several empirical equations were developed to estimate the maximum scour depth around side-by-side bridge piers under both open channel and ice-covered flow conditions. In addition to the experimental study, the numerical study was also done for the finest and the coarsest sediment types. The numerical study was in good agreement with the experimental study. The simulated result of local scour around the bridge piers represents information regarding the scour depth, morphological changes, and deposition patterns in the vicinity of the bridge piers.

TABLE OF CONTENTS

CO-AUTHORSHIP

Regarding all the chapters in this dissertation, I was the primary investigator whose responsibility was to design the experimental plan, collect, process and to interpret the data. In terms of the formation of the manuscripts, my duty was to write them and to implement reviewers' comments and their feedback into the final versions of the dissertation. However, it would be surely impossible to do this amount of work alone. Therefore, I would like to acknowledge Dr. Sui who truly contributed to the finalization of the manuscripts, supervision of the experimental design, data analysis of the current research and, whereby, he is included in authorship of all the corresponding publications. Further, Yuquan Li, who assisted me in doing the experiments throughout the field work, is included in a publication to acknowledge his contribution. Additionally, Dr. Todd Whitcombe and Dr. Ramaswami Balachandar truly contributed to this work by making some rich comments to some of the manuscripts are also included in some of the publications.

Publications and authorships stemming from this dissertation (submitted, accepted or published)

1) Namaee, M. R., & Sui, J. (2018). Local scour around two side-by-side cylindrical bridge piers under ice-covered conditions. International Journal of Sediment Research. (Published online) (Chapter 3.1) [https://doi.org/10.1016/j.ijsrc.2018.11.007]

2) Namaee, M. R., & Sui, J. (2018). Impact of armor layer on the depth of scour hole around side-by-side bridge piers – an experimental study using non-uniform sands. Journal of Hydrology and Hydromechanics. (Accepted) (Chapter 3.2)

3) Namaee, M. R., & Sui, J. (2018). Effects of ice cover on the incipient motion of bed material and shear stress around side-by-side bridge piers. Cold Region Science and Technology. (Under revision) (Chapter 3.3)

4) Namaee, M. R., Sui, J. & Whitcombe, T., (2018). Scour patterns and velocity profiles around bridge piers under ice-covered flow. ASCE Journal of Hydraulic Engineering, (Submitted). (Chapter 3.4)

5) Namaee, M. R., & Sui, J. (2019). Three-dimensional numerical modeling of local scour around bridge piers under open channel and ice-covered flow condition, (Submitted). (Chapter 3.5)

6) Namaee, M. R., Li, Y., & Sui, J. (2018). Effects of ice cover on local scour around bridge piers in non-uniform sand bed. Proceedings of the 6th International Conference on Estuaries and Coasts (ICEC-2018), University of Caen Basse-Normandie, France, August 20-23, 2018 (Chapter AI-1)

7) Namaee, M. R., Li, Y., Sui, J., & Whitcombe, T. (2018). Comparison of three commonly used equations for calculating local scour depth around bridge pier under ice-covered flow condition. World Journal of Engineering and Technology, 6 (02), 50. (Chapter AI-2)

List of Tables

List of Figures

ACKNOWLEDGEMENT

Firstly, I would like to express my sincere gratitude to my supervisor Dr. Jueyi Sui for his continuous support of my Ph.D. study and related research, for his patience, motivation, and immense knowledge. His guidance helped me in all the time of research and writing of this dissertation. I could not have imagined having better advisor and mentor for my Ph.D. study.

Besides my supervisor, I would like to thank the rest of my dissertation committee member: Dr. Jianbing Li, Dr. Liang Chen, Dr. Samuel Li and my co-supervisor Dr. Youmin Tang for their insightful comments and encouragement. I am also grateful to Dr. Peng Wu for his in-depth knowledge which encouraged me to look at my research from a more in-depth perspective.

My sincere thanks also go to Dr. Phil Owens and Dr. Ellen Petticrew who provided me an opportunity to stay and do my research at The Dr. Max Blouw Quesnel River Research Center (QRRC), and who gave me access to the laboratory and research facilities. Huge thanks are extended to QQRC staff (Lazlo Enyedy and Michael Allchin) and my friends (Todd French and Yuquan Li) without whom it would be impossible to conduct this research.

I am also grateful to Dr. George Jones and Dr. Alia Hamieh who provided me with teaching contracts throughout my Ph.D. which helped me financially. I would also like to thank the staff and all the wonderful friends I met at The University of Northern British Columbia and Prince George who were really welcoming and supportive of foreign students.

I would like to express my gratitude to Dr. Bill McGill, Dr. David Connell, Dr. Peter Jackson and Dr. Todd Whitcombe as my course supervisors in my first year of Ph.D., who widened my scientific perspective and assisted me to understand the interaction between natural science and social science. My appreciation also goes to my classmates who presented different subjects which made me keener on different aspects of science.

Last but not the least, I would like to thank my beloved family: my parents, my sisters and my brother-in-law and my newly-born niece (Artemis) for supporting me spiritually and financially throughout writing this dissertation and especially in my life.

1. INTRODUCTION

Local scour is the abrupt decrease in bed elevation near a pier due to erosion of bed material in the vicinity of the local flow structure induced by the pier (Shen et al., 1969). Overlooking the local scour phenomenon in the bridge pier design might possibly result in huge financial cost or even high casualty rate. According to a broad collection of bridge failure data worldwide assembled by Imhof (2004), natural hazard is the principal cause of bridge failure as it amounts to approximately 30% of all collected bridge collapse cases (Figure 1-1). Among the natural hazard causes listed, flooding or scour is responsible worldwide for about 60% of the failure cases (Figure 1-2). Due to the local scour, the insertion depth of the pile reduces as the scour depth around the pile grows, which is directly associated with the stability of the pier. The deeper the depth of local scour around the pier, the more vulnerable it becomes which leads to bridge collapse in the most extreme case (Zhang et al, 2005).

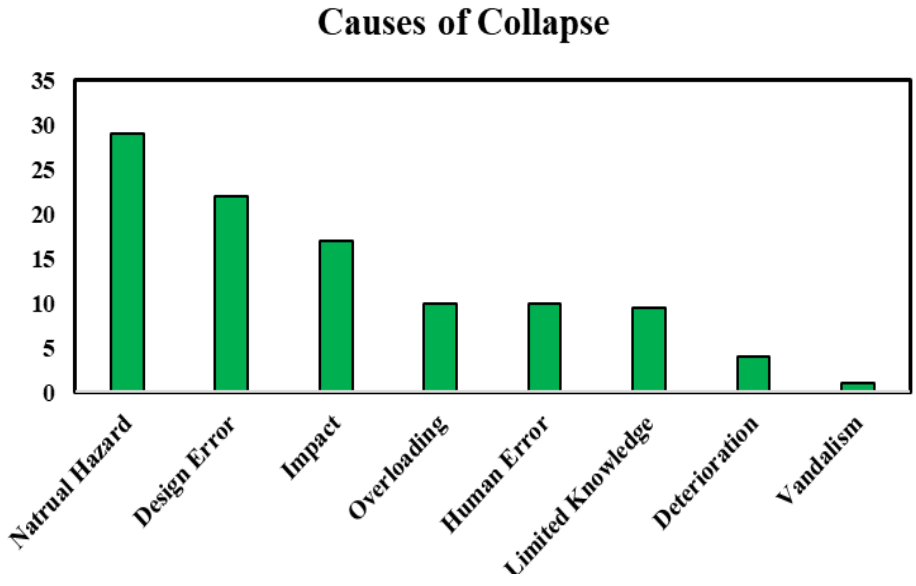

Figure 1–1: Main causes of bridge failure (Adopted by Imhof, 2004)

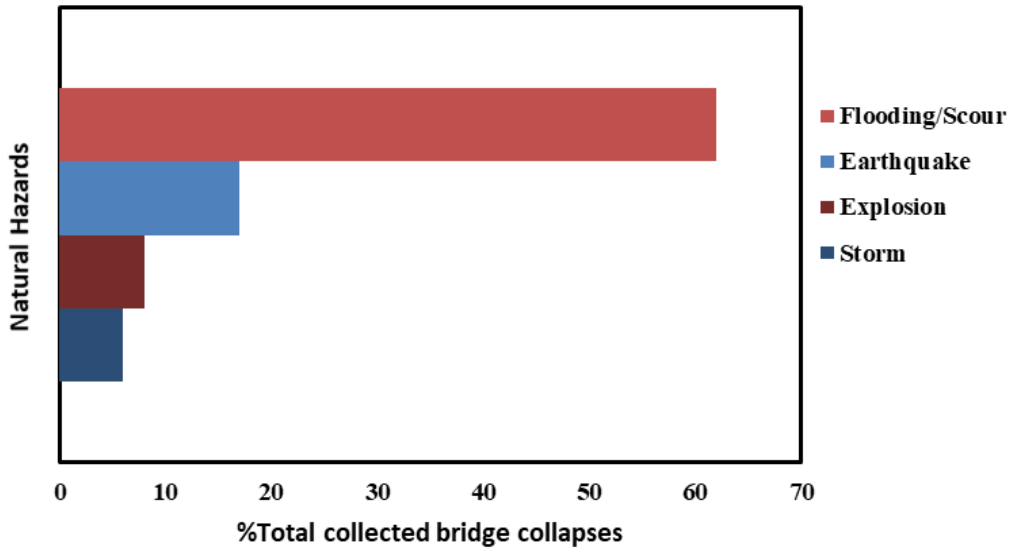

Figure 1–2: Different natural hazards causing bridge collapse (Adopted by Imhof, 2004)

The Federal Highway Administration (FHWA) has estimated that 60% of bridge failure cases in the USA are due to scour (FHWA, 1988; Parola et al, 1997) and on average, approximately 50 to 60 bridges collapse in the USA annually. Wardhana & Hadipriono (2003) studied 500 failures of bridge structures in the United States between 1989 and 2000 and reported that the most frequent causes of bridge failures were due to floods and scour. On average, the age of the 500 failed bridges was 52.5 years and its range was from 1 to 157 years (Brandimarte et al, 2012). Bridge damage and failure have huge negative social and economic impacts in terms of reconstruction costs, maintenance and monitoring of existing structures, the disruptions of traffic flow and, in some life-threatening cases, the cost of human lives (Brandimarte et al 2012). In a broad research on bridge scour, the Federal Highway Administration (Brice and Blodgett, 1978) reported that damages to bridges and highways from major regional floods in 1964 and 1972 is equivalent to approximately 100 million US dollars per event. A report of road administration declared that scour caused by rivers results in hefty expenses of 36 New Zealand million dollars per year in New Zealand (Macky, 1990). Hereby, it is necessary to consider scour as one of the most important causes of

bridge failure when designing the bridge foundation (Briaud et al, 2006). Moreover, a precise prediction of scour depth will not only prevent those bridge failures which are the consequence of underestimation of scour depth, but also will efficiently reduce unnecessary construction cost of those bridge piers in which scour depths are overestimated. Many hydraulic researchers have done experiments to investigate the local scour around bridge piers and develop empirical equations to estimate the maximum scour depth (Ettema et al., 2011; Melville, 1997; Melville & Sutherland, 1988; Richardson et al., 2001; Sheppard et al., 2013).

A great number of bridges are constructed in extreme cold regions whose piers are exposed to the impact of ice in addition to the local scour around the piers. These types of bridge piers have not been thoroughly examined in terms of flow field and prediction of maximum scour depth around them. It has been proved that the formation of a stable ice cover effectively doubles the wetted perimeter compared to open channel conditions, alters the hydraulics of an open channel by imposing an extra boundary to the flow, causing the velocity profile to be shifted towards the smoother boundary (channel bed) and adding up to the flow resistance (Sui et al., 2010; Wang et al., 2008). Besides, the influence of an ice cover on a channel involves complex interactions among the ice cover, ice roughness, fluid flow sediment, bed geometry, water depth, and channel geometry and this complex interaction can have a dramatic effect on the sediment transport process (Hains, 2004). The investigation into scour under the ice was prompted by the collapse of a bridge over the White River in White River Junction, Vermont in 1990. It is interesting to know that the bridge had survived more dramatic ice and flood events during its service life than the one that led to the failure of the bridge piers. The failure of the bridge piers was the result of multiple bridge pier scour cycles which had already undermined the foundation of the piers (Zabilansky, 1996). In order to get a better understanding of the flow field and scouring process around bridge piers under

ice-covered condition, my PhD dissertation conducted a comprehensive experimental study on the local scour around bridge pier, by carrying out three sets of flume experiments in a non-uniform bed by incorporating four different sets of circular bridge piers with a fixed distance in-between under open, rough and smooth ice-covered flow condition.

1.1 Definition of scour and different types of scour

Scouring can be defined as a process due to which the sediment particles around the surroundings of the abutment or pier of the bridge, gets eroded and removed over a certain depth which is called scour depth (Chang, 1992). Bed scour may be a natural occurrence or due to man-made changes to a river (Maddison, 2012). Brandimarte et al. (2012) state that scour at bridge foundation is typically as the result of the joint impacts of three different scour processes (general scour, contraction scour and local scour I the vicinity of the piers) that may arise either independently or concurrently. General scour (degradation) is defined as the general dropping in the sediment bed by the kinetic energy of the oncoming flow which can occur more rapidly during the flood and can affect the reach of the river on which the bridge is located, while aggradation involves the deposition of material eroded from the channel or watershed upstream of the bridge (Richardson et al, 1993). Figure 1-3 illustrates a bridge damage case in Malaysia due to flooding and scouring at the pier. Rivers that transport significant amounts of bed material are most susceptible to scour and channel instability which includes sand-bed rivers and upland gravel bed rivers (Maddison, 2012). The main causes of general scour that induce aggradation or degradation of the bed channel are either due to human activities, such as land-use changes (urbanization, deforestation); dam construction, reservoir construction, channel alterations, river bed material mining or due to natural phenomena, such as channel straightening, climate changes and land activities such as landslides, mudflows (Brandimarte, et al. 2012).

Figure 1–3: General scouring of river bed at Sg. Jeniang, Kedah

Contraction scour occurs when the cross-section area of flow of a stream at flood stage is reduced, either by a natural contraction or bridge. From continuity principle, a decrease in flow area leads to an increase in average velocity and bed shear stress through the contraction. Therefore, there is an increase in erosive forces in the contraction. Because of that, more bed material is removed from the contracted reach than is transported into the reach. This increase in transport of bed material from the reach lowers the natural bed elevation (Richardson et al, 1993). This lowering may be uniform or non-uniform across the bed. Non-uniform contraction scour means that the depth of scour may be deeper in some parts of the cross section. As the bed elevation is lowered, the flow area increases and, in the riverine situation, the velocity and shear stress decreases until relative equilibrium is reached; i.e., the quantity of bed material that is transported into the reach is equal to that removed from the reach, or the bed shear stress decreases to a value such that no sediment is transported out of the reach. The natural process of scouring can also be impacted by the placement of the artificial obstruction in the way of river flow, such as weirs and piers (Richardson et al, 1993) which triggers local scour around bridge piers and is the main interest in

this dissertation. The local scour around bridge foundations usually results from the joint effect of contraction scour, due to the flow velocity increase, which is the result of the reduction of the channel section, and the pier and abutment scour which is the result of the (local) alteration of the flow field induced by piers and abutments (Graf, 1998). Figure 1-4 illustrates the contraction scour due to narrowing of the flow cross section and local scour around bridge piers and abutments. Total scour is the addition of long-term degradation of the river bed (general scour), contraction scour at the bridge and local scour at the piers or abutments. In the process of local scour, the material from around piers, abutments, embankments would be removed because of the flow alteration induced by the obstruction of the flow (Richardson & Davis, 2001). Compared to general scour and constriction scour, local scour can cause serious damage to the bridge because it specifically occurs around the bridge piers.

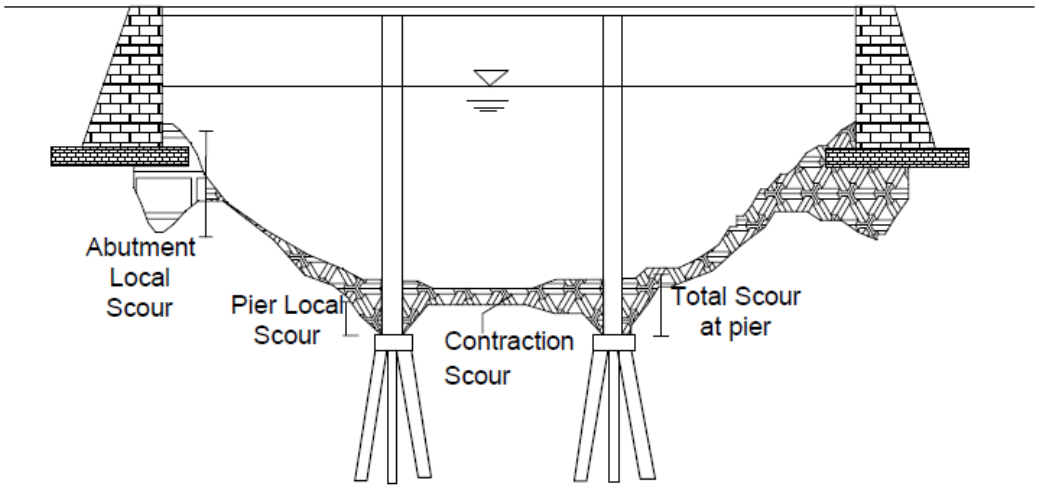

Figure 1–4: Sketch of the type of scour that can occur at a bridge crossing (Adapted from Brandimarte et al. 2012)

1.2 Local scour characteristics around bridge piers in open channels

The main feature of the flow around a pier is the system of vortices which develop about the pier. These vortex systems are the basic mechanism of local scour, which has long been described by investigators (Tison, 1961; Breusers et. al., 1977; Chabert & Engeldinger, 1956; Laursen and Toch, 1956; Shen et. al.,1969; Melville, 1975; Hjorth, 1975; Melville and Raudkivi 1977; Ettema, 1980; Baker, 1981; Jain, 1980; Raudkivi and Ettema, 1983; Melville and Sutherland, 1988; Kothyari, 1998; Dargahi, 1990; Yanmaz and Altimbilek, 1991; HEC-18, 1991; Dey, 1997; Ahmed and Rajaratnam, 1998; Graf and Istiarto, 2002). It has been described that, depending on the type of pier and freestream conditions, these vortex systems can be characterized by three basic systems: downflow, horseshoe vortices, and wakes (Laird, 1971; Dargahi, 1989,1990; Ahmed and Rajaratnam, 1998; Ansari et al, 2002; Graf and Istiarto 2002). Figure 1-5 illustrates the flow and scour pattern around a circular pier. As it is depicted in Figure 1-5, the strong vortex motion caused by the existence of the pier entrains bed sediments from around the pier base (Lauchlan & Melville, 2001). The downflow rolls up while it continues to dig a hole through interaction with the oncoming flow. Near the water surface, the water depth is increased, and a vertical pressure gradient is developed due to the stagnation of the approaching flow. The vortex then extends downstream along the sides of the pier. This vortex is often referred to as a horseshoe vortex because of its great similarity to a horseshoe (Breusers et al., 1977). The primary vortex then extends to the downstream of the piers and loses its identity after some distances. In the corner of downstream piers, the flow accelerates and leads to the development of concentrated vortices, which are termed as wake vortices. Wake vortices are created due to the separation of the flow upstream and downstream of the pier corners (Zhang, 2005; Kwan & Melville, 1994).

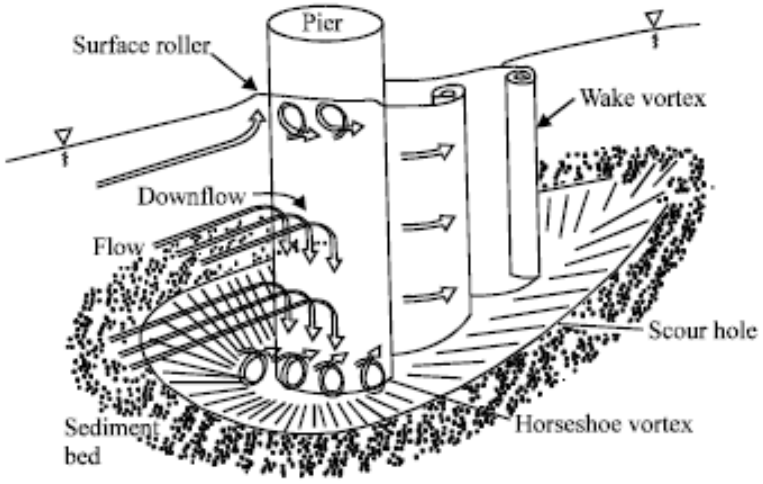

Figure 1-5: Illustration of the flow and scour pattern at a circular pier (Masjedi et al, 2010)

1.3. Clear-water and live-bed scour

There are two main classifications of local scour at piers based on the mode of sediment transport by the approaching stream, namely clear-water scour and live-bed scour. These classifications depend on the ability of the flow approaching the bridge to transport bed material. Distinguishing between these two types of scour is important because both the development of the scour hole with time and the relationship between scour depth and approach flow velocity depends on the type of scour (Raudkivi & Ettema, 1983). Laursen (1960) was the first to distinguish between live-bed and clear-water scour for both contraction and local scour (Richardson, 1996). Two conditions might occur for contraction and local scour which are clear-water and live-bed scour. Clear-water scour occurs when there is no movement of the bed material in the flow upstream of the crossing or if there is any movement of the bed materiel, it would be in suspension through the scour hole at the pier at less than the capacity of the flow. This happens when the shear stress exerted on the sediment by the flow is less than the critical shear stress of the sediment. Under clear-water scour, the maximum scour depth is reached more gradually and once it is developed, the flow can no longer remove sediment from the scour hole. Clear-water scour reaches its maximum over a longer

period than live-bed scour (Chee, 1982; Melville, 1984; Richardson & Davis, 2001). Chabert and Engeldinger (1956) observed that the equilibrium clear-water scour depth is 10% greater than live bed scour depth (Figure 1-6). This is because clear-water scour occurs mainly in coarse-bed material streams. On the other hand, live-bed scour occurs when there is transport of bed material from the upstream reach into the crossing (Raudkivi & Ettema, 1983). This happens when the shear stress exerted on the sediment by the flow is greater than the critical shear stress of the sediment. Under live-bed conditions, the depth of local scour develops more rapidly compared to clear-water scour, then it oscillates about the equilibrium scour depth due to spreading bed-form.

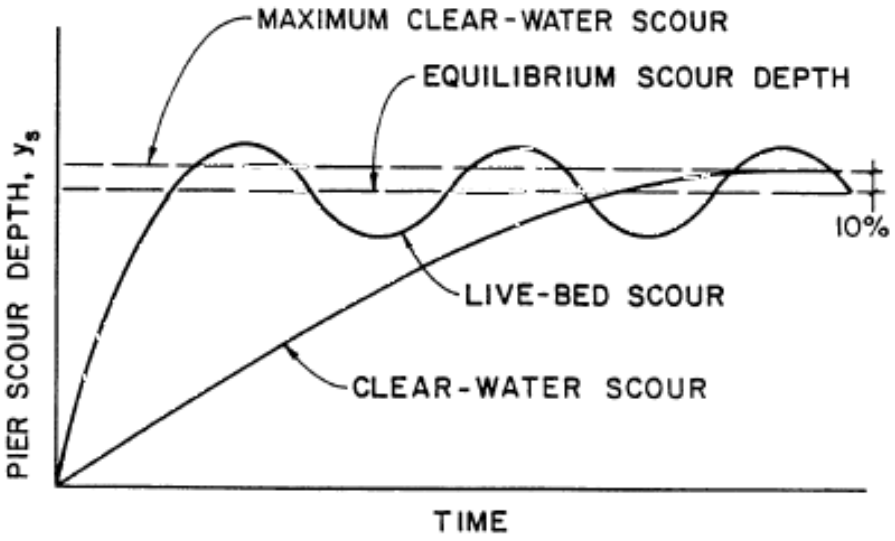

Figure 1-6: Pier scour depth in a sand-bed stream as a function of time (Richardson and Davis, 2001)

Critical shear velocity is used to determine the velocity associated with the initiation of motion. They are used as an indicator for clear-water or live-bed scour conditions. If the mean velocity (V) in the upstream reach is equal to or less than the critical shear velocity (V_c) of the median diameter (D_{50}) of the bed material, then contraction and local scour will be clear-water scour. On the other hand, if the mean velocity is greater than the critical shear velocity of the median bed material size, live-bed scour will occur. This method can be applied to any unvegetated channel or overbank area

to determine whether scour is clear-water or live-bed. (Richardson et al, 1993). Sheppard, et. al. (2013) stated that the sediment critical velocity (V_c) can be estimated from Shields' diagram, using Equations (1-1) to (1-4). It should be mentioned that shields diagram will be explained in the upcoming section:

$$u^* = [16.2D_{50}(\frac{9.09\times10^{-6}}{D_{50}} - D_{50}(38.76+9.6\ln(D_{50})) - 0.005)]^{\frac{1}{2}} \quad (1\text{-}1)$$

$$\mathrm{Re} = \frac{u^* D_{50}}{2.32\times10^{-7}} \quad (1\text{-}2)$$

For 5<Re<70

$$V_c = 2.5u^* \ln[\frac{73.5y_1}{D_{50}(\mathrm{Re}(2.85-0.58\ln(\mathrm{Re})+0.002\mathrm{Re})+\frac{111}{\mathrm{Re}}-6)} \quad (1\text{-}3)$$

For Re>70

$$V_c = 2.5u*\ln(\frac{2.21y_1}{D_{50}}) \quad (1\text{-}4)$$

In which u* is friction (shear) velocity ($\sqrt{\frac{\tau_0}{\rho}}$) [L/T]; D_{50} is median grain size; y_1 is average flow depth in the upstream main channel [L] and τ_0 is bed shear stress [F/L^2].

1.4 Sediment transport in a river Channel

In terms of mode of sediment particle motion, there are three modes of particle motion: (a) rolling and sliding (traction), saltation (hopping) and suspended motion. That portion of the sediment load that is transported along the bed by sliding, rolling or hopping is bedload. Bedload initiates when bed shear stress exceeds the critical value for the incipient motion of particles. With increasing bed shear stress or shear velocity, the particles acted on turbulent flow will regularly jump or saltate (Van Rijn, 1984). Suspended load is the type of sediment that is carried in the body of the flow

and moves at the same velocity as the flow. It particularly occurs for a small particle (e.g. Clay and fine silt) because these types of particles with a large relative surface area are held in suspension more easily due to the electrostatic attraction between the unsatisfied charges on the grain's surface and the water molecules. This force, tending to keep the particle in the flow, is large compared to the weight of the particle (Van Rijn, 1984). The total load is the sum of bed load and suspended load. In most natural rivers, sediments are mainly transported as suspended load, while the bed load transport rate is about 5-25% of that in suspension (Yang, 2003).

1.5 Importance of bed shear stress and methods to predict it

Bed shear stress provides an index of fluid force per unit area on the stream bed, which has been related to sediment mobilization and transport in many theoretical and empirical treatments of sediment transport. Bed shear stress and shear velocity are fundamental variables in river studies to calculate the transport field and the scour, deposition and channel change (Wilcock, 1996). The difficulty of estimating these variables accurately, particularly in complex flow fields when flow is highly three-dimensional, has long been recognized (Biron et al, 2004). One of the most popular methods to calculate bed shear stress is to use the reach-average bed shear stress in which $\tau_0 = \rho g R S_f$ where τ_0 is bed shear stress, ρ is water density, g is acceleration due to gravity, R is hydraulic radius and S_f is the energy slope. However, this method is not appropriate for local small-scale estimates of the variation in shear stress and it lacks accuracy (Babaeyan-Koopaei et al., 2002). There are totally four different methods to predict local bed shear stress, which are log profile, drag, Reynolds and turbulent kinetic energy (TKE) with more accuracy. Until recently, Reynolds stress and the turbulent kinetic energy method were not used broadly because of the difficulty in obtaining detailed turbulence measurements close to the bed in natural rivers (Dietrich and Whiting, 1989; Wilcock, 1996). Fortunately, the development of measuring devices such as

the Acoustic Doppler Velocimeter (ADV) has allowed comprehensive field measurements of turbulent velocity fluctuations in the three components of velocity at high frequencies with small errors in the Reynolds shear stress (McLelland & Nicholas, 2000). Biron, et. al., 2004 compared shear stress estimated from the log profile, drag, Reynolds and turbulent kinetic energy (TKE) approaches in a laboratory flume in a simple boundary layer, over Plexiglas, sand and in a complex flow field around deflectors. They concluded that in a complex flow field around deflectors, the TKE method provided the best estimate of shear stress as it is not affected by local streamline variations and it considers the increased streamwise turbulent fluctuations close to the deflectors. The turbulent kinetic energy (TKE) is $\tau = C_1[0.5\rho(u'^2 + v'^2 + w'^2)]$. In which, ρ is the flow density, C_1=0.19 is a proportionality constant and u′, v′, w′ are turbulence fluctuations in the longitudinal, transverse and vertical directions, respectively. For the local scour in open channel, a flow resistance calculation leads directly to the estimation of the shear velocity associated with the bed surface drag. To estimate sediment transport rate under ice cover, it is first necessary to estimate flow resistance (or a relationship between flow depth and mean velocity of the flow), and then the flow drag on the bed. As it was mentioned earlier, ice cover presence alters mean flow distribution and flow turbulence characteristics. The flow velocity profile under ice cover can be categorized as upper portion and lower portion, which are divided by the locus of the point of the maximum velocity. The upper portion of the flow is mainly affected by the ice cover and the lower portion of the flow is mainly affected by river bed (Sui et al, 2010).

1.6 Shields Parameter and importance of critical shear stress

As it was mentioned earlier, for a particle to become entrained, the bed or boundary shear stress caused by the water flowing parallel to the stream bed must exceed a critical shear stress. In other words, the moment where the directive forces (shear forces) overcome preventive forces (inertia,

friction) is known as the moment of incipient motion and is the threshold of particle entrainment. The shear stress at this threshold is known as the critical shear stress (Wiberg & Smith 1987). Figure 1-7 illustrates these forces. This critical shear stress is a function of both the bed sediment and the condition of the sediments (Beltaos et al., 2011). The threshold when the two forces are equivalent is the critical condition at which the directive forces are just balancing the resisting forces (Wiberg & Smith 1987). Totally, of the total sediment load, there are two kinds of distinctive sediment types, the bed load and the suspended load. Mathematically, if the shear stress is higher than the critical shear stress, and less than the critical shear stress for initiation of suspended particle, the sediments will start to move which is called bedload transport and the bed load transport is in shape of Traction (rolling & sliding) or saltation (hopping). However, if the shear stress is higher than the critical shear stress for initiation of suspended particle, the sediment starts to move in suspension (Hasanzadeh, 2012). Dissolved load is material, especially ions, that are carried in solution by a stream which is not within the scope of this research and it should be noted that if the bed shear stress is less than critical shear stress there would be no motion (Figure 1-8).

$$\tau < \tau_{cr} \qquad \text{no motion} \qquad (1\text{-}5)$$

$$\tau_{cr} \leq \tau \leq \bar{\tau}_{cr} \qquad \text{bed load transport} \qquad (1\text{-}6)$$

$$\tau \geq \bar{\tau}_{cr} \qquad \text{bed \& suspended loads transport} \qquad (1\text{-}7)$$

Where τ is bed shear stress, τ_{cr} is critical shear stress or shear stress of exact moment at which sediment particle initiates, $\bar{\tau}_{cr}$ is critical shear stress for initiation of suspended particle.

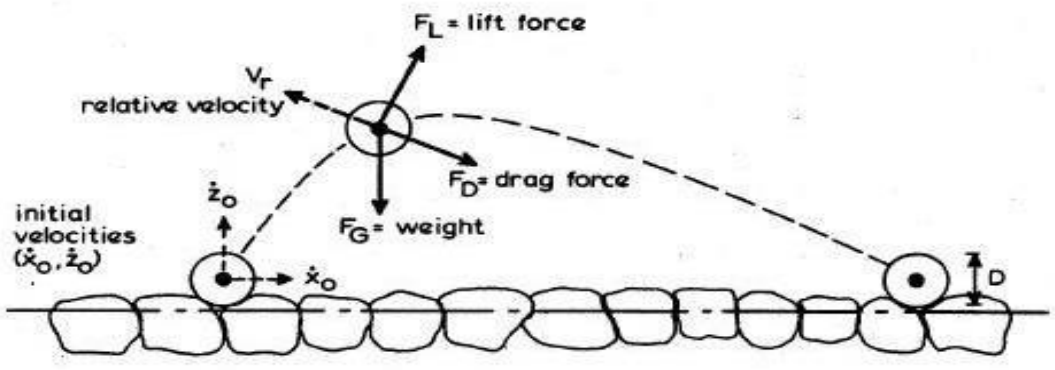

Figure 1-7: Forces acting on a sediment particle include gravity (F_G), lift (F_L), drag (F_D), and resistance or friction (Fr) (van Rijn, 1984)

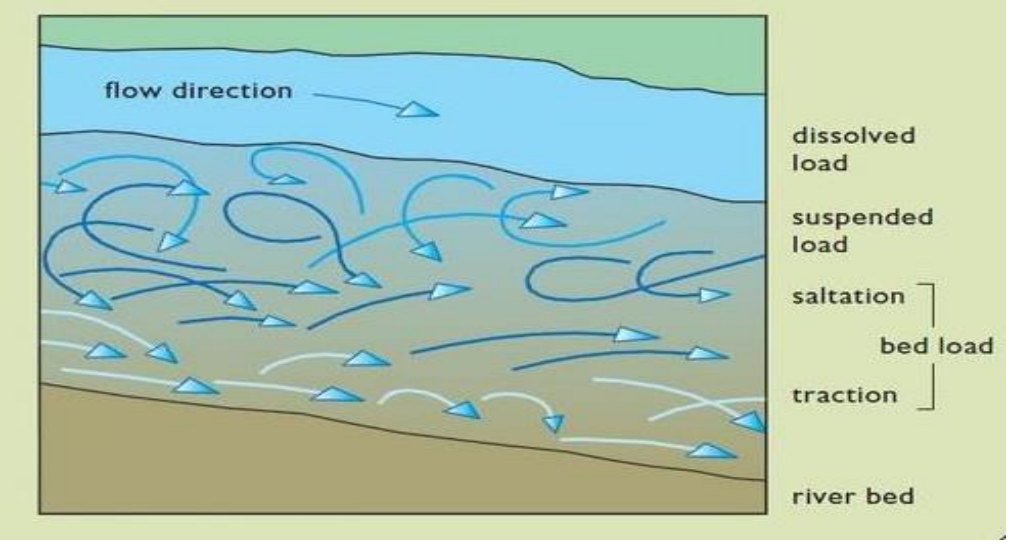

Figure 1-8: Types of sediment loads in rivers (Louck, 2005)

1.7 The Shields diagram

Several studies (Brownlie, 1983; Liu, 1999; Van-Rijn, 1993; Hasanzadeh, 2012) stated that the Shields diagram is properly defined to describe sediment movement and used the critical shear stress parameter to describe the flow conditions affecting on the movement of sediment particles. It should be mentioned that shield diagram represents the relationship between critical Shields parameter and the hydraulic conditions of the flow at the bottom of the channel which is expressed

in term of particle Reynolds number. The amount of particle Reynolds number depends on the determination of the diameter of a particle which is usually taken as the average grain size (D_{50}) and the shear velocity values.

$$\theta_{cr} = \frac{U_{*_{cr}}^2}{(s-1)\times g \times D_{50}} = \frac{\tau_{cr}}{(s-1)\times \rho \times g \times D_{50}} \quad (1\text{-}8)$$

$$\mathrm{Re}_* = \frac{U_{*cr} \times D_{50}}{\upsilon} \quad (1\text{-}9)$$

$$\theta = \frac{U_*^2}{(s-1)\times g \times D_{50}} = \frac{\tau}{(s-1)\times \rho \times g \times D_{50}}, U_* = \sqrt{gRS} \quad (1\text{-}10)$$

Where Θ is dimensionless mobility Shields parameter, Θ_{cr} is dimensionless critical mobility Shields parameter, Re* is dimensionless Reynolds particle number, U* is shear velocity (m/s), U_{cr}* is critical shear velocity (m/s), τ is shear stress (N/m^2), τ_{cr} critical shear stress (N/m^2), υ is kinematics viscosity (m^2/s), D_{50} is median diameter of particle (m); S is relative density (ρ_s/ρ). Therefore, above equations are considered a mathematical formula to describe the initiation of sediment movement. Sediment particle starts moving when the mobility Shields parameter value becomes greater than a critical Shields parameter which is shown in the following equations. Figure 1-9 illustrates Shields diagram, which represents the relationship between a critical mobility Shields parameter and a Reynolds number of sediments.

$$U_* > U_{*cr} \quad (1\text{-}11)$$

$$\tau_b > \tau_{bcr} with \ \ \tau_{bcr} = \rho \times U_{*cr} \quad (1\text{-}12)$$

$$\theta > \theta_{cr} with \ \theta_{cr} = \frac{U_{*cr}^2}{(S-1)\times g \times D_{50}} \quad (1\text{-}13)$$

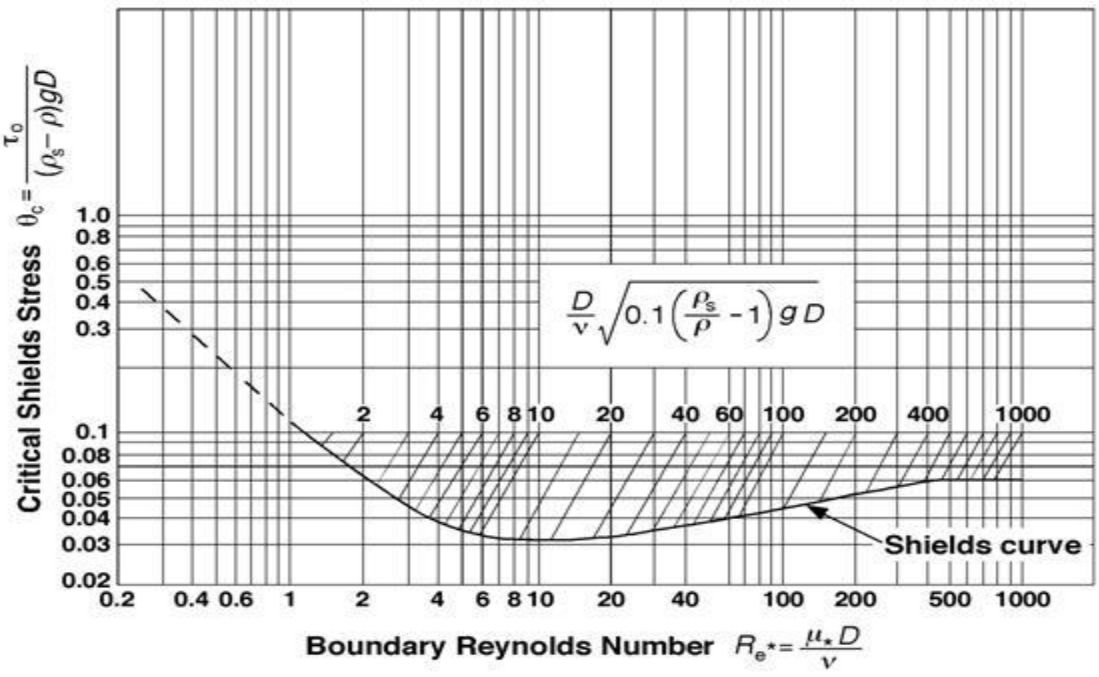

Figure 1-9: The Shield's Diagram (Cao, 2006)

1.8 The modified shields diagram

Madsen & Grant (1977) pointed out the difficulty of applying the shields diagram due to the presence of U^*_{cr} in both axes of the diagram. Therefore, they worked to use a new variable instead of Reynolds number on the horizontal axis of diagram as it is shown in Figure 1-10. This figure indicates the relation between the critical Shields parameter in the Y-axis and new variable which is sediment-fluid parameter (S^*) in the X-axis. S^* Value is calculated from the following equation:

$$S^* = \frac{D_{50}}{4\nu}\sqrt{(s-1)gD_{50}} = \frac{\mathrm{Re}^*}{4\sqrt{\theta_c}} \qquad (1\text{-}14)$$

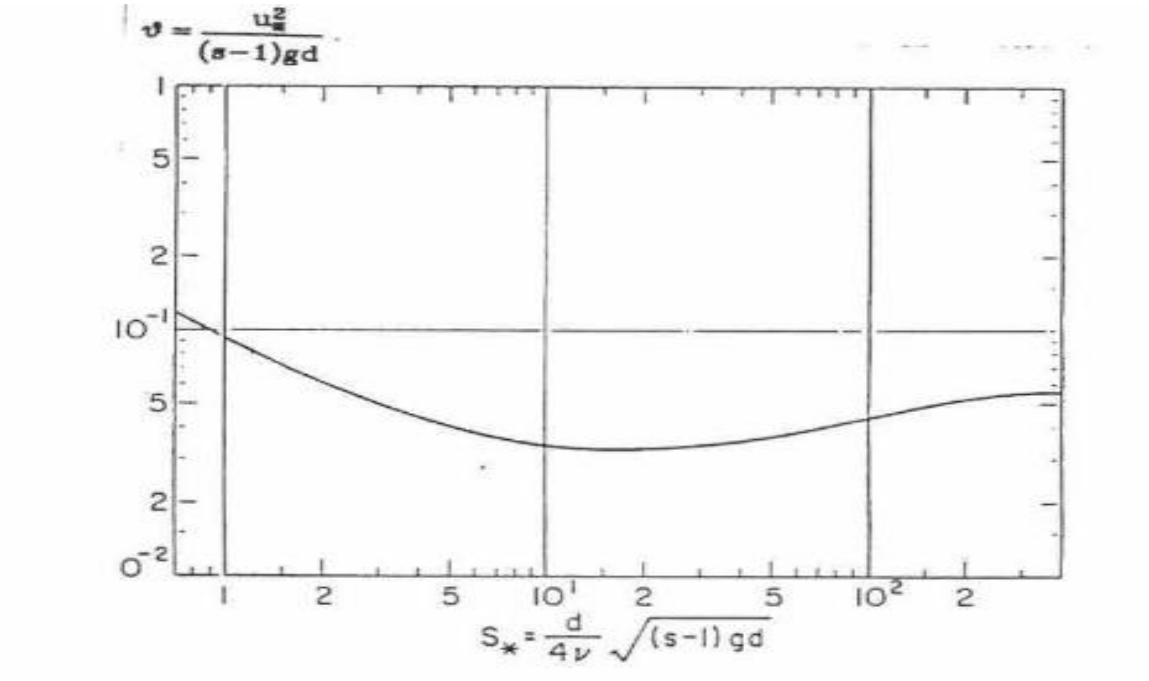

Figure 1-10: Indicates the relation between the critical Shields Parameter (Θc) and Sediment-Fluid Parameter (S*) (Madsen & Grant, 1977)

1.9. Bridge scour prediction

It has been found that bridge scour is related to many factors such as the geometry of the channel, dynamic properties of the flow and geometry of the bridge piers and abutments (Deng and Cai, 2009). Predicting bridge scour using the available information of these factors prior to or during flood events is highly crucial in preventing disastrous failures of bridges and possible loss of life. Scour prediction practice can be generally categorized into two groups which are prediction of bridge scour using empirical equations and prediction of bridge scour using other methods, such as neural networks and numerical modelling (Deng and Cai, 2009). By incorporating these two methods, the final scour depth and real-time scour depth can be predicted.

1.10 Predicting bridge scour using empirical equations

In the past few decades, many researches have been done to estimate the maximum scour depth, which is the main reason of bridge failure, around bridge piers. (Laursen and Toch, 1956; Liu et al. 1961; Tison, 1961; Shen et al., 1969; Breusers, et al., 1977; Jain and Fischer, 1980; Raudkivi 1986; Melville and Sutherland, 1988; Froehlich, 1989; Melville, 1992; Abed and Gasser, 1993; Richardson and Richardson, 1994; Melville, 1997; Coleman et. al., 2003; Dey & Barbhuiya, 2005; Dey & Raikar, 2005; Heza et al., 2007; Sheppard et al., 2013). However, due to the difference between site and laboratory conditions and the limitation of collected data specifically those of small-scale laboratory flumes, the development of these formulae has a great deal of uncertainty and limitations with respect to the factors considered in constructing the scour model, parameters used in the equation, laboratory or site conditions, etc. It is noteworthy to mention that it is generally believed that most existing equations might overestimate the scour depth and are generally conservative deductions from comparative studies by different researchers based on the conducted laboratory experiments and field tests (Johnson and Ayyub 1996; Melville 1997; Ataie-Ashtiani & Beheshti, 2006; Lu et al. 2008). In this section, a brief review of some of the most common equations is presented.

1.10.1 Colorado State University equation

Among all the equations, one of the most commonly used pier scour equations in the United States is the Colorado State University equation (Deng and Cai, 2009) recommended by the U.S. Department of Transportation's Hydraulic Engineering Circular No. 18 (HEC-18) (Federal Highway Administration 1993), which is expressed as follows:

$$d_s = 2.0 y K_1 K_2 K_3 (b/y)^{0.65} Fr^{0.43} \quad (1\text{-}15)$$

Where d_s=scour depth; y=flow depth at the upstream of the pier; K_1, K_2, and K_3=correction factors for the pier nose shape, angle of attack flow, and bed condition, respectively; b=pier width; and Fr=Froude number. It is recommended in the HEC-18 that the limiting value of d_s/y is 2.4 for Fr<0.8 and 3.0 for Fr>0.8. Eq. (1-15) was developed from laboratory data and was recommended for both live-bed and clear-water conditions. A few other commonly used equations are also listed in the following section. For the purpose of simplification, repeated terms in the following equations will not be explained again.

1.10.2 Neil (1964) equation

Equation presented by Neil (1964), which was developed from the design curves by Laursen and Toch (1956).

$$d_s = 1.35 b^{0.7} y^{0.3} \tag{1-16}$$

Shen's equation (Shen et al. 1969)

$$d_s = 0.00022 \left(\frac{Vb}{\nu} \right)^{0.3} \tag{1-17}$$

Where V=average velocity of approach flow and $\nu=1\times10^{-6}$ m^2/s.

1.10.3 Jain and Fisher equation (1979)

$$\begin{cases} d_s = 2.0 b (Fr - Fr_c)^{0.25} (\frac{y}{b})^{0.5} \; for (Fr - Fr_c) > 0.2 \\ d_s = 1.85 b (Fr_c)^{0.25} (\frac{y}{b})^{0.5} \; for 0 < (Fr - Fr_c) \end{cases} \tag{1-18}$$

Where Fr_c=critical Froude number. For $0<(Fr-Fr_c)<0.2$, the larger of the two scour depths computed using the two equations is used.

1.10.4 Froehlich equation (Froehlich 1989)

$$d_s = 0.32 b \phi F^{0.2} \left(\frac{b_e}{b}\right)^{0.62} \left(\frac{y}{b}\right)^{0.46} \left(\frac{b}{D_{50}}\right)^{0.082} \quad (1\text{-}19)$$

Where ϕ=coefficient based on the shape of the pier nose; b_e=width of the bridge pier projected normal to the approach flow; and D_{50}=median grain size of bed material.

1.10.5 Melville and Sutherland equation (1988):

$$d_s = K_1 K_d K_y K_a K_s b \quad (1\text{-}20)$$

Where K_I=flow intensity factor; K_d=sediment size factor; K_y =flow depth factor; Ka=pier alignment factor; and K_s=pier shape factor.

1.11 Bridge scour modeling

As discussed earlier, bridge scour is a very complicated hydraulic process which involves the interaction between the flow around a bridge pier or abutment and the erodible bed surrounding it and it is dependent on many hydraulic factors such as geometry of the channel, dynamic hydraulic properties of the flow, geometry of the bridge piers and abutments (Deng & Cai, 2009). To study the complicated bridge scour process, different numerical models as well as laboratory models have been developed in the past few decades. In this section, these types of hydraulic modelling would be discussed more in details.

1.11.1 Laboratory models

Laboratory models are very common and trustworthy in the design of different hydraulic problems. One of the most important advantages of laboratory studies of bridge scour is that they can be very helpful in terms of getting a better and clearer understanding of the effect of different variables and parameters associated with scour and therefore improve the scour prediction equations.

Besides, they can be useful to develop alternative or improved scour countermeasures which is primarily important during floods (Deng & Cai, 2009). As it was mentioned before, a numerous laboratory researches have been done to investigate bridge pier scours. For instance, a large circular pier at the Imbaba Bridge with a scale of 1:60 was constructed at the Hydraulics and Sediment Research Institute to study the deep scour hole downstream of one of the major bridges across the Nile River (Abed & Gasser, 1993). In order to do so, a series of clear-water scour tests were performed to investigate the causes of the local scour downstream the circular pier. It was found that the large scour hole downstream the circular pier was formed by the turbulent velocity fields at the intersection of the wake vortex streams from adjacent piers which was enlarged by the confluence flow. Based upon the results of this investigation, an empirical formula was developed to predict the wake and confluence maximum local scour depth downstream of a circular pier for a clear-water condition. Umbrell et al. (1998) put a tilting fume with the dimension of 21.3 m long, 1.8 m wide, and 0.6 m deep in practice to investigate clear-water bridge contraction scour caused by pressure flow beneath a bridge without the localized effect of piers or abutments. In their laboratorial experiment, different factors such as approach velocity, pressure-flow velocity under the bridge deck, and sediment size were studied. Sheppard & William (2006) studied the local clear-water and live-bed scour using laboratory tests for a range of water depths and flow velocities with two different uniform cohesionless sediment diameters (0.27 and 0.84 mm) and a circular pile with a diameter of 0.15 m. The tests were done in a tilting flume located in the Hydraulics Laboratory at the University of Auckland in Auckland, New Zealand. In their experiments, large bed forms were observed to travel through the scour hole during a number of the live-bed scour tests and they concluded that Sheppard's equations appeared to perform well for the range of conditions covered by the experiments.

1.11.2 Numerical models

Since experiments are sometimes very costly and time-consuming, application of Computational fluid dynamics (CFD) models has become greatly popular among many hydraulic researchers. Computational fluid dynamics (CFD) can be defined as a branch of fluid mechanics that uses numerical methods and algorithms to solve and investigate problems involving fluid flows. The term "CFD model" is commonly used to refer to a high-order numerical model capable of solving complex flow situations with relatively few simplifications such as three-dimensional, multi-fluid, compressible. (Toombes & Chanson, 2011). Not only CFD models can save time and money but also, they are free of scaling effect and can be used for various types of geometry and hydraulic conditions of a specific hydraulic problem, in this case, it is unnecessary to set up an entirely new experimental setup. Besides, usage of modern laboratorial equipment is very costly and there would be always experimental errors in the system which sometime cannot be simply neglected. That's why most CFD numerical models have been developed along with laboratory models and their results have been compared with each other in order to verify the validity, reliability and accuracy of them. In the case of numerical modelling of scour around bridge pier, most CFD numerical models have not been very accurate and precise due to extremely complex 3D flow field around bridge piers as well as lack of an accurate sediment transport equations in them. It should be mentioned that the application of the sediment transport equation is to predict the complex process of scouring around bridge piers. That is why many hydraulic researchers have devoted their investigations to develop sediment transport equation (e.g. Wu et al., 2000a; Olsen, 1998; Feurich & Olsen, 2011; Zhu et al, 2012). Regardless of deficiency of numerical model in an accurate prediction of scour pattern around bridge piers, in this section, some of the most significant studies on scour around bridge pier will be presented. Fukuoka et al. (1994) developed

a three-dimensional (3D) numerical simulation model for the local scour around a bridge pier. Their study demonstrated that the developed numerical model can accurately obtain solutions that are in good agreement with the experimental results of the local scour from the large-scale hydraulic model. Richardson & Panchang (1998) used a fully 3D hydrodynamic model to simulate the flow occurring at the base of a cylindrical bridge pier within a scour hole. The results of the numerical simulation were also compared with laboratory observations by Melville and Raudkivi (1977). Relatively good agreements were attained between these studies quantitatively and qualitatively. It was concluded that the discrepancies between the results of the two studies might be due to the parameters chosen in the numerical model. Besides, numerical results for bridge scour were also compared to empirical equations. Young et al. (1998) developed a numerical model for clear-water abutment scour depth along with an independent 3D finite element model. In their study, the predicted scour depths were in good agreement with the predicted results from the finite element model. They also concluded, from a comparative study, that the HEC-18 (Federal Highway Administration (1993) prediction overestimates measurement by 22%. Salaheldin et al. (2004) inspected the performance of several turbulence models (the standard, the RNG, the realizable k-ε model and RSM model) in simulating three-dimensional flow around bridge piers by using FLUENT. The results specified that despite the overestimation of near bed velocity field, standard k-ε and RNG k-ε models are able to simulate 3D-flow around the bridge piers accurately.

1.11.3 Hydrodynamic model

Numerical model of turbulent flow is one of the most complicated fields in hydraulic engineering. To simulate a wide variety of hydrodynamic problems, several commercially CFD models are most common and available for the numerical simulation, such as FLUENT and FLOW-3D. The

commercially available CFD package FLOW-3D is one of the most recent practical CFD model for simulation of hydraulic models and is my first choice to be used to simulate this hydraulic problem. FLOW-3D uses a finite-volume approach to solve the RANS equations by implementing of the Fractional Area/Volume Obstacle Representation (FAVOR) method to define an obstacle (FLOW-3D User's Manual, 2000). The general governing RANS and continuity equations for an incompressible flow, including the FAVOR variables, are given by:

$$\frac{\partial x}{\partial x_i}\left(u_i A_i\right) = 0 \tag{1-21}$$

$$\frac{\partial u_i}{\partial t} + \frac{1}{V_F}\left(u_j A_j \frac{\partial u_i}{\partial x_j}\right) = -\frac{1}{\rho}\frac{\partial P}{\partial x_i} + g_i + f_i \tag{1-22}$$

where u_i represents the velocities in the x_i directions which are x, y, z-directions; t is time; A_i is the fractional area open to flow in the subscript directions; V_F is the volume fraction of fluid in each cell; ρ is fluid density; p is hydrostatic pressure; g_i is gravitational acceleration in the subscript directions; and f_i represents the Reynolds stresses for which a turbulence closure model is required (Kim, D. G., 2007). To numerically solve the free surface profile over the side weir, it is important that the free surface is accurately tracked. In FLOW-3D, the free surface is defined in terms of the volume of fluid (VOF) function, F, which represents the volume of fraction occupied by the fluid (FLOW-3D User's Manual, 2000). A two-equation renormalized group theory model (RNG model), as outlined by Yakhot & Orszag (1986) was used for turbulence closure. The RNG model is known for an accurate description of low intensity turbulence flows and flows having strong shear regions (Dargahi, 2010). For each cell, values of the state variables are solved at discrete times using a staggered grid technique. The staggered grid places all dependent variables at the center of each cell except for the velocities and the fractional areas (FLOW-3D User's Manual,

2000). Velocities and fractional areas are in the center of the cell faces normal to their associated direction. Pressures and velocities are coupled by using SOR (Successive over Relaxation) method which is a semi- implicit method. This semi-implicit formulation of the finite difference equations allows for an efficient solution of low speed and incompressible flow problems (Dargahi, 2010). Over the years, many numerical investigations of the sediment transport have been published (e.g. Wu, et al., (2000b); Olsen, (2009); Olsen & Kjellesvig, (1998); Zhu & Liu, (2012). Wu et al. (2000b) obtained a formula for the fractional bed load transport by regression analysis in which the effects of different sediment sizes is included. Compared to the turbulent flow, sediment transport around bridge piers under ice cover involves much more complexity. In the local scour hole, the bed slope is relatively steep, and this will greatly affect the bed load transport rate.

1.11.4 Turbulence models

FLOW-3D gives the user the choice of three turbulent k-ε models: The standard model as introduced by Launder & Spalding, (1983). The Renormalization Group (RNG) model designed by Yakhot & Orszag (1986) and the realizable model designed by Shih et al, (1995).

- **The standard k−ε:** The standard k−ε model has been the most widely used two equation models since it was introduced by Launder & Spalding, (1983). As a result, its strengths and weaknesses are well known. According to Wilcox (1998), it is generally inaccurate for flows with adverse pressure gradient (and therefore also for separated flows). The standard k-ε model is a semi-empirical model based on model transport equations for the turbulence kinetic energy (k) and its dissipation rate (ε). The model transport equation for k is derived from the exact equation, while the model transport equation for ε is obtained using physical reasoning and bears little resemblance to its mathematically exact counterpart. The mathematical surgery involved in closing the ε-equation is more far-reaching than the k equation. As a result, many of the shortcomings of the

standard k – ε model are due to the inaccuracy of the ε equation. The closure coefficients are found through calibration with experimental data for fundamental turbulent shear flows such as incompressible equilibrium flow past a flat plate. Naturally, the closures are less reliable for complex turbulent flows and care must be taken when interpreting results. Motion equation of viscous incompressible fluid (Navior-Stokes equation) can be written as:

$$\frac{\partial u_i}{\partial t} + u_j \frac{\partial u_i}{\partial x_j} = f_i - \frac{1}{\rho}\frac{\partial p}{\partial x_i} + \nu \frac{\partial^2 u_i}{\partial x_j \partial x_j} \tag{1-23}$$

Substituting $u_i = \overline{u}_i + u_i'$, $p = \overline{p} + p'$ into equation (1-23), and taking time-averaging, The Reynolds equation can be obtained as follows:

$$\frac{\partial \overline{u}_i}{\partial t} + \overline{u}_j \frac{\partial \overline{u}_i}{\partial x_j} = f_i - \frac{1}{\rho}\frac{\partial \overline{p}}{\partial x_i} + \frac{1}{\rho}\frac{\partial}{\partial x_j}\left(\mu \frac{\partial \overline{u}_i}{\partial x_j} - \rho \overline{u_i' u_j'}\right) \tag{1-24}$$

Where $-\rho\,\overline{u_i' u_j'}$ is Reynolds stress. Standard k−ε models are employed as follows:

$$\frac{\partial k}{\partial t} + \overline{u}_i \frac{\partial k}{\partial x_i} = \frac{\partial}{\partial x_i}\left(\nu + \frac{\nu_t}{\sigma_k}\frac{\partial k}{\partial x_i}\right) + \nu_t \left(\frac{\partial \overline{u}_i}{\partial x_j} + \frac{\partial \overline{u}_j}{\partial x_i}\right)\frac{\partial \overline{u}_i}{\partial x_j} - \varepsilon \tag{1-25}$$

$$\frac{\partial \varepsilon}{\partial t} + \overline{u}_l \frac{\partial \varepsilon}{\partial x_l} = \frac{\partial}{\partial x_l}\left[\left(\nu + \frac{\nu_t}{\sigma_\varepsilon}\right)\frac{\partial \varepsilon}{\partial x_l}\right] - C_{\varepsilon 1}\frac{\varepsilon}{k}\nu_t \left(\frac{\partial \overline{u}_i}{\partial x_l} + \frac{\partial \overline{u}_l}{\partial x_i}\right)\frac{\partial \overline{u}_i}{\partial x_l} - C_{\varepsilon 2}\frac{\varepsilon^2}{k} \tag{1-26}$$

$$\nu_t = C_\mu \frac{k^2}{\varepsilon} \tag{1-27}$$

The empirical constants of standard k−ε models can be taken according to Table 1-1.

Table 1-1 Empirical Constants for the standard k−ε

C_μ	$C_{\varepsilon 1}$	$C_{\varepsilon 2}$	σ_k	σ_ε
0.09	1.44	1.92	1.0	1.3

- **The RNG k-ε model:** A more recent version of the k−ε model has been developed by Yakhot & Orszag (1986). Using techniques from renormalization group theory, they developed a new k−ε model which is known as the RNG model. The main difference between the RNG and the standard k−ε models is in the expression for $C_{\varepsilon 2}$, which alters the form of the dissipation term. The RNG model decreases dissipation in regions of high mean strain rates. This should make the RNG more suitable for non-equilibrium flows, such as flows with adverse pressure gradients. The empirical constants of the RNG k-ε models can be taken according to Table 1-2.

Table 1-2: Empirical Constants for the RNG k-ε model

$C_{1\varepsilon}$	$C_{2\varepsilon}$	σ_ε	σ_k
1.42	1.68	0.72	0.72

- **Realizable k-ε model**: The realizable k−ε model was developed by Shih, et al (1995). In the standard k−ε model, the normal Reynolds stress u_2 becomes negative (non-realizable) when the strain rate is large. Large strain rates can also cause the Schwartz inequality for shear stresses to be violated. To overcome these problems, the realizable k−ε model makes the eddy-viscosity coefficient, C_v, dependent on the mean flow and turbulence parameters. The notion of variable C_v has been suggested by many authors and is well substantiated by experimental evidence. For example, C_v is found to be around 0.09 in the defect layer of an equilibrium boundary layer, but only 0.05 in a strong shear flow. Of note, in the realizable model, C_v can be shown to recover this standard value of 0.09 for simple equilibrium flows. The empirical constants of The Realizable k-ε model can be taken according to Table 1-3.

Table 1-3: Empirical Constants for Realizable k-ε model

$C_{1\varepsilon}$	C_2	σ_ε	σ_k
1.44	1.9	1.2	1.0

1.11.5. Free surface Tracking (VOF Method)

Several methods have been used to approximate free surface. A simple, but powerful method is VOF (Hirt & Nichols, 1981). This method is proved to be more flexible and effective than other methods for simulating complex free surface problems. Volume of Fluid (VOF) model is designed for two or more immiscible fluids, where the position of the interface between the fluids is of interest. In each cell of a mesh, it is usual to use only one value for each dependent variable defining the fluid state. Therefore, using several points in a cell to define the region filled by a certain fluid seems unnecessary. Supposing that a function F is defined in such a way whose value is unity at any point occupied by a certain fluid and is zero otherwise. The average value of F in a cell would then represent the fractional volume of the cell occupied by a certain fluid. Particularly, a unit value of F would correspond to a cell full of a certain fluid, while a zero value would indicate that the cell contained no this fluid. Cells with F values within the range of zero and one must then contain a free surface. For air-water flow field, a single set of momentum equation is shared by air and water, and the volume fraction of each of the fluids in each computational cell is tracked throughout the domain. In each cell, the summation of the volume fractions of air and water is unity. Therefore, an extra variable, the volume fraction of air or water is presented. If F_W denotes the volume fraction of water, then the volume fraction of air (F_a) can be expressed as:

$$F_a = 1 - F_w \tag{1-28}$$

Once the volume fraction of air and water is known at each location, the fields for all variables and properties are shared by air and water and represent volume-averaged values. Thus, the variables and properties in any given cell are either purely representative of water or air, or representative

of a mixture of them, depending upon the volume fraction values. The tracking of the interface between air and water is accomplished by the solution of the continuity equation with the following form:

$$\frac{\partial F_a}{\partial t} + u_i \frac{\partial F_a}{\partial x_i} = 0 \tag{1-29}$$

The value of F_a in a cell represents the fractional volume of the cell occupied by air. In particular, F_a=1 will correspond to a cell full of air, while F_a=0 will indicate that the cell is full of water. Therefore, the interface information can be known according to the value of F_a. In summary, the VOF technique can locate free surface as well as a distribution of air concentration because it follows regions rather than surfaces.

1.12 Scour around multiple pile bridge piers

Nowadays, multiple pile bridge piers have become tremendously common in bridge design for geotechnical and economic reasons. These types of pier not only can significantly reduce construction costs but also are more practical and efficient (Ataie-Ashtiani & Beheshti 2006). In this section, some of the most fundamental studies of scour around multiple pile bridge piers is presented. Chow and Herbich's study in 1978 did the first study introducing wave scour at pile groups. They studied the wave scour around 3-legged pile structures, 4-legged pile structures and 6-legged pile structures. Hannah (1978) studied 2-pile tandem, 2-pile side by side, 2-pile staggered, 3-pile tandem, 4-pile square and 6-pile rectangular arrangements in steady current. It was concluded that due to progressive protrusion of a pile cap into the flow, scour depths increase and the pile cap very quickly becomes the dominant feature causing local scour. Salim & Jones (1996) studied the scour around submerged and unsubmerged pile groups and presented equations for the effect of pile spacing and angle of attack at pile groups. They observed that the scour depth decreases as the spacing between the piles increases. Zhao and Sheppard (1998) investigated the

effect of flow skew angle on local scour at pile groups. Sumer and Fredsøe (1998) studied wave scour around groups of piles with different configurations (2-pile, 3-pile including the triangular group, and 4×4 arrangements). Ataie-Ashtiani and Beheshti 2006, did 112 experiments including a variety of conditions including different pile group arrangements, spacing, flow rates, and sediment grain sizes under steady clear-water scour conditions. It was concluded that the scour at a pile group is different from that around a single pile, depending on the pile spacing and for very small pile spacing, the pile group behaves as a single body. Besides, for the two-pile side-by-side arrangement, the scour depth increases by as much as a factor of 1.5, while this value for the tandem arrangement is about 1.2. Sheppard and Jones (1998) conducted experiments on complex pier components (pile group, pile cap, and columns) and presented a superposition procedure that combines scour depth predictions for the individual components to obtain a prediction for scour at the composite structure. Sumer et al. (2005) described the scour geometry for pile groups with varying pile spacing. According to them, scour around pile groups is caused by two mechanisms. Those causing local scour at individual piles, and those causing a global scour (the general lowering of the bed) over the entire area of the pile group. As pile spacing decreases, the scour holes at individual piles overlap and, at the limit, merge into one large scour-hole. Mostafa (2011) did an experimental study of scour around single pile and different configurations of pile groups exposed to waves and currents. Four different sets of experiments were used in this study: single pile, group of two piles with side-by-side arrangement, group of two piles with tandem arrangement and group of three piles. It was concluded that the case of side-by-side pile arrangement induced more scour compared to the case of tandem pile arrangement and the case of three piles with triangular arrangement. Although a great number of studies have been done about scour around single piers over the past decade or so, less studies have been done about scour at

pile groups and to the authors' knowledge, no study is yet available investigating scour under ice cover for pile groups.

1.13 Impact of ice on the bridge pier scouring

Many rivers become ice-covered during the winter months. Engineers and resource managers often overlook the winter season even though most rivers in Canada and northern parts of the United States, Europe, and Asia are annually affected by ice. The reason why the winter season is overlooked is that all the design criteria are often centered on large open channel flow event; however, this is a dangerous assumption because there are some ice-affected sediment processes that are essential to consider for safe civil engineering designs (Turcotte et al., 2011). Ice-cover presence can cause significant damage on the foundation of bridges that requires expensive repairs. One very recent example has happened at the upstream of Melvin Price Lock and Dam where ice-induced scour was repaired at a cost more than $1,000,000 and the scour hole re-appeared within a year of the repair (Carr & Dahl, 2017). Ice-cover presence imposes a floating solid boundary on the upper surface of the flow which will lead to increase in channel flow resistance and causes redistribution of velocity gradient over its depth (Ashton, 1986; Smith & Ettema, 1995; Sui et al., 2010). Besides, ice-cover causes changes in the hydraulic characteristics of flow such as bed shear stress distribution and sediment transport rate (Lau and Krishnappan, 1985). Although the problem of scour around bridge pier has been broadly studied and documented by several investigators (Chabert & Engeldinger, 1956; Laursen and Toch 1956; Shen et. al., 1969; Melville, 1975; Hjorth 1975; Melville & Raudkivi, 1977; Ettema, 1980; Baker, 1981; Jain, 1981; Raudkivi & Ettema, 1983; Melville & Sutherland, 1988; Kothyari, 1989; Dargahi, 1990; Yanmaz & Altimbilek, 1991; HEC-18 (1991), Dey, 1997; Ahmed and Rajaratnam 1998; Graf & Istiarto, 2002), this issue has not been properly scrutinized under ice-covered flow condition. The lesser number of studies on

the scour around bridge pier under ice-covered flow condition is due to the inherent difficulty in collecting field data while ice is present and complications in lab measurements representing differing scales and temperature effects (Moore & Landrigan, 1999). Some of the most significant studies on scour under ice cover will be presented in the following section. Krishnappan (1984) did experiments to test the validity of a turbulent flow model (k-ε model), first introduced by Lau & Krishnappan, (1981). Thirty-two flows were tested all together. Seventeen of them were free-surface flows, and the remaining fifteen were flows with top cover. For flows with top cover, three types of covers were tested which were natural ice cover, plywood cover and plywood covered with "Mactac." The natural ice cover was formed by reducing the temperature in the cold room to -10° C and maintaining it at that value overnight. Their method uses the k-ε turbulence model to numerically determine velocity distribution and suspended-sediment concentration. The study indicates that this model can predict the average flow properties in such flows with reasonable accuracy and it is recommended that this turbulent model can be used for practical applications when predicting time-averaged flow properties in flows with and without top cover. It is based on the assumptions that bed-load transport can be estimated by treating an ice-covered flow as a two-layer flow divided at the elevation of the velocity maximum. However, their findings showed a great deal of limitation for dune regime. Hereby, flume experiments done by Smith and Ettema (1997) revealed that the two-layer assumption is especially insufficient for characterizing flow resistance and sediment transport in the dune regime, because bedform geometry and the macroscale turbulence structures within an ice-covered flow increase with the full depth of flow. This finding was not considered in Krishnappan, (1984) because their flume experiments were done with a bed in the ripple regime. It should be mentioned that ripple geometry principally increases with bed sediment size rather than flow depth and is insensitive to ice-cover presence.

Lau & Krishnappan (1985) developed a method to calculate sediment transport in ice-covered flows. This study revealed very important characteristics of flow under ice-cover conditions. It was concluded that the presence of ice is greatly influential on the dynamics of flow and sediment transport in a river. The ice cover almost doubles the wetted perimeter leading to increase in the total boundary shear and flow depth and a decrease in the average velocity. However, the bed shear stress and the eddy viscosity are both smaller than the corresponding free-surface flow values. It was also concluded that the reduction in the bed shear stress results in significant changes on sediment transport and lessens the ability of the flow to entrain and suspend sediment. Since, the sediment transport rate is very sensitive to changes in bed shear stress, decrease in sediment concentration and flow velocity noticeably reduces the suspended sediment transport. Another remarkable study on local scour around bridge piers was done by Zabilansky (1996). In his research, he developed an instrumentation package for measuring and monitoring ice forces on a bridge pier and for monitoring the development of bed scour due to ice and open-water floods. It was concluded that the faster velocity resulted in more aggressive bed scour and the bulk of the scour occurred in the initial stages of breakup while the ice sheet was still intact. Once the ice sheet broke up and the ice was free floating, the scour activity died down. Zabilansky & White (2005) investigated the impact of ice cover on scour in narrow rivers. It was concluded that when discharge increases above the freeze-up datum, the pressurized flow condition, combined with the rough underside of the ice, will cause the maximum velocity in the flow to both increase and shift closer to the bed. The result will be increased shear stresses on the bed which results in live-bed scour. Moreover, the increase in shear stress on the bed due to the ice-cover accelerates the scour around bridge piers. Ackermann et al. (2002) performed a laboratory investigation on the effect of ice cover on local scour around circular bridge under rough, smooth and open channel condition

for a uniform sand type with D_{50}= 31.8 mm. It was found that covered flows gave larger scour depths for all flow velocities, although the scour development followed a similar pattern for both covered and free surface flow conditions**.** Hains & Zabilansky (2004) carried out twenty test using mean flow velocity in the clear water scour range under open water, floating and fixed ice-cover. Styrofoam was used to simulate both smooth and rough surface. It was found that under clear-water scour, the equilibrium scour depths for the fixed and floating covers were similar, but up to 21% higher than those found for open water. Ettema et al. (2000) proposed a method for estimating rates of sediment transport in ice-covered alluvial channels. The method extends existing, open-water procedures for estimating rates of sediment transport to conditions of ice-covered flow. This study uses laboratory flume data to enable sediment transport in covered flow to be estimated using procedures for estimating rates of sediment transport in open-water flow. In other words, the proposed method smooths the extension of suitable open-water procedures to ice-covered flow conditions. Based on a series of experiments under both ice-covered and free surface conditions, Wang et al. (2008) discusses the impact of flow velocity and critical shear Reynolds number on incipient motion of bed material. It was found that the deeper the flow depth under ice cover, the higher the flow velocity needed for the incipient motion of bed material. Besides, the location of the maximum velocity moves to the bed with increase in the ratio of undercover resistance coefficient to the resistant coefficient of channel bed (n_i/n_b). Therefore, since near-bed velocity is higher under ice-covered conditions, a higher shear stress is exerted on the river bed. A series of experiments for the incipient motion of frazil particles under ice cover have been carried out by Sui et al. (2010) in laboratory under different flow and boundary conditions. To investigate the impacts of ice cover on the incipient motion of frazil particles, foam panels were used to simulate smooth ice cover. To study the impact of rough ice cover on the incipient motion of frazil particles,

the foam panels were modified by adding small wood pieces to create rough underside surface. Measurements on flow velocities across the measuring cross-section at different water depths have been conducted to compare the velocity profile under different flow and boundary conditions. It was found that less critical dimensionless shear stress for incipient motion was needed if the sediment size is smaller. Moreover, the velocity profile under ice cover is entirely different compare to the velocity profile in open channels because the presence of an ice cover causes the velocity profile to be shifted towards the smoother boundary (channel bed) and adding up to the flow resistance. The most recent study on scour around bridge piers was done by Hirshfield (2015). In her dissertation, 54 flume experiments were completed investigating scour around a single pier under open, smooth and rough ice cover conditions. She used two different circular piers with diameters of 11 cm and 22 cm in non-uniform sediments under rough, smooth and open channel conditions. It was concluded that scour depth is greater under rough ice cover compared to open channel conditions for 60 percent of experiments and it is greater under smooth ice cover compared to open channel conditions for 53 percent of experiments and the smallest grain size yielded the larger pier depth under all channel cover and vice versa.

1.14 Hydraulic characteristics of ice scour

The impact of ice cover on the annual sediment transport budget in cold regions can be significant (Lawson et al., 1986). As it was mentioned earlier, due presence of ice on the water surface and limitation in its measurement, the impact of ice cover on the annual sediment transport is often neglected in sediment budgets (Knack & Shen, 2015). The presence of ice has been found to increase local clear-water scour depth at bridge piers by 10%–35% (Hains & Zabilansky, 2004; Ackermann et al., 2002). For bridge abutments, flume experiments revealed that with larger ice cover roughness, scour increased (Wu et al., 2014). For example, a bridge at White River Junction

whose foundation collapsed was found to have weakened because of recurring scour and redeposition of non-structural fill (Zabilansky & White, 2005). The velocity profile under ice-covered condition, is totally different compared to open channel flow. An ice cover changes the velocity profile in a river, with the ice acting as a flow boundary on the water (Sui et al., 2010). Under ice-covered condition, the maximum velocity occurs between the bed and the bottom of the ice cover and is dependent on the relative roughness of the two boundaries. The velocity drops to zero at each boundary due to the no-slip boundary condition, resulting in a parabola-shaped profile (Muste et al. 2000; Zabilansky et al., 2006). Figure 1-11 shows Velocity profile for open water and floating smooth and rough covers from experiments.

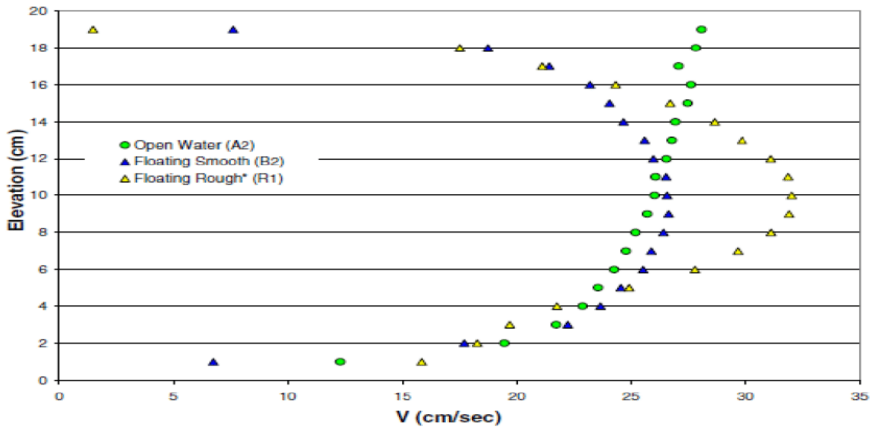

Figure 1-11: Velocity profile for open water and floating smooth and rough covers from experiments (Zabilansky et al., 2006)

1.15 Sediment transport under ice-covered flow

The ratio between suspended load and bed load, vertical distribution of suspended sediment and vertical diffusivity is affected by the presence of ice for flows under ice-covered condition (Prowse, 1993). It should be noted that the impact of ice on sediment transport in a stream is typically most significant during ice formation and breakup (Ettema & Kempema 2012). For

example, during breakup on the Liard, Saint John, and Lower Nelson Rivers in Canada, it was observed that suspended sediment loads around 10 times that of open-water or ice-covered conditions (Prowse 1993). The magnitude of any sediment transport will depend on the impact of ice on the shear stress, especially if it exceeds the critical shear stress of incipient motion of sediment. Furthermore, under conditions where erosion occurs, the magnitude of erosion is a function of water depth, ice thickness, and ice roughness (Ettema & Kempema, 2012). Besides, Variation in thickness through an ice jam can lead to variations in sediment transport capacity and can affect general scour and deposition (Beltaos et al., 2007). Ice cover can either increase or decrease bed load and suspended sediment transport depending on the type of ice cover acting on water surface (Prowse 2001; Ettema & Kempema 2012). If an ice cover is floating or a jam is restricting flow, the drop-in flow can reduce the transport of both suspended and bed-load sediment which leads to deposition (Ettema &Kempema 2012). However, if an ice is attached and is not floating type, the restraint on the cross-sectional area causes increased velocity and sediment transport capacity (Zabilansky, 1996; Hirshfield & Sui 2011). The rate of sediment transport for these two cases will be discussed more thoroughly in this section. In the case of smooth floating ice, the wetted perimeter increases causing a decrease in velocity and lower bed shear stress that, in turn, result in a loss in sediment transport capacity (Ettema, 2002; Turcotte et al., 2011). However, the magnitude of the loss in sediment transport capacity and the possibility of general or local scour depends on the roughness of ice, change in resistance near melt times, irregularity in thickness, depth of flow beneath ice that is jammed, whether the cover is attached to the shore, and the presence of structures (Wang et al. 2008). Muste et al. (2000) concluded that the presence of a rough cover in a flume reduced overall rates of sediment transport but amplified the proportion of sediment moving in suspension. In the case of an attached cover, the restraint on the cross-

sectional area causes increased velocity and sediment transport capacity (Zabilansky 1996; Hirshfield and Sui 2011). As it was mentioned earlier, the presence of ice cover also tends to shift the velocity maximum closer to the bed, increasing erosion (Zabilansky et al. 2006). Rougher ice can push the maximum velocity even further towards the bed to reduce and loose energy, causing scour (Hains & Zabilansky, 2004). Therefore, a lower average velocity threshold is needed in an ice-covered flow to reach critical shear stress for bed deformation compared to an open-water flow (Beltaos et al., 2007). Increased turbulence near the bed caused by an ice cover as well as increase in velocity profiles magnifies around bridge piers, abutments, and other hydraulic structures causing a more intensified localized scour (Beltaos et al. 2007). An increase in velocity, and thus erosion, is more intense at thickened parts of ice covers (Mercer & Cooper, 1977). However, increased depth can lower the probability of erosion, as the maximum velocity will be farther away from the bed (Hirshfield & Sui, 2011). Larger ice roughness also tends to push the maximum velocity further to the bed, increasing the gradient between the maximum and minimum velocities and increasing scour (Hirshfield & Sui, 2011). Increased ice roughness can occur due to dynamic growth in steep, narrow rivers or due to waves that can occur as ice covers remain in place through the winter season (Zabilansky et al., 2006).

1.16 Transverse flow distributions under ice-covered flow

In terms of transverse flow distributions and velocities of secondary currents, ice cover can impact flows in an existing thalweg, altering the position of the thalweg and changing the morphology of the stream which in an extreme case will lead to bank and bed erosion (Beltaos et al., 2007). Ettema & Daly (2004) stated that thalweg shifts can accelerate localized erosion and develop scour holes which is possible to make permanent bed deformations. For example, on the Missouri River in Culbertson, Montana, a thalweg shift from a primary flow channel to a secondary channel with

different roughness resulted in erosion of the bed and banks of the secondary channel (Zabilansky et al. 2006). Shifting in the position of thalweg may also reduce velocities and provide locations for frazil deposition (Ettema, 2002). Sui et al., (2006) stated that this frazil deposition decreases the cross-sectional area and increases velocity and subsequent scour. Figure 1-12 compares velocity and suspended sediment concentration distributions between covered flow and free surface flow (Lau et al, 1985)

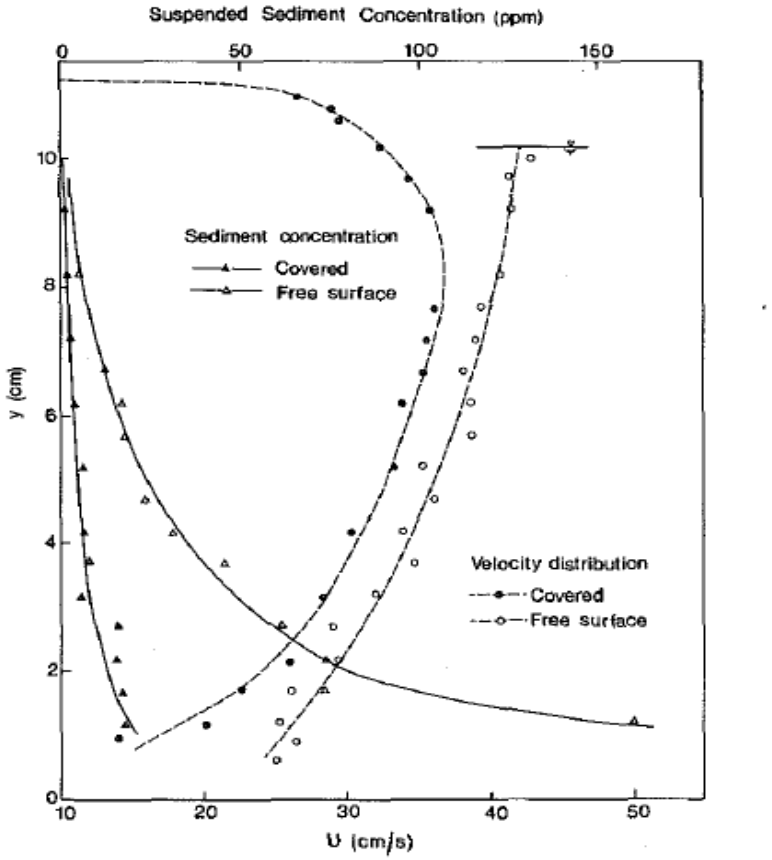

Figure 1-12: Comparison of velocity and suspended sediment concentration distributions between covered flow and free surface flow (Lau & Krishnappan)

1.17 Research objectives

As it was mentioned earlier, scour around bridge pier under ice cover conditions needs to be scrutinized more in details. My study aims at contributing to the understanding of local scour under

open and ice-covered flow conditions around two side-by-side bridge piers by incorporating four different sets of circular bridge piers with a fixed distance from each other. Besides, in order to consider the non-uniformity of sediment, three different types of bed materials are used. The main objectives of this study are listed as follows.

1.17.1 Objective one

The hydraulic characteristics of velocity distribution around bridge piers under ice cover

The velocity distribution under ice cover is totally different to that of an open channel. Under ice-covered flow condition, a new boundary is added to the surface of water which causes the velocity to drop to zero at ice cover and the channel bed due to the no-slip boundary condition, resulting in a parabola-shaped profile (Muste et al. 2000; Prowse 2001; Ettema and Daly 2004; Zabilansky et al. 2006). Besides, under ice-covered condition, the maximum velocity occurs between the bed and the bottom of the ice cover and is dependent on the relative roughness of ice cover roughness and the channel bed roughness. In this study, the velocity distribution of flow under ice-covered and open channel flow conditions will be measured by means of SonTek 16 MHz Acoustic Doppler Velocimeter (ADV). The main objective is to analyze the velocity profile distribution between open channel and ice-covered flow condition

1.17.2 Objective two

The impact of flow depth and approaching velocity on scour around bridge piers under ice-covered and open-channel flow condition

The well-known dimensionless number which includes approach velocity and flow depth and is one of the most influential dimensionless parameters in prediction of scour depth is Froude number (Froehlich, 1989). Froude number, Fr, is a dimensionless value that describes different flow

regimes of open channel flow. It can be interpreted as the ratio of water velocity to wave velocity. At critical flow (Fr=1) water velocity equals wave velocity so any disturbance to the surface will remain stationary. In subcritical flow (Fr<1) the flow is controlled from a downstream point and information is transmitted upstream. This condition leads to backwater effects. Supercritical flow (Fr>1) is controlled upstream and disturbances are transmitted downstream (Douglas et al 1995). Another important dimensionless parameter which considers both the mean particle size of the sediments (D_{50}) and inertia force is densimetric Froude number (Khwairakpam et al, 2012). In the proposed experimental study, different combinations of flow velocity and flow depth are incorporated to make a wide range of Froude number and densimetric Froude number in subcritical flow regime. The ultimate purpose of this objective is to measure the real-time and maximum scour depth under different flow conditions in terms of velocity and water depth for ice-covered and open channel flow and interpret their possible difference which can lead to derivation of useful scour predictive formula.

1.17.3 Objective three

The impact of non-uniformity of sediment on local scour around bridge piers under ice-covered and open-channel flow condition

Most of the existing researches on bridge piers use uniform sediment which is not an appropriate representative of natural river system and can result in excessively conservative design values for scour in low risk or non-critical hydrologic conditions. In the present study, flume experiments are completely investigating local scour around two adjacent circular bridge piers with non-uniform bed. To represent non-uniform sediment condition, three different bed materials with average particle size (D_{50}) of 0.47 mm, 0.50 mm, 0.58 mm are used. The purpose of using non-uniform

sediment bed is to represent a more actual prototype of a natural river as well as analyzing the scour depths between these three different sediments.

1.17.4 Objective four

Difference between scour patterns of two side-by-side bridge piers with a single bridge pier

As it was discussed earlier, multiple pile bridge piers have become greatly common in bridge design for geotechnical and economic reasons. Scour around pile groups is caused by 2 mechanisms: Those causing local scour at individual piles, and those causing a global scour (the general lowering of the bed) over the entire area of the pile group (Sumer et al, 2005). To the author's knowledge, there has not been a comprehensive study on scour for two side-by-side bridge piers under ice-covered flow condition and most of the studies have been done for single bridge. The main objective of this proposal is performing a more comprehensive study on scour around two side-by-side bridge piers by incorporating four different sets of circular bridge piers with a fixed distance from each other under open, rough and smooth ice-covered flow condition. Totally, 3 sets of flume experiments will be carried out in a non-uniform bed and suitable mathematical models regarding scour estimation of bridge piers for open and ice-covered flow condition will be developed.

1.17.5 Objective five

Impacts of two different types of ice cover on local scour under ice cover

As it was mentioned earlier, the presence of ice cover causes fundamental changes in the properties of flow. Since ice cover is the most important parameter in this study, it has been decided to use two different types of ice cover to represent impact of ice-roughness on local scour around bridge piers which are rough and smooth ice covers. In order to simulate ice cover, 13 panels of Styrofoam

with dimensions of 1.2 m × 2.4 m (4×8 foot) will be used to cover nearly the entire surface of flume. Styrofoam density is 0.026 gr/cm^3 and it will get floatable during the experiments when the water flows beneath it. The smooth ice cover is the even surface of the original Styrofoam panels while the rough ice cover is made by attaching small Styrofoam cubes to the bottom of the smooth cover. The dimensions of Styrofoam cubes are 25 mm×25 mm× 25 mm and are spaced 35 mm apart. The main objective of using two different types of ice cover is to more realistically examine the impact of them on local scour depth around bridge piers as well as proposing a more general scour predictive formula which will have a wider application in bridge engineering design.

1.17.6 Objective six

Dimensional analysis of variables impacting the local scour around bridge piers

Scour at piers is influenced by various parameters including duration of scour hole equilibrium time; pier characteristics such as pier size, pier shape and angle of attack; sediment characteristics such as sediments density and sediment cohesion, approaching flow characteristics such as flow depth and flow velocity, properties of fluid such as fluid density and fluid viscosity, flume characteristics such as flume width, flume slope and flume roughness. The relationship showing the influence of various parameters on the maximum scour depths at piers can be given in functional form as follows:

$$y_{max} = f(K_s, K_\theta\, C, y_0, U, W, D, \rho_w, \rho_S, g, \mu, D_{50}, S_0, n_i, n_b, T_0, G) \quad (1\text{-}30)$$

In which y_{max} is maximum scour depth; f is function symbol; K_s is simplified pier shape coefficient which is one for circular bridge piers (Melville and Sutherland 1998); K_θ is factor for angles between approach flow and pier axial; C is cohesion of the sediment particles; y_0 is approaching flow depth; U is approaching velocity; W is channel width; D is pier diameter; ρ_w is water density;

ρ_s is sand density; g is acceleration due to gravity; μ is dynamic viscosity of fluid; D_{50} is particle mean diameter; S_0 is the longitudinal channel slope; n_i and n_b are the roughness of the ice cover and the channel bed and T_0 is time needed for the scour depth to reach to the equilibrium condition. Hereby, the following dimensionless parameters are effective in scour under the present experimental conditions:

$$y_{max}/y_0 = f(U/(\sigma g D_{50})^{0.5}, U/(g y_0)^{0.5}, n_i/n_b, D_{50}/W, D_{50}/y_0, y_0/D, y_0/W, D/D_{50}, W/D, \rho_s/\rho_w, G/D) \quad (1\text{-}31)$$

In order to simplify the above equation and select the most dominant parameters to develop an equation for prediction of scour under open channel and ice-covered flow condition, linear regression and sensitivity analysis for each of the dimensionless parameters will be developed and corresponding statistical analysis will be done

1.17.7 Objective seven

CFD simulation of local scour around bridge piers under ice cover

Due to the uncertainties involved in the physical study, such as idealized flow condition, uniform sediments, simplified geometries, formulae derived from this approach are appeared to overestimate the scour depth obtained from field measurements. Physical experiments can overcome some of the shortcomings, but they are usually time-consuming and highly cost in model construction and experimentation. In viewing these aspects, recently, the computer-based numerical simulation becomes an alternative and promising way to deal with local scour. Computational Fluid Dynamics (CFD) has emerged as a powerful hydraulic engineering design and analysis tool along with experimental study. Due to the complex 3D flow field and limitations of computer capabilities, numerical studies about the local scour around bridge piers or piers are not well addressed as experimental studies. In the present research, hydraulic model will be

employed to simulate the flow field around a bridge pier under ice cover and sediment model will be used to calculate the variation of channel bed elevation. Numerical results will also be compared with original experimental data.

1.18 The innovations of the research

This research is associated with local scour around four different set of side-by-side bridge piers under different flow conditions in term of approaching velocity and flow depths. As the proposed experimental focuses on the local scour around bridge piers under ice cover conditions. The study has the following innovations.

1. The entire process of local scour around bridge piers under ice covered conditions will be carried out by a series of large-scale flume experiments;
2. The local scour process under different flow conditions, namely, open channel, smooth, rough cover will be compared;
3. The local scour process will be performed under three different bed materials with average particle size (D_{50}) of 0.47 mm, 0.50 mm, 0.58 mm are used.
4. Through Dimensional Analysis, empirical formulae to estimate the scour depth under ice covers will be derived;
5. Simulation of flow around bridge pier under ice-covered condition

2. EXPERIMENTAL SETUP

Experiments are carried out at the Quesnel River Research Centre, Likely, BC, Canada in a large-scale flume. The flume is 40 m long, 2 m wide and 1.3m deep. The longitudinal slope of the flume bottom is 0.2 percent. Three supply valves and two different tailgates with the height of 100 mm and 200 mm are used to make different range of flow conditions in term of velocity and flow depth. Inlet discharge is supplied by means of three pumps under two tailgates and one tailgate configuration. The highest discharge is when all the pumps are simultaneously in action and it is exclusively for two-tailgate configuration in order to avoid live-bed scour. Figure 2-1 shows two pumps in action.

Figure 2-1: Two pumps in action

A holding tank with a volume of nearly 90 m^3 is located at the upstream of the flume to keep a constant head in the experimental zone. It should be noted that the holding tank is 40 m in length, 2 m in width and 1.3 m in depth. At the end of the holding tank, water overflows from a rectangular weir to the flume. In order to protect the flume from weather elements and keep running experiments safe, the whole length of the flume (40 m) is covered with plastic cover. Two sand boxes with the depth of 0.30 m are filled with non-uniform sediment with average particle size

(D_{50}) of 0.47 mm, 0.50 mm, 0.58 mm. The first sand box is 5.6 m in length and the second sand box is 5.8 m in length. The distance between the sand boxes is 10.2 m. Four different pairs of bridge piers with diameter of 60 mm, 90 mm, 110 mm and 170 mm are used. Bridge piers are constructed from PVC plumbing pipe and are circular in shape. Figure 2-2 shows measuring points around the bridge piers.

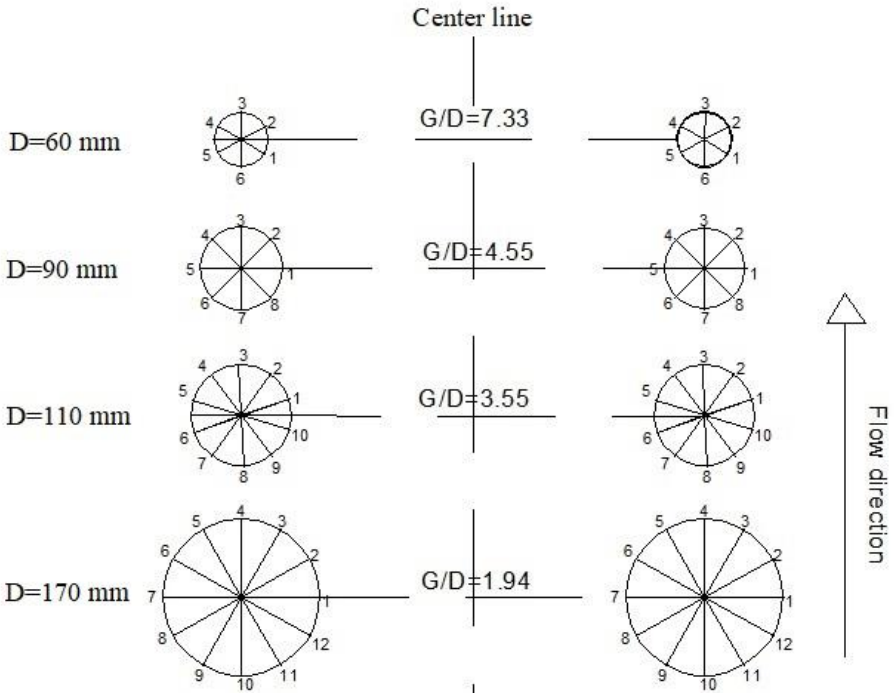

Figure 2–2: Measuring points around the bridge piers

A transparent viewing window is constructed inside each of the sand boxes which makes it possible to observe the process of scouring around bridge piers through it. A rectangular weir is used in the middle of the flume at 40 m in order to create a constant head. Since the flow of water is turbulent while entering the flume, a flow diffuser is placed at the downstream of the rectangular to dissipate the turbulence in the flow of water. A pair of bridge piers are placed inside both sand boxes with the constant distance of 0.50 m from each other and are fixed to the bottom of the flume. Since there is one pair of bridge piers in each of the sand boxes, two experiments are being done

simultaneously in each experimental run. The left bride piers are placed at 0.25 m and the right bridge piers are placed at 0.25 m from the center line of the flume in each of the sand boxes. Figure 2-3 and Figure 2-4 show the downstream view of the bridge piers in both sand boxes while the experiment is running.

Figure 2-3: Downstream view of the bridge piers with rough ice cover on

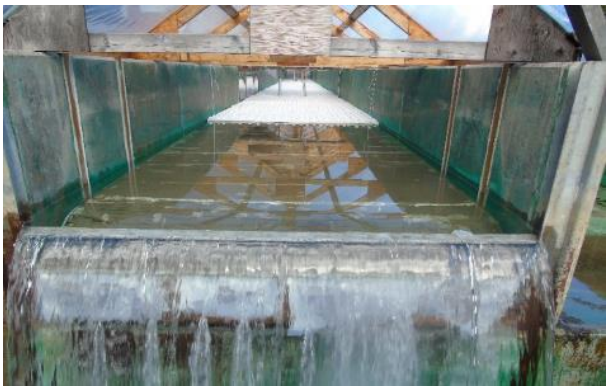

Figure 2-4: Downstream view of the bridge piers with rough ice cover on and larger tail gate in action

The first configuration consisted of 60 mm bridge pier in the first sand box and 90 mm bridge pier in the second sand box and the second configuration consisted of 110 mm bridge pier in the first sand box and 170 mm bridge pier in the second sand box. The water depth in the flume is adjusted by the position of the tailgates. Since the sediment needs to be restored, after each sand box, a sediment trap will be installed to collect sediment during and after experiments. In front of the first sand box, a 2D flow meter by Sontek Incorporated was installed to measure the approaching flow velocity, water depth and mainly the inflow discharge during the experiment (Figure 2-5).

Figure 2-5: The SonTek-IQ used to collect flow (area-velocity) and volume data

A staff gauge is also installed in the middle of each sand box to manually verify water depth. The scour hole velocity field is measured by using a 10-Mhz Acoustic Droppler Velocimeter (ADV) (Figure 2-6).

Figure 2-6: 10-Mhz Acoustic Droppler Velocimeter (ADV) in practice used to measure velocity field around bridge piers

108 Experiments (36 experiment for each type of the sand) will be conducted under open channel, smooth ice and rough ice conditions. In order to simulate ice cover, 13 panels of Styrofoam with dimensions of 1.2 m × 2.4 m (4×8 foot) are used to cover nearly the entire surface of flume. Styrofoam density was 0.026 gr/cm^3 and it will get floatable during the experiments when the

water flows beneath it. In the present study, two types of ice cover are used, namely smooth cover and rough cover. The smooth ice cover is the even surface of the original Styrofoam panels while the rough ice cover is made by attaching small Styrofoam cubes to the bottom of the smooth cover. The dimensions of Styrofoam cubes are 25 mm×25 mm× 25 mm and are spaced 35 mm. In order to avoid the turbulence effect of incoming flow on the Styrofoam especially at high discharges, the position of first Styrofoam is decided to start from the middle of the flow diffuser section. In this case, the flow will get less turbulent while reaching the first Styrofoam. It should be mentioned that at the beginning of each experiment, the flume is slowly filled to avoid initial scouring. The durations of the experimental runs until scour hole reaches to equilibrium condition is chosen 24 h which is based on the previous experiment on single bridge pier (Hirshfield, 2015) and experiment on scour around bridge abutment (Wu et al, 2015) and my own observation. In addition, it was observed that after a period of 6 hours, the material which was transported into the scour hole was nearly at the same rate at which it was transported out and there was not any significant difference (less than 1.5 mm) in scour depth. Therefore, the maximum scour depths obtained after 24 h are adopted as the equilibrium scour depths. After 24h, the flume is gradually drained. The scour depth is manually measured along the outside lines of the circular bride piers. Figure 2-7 shows the experimental setup.

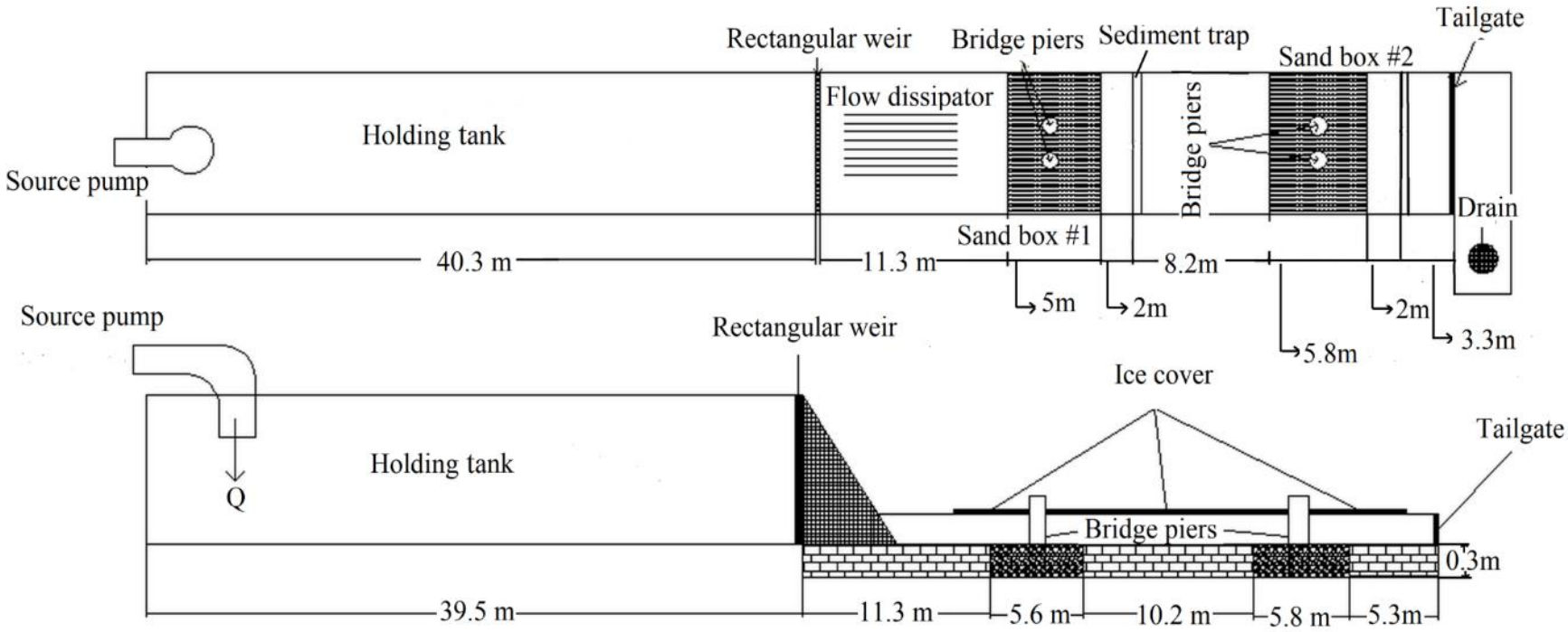

Figure 2-7: Experimental setup

2.1 Measurement apparatus

As it was mentioned before, measurement of components of velocity in x, y and z directions can be very useful in determination of shear velocity, turbulent kinetic energy and flow field characteristics around bridge piers. Recently, Acoustic Doppler Velocimeter (ADV) has been widely used to determine the flow field around in turbulent flow (Zhang et al. 2005). (ADV) is designed to record instantaneous velocity components at a single-point with such a relatively high frequency which can be consequently used to determine the turbulent properties and the bed shear stress (Chanson, 2008). In this study, to measure the flow field in the scour hole around the bridge piers under ice cover, a SonTek 10MHz Acoustic Doppler Velocimeter (ADV) which is known for its accuracy, portability, reliability and ease of operation is used. The ADV is a high-precision instrument used to measure 3D water velocity in a wide range of environments including laboratories, rivers, estuaries, and the ocean that can be used to compute the mean velocity, Reynolds stresses, shear stresses, turbulent kinetic energy and other hydraulic parameters (Cea & Pena, 2007). The ADV measures the velocity in the sampling volume located at the intersection of the transmitted and received acoustic beam as shown in Figure 2-8. As it is clear in the figure, the probe head includes one transmitter and three receivers. The 3D down-looking ADV receiver used in this study is focused in a sampling volume located 0. 10 m below the transmitter. An ADV system records simultaneously nine values with each sample: three velocity components, three signal strength values and three correlation values. Signal strengths and correlations are used primarily to determine the quality and accuracy of the velocity data. One of the most important issues regarding the ADV measurement is noise from ADV. The existence of Doppler noise from the ADV always can occur when measuring the velocity. Noise also occurs when a high level of turbulence exists at the measuring location. Hence, the examination and filtering of the signal is needed before analyzing the mean point velocity and turbulent kinetic energy (Nikora & Goring,

1998). In other words, "raw" ADV velocity data are not "true" turbulent velocities and they should never be used without adequate post-processing (Nikora & Goring, 1998). One method of dealing with this noise is to filter the data according to the value of a correlation coefficient that is a measure of the coherence of the return signals from two successive acoustic pulses (Goring & Nikora, 2002). In this research, scour hole velocity and approach velocity will be analyzed and filtered using the WinADV software supplied by Sontek. Velocity data will be filtered for correlations values above 70 (SonTek, 1997).

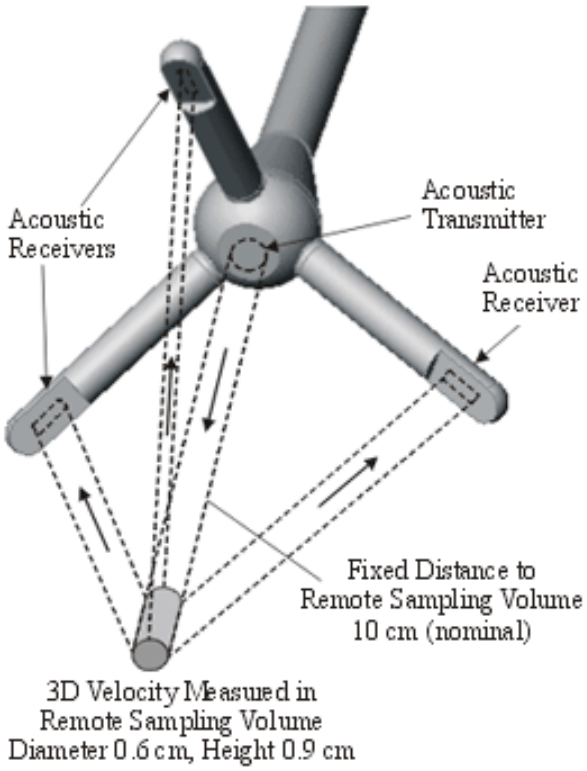

Figure 2-8: 3D-down looking ADV probe
(http://www.sontek.com/productsdetail.php?Argonaut-ADV-6)

2.2 Reference

Abed, L., and Gasser, M. M. (1993). Model study of local scour downstream bridge piers. Proceedings of the National Conference of Hydraulic Engineering, San Francisco, 1738–1743.

Ackermann, N. L., Shen, H. T., Olsson, P., & Squire, V. A. (2002, December). Local scour around circular piers under ice covers. Proceedings of the 16th International Symposium on Ice, IAHR, Dunedin, New Zealand (pp. 2-6).

Ahmed, F., & Rajaratnam, N. (1998). Flow around bridge piers. Journal of Hydraulic Engineering, 124(3), 288-300.

Ansari, S. A., Kothyari, U. C., & Ranga Raju, K. G. (2002). Influence of cohesion on scour around bridge piers. Journal of Hydraulic Research, 40(6), 717-729.

Ashton, G. D. (1986). River and lake ice engineering. Water Resources Publication.

Ataie-Ashtiani, B., & Beheshti, A. A. (2006). Experimental investigation of clear-water local scour at pile groups. Journal of Hydraulic Engineering, 132(10), 1100-1104.

Babaeyan-Koopaei, K., Ervine, D. A., Carling, P. A., & Cao, Z. (2002). Velocity and turbulence measurements for two overbank flow events in River Severn. Journal of Hydraulic Engineering, 128(10), 891-900.

Baker, C. J. (1981). New design equations for scour around bridge piers. Journal of Hydraulic Engineering, 107(4), 507-511.

Beltaos, S., Miller, L., Burrell, B. C., & Sullivan, D. (2007). Hydraulic effects of ice breakup on bridges. Canadian Journal of Civil Engineering, 34(4), 539-548.

Beltaos, S., Carter, T., & Prowse, T. (2011). Morphology and genesis of deep scour holes in the Mackenzie Delta. Canadian Journal of Civil Engineering, 38(6), 638-649.

Biron, P. M., Robson, C., Lapointe, M. F., & Gaskin, S. J. (2004). Comparing different methods of bed shear stress estimates in simple and complex flow fields. Earth Surface Processes and Landforms, 29(11), 1403-1415.

Brownlie, W. R. (1983). Flow depth in sand-bed channels. Journal of Hydraulic Engineering, 109(7), 959-990.

Breusers, H. N. C., Nicollet, G., & Shen, H. W. (1977). Local scour around cylindrical piers. Journal of Hydraulic Research, 15(3), 211-252.

Brandimarte, L., Paron, P., & Di Baldassarre, G. (2012). Bridge pier scour: A review of processes, measurements and estimates. Environmental Engineering & Management Journal (EEMJ), 11(5).

Briaud, J. L., & Hunt, B. E. (2006). Bridge Scour & the Structural Engineer. Structure Magazine, p. 59-61.

Brice J.C., Blodgett J.C., (1978), Countermeasures for hydraulic problems at bridges, Federal Highway Administration Report FHWA-RD-78-162

Carr, M. L., & Dahl, T. A. (2017). Review of Ice Induced Scour Impacts to Navigation and Structures (No. ERDC SR-17-3). ERDC Hanover United States.

Cao, Z., Pender, G., & Meng, J. (2006). Explicit formulation of the Shields diagram for incipient motion of sediment. Journal of Hydraulic Engineering, 132(10), 1097-1099.

Cea, L., Puertas, J., & Pena, L. (2007). Velocity measurements on highly turbulent free surface flow using ADV. Experiments in fluids, 42(3), 333-348.

Chanson, H. (2008). Acoustic Doppler velocimetry (ADV) in the field and in laboratory: practical experiences. In International Meeting on Measurements and Hydraulics of Sewers IMMHS'08, Summer School GEMCEA/LCPC (pp. 49-66). Department of Civil Engineering at The University of Queensland.

Chang, H. H. (1992). Fluvial Processes in River Engineering, 425 pp., John Wiley, New York
Chabert, J., & Engeldinger, P. (1956). Etude des affouillements autour des piles des ponts. Laboratoire National d'Hydraulique, Chatou, France (in French)

Chee, R. K. W. (1982). Live-bed scour at bridge piers. Rep. No. 290, School of Engineering, University of Auckland, Auckland, New Zealand.

Coleman, S. E., Lauchlan, C. S., & Melville, B. W. (2003). Clear-water scour development at bridge abutments. Journal of Hydraulic Research, 41(5), 521-531.

Chow, W. Y., & Herbich, J. B. (1978). Scour around a group of piles. Proceedings of Tenth Annual Offshore Technology Conference.

Dargahi, B. (1989). The turbulent flow field around a circular cylinder. Experiments in Fluids, 8(1), 1-12.

Dargahi, B. (1990). Controlling mechanism of local scouring. Journal of Hydraulic Engineering, 116(10), 1197-1214.

Dargahi, B. (2010). Flow characteristics of bottom outlets with moving gates. Journal of Hydraulic Research, 48(4), 476-482.

Dey, S. (1997). Local scour at piers, Part I: A review of developments of research. International Journal of Sediment Research. Beijing, China, 12(2), 23-46.

Dey, S., & Barbhuiya, A. K. (2005). Time variation of scour at abutments. Journal of Hydraulic Engineering, 131(1), 11-23.

Dey, S., & Raikar, R. V. (2005). Scour in long contractions. Journal of Hydraulic Engineering, 131(12), 1036-1049.

Deng, L., & Cai, C. S. (2009). Bridge scour: Prediction, modeling, monitoring, and countermeasures. Practice periodical on structural design and construction, 15(2), 125-134.

Dietrich, W. E., & Whiting, P. (1989). Boundary shear stress and sediment transport in river meanders of sand and gravel. River meandering, American Geophysical Union Water Resources Monograph, p.1–50

Douglas, J. F., Gasiorek, J. M., & Swaffield, J. A. (1995). Fluid Mechanics, (Essex, UK, Longman Scientific and Technical)

Ettema, R. (1980). Scour at bridge piers. Dissertation presented to the University of Auckland, at Auckland, New Zealand, in partial fulfillment of the requirements for the degree of Doctor of Philosophy in Engineering

Ettema, R., Braileanu, F., & Muste, M. (2000). Method for estimating sediment transport in ice-covered channels. Journal of Cold Regions Engineering, 14(3), 130-144.

Ettema, R. (2002). Review of alluvial-channel responses to river ice. Journal of Cold Regions Engineering, 16(4), 191-217.

Ettema, R., & Daly, S. F. (2004). Sediment transport under ice. ERDC/CRREL TR-04-20. Hanover, NH: U.S. Army Engineer Research and Development Center

Ettema, R., Melville, B. W., & Constantinescu, G. (2011). Evaluation of bridge scour research: Pier scour processes and predictions. Washington, DC: Transportation Research Board of the National Academies.

Ettema, R., & Kempema, E. W. (2012). River-Ice Effects on Gravel-Bed Channels. In: M. Church, P. Biron and A. Roy, Eds., Gravel-Bed Rivers: Processes, Tools, Environments, Wiley- Blackwell, Oxford, 2012, pp. 525-540.

FHWA, Evaluating Scour at Bridges, NH1-01-001, Federal Highway Administration, Washington, DC, USA, 4th edition, 1988.

Feurich, R., & Olsen, N. R. B. (2011). Three-dimensional modeling of nonuniform sediment transport in an S-shaped channel. Journal of Hydraulic Engineering, 137(4), 493-495.

Flow Science, Inc. (2000). FLOW-3D User's Manual.

Froehlich, D. C. (1989). Local scour at bridge abutments. In Proceedings of the 1989 National Conference on Hydraulic Engineering (pp. 13-18).

Fukuoka, S., Tomita, K., Hotta, T., & Miyagawa, T. (1994). Practical numerical simulation of local scour around a bridge pier. Doboku Gakkai Ronbunshu, 1994(497), 71-79.

Graf, W. H. A. (1998). Fluvial hydraulics: Flow and transport processes in channels of simple geometry (No. 551.483 G7).

Graf, W. H., & Istiarto, I. (2002). Flow pattern in the scour hole around a cylinder. Journal of Hydraulic Research, 40(1), 13-20.

Goring, D. G., & Nikora, V. I. (2002). Despiking acoustic Doppler velocimeter data. Journal of Hydraulic Engineering, 128(1), 117-126.

Hains, D., L.J. Zabilansky, and R.N. Weisman (2004). An experimental study of ice effects on scour at bridge piers. Cold Regions Engineering and Construction Conference and Expo, (16–19 May 2004, Edmonton, Alberta).

Hains, D.B. (2004). An experimental study of ice effects on scour at bridge piers. Ph.D. Dissertation, Lehigh University, Bethlehem, PA.

Hjorth, P. (1975). Studies on the nature of local scour. Inst. för Teknisk Vattenresurslära, Lunds Tekniska Högskola, Lunds University

Hannah, C. R. (1978). Scour at pile groups. Research report no. 28-3, Civil Engineering Department, University of Canterbury, Christchurch, New Zealand

Hassanzadeh, Y. (2012) Hydraulics of Sediment Transport, Hydrodynamics – Theory and Model, edited by Zheng, J.-H., ISBN: 978-953-51-0130-7, In Tech, available at: http://www.intechopen.com/books/hydrodynamics-theory-and-model/hydraulics-of-sediment-transport.

HEC-18. Evaluating scour at bridges. (1991). Hydraulic Engineering Circular No. 18, Federal Highway Administration (FHWA), USDOT, Washington, D.C.

Heza, Y. B. M., Soliman, A. M., & Saleh, S. A. (2007). Prediction of the scour hole geometry around exposed bridge circular-pile foundation. Journal of Engineering and Applied Science, 54(4), 375.

Hirshfield, F. (2015). The impact of ice conditions on local scour around bridge piers (Doctoral dissertation, University of Northern British Colombia.

Hirshfield, F., & Sui, J. (2011). Sediment Transport under Ice Conditions. In Sediment Transport. Intech Open Limited

Hirt, C. W., & Nichols, B. D. (1981). Volume of fluid (VOF) method for the dynamics of free boundaries. Journal of computational physics, 39(1), 201-225.

Imhof, D. (2004). Risk assessment of existing bridge structures (Doctoral dissertation, University of Cambridge).

Jain, S. C., & Fischer, E. E. (1979). Scour around bridge piers at high Froude numbers. Report. no. FHWA-RD-79-104. Washington, DC, USA: Federal Highway Administration

Jain, S. C., & Fischer, E. E. (1980). Scour around bridge piers at high flow velocities. Journal of the Hydraulics Division, 106(11), 1827-1842.

Johnson, P. A., & Ayyub, B. M. (1996). Modeling uncertainty in prediction of pier scour. Journal of hydraulic engineering, 122(2), 66-72.

Khwairakpam, P., Ray, S. S., Das, S., Das, R., & Mazumdar, A. (2012). Scour hole characteristics around a vertical pier under clear water scour conditions. ARPN J. Eng. Appl. Sci, 7(6), 649-654.

Kim, D. G. (2007). Numerical analysis of free flow past a sluice gate. KSCE Journal of Civil Engineering, 11(2), 127-132.

Knack, I., & Shen, H. T. (2015). Sediment transport in ice-covered channels. International Journal of Sediment Research, 30(1), 63-67.

Kothyari, U. C. (1989). Scour around bridge piers. Ph.D. Dissertation, University of Roorkee, Roorkee, India

Krishnappan, B. G. (1984). Laboratory verification of turbulent flow model. Journal of hydraulic engineering, 110(4), 500-514

Kwan, R. T., & Melville, B. W. (1994). Local scour and flow measurements at bridge abutments. Journal of Hydraulic Research, 32(5), 661-673

Laird, A. D. (1971). Eddy formation behind circular cylinders. Journal of the Hydraulics Division, 97(6), 763-775.

Lau, Y. L., & Krishnappan, B. G. (1981). Modeling transverse mixing in natural streams. Journal of the Hydraulics Division, 107(2), 209-226.

Lau, Y. L., & Krishnappan, B. G. (1981). Ice cover effects on stream flows and mixing. Journal of the Hydraulics Division, 107(10), 1225-1242.

Lau, Y. L., & Krishnappan, B. G. (1985). Sediment transport under ice cover. Journal of Hydraulic Engineering, 111(6), 934-950.

Launder, B. E., & Spalding, D. B. (1983). The numerical computation of turbulent flows. In Numerical Prediction of Flow, Heat Transfer, Turbulence and Combustion (pp. 96-116).

Laursen, E. M., & Toch, A. (1956). Scour around bridge piers and abutments. Bull. No. 4, Iowa Highways Research Board, Ames, Iowa.

Lauchlan, C. S., & Melville, B. W. (2001). Riprap protection at bridge piers. Journal of Hydraulic Engineering, 127(5), 412-418.

Laursen, E. M. (1960), Scour at Bridge Crossings. Journal of Hydraulic Division. 92 (3), 39-54.

Lawson, D. E., E. F. Chacho Jr., B. E. Brockett, J. L. Wuebben, and C. M. Collins. (1986). Morphology, Hydraulics and Sediment Transport of an Ice-Covered River: Field Techniques and Initial Data. CRREL Report 86-11. Hanover, NH: Cold Regions Research and Engineering Laboratory.

Liu, H. K., Chang, F. F., & Skinner, M. M. (1961). Effect of bridge constriction on scour and backwater. Civil Engineering Section, Colorado State University.

Liu, Z. (1999). Sediment transport, Aalborg University press, Denmark

Lu, J. Y., Hong, J. H., Su, C. C., Wang, C. Y., & Lai, J. S. (2008). Field measurements and simulation of bridge scour depth variations during floods. Journal of Hydraulic Engineering, 134(6), 810-821.

Macky G.H., (1990), Survey of roading expenditure due to scour, Report CR 90.09, DSIR Hydrology Centre, Christchurch, New Zealand.

Madsen, O. S., & Grant, W. D. (1977). Quantitative description of sediment transport by waves. In Coastal Engineering 1976 (pp. 1092-1112).

Maddison, B. (2012). Scour failure of bridges. Proceedings of the Institution of Civil Engineers-Forensic Engineering, 165(1), 39-52.

Masjedi, A., Bejestan, M. S., & Kazemi, H. (2010). Effects of bridge pier position in a 180-degree flume bend on scour hole depth. J. Appl. Sci, 10(8), 670-675.

McLelland, S. J., & Nicholas, A. P. (2000). A new method for evaluating errors in high-frequency ADV measurements. Hydrological Processes, 14(2), 351-366.

Mercer, A. G., & Cooper, R. H. (1977, May). River bed scour related to the growth of a major ice jam. In Proceedings of the 3rd National Hydrotechnical Conference (pp. 30-31).

Melville, B. W. (1975). Local scour at bridge sites. Report No. 117. University of Auckland, School of Engineering, New Zeeland (Doctoral dissertation)

Melville, B. W., & Raudkivi, A. J. (1977). Flow characteristics in local scour at bridge piers. Journal of Hydraulic Research, 15(4), 373-380.

Melville, B. W., & Sutherland, A. J. (1988). Design method for local scour at bridge piers. Journal of Hydraulic Engineering, 114(10), 1210-1226.

Melville, B. W. (1984). Live-bed scour at bridge piers. Journal of Hydraulic Engineering, 110(9), 1234-1247.

Melville, B. W. (1992). Local scour at bridge abutments. Journal of Hydraulic Engineering, 118(4), 615-631.

Melville, B. W. (1997). Pier and abutment scour: integrated approach. Journal of hydraulic Engineering, 123(2), 125-136.

Mostafa, Y. E., & Agamy, A. F. (2011). Scour around single pile and pile groups subjected to waves and currents. International Journal of Engineering Science and Technology, IJEST, 3(11), 8160-8178.

Moore, J. N., & Landrigan, E. M. (1999). Mobilization of metal-contaminated sediment by ice-jam floods. Environmental Geology, 37(1-2), 96-101.

Muste, M., Braileanu, F., & Ettema, R. (2000). Flow and sediment transport measurements in a simulated ice-covered channel. Water resources research, 36(9), 2711-2720

Neil, C. R. (1964). River bed scour, a review for bridge engineers, Contract No. 281. Research Council of Alberta, Calgary, Alta., Canada.

Nikora, V. I., & Goring, D. G. (2002). Fluctuations of suspended sediment concentration and turbulent sediment fluxes in an open-channel flow. Journal of Hydraulic Engineering, 128(2), 214-224.

Olsen, N. R., & Kjellesvig, H. M. (1998). Three-dimensional numerical flow modeling for estimation of maximum local scour depth. Journal of Hydraulic Research, 36(4), 579-590.

Parola, A. C., Hagerty, D. J., Mueller, D. S., Melville, B. W., Parker, G., & Usher, J. S. (1997). The need for research on scour at bridge crossings. In Stream Stability and Scour at Highway Bridges: Compendium of Stream Stability and Scour Papers Presented at Conferences Sponsored by the Water Resources Engineering (Hydraulics) Division of the American Society of Civil Engineers (pp. 1020-1020). ASCE.

Prowse, T. D. (1993). Suspended sediment concentration during river ice breakup. Canadian Journal of Civil Engineering, 20(5), 872-875.

Richardson, E. V., Harrison, L. J., Richardson, J. R., & Davis, S. R. (1993). Evaluating scour at bridges (No. HEC 18 (2nd edition)).

Richardson, E. V., Richardson, J. R., & Edge, B. E. (1993). Scour at highway structures in tidal waters. In Hydraulic Engineering (pp. 1206-1211). ASCE.

Richardson, J. R., & Richardson, E. V. (1994). Practical method for scour prediction at bridge piers. In Hydraulic Engineering (pp. 1-5). ASCE.

Richardson, E.V. (1996), History of Bridge Scour Research and Evaluations. In Stream Stability and Scour at Highway Bridges: ASCE compendium of papers ASCE water resources engineering conferences 1991 to 1998. Richardson, E. V. and Lagasse, P. F. (eds.), Anaheim: pp: 15-40

Richardson, J. E. and Panchang, V. G. (1998). "Three-dimensional simulation of scour-induced flow at bridge piers." J. of Hydraulic Engineering, ASCE, 124, 530-540.

Richardson, E. V., Davis, S. R., (2001). Evaluating scour at bridges. HEC18 FHWA NHI-001, Federal Highway Administration, US Department of Transportation, Washington, DC.

Raudkivi, A. J., & Ettema, R. (1983). Clear-water scour at cylindrical piers. Journal of Hydraulic Engineering, 109(3), 338-350.

Raudkivi, A. J. (1986). Functional trends of scour at bridge piers. Journal of hydraulic engineering, 112(1), 1-13.

Salaheldin, T. M., Imran, J., & Chaudhry, M. H. (2004). Numerical modeling of three-dimensional flow field around circular piers. Journal of Hydraulic Engineering, 130(2), 91-100.

Salim, M., & Jones, J. S. (1996). Scour around exposed pile foundations. In North American Water and Environment Congress & Destructive Water (pp. 2202-2211). ASCE.

Shen, H., Schneider, V. R., and Karaki, S. (1969). Local scour around bridge piers Journal of the Hydraulics Division, 95(6), 1919–1940

Sheppard, D. M., & Jones, J. S. (1998). Scour at complex pier geometries. In Stream Stability and Scour at Highway Bridges: Compendium of Stream Stability and Scour Papers Presented at Conferences Sponsored by the Water Resources Engineering (Hydraulics) Division of the American Society of Civil Engineers (pp. 365-370). ASCE.

Sheppard, D. M. (2003). Large-scale and live-bed local pier scour experiments Coastal Engineering Technical Rep. No. 133. Civil and Coastal Engineering Dept., Univ. of Florida, Gainesville, Fla.

Sheppard, D. M., & Miller Jr, W. (2006). Live-bed local pier scour experiments. Journal of Hydraulic Engineering, 132(7), 635-642.

Sheppard, D. M., Melville, B., & Demir, H. (2013). Evaluation of existing equations for local scour at bridge piers. Journal of Hydraulic Engineering, 140(1), 14-23.

Shih, T. H., Liou, W. W., Shabbir, A., Yang, Z., & Zhu, J. (1995). A new k-ϵ eddy viscosity model for high Reynolds number turbulent flows. Computers & Fluids, 24(3), 227-238.

Smith, B. T., & Ettema, R. (1995). Ice-cover influence on flow and bedload transport in dune-bed channels (Doctoral dissertation, University of Iowa.).

SonTek. 1997. Pulse coherent Doppler processing and ADV correlation coefficient. SonTek Technical Notes. www.sontek.com

Sui, J., Hicks, F. E., & Menounos, B. (2006). Observations of riverbed scour under a developing hanging ice dam. Canadian Journal of Civil Engineering, 33(2), 214-218.

Sui, J., Wang, J., Yun, H. E., & Faye, K. (2010). Velocity profiles and incipient motion of frazil particles under ice cover. International Journal of Sediment Research, 25(1), 39-51.

Sumer, B. M., Fredsøe, J., & Bundgaard, K. (2005, January). Global and local scour at pile groups. In the Fifteenth International Offshore and Polar Engineering Conference. International Society of Offshore and Polar Engineers

Tison, L. J. (1961). Local scour in rivers. Journal of Geophysical Research, 66(12), 4227-4232.

Toombes, L., & Chanson, H. (2011). Numerical limitations of hydraulic models. In Proceedings of the 34th World Congress of the International Association for Hydro-Environment Research and Engineering: 33rd Hydrology and Water Resources Symposium and 10th Conference on Hydraulics in Water Engineering (p. 2322). Engineers Australia.

Turcotte, B., Morse, B., Bergeron, N. E., & Roy, A. G. (2011). Sediment transport in ice-affected rivers. Journal of hydrology, 409(1), 561-577.

Umbrell, E. R., Young, G. K., Stein, S. M., & Jones, J. S. (1998). Clear-water contraction scour under bridges in pressure flow. Journal of Hydraulic Engineering, 124(2), 236-240.

Van Rijn, L. C. (1984). Sediment transport, part I: bed load transport. Journal of hydraulic engineering, 110(10), 1431-1456.

Wang, J., Sui, J., & Karney, B. (2008). Incipient motion of non-cohesive sediment under ice cover – an experimental study. Journal of Hydrodynamics, 20(1), 117-124.

Wardhana, K., & Hadipriono, F. C. (2003). Analysis of recent bridge failures in the United States. Journal of performance of constructed facilities, 17(3), 144-150.

Wilcock, P. R. (1996). Estimating local bed shear stress from velocity observations. Water Resources Research, 32(11), 3361-3366.

Wilcox, D. C. (1998). Turbulence modeling for CFD (Vol. 2, pp. 103-217). La Canada, CA: DCW industries.

Wiberg, P. L., & Smith, J. D. (1987). Calculations of the critical shear stress for motion of uniform and heterogeneous sediments. Water resources research, 23(8), 1471-1480.

Wu, W., Rodi, W., Wenka T, (2000a). 3D numerical modeling of flow and sediment transport in open channels. Journal of Hydraulic Engineering, ASCE, 126(1): 4-15.

Wu, W., Wang, S., Jia, Y., (2000b). Nonuniform sediment transport in alluvial rivers. Journal of Hydraulic research, 38(6): 427-434.

Wu, P., Hirshfield, F., & Sui, J. Y. (2015). Local scour around bridge abutments under ice covered conditions-an experimental study. International Journal of Sediment Research, 30(1), 39-47.

Yakhot, V., & Orszag, S. A. (1986). Renormalization-group analysis of turbulence. Physical review letters, 57(14), 1722.

Yanmaz, A. M., & Altinbilek, H. D. (1991). Study of time-dependent local scour around bridge piers. Journal of Hydraulic Engineering, 117(10), 1247-1268.

Yang, C. T. (2003). Sediment Transport, Theory and Practice. KRIEGER Publishing Company, Malabar, Florida, pp: 90-140

Young, T. L., Ronan, S. M., Alvear, A. B., Wildenberg, S. C., Oetting, W. S., Atwood, L. D., ... & King, R. A. (1998). A second locus for familial high myopia maps to chromosome 12q. The American Journal of Human Genetics, 63(5), 1419-1424.

Zabilansky, L. J. (1996). Ice force and scour instrumentation for the White River, Vermont (No. CRREL-SR-96-6). Cold Regions Research & Engineering Lab, Hanover

Zabilansky, L. J., and K. D. White (2005), Ice cover effects on scour in narrow rivers, Ice Engineering, U.S. Army Cold Regions Research and Engineering Laboratory (CRREL), TN-05-3. (Available at http://www.crrel.usace.army.mil/library/technicalnotes/TN05-3.pdf

Zabilansky, L. J., Hains, D. B., & Remus, J. I. (2006). Increased bed erosion due to ice. In Current Practices in Cold Regions Engineering (pp. 1-12).

Zhao, G., and Sheppard, D. M. (1998). The effect of flow skew angle on sediment scour near pile groups. Compilation of Conf. Scour Papers (1991–1998), ASCE, Reston, VA

Zhang, H., Nakagawa, H., Ishigaki, T., Muto, Y., & Baba, Y. (2005). Three-dimensional mathematical modeling of local scour. Journal of applied mechanics, 8, 803-812.

Zhang, H., Nakagawa H., Ishigawa, T., & Muto, Y. (2005). Prediction of 3D flow field and local scouring around spur dykes. Proceedings of hydraulic engineering, 49, 1003-1008.

Zhu, Z. W., & Liu, Z. Q. (2012). CFD prediction of local scour hole around bridge piers. Journal of Central South University, 19(1), 273-281.

RESULTS AND DISCUSSION

3.1 Local scour around two side-by-side cylindrical bridge piers under ice-covered conditions

Scour is the local lowering of the stream bed elevation which occurs around a structure constructed in flowing water, such as bridge piers, abutments, spur dikes, jetties, and breakwaters (Melville & Coleman, 2000). As noted by Briaud et al. (2006), 1502 bridges collapsed due to bridge scour between 1966 and 2005. Wardhana and Hadipriono (2003) studied 500 cases of bridge structure failures in the United States between 1989 and 2000 and stated that the most common causes of bridge failures were floods and scour. The scour around bridge infrastructure is extremely difficult to track due to the complexity of the flow structure around this infrastructure. An accurate prediction of scour depth around bridge infrastructure will not only prevent bridge failures, which are the consequence of underestimation of scour depth, but also will efficiently reduce unnecessary, over-estimated construction cost. Many hydraulic researchers have done experiments to investigate the local scour around bridge piers and develop empirical equations to estimate the maximum scour depth (Ettema et al., 2011; Melville, 1997; Melville & Sutherland, 1988; Richardson et al., 2001; Sheppard et al., 2013; Williams et al., 2013). However, due to different laboratory conditions and limitations on data collection, specifically in small-scale laboratory flumes, most of the empirical equations for determining scour depth have a great deal of uncertainty and substantial limitations. Moreover, bridges constructed in rivers in cold regions are exposed to the impact of ice in addition to the local scour around bridge piers. The influence of ice cover on a channel involves in complex interactions among the ice cover, fluid flow, and channel geometry. This complex interaction can have a dramatic effect on the sediment transport process (Hains et al., 2004). The formation of a stable ice cover in natural rivers effectively doubles the wetted perimeter compared to open channel conditions and causes the maximum velocity to be lowered towards the channel bed (Sui et al., 2010; Wang et al., 2008). Zabilansky and White (2005) investigated the impact of ice cover on scour in narrow rivers.

It was found that when discharge increases above the freeze-up datum, the pressurized flow condition, combined with the rough underside of the ice, will cause the maximum velocity in the flow to increase and shift closer to the bed. Using uniform sand as the bed material, Ackermann et al. (2002) reported that covered flow results in larger scour depths compared to open channel flow, although the scour development follows a similar pattern for both covered and open channel flow conditions. Sui et al. (2008, 2009) studied the impacts of ice cover on local scour caused by square jets compared to those under open channel flow conditions. Wu et al. (2015a) studied the effect of relative bed coarseness, flow shallowness, and pier Froude number on local scour around a bridge pier and reported that the scour depth under covered conditions is larger compared to that under open channel flow conditions. Wu et al. (2014b) investigated scour morphology around a bridge abutment under ice cover. It was found that, at different locations around the abutment, the sediment sorting process under ice cover was more obvious. Wu et al. (2015b) studied the impact of ice cover on local scour around bridge abutments. Hirshfield (2015) did 54 flume experiments to investigate local scour around a single pier under open channel, smooth covered and rough covered flow conditions. It was concluded that the scour depth under rough cover is 60% greater compared to that under open channel conditions for 60 percent of the experiments; and the scour depth under smooth cover is 53% greater than that under open channel conditions. Multiple pile bridge piers have become more common in recent years in bridge design for geotechnical and economic reasons. These types of pier not only can significantly reduce construction costs but also are more practical and efficient (Ataie-Ashtiani & Beheshti, 2006). However, the mechanisms of the scouring process around pile groups are much more complex. According to Hannah (1978), if the pier spacing ratio is 0.25, the maximum scour depth around side-by-side piers is about 50% more than that around a single pier and for $G/D < 0.25$, the two side-by-side piers can be assumed to act as a single bridge pier (where G represents the bridge spacing distance

and *D* represents the diameter of the bridge pier). Ataie-Ashtiani and Beheshti (2006) investigated local scour for different pier arrangements and with different bridge pier spacings. It was found that with an increase in the space between the two piers, scour depth is reduced. To the authors' knowledge, all reported research regarding local scour around pile groups has been done under open channel flow conditions (Ataie-Ashtiani & Beheshti, 2013; Hannah, 1978; Melville & Coleman, 2000). As pointed out by Ettema et al. (2011), the impact of ice cover on bridge pier scour is still unknown and needs further investigation. In this regard, a more in-depth study has been done here to investigate the impact of ice cover on local scour around four pairs of side-by-side bridge piers under different sediment compositions and flow conditions.

3.1.1. Methodology

Experiments were done in a large-scale flume at the Quesnel River Research Centre of the University of Northern British Columbia. The flume was 38.2 m long, 2 m wide and 1.3 m deep. Since the experimental flume was long, in order to generate a higher velocity as well as to avoid large amount of energy dissipation for the second sand box which would ultimately lead to smaller scour depth, the relatively steep slope of 0.2% was used. Figure 3.1 shows a plan view and a side view of the experimental flume. A holding tank with a volume of 90 m^3 was located at the upstream end of the flume to maintain a constant discharge during the experimental runs. To create different velocities, three input valves were connected to control the inlet volumetric discharge. At the end of the holding tank and upstream of the main flume, water overflowed from a rectangular weir into the flume. Two sand boxes were constructed in the flume. Both had a depth of 0.30 m and were 10.2 m apart. The lengths of the sand boxes were 5.6 m and 5.8 m. In each sand box, a pair of bridge piers was placed. Three natural non-uniform sediment compositions with median grain sizes of 0.50, 0.47, and 0.58 mm were used. It should be noted that the selection of these three sands was based on their availability

in the research center. This selection also was based upon the fact that the masonry (D_{50} = 0.47 mm), concrete (D_{50} = 0.58 mm) and bedding sand (D_{50} = 0.50 mm) were the three most common sands already excavated from the surrounding mines (Hirshfield, 2015). Four pairs of cylindrical bridge piers with diameters of 60, 90, 110, and 170 mm were used, and each pier was offset from the centre line by 0.25 m, as illustrated in Figure 3-2. The bridge pier spacing ranges from 1.94 to 7.33 relative to D as illustrated in Figure 3.2. The water level in the flume was controlled by the downstream tailgate.

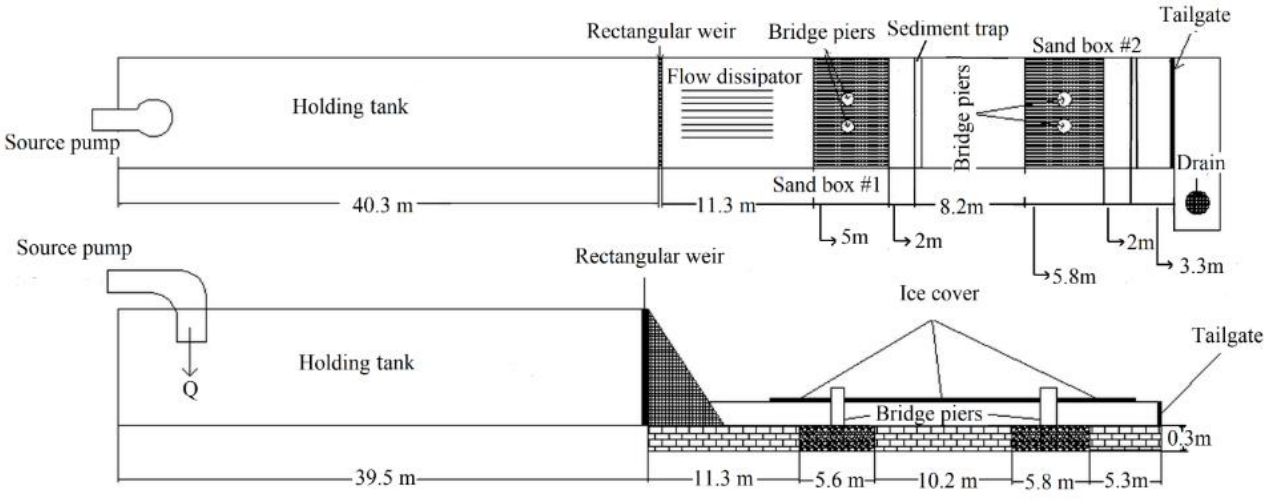

Figure 3–1: Plan view and side view of the experimental flume.

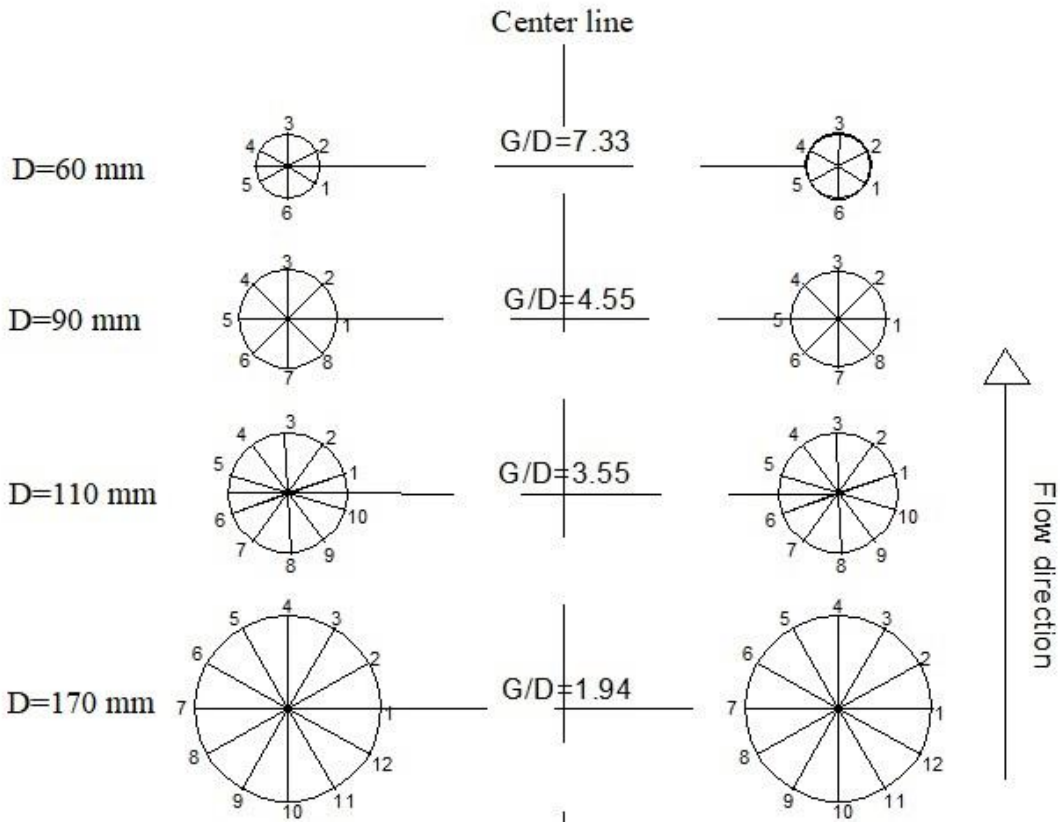

Figure 3–2: The spacing ratio and measuring points around the circular bridge piers

In front of the first sand box, a SonTek two-dimensional (2*D*) Flow Meter was installed to measure flow velocities and water depth. A staff gauge was also installed in the middle of each sand box to manually verify the water depth. The velocity fields in the scour holes were measured using a 10-MHz Acoustic Doppler Velocimeter (*ADV*). The *ADV* is a high-precision instrument that can be used to measure three-dimensional (3*D*) flow velocity in a wide range of environments including laboratories, rivers, estuaries, and the ocean (Cea et al., 2007). Styrofoam panels were used to represent ice cover and covered the entire surface of the flume. Two types of model ice cover were used, namely smooth cover and rough cover. The smooth cover was the smooth surface of the original Styrofoam panels while the rough cover was made by attaching small Styrofoam cubes to the bottom of the smooth cover. The dimensions of Styrofoam cubes were 25 mm × 25 mm × 25 mm and they

were spaced 35 mm apart. Although ice accumulation in natural rivers is assumed to be floating, Hains et al., (2004) claimed that fixed rough ice covers cause the deepest local scour around bridge piers compared to those of floating covers and smoother ice, because the rigid ice cover causes the maximum velocity to be closer to the bed. 108 Experiments (36 experiments for each sediment type) were done under open channel, smooth covered, and rough covered conditions. In terms of different boundary conditions (open channel, smooth, and rough covered flows), for each sediment type and each boundary condition, 12 experiments were done. Throughout the calibration stage of the experiments, local scour around bridge piers was carefully watched hourly for any changes in the scour depths. It was observed that after approximately a period of 6 hr, no significant change in scour depth was observed and scour hole equilibrium depth was achieved. The experiment was continued for 24 hr and again no obvious change in scour depth was observed. A limited number of experiments were also extended to 38 hr and there was not any change in scour depth between 24-hr and 38-hr experiments. Further, according to Wu et al. (2014a), who did a lot of experiments regarding local scour around a semi-circular bridge abutment, the time for development of equilibrium scour depth was 24 hr. Based on the current experimental results and the results of Wu et al. (2014a), the experimental run time of 24 hr was chosen. After 24 hr, the flume was gradually drained, and the scour and deposition pattern around the piers was measured. To accurately read the scour depth at different locations and to draw scour hole contours, the outside perimeter of each bridge pier was equally divided and labeled. The measurement of the scour hole was subject to an error of +/-0.3 mm. Of note, there are three types of similitude: geometric, kinematic, and dynamic. Geometric similarity is similarity of shape and dimensions. According to geometric similarity, the model and its prototype are identical in shape but differ only in size. Kinematic similarity is similarity of motion. According to kinematic similarity, the ratios of the velocities at all corresponding points in the flows are the

same. Dynamic similarity is similarity of forces. According to dynamic similarity, the forces that act on a system in the model and prototype must be in the same ratio throughout the entire flow field (Yang, 2005). In fact, it is not practical for a physical model of local scour around a bridge pier to satisfy all these similarities because of extremely complicated flow conditions. In scour modelling, inertial, gravitational, and viscous forces are very significant for defining similarity (Heller, 2011). In terms of kinematic and dynamic similarity, the pier Reynolds number (Re_b) which is a measure of the ratio of the inertia force on an element of fluid to the viscous force on the element is usually high and scale effects related to Re_b are negligible (Heller, 2011). Therefore, the Froude number (Fr) which is a measure of the ratio of the inertia force to gravity force is considered as the most applicable and experimental design follows to this form of similitude (Heller, 2011). In the current study, flows of all experimental runs in the flume were turbulent ($Re_b > 4{,}000$) and subcritical ($Fr < 1$) which occurs in most rivers where inertial forces are dominant. Of note, the flow Reynolds number was in the domain of turbulent flow (It ranged from 4802 to 39030). Of note, in open channel, it is common to use flow Froude number rather than flow Reynolds number in order to do kinematic and dynamic similarity. One of the issues raised by placement of a bridge pier is the blockage of the flow cross section. The blockage or wall interference refers to the influence of the side walls of a test section on the local scour depth. Chiew (1984) suggested that if the ratio of pier size to channel width is less than 10 percent ($D/W < 10\%$), the sidewalls will have no significant impact on flow characteristics and the scour profile. Significant sidewall effects in terms of scour occurring very close to the sidewall are present in the study done by Sheppard et al. (2004) in which the blockage ratio is 15%. In the current study, the ratio of D/W ranges from 6 to 17%. Therefore, in order to minimize the impact of the blockage ratio, the 170-mm pier whose blockage ratio exceed 15% was located in the second sand box. Further, as suggested by Ettema (1980), when $D/D_{50} < 25$, individual grains are

relatively large compared to the scour hole and entrainment of sediment particles is hindered because the porous bed dissipates some of the energy of the down flow. Considering the work of Ettema (1980), Breusers and Raudkivi (1991) confirmed that relative scour depth is not affected by particle size when $D/D_{50} > 25$. Yanmaz (2002) observed that relative scour depth is not affected by the particle size when $D/D_{50} > 50$. In the current study, the ratio of D/D_{50} ranges from 206.9 to 723.4 in order to avoid the impact of D/D_{50} (the relative pier size) on scour depth.

3.1.2. Results and discussion

- **Scour patterns and deposition patterns**

Figure 3-3a shows scour depths around the 9-cm-piers and Figure 3-3b shows the scour and deposition patterns at the pier face for the 9-cm-piers under different boundary conditions for $D_{50} =$ 0.50 mm. The results indicate that, regardless of the roughness of ice cover and the grain size of sediment, the maximum scour depths always occurred at the upstream, front face of the bridge piers. The downflow generated by the flow hitting the upstream face of the pier, acts like a vertical jet which erodes a groove in front of the pier. Under covered conditions, the strength of this downflow jet is intensified. The eroded sand particles are carried around the pier by the combined action of accelerating flow and the spiral motion of the horseshoe vortex (Hafez, 2016). Melville and Coleman (2000) declared that the wake-vortex system acts like a vacuum cleaner sucking up stream bed material and carrying the sediment moved by the horseshoe vortex system and by the downward flow to the downstream side of the pier. However, wake vortices are not as strong as the horseshoe vortices, and, therefore, are not able to carry the same amount of sediment load as that carried by the horseshoe vortex. Hereby, sediment deposition occurs downstream of bridge piers in the form of a deposition mound, as clearly shown in Figure 3-3b. Figure 3-4(a-b) shows the scour depth contours around the 9-cm-piers for sediment of $D_{50} =$ 0.50 mm under rough covered and open channel flows. These scour

depth contours are mapped using Surfer 13 Plotting Software (Golden Software Incorporated, U.S). The deepest point of the scour hole is clearly at the front face of the bridge piers and the deposition mound is located downstream of the bridge piers. Under the rough covered flow, both the maximum scour depth and maximum deposition height are clearly greater than that of the open channel flow. By plotting the scour depth contours, the horseshoe vortex which is the primary reason for the local scour phenomenon, must have occurred closer to the channel bed which led to a greater scour depth under the rough covered flow conditions. The results also indicate that under the rough covered flow conditions, more sediment deposition develops at the downstream side of bridge piers and the deposition mound is wider than those under open channel flow and smooth covered flow conditions. Moreover, a more intense irregular deposition mound was observed downstream of the piers, as shown in Figure 3-4b. The reason for this deposition might be due to the velocity distribution changes and greater strength of the horseshoe vortex near the bed surface under ice covered conditions. Similar scour/deposition patterns have been observed for other bridge piers regardless of sediment type and pier size. The height of the deposition mound downstream of the bridge piers depends on the depth of the scour hole upstream of the bridge pier as well as on the interaction between horseshoe vortices and wake vortices. The results indicate that, the higher the velocity of approaching flow under rough covered flow conditions, the larger the deposition mound downstream of the bridge pier.

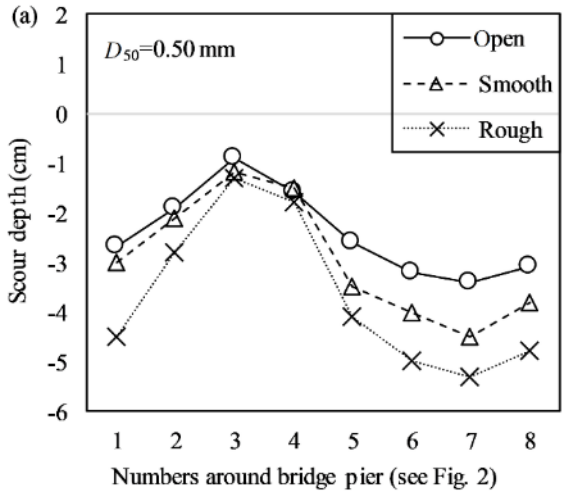

Figure 3–3a: Variation of scour depth around the 9-cm-piers for D_{50}= 0.50 mm type under open, smooth, and rough covered flow conditions

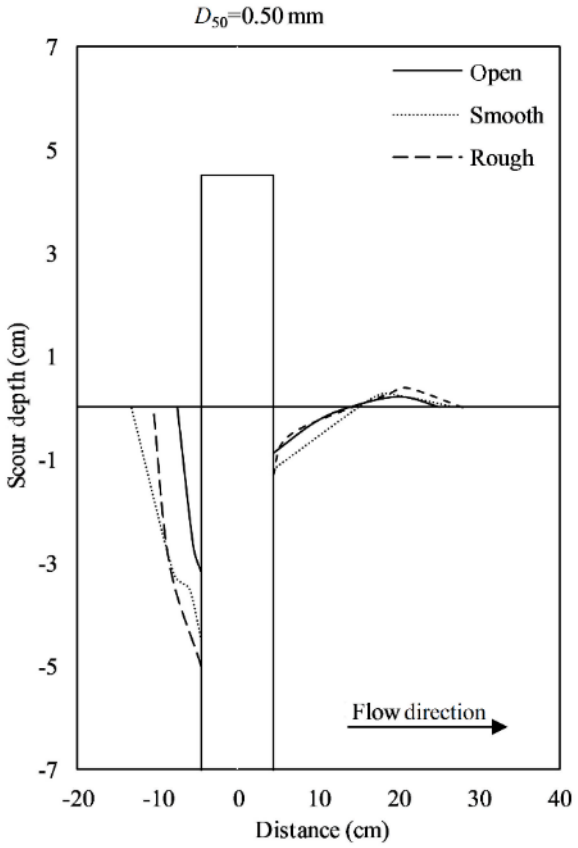

Figure 3–3b: Scour and deposition patterns at the pier face of the 9-cm-piers under open channel, smooth, and rough covered flow conditions (D_{50} = 0.50 mm).

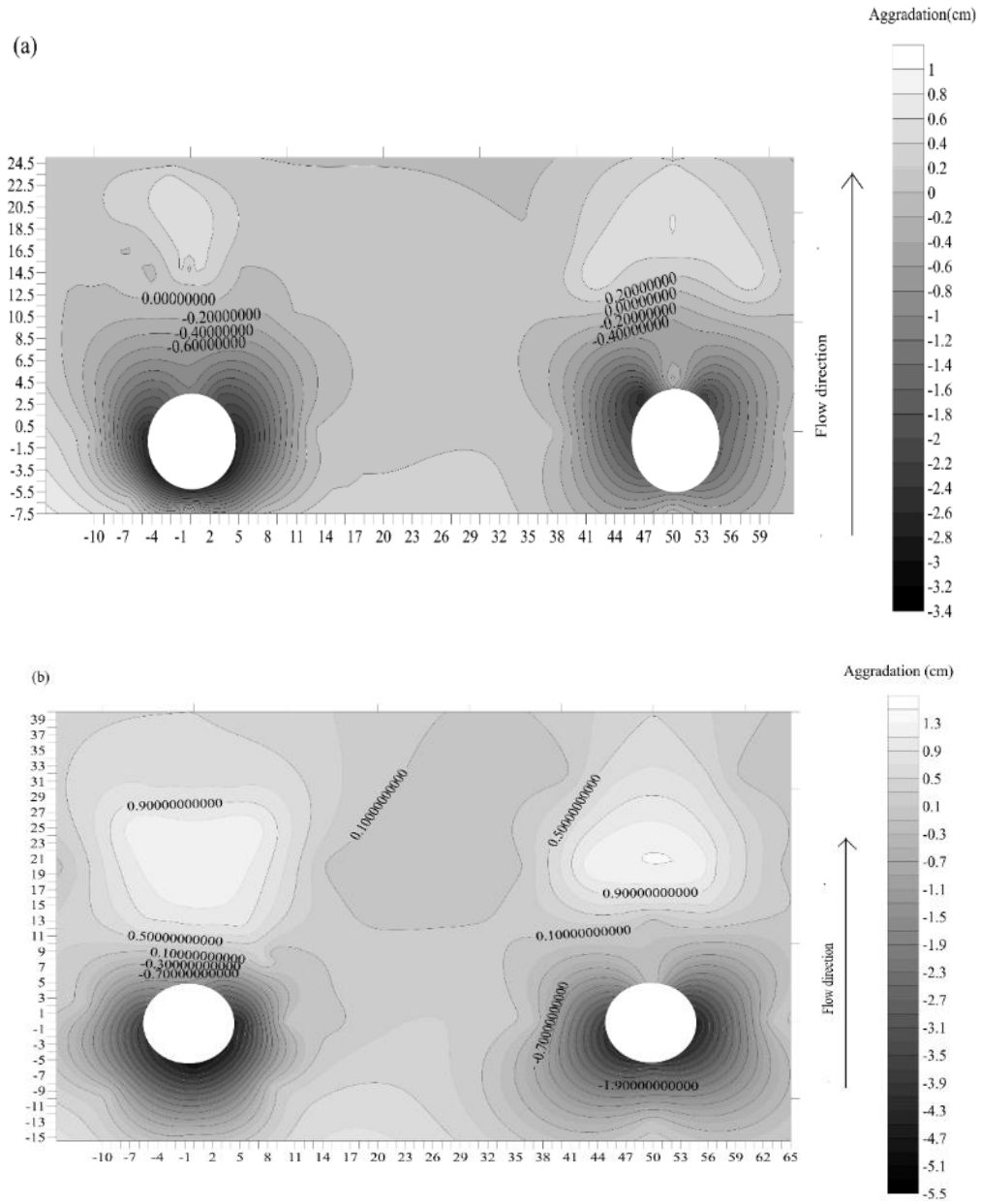

Figure 3–4: (a) Contours of scour holes and deposition mounds around the 9-cm-piers under open channel flow conditions (D_{50} = 0.50 mm) and (b) Contours of scour holes and deposition mounds around the 9-cm-piers under rough covered condition (D_{50} = 0.50 mm).

- **Effect of pier spacing distance on the scour patterns**

Figure 3-5 shows the ratio of the maximum scour depth to the depth of approaching flow (y_{max}/y_0, termed as relative *MSD*) against the ratio of pier spacing distance to pier diameter (*G/D*, termed as bridge pier spacing ratio) for D_{50} = 0.50 mm. In Figure 3-5, the Froude number ranges from 0.072 to 0.270 and *G/D* ranges from 3.54 to 7.33. In the current study, the Froude number in the first sand box was higher than that in the second sand box because of the longitudinal slope of the bed channel and the dissipation of momentum of the flow due to friction. In the first sand box, either the 9-cm-diameter piers or the 11-cm-diameter piers were placed; and in the second sand box, either the 6-cm-diameter piers or the 17-cm-diameter piers were placed. More experiments should have been done to place either the 17-cm piers or the 6-cm piers in the first sand box (under the same flow condition); and either the 9-cm-piers or the 11-cm piers in the first sand box (under the same flow condition). However, due to budget limitations and time constraints, those experimental runs have not been done. According to Figure 3-5, the relative *MSD* decreases with the increase in *G/D*. Also, for the same bridge pier spacing ratio (*G/D*) and for the same sediment, the relative *MSD* under open channel flow conditions is the lowest, and the relative *MSD* under the rough covered flow reaches the highest. Figure 3-6 shows the changes of the pier Reynold number (Re_b) with the pier spacing ratio (*G/D*) for D_{50} = 0.50 mm. The pier Reynolds number is defined as:

$$\mathrm{Re}_b = \frac{UD}{\nu} \qquad (3\text{-}1\text{-}1)$$

Where *U* is the average velocity of the approaching flow; *D* is the diameter of the bridge pier, and *v* is the kinematic viscosity. As shown in Figure 3-6, the pier Reynold number (Re_b) decreases with increases in *G/D*. Hopkins et al. (1980) stated that the strength of the horseshoe vortex system is a function of the pier Reynolds number (Re_b). Therefore, it can be concluded that the strength of

horseshoe vortices, which is a function of Re_b, decreases with the increase in the pier spacing ratio. Therefore, the smaller the pier size (D) and the larger the pier spacing (G), the weaker the horseshoe vortices around bridge piers, which will result in shallower scour depths around the bridge piers. According to Figure 3-6, under the same flow condition (velocity and flow depth), the lowest pier Reynolds number (Re_b) occurred under the open channel flow conditions, and the maximum pier Reynolds number (Re_b) occurred under rough covered flow condition. However, with an increase in the pier spacing ratio, the pier Reynolds number under rough covered flow conditions, gets closer to those of the smooth covered and open channel flow conditions, implying that the influence of ice cover on pier Reynolds number diminishes as the pier spacing distance increases.

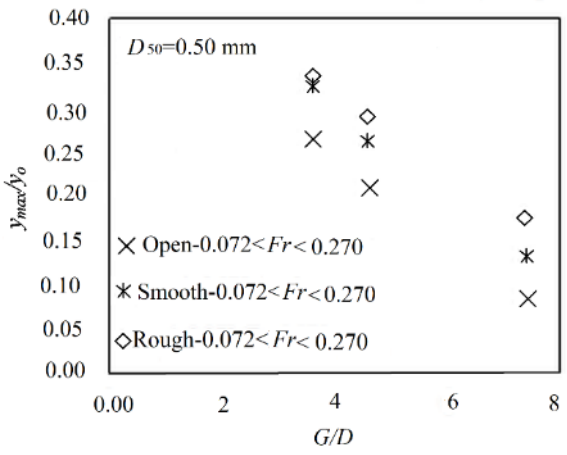

Figure 3–5: Relative MSD (y_{max}/y_0) against pier spacing (G/D) under open channel, smooth, and rough covered flow conditions (D_{50} = 0.50 mm).

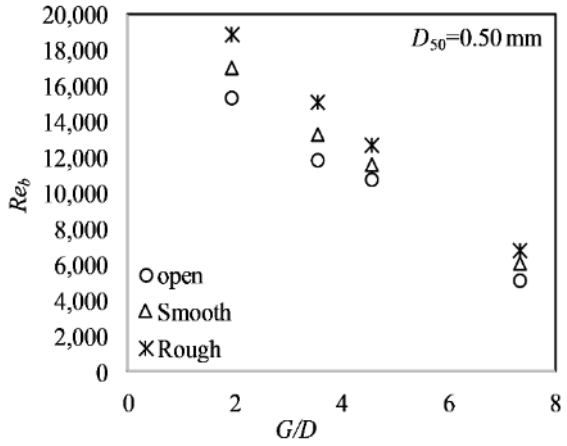

Figure 3–6: Variation of pier spacing (G/D) with respect to pier Reynolds number (Re_b).

- **Effects of flow Froude Number on scour depth**

Figure 3-7(a-c) shows the impacts of flow Froude number (Fr) on the relative MSD for D_{50} = 0.50 mm under open channel, smooth covered, and rough covered flow conditions, respectively. Overall, regardless of flow cover, the larger the flow Froude number, the greater the relative MSD. Under open channel flow conditions, both the 11-cm-piers and 9-cm-piers which are exposed to flows with higher Froude numbers have deeper scour holes (Figure 3-7a). For flow with lower Froude numbers,

the average depths of scour holes around the 17-cm-piers and 6-cm-piers are 0.14 and 0.09 cm, respectively. While for flow with higher Froude number, the average depths of scour holes around the 11-cm-piers and 9-cm-piers are 0.27 and 0.21 cm, respectively. Regarding the flow under smooth and rough covered conditions, similar trends as for open channel flow condition is seen between *MSD* and Froude number (Figure 3-7b, c). Regardless of the pier size, a deeper scour hole results under both smooth and rough covered flow conditions compared to that under open channel flow conditions which signifies the impact of flow cover on the scour pattern as well as on the characteristics of the flow field around the piers. Under nearly the same Froude number and bed sediment type, the largest scour depth occurs under rough covered flow conditions which indicates that the cover roughness plays an important role in the local scour around the bridge pier. Also, the impact of Froude number on each individual bridge pier under different cover conditions has been examined, as shown in Figure 3-7d. According to Figure 3-7d, the relative *MSD* for the 6-cm pier under rough covered flow conditions is greater than those under both smooth covered and open channel flow conditions. Besides, for flow with larger Froude numbers, the difference between the relative *MSD* under the rough covered flow conditions and those under both smooth covered and open channel flow conditions becomes more distinct, implying that the effect of the larger Froude number is more dominant under rough covered flow conditions. According to Figure 3-7e, the relative *MSD* around the 17-cm pier in the channel bed with the finest sediment is obviously larger than that with the coarsest sediment. Similarly, the impact of Froude number on relative *MSD* becomes more distinct for higher values of Froude number. Similar trends have been observed for local scour around other piers. According to Wu et al. (2014a), the dimensionless shear stress increases with the increase in Froude number. Therefore, for the same Froude number, the finer the sediment in the channel bed,

the lower the dimensionless shear stress is needed to initiate motion of the sediment. This is the reason that larger scour depths occur for flow with higher Froude numbers.

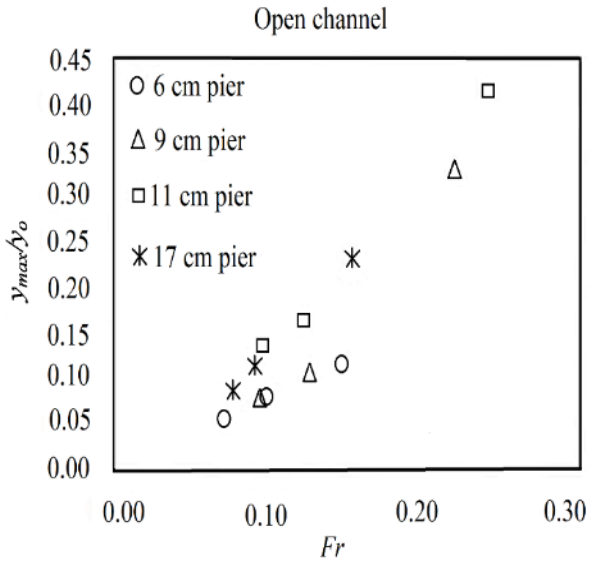

Figure 3–7a: Variation of the relative MSD (y_{max}/y_0) against flow Froude number (Fr) under open channel flow conditions (D_{50} = 0.50 mm);

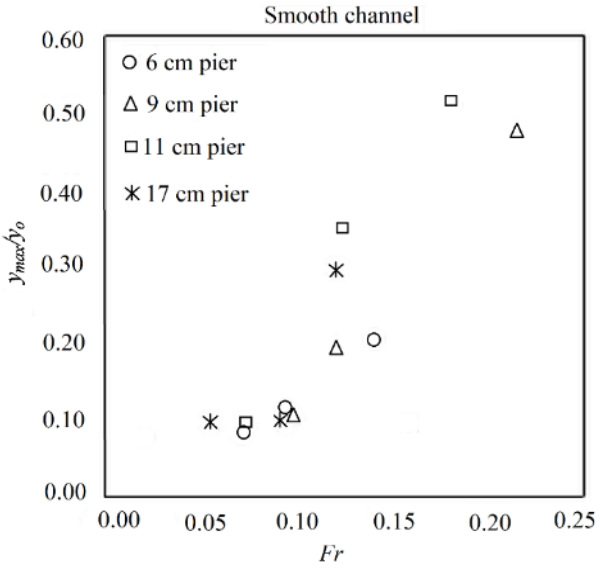

Figure 3–7b: Variation of the relative MSD (y_{max}/y_0) against flow Froude number (Fr) under smooth covered flow conditions (D_{50} = 0.50 mm);

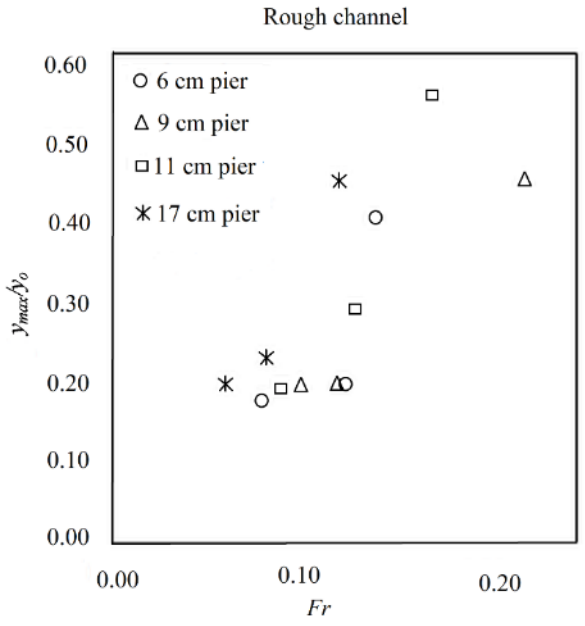

Figure 3–7c: Variation of the relative MSD (y_{max}/y_0) against Froude number (Fr) under rough covered flow conditions (D_{50} = 0.50 mm)

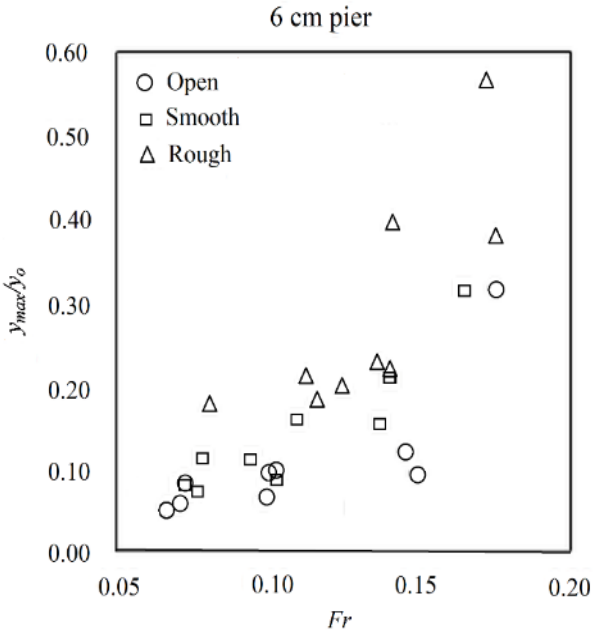

Figure 3–7d: Variation of the relative MSD (y_{max}/y_0) against Froude number (Fr) for the 6 cm-pier under different flow conditions;

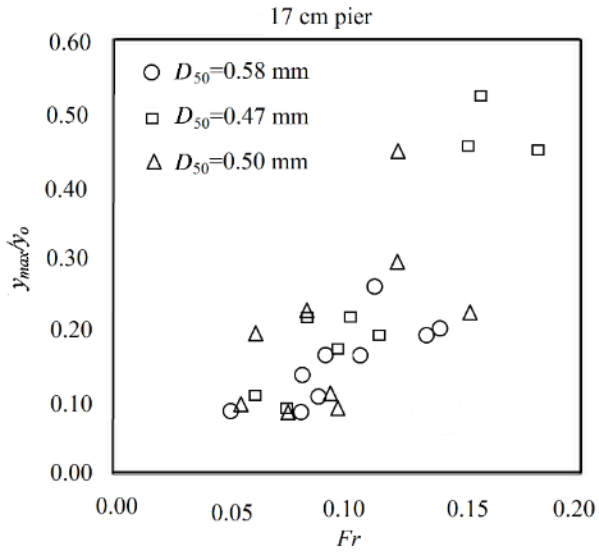

Figure 3–7e: Variation of the relative MSD (y_{max}/y_0) against Froude number (Fr) for the 17 cm-pier under different flow conditions for three D_{50} values

- **Effects of grain size of sediment on scour depth**

The grain size of bed material is another important variable affecting the depth of the scour hole. Figure 3-8(a-c) shows the impact of grain size of sediment on local scour depth around the 11-cm-pier under open channel, smooth covered, and rough covered flow conditions, respectively. According to Figure 3-8, under nearly the same flow condition (same flow Froude number), as the grain size of the bed material gets larger, the depth of the scour hole around the bridge piers gets smaller. Regardless of flow cover, the difference between depths of scour holes is obvious between the finest bed material (D_{50} = 0.47 mm) and the other coarser types of sediment. Experimental results showed that, for other piers with different diameters, similar relation between scour depth and grain size of bed material exists. A sediment particle starts to move when the shear stress acting on it is greater than the resistance force. The magnitude of shear stress required to move a particle is known as the critical shear stress (τ_{cr}). The greater the dimensionless shear stress, the greater the capacity for sediment transport (Wiberg & Smith, 1987). As the median grain size and density of the sediment

particles increase, the value of the dimensionless shear stress decreases. Therefore, the larger the median grain size, the lower the dimensionless shear stress for initiating motion for the sediment particles. Results of the current study showed that, for these three sands, the relative *MSD* increases with the increase in Froude number. Also, the increasing rate of the relative *MSD* is highest around bridge piers for a channel bed with the finest sediment particles. Thus, it can be concluded that, since dimensionless shear stress increases with Froude number, the relative *MSD* increases with dimensionless shear stress. Therefore, for the channel bed with the finest sediment, the dimensionless shear stress which represents the capacity for sediment transport is highest compared to those of other types of sediment.

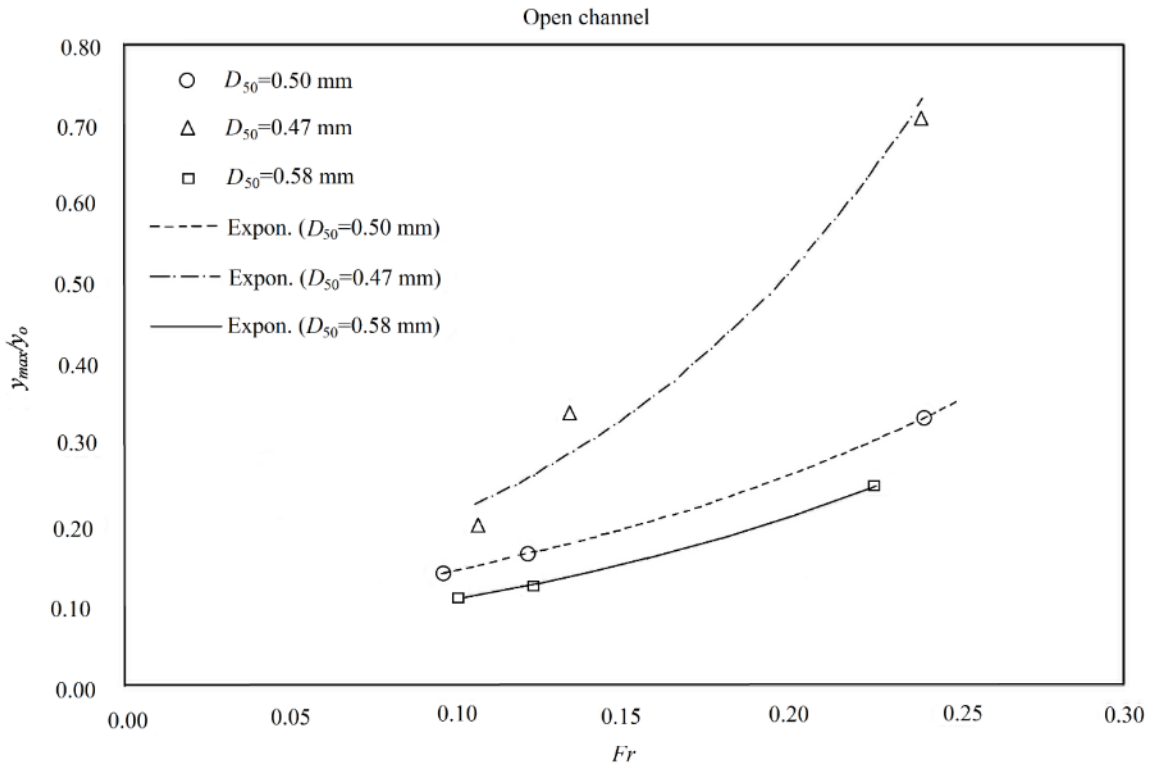

Figure 3–8a: The impact of sediment size on local scour around the 11-cm-pier under open channel flow conditions;

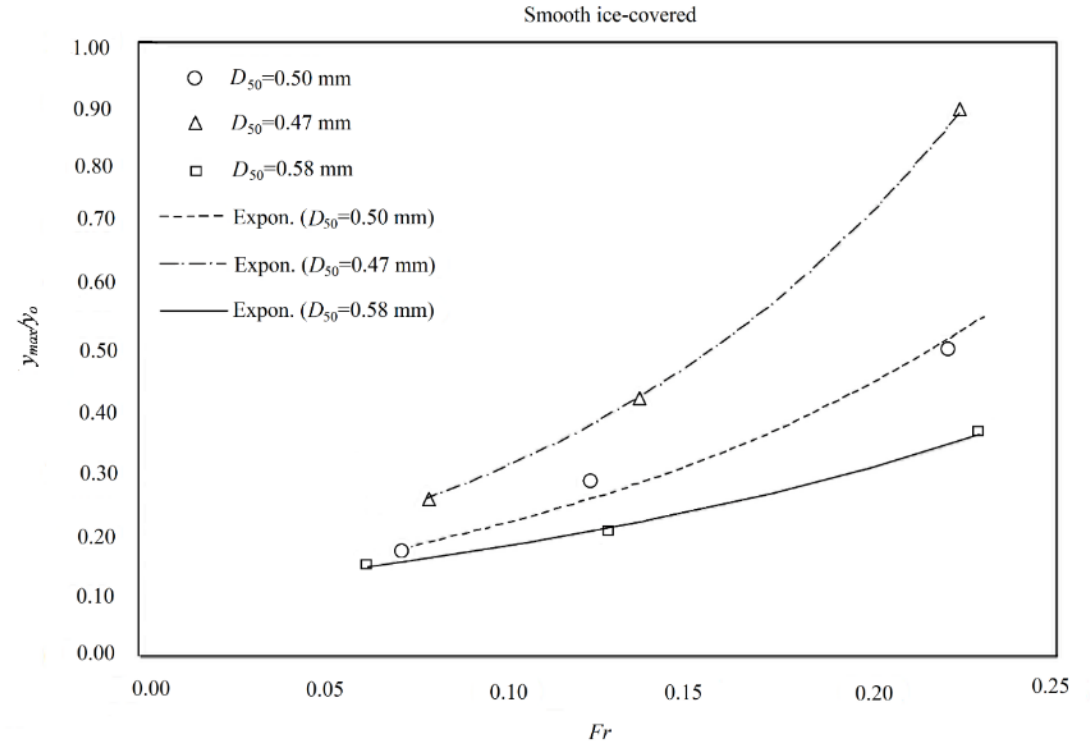

Figure 3–8b: The impact of sediment size on local scour around the 11-cm-pier under smooth covered flow conditions;

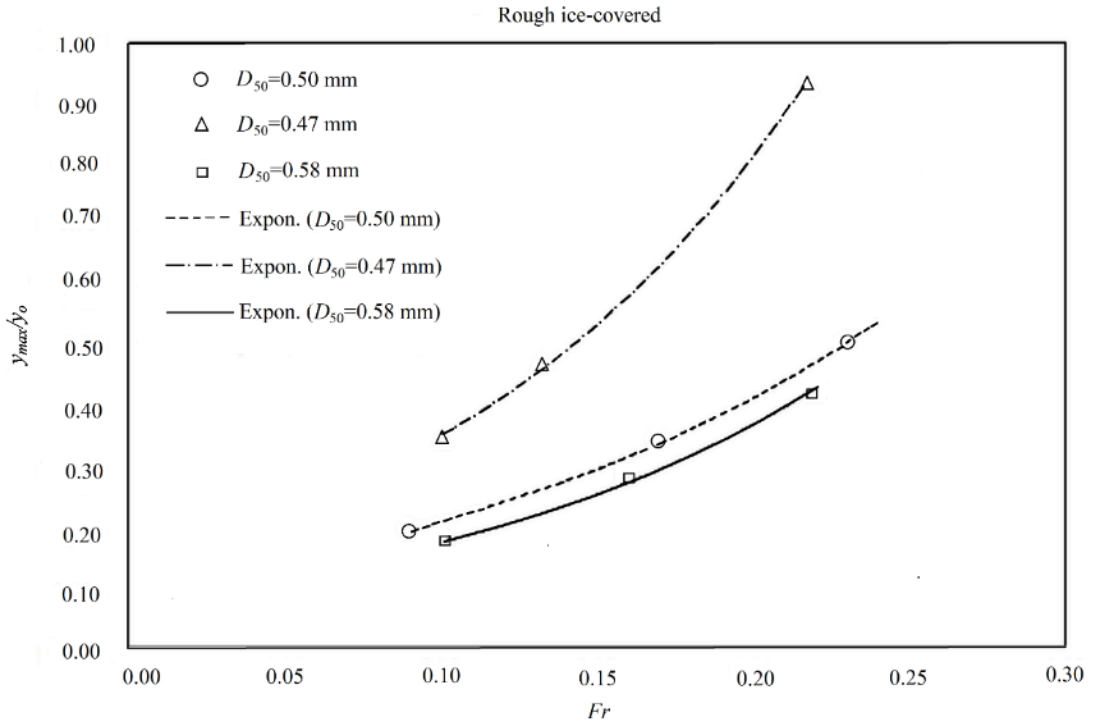

Figure 3–8c: The impact of sediment size on local scour around the 11-cm-pier under rough covered flow conditions.

- **Formula for determining the maximum depth of the scour hole**

Overall, the depth of scour holes around bridge piers under covered conditions depends on flow intensity, pier size, grain size of the bed material, spacing distance between side-by-side piers, and roughness of the channel bed and ice cover. The scour depth can be described by the following relation,

$$y_{max} = f(G, y_0, U, g, \rho_w, \rho_s, D, D_{50}, n_b, n_i) \tag{3-1-2}$$

Where, y_{max} is the maximum depth of scour hole; y_0 is the depth of approaching flow; g is the gravitational acceleration; ρ_s is the density of the sediment; ρ_w is the density of water and n_i and n_b are the roughness coefficients of the model ice cover and the channel bed, respectively. Using dimensional analysis, the relative *MSD* can be described as follows,

$$\frac{y_{max}}{y_0} = f\left(\frac{U}{\sqrt{gy_0}}, \frac{n_i}{n_b}, \frac{D_{50}}{y_0}, \frac{\rho_s}{\rho_w}, \frac{G}{D}\right) \tag{3-1-3}$$

The first dimensionless variable is the Froude number of the approaching flow. In the current study, the Froude number of the approaching flow is less than 1, implying the flow in the flume is subcritical flow. Considering the dominant parameters affecting the scouring process under both open channel and covered flow conditions, regression analysis of the relative *MSD* against each of the other dimensionless variables has been done, and the corresponding statistical analysis has been done. The general form of regression analysis is as follows,

$$\frac{y_{max}}{y_0} = A\,Y + B \tag{3-1-4}$$

Where, Ψ is the dimensionless variables from Eq. 3-1-3, and A and B are constants. The statistical analysis for each of the dimensionless variables includes calculations of the associated coefficient of determination (R^2), P-value, Theil's coefficient (α), the Mean Absolute Error (*MAE*), and the Root Mean Square Error (*RMSE*). The Theil's coefficient (α), Mean Absolute Error (*MAE*) and Root Mean Square Error (RMSE) are computed using the following equations, respectively:

$$\alpha = \frac{\sqrt{\frac{1}{n}\sum_{i=1}^{n}\left\{\left(y_{\max}\right)_C - \left(y_{\max}\right)_O\right\}^2}}{\sqrt{\frac{1}{n}\sum_{i=1}^{n}\left(y_{\max}\right)_C^2} + \sqrt{\frac{1}{n}\sum_{i=1}^{n}\left(y_{\max}\right)_O^2}} \tag{3-1-5}$$

$$MAE = \frac{1}{n}\sum_{i=1}^{n}|e_i| \tag{3-1-6}$$

$$RMSE = \sqrt{\sum_{i=1}^{n}\frac{e_i^2}{n}} \tag{3-1-7}$$

where α is Theil's coefficient (α = 0 for a model yielding a perfect forecast and α = 1 for an unsuccessful model); $(y_{max})_0$ is the maximum depth of the scour hole obtained from experimental runs, and $(y_{max})_C$ is the predicted maximum depth of the scour hole obtained using the developed formula; e_i is the error in predicting the maximum depth of scour hole for event *i* of the record using the developed formula; and n is number of datasets. Hereby, the values of α, *MAE* and *RMSE* obtained from Eqs. 3-1-5 to 3-1-7 are smaller, implying a more successful prediction of the maximum depth of the scour hole using the developed formulae. The *P*-value, which is a number between 0 and 1, gives the evidence against a null hypothesis. The smaller the *P*-value (typically ≤ 0.05), the stronger the evidence that the null hypothesis is not true (Storey & Tibshirani, 2003). Table 3-1 lists the results of the regression analysis between the relative *MSD* and other parameters as given in Eq. 3-1-3 under

open channel, smooth covered, and rough covered flow conditions. The second column of Table 3-1 gives values of slope of the regression line, which represent the rate of change in the relative *MSD* as the dimensionless variables change (such as *Fr*). A negative value of the regression slope indicates that the relative *MSD* decreases with respect to the associated variable (such as the pier spacing ratio, *G/D*), whilst a positive value indicates that the relative *MSD* increases with respect to the associated variable. The results show that the relative *MSD* increases with the Froude Number (*Fr*) which implies that the higher the Froude number (higher velocity and/or shallower water depth), the deeper the scour hole will be. The relative *MSD* against the roughness ratio (n_i/n_b) has a positive slope, indicating that as the model ice cover gets rougher, the depth of scour hole increases. The linear regression between the relative *MSD* and D_{50} or y_0 (Table 3-1) shows that as D_{50} or y_0 decreases, the relative *MSD* increases which means that as the sediment gets coarser of the flow gets deeper, the relative *MSD* decreases. However, according to Table 3-1 the relative *MSD* increases with increases in the ratio of D_{50}/y_0. The regression coefficient between the relative *MSD* and the specific gravity of sediment (ρ_s/ρ_w) indicates that sediment having a higher density ($D_{50} = 0.47$ mm) is expected to have a deeper scour hole. In terms of the bridge pier spacing distance, since it was not possible to examine a variety of pier spacings, the pier spacing ratio is not as influential as might be was expected. However, the negative regression coefficient between the relative *MSD* and the pier spacing (*G/D*) indicates that the relative *MSD* increases as *G/D* decreases. In other words, as the piers get closer to each other and the pier diameter gets larger, the relative *MSD* increases correspondingly. Finally, by considering the (R^2), *P*-value, *MAE*, and *RMSE* of the regression equations using the various dimensionless variables as listed in Table 3-1, the dimensionless groups which have a strong relation with the relative *MSD* are chosen for further analysis, and can be expressed as follows:

$$\frac{y_{max}}{y_0} = f\left(\frac{u}{\sqrt{gy_0}}, \frac{n_i}{n_b}, \frac{D_{50}}{y_0}, \frac{G}{D}\right) \quad (3\text{-}1\text{-}8)$$

Eq. 3-1-8 implies that the relative *MSD* of scour holes around the side-by-side bridge piers primarily depends on the Froude number of the approaching flow, the grain size of sediment, the spacing distance between piers, the bridge pier diameter and the roughness coefficient of the channel bed and the model ice cover. As shown in Figure 3-9, although the data points are scattered, under the condition of nearly the same flow Froude number and same bed material (i.e., D_{50} = 0.47 mm), the relative *MSD* around a bridge pier under rough covered flow conditions is maximum compared to those under both smooth covered and open channel flow conditions.

Table 3-1: The values of the intercept, R^2, P-value, α, MAE, and RMSE of the dimensionless parameters with respect to Eq. 3-1-3

	Coefficients	Intercept	*R* Square	*P*-value	*α*	*MAE*	*RMSE*
Fr	3.201	-0.141	0.651	5.3E-26	0.167	0.077	0.103
n_i/n_b	0.118	0.201	0.45	0.0061	0.311	0.139	0.182
D_{50}/y_0	99.259	-0.061	0.416	2.9E-14	0.236	0.108	0.143
ρ_s/ρ_w	0.421	-0.415	0.074	0.004	0.309	0.136	0.181
G/D	-0.011	0.314	0.017	0.0184	0.324	0.141	0.187
D_{50}	-1198.98	0.878672	0.08772	0.001856	0.295	0.135	0.180
y_0	-0.194	0.23	0.37	1.63E-12	0.229	0.107	0.139

The experiments showed that, similar results were obtained for other sediment grain sizes. Figure 3-10 (a-c) shows the dependence of the relative *MSD* on flow Froude number (*Fr*) and grain size of sediment (D_{50}) under different boundary conditions (open channel, smooth covered, and rough covered flow conditions). According to Figure 3-10, under nearly the same Froude number (*Fr*), regardless of flow cover, the relative *MSD* is deepest around piers in the finest sand bed (D_{50} = 0.47

mm). According to Figure 3-9 and Figure 3-10, the deepest scour hole around a bridge pier occurs in the finest sand bed under rough covered flow conditions. One can observe that results for sediment sizes 0.47 and 0.50 mm seem close. Since the median grain size of sediment of 0.47 mm is very close to that of 0.50 mm, this small difference resulted in a very close critical shear stress which defines the threshold for sediment transport.

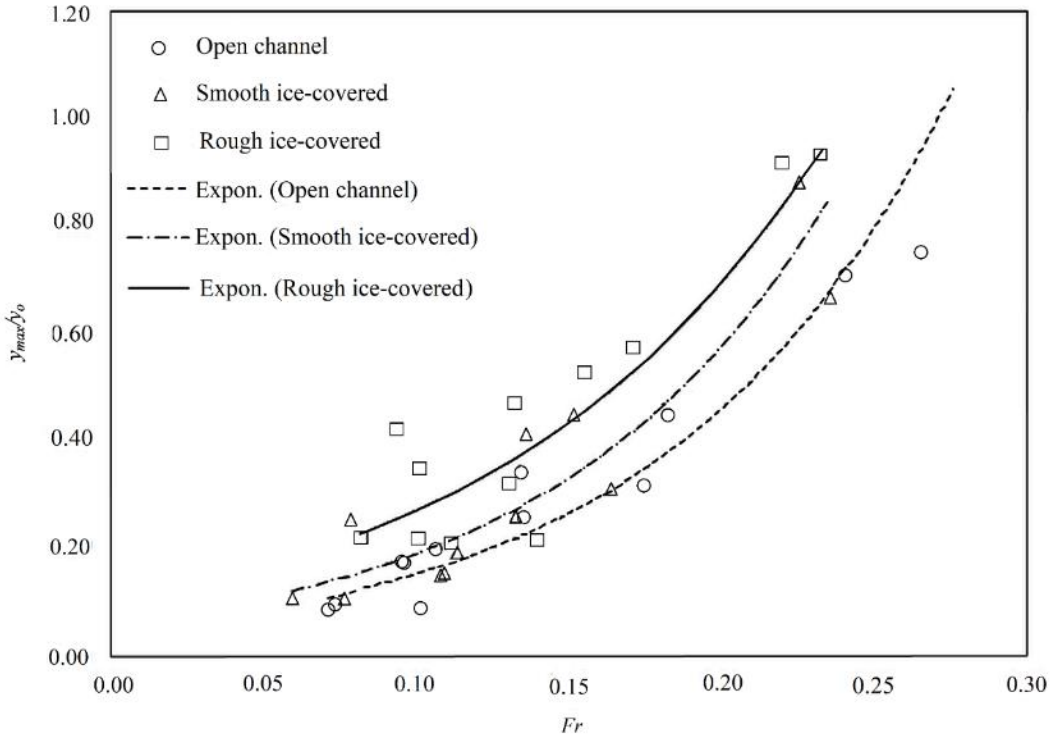

Figure 3–9: Dependence of the relative MSD (y_{max}/y_0) on flow Froude number (Fr) under covered conditions compared to that under open channel flow conditions (D_{50} = 0.47 mm)

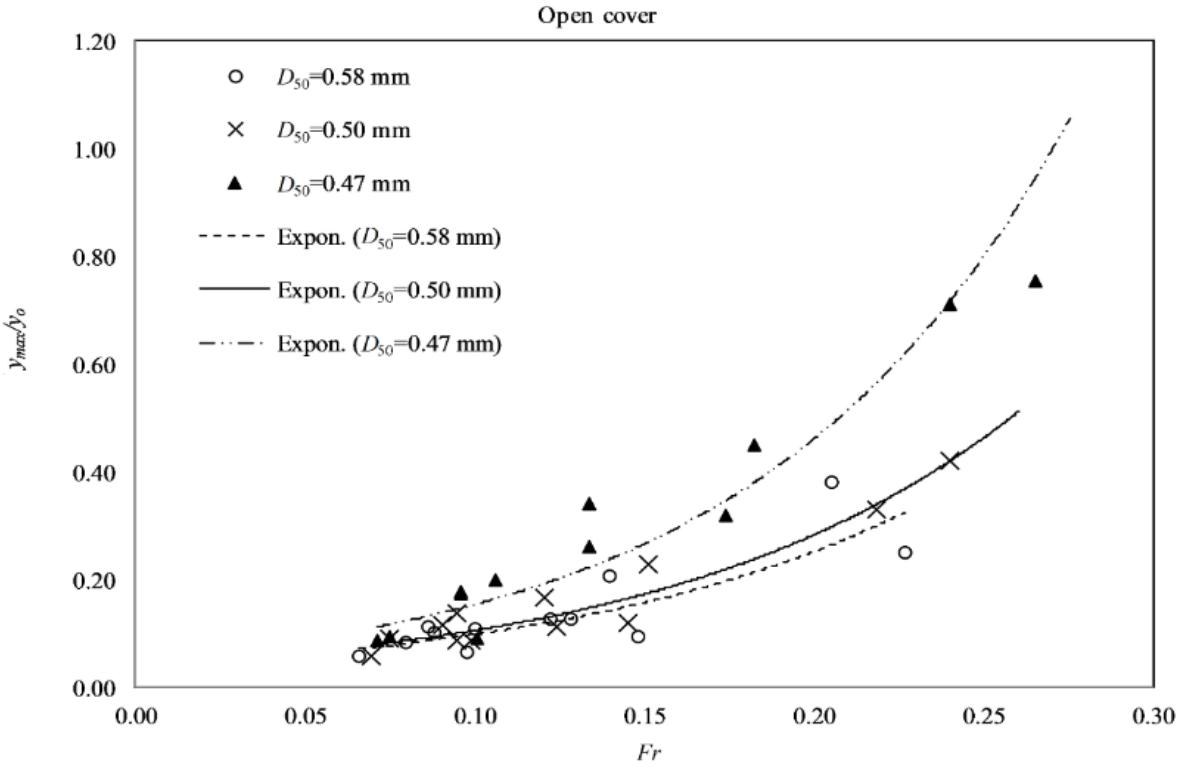

Figure 3–10a: Dependence of the relative MSD (y_{max}/y_0) on flow Froude number (Fr) and grain size of sediment (D_{50}) under open channel flow condition

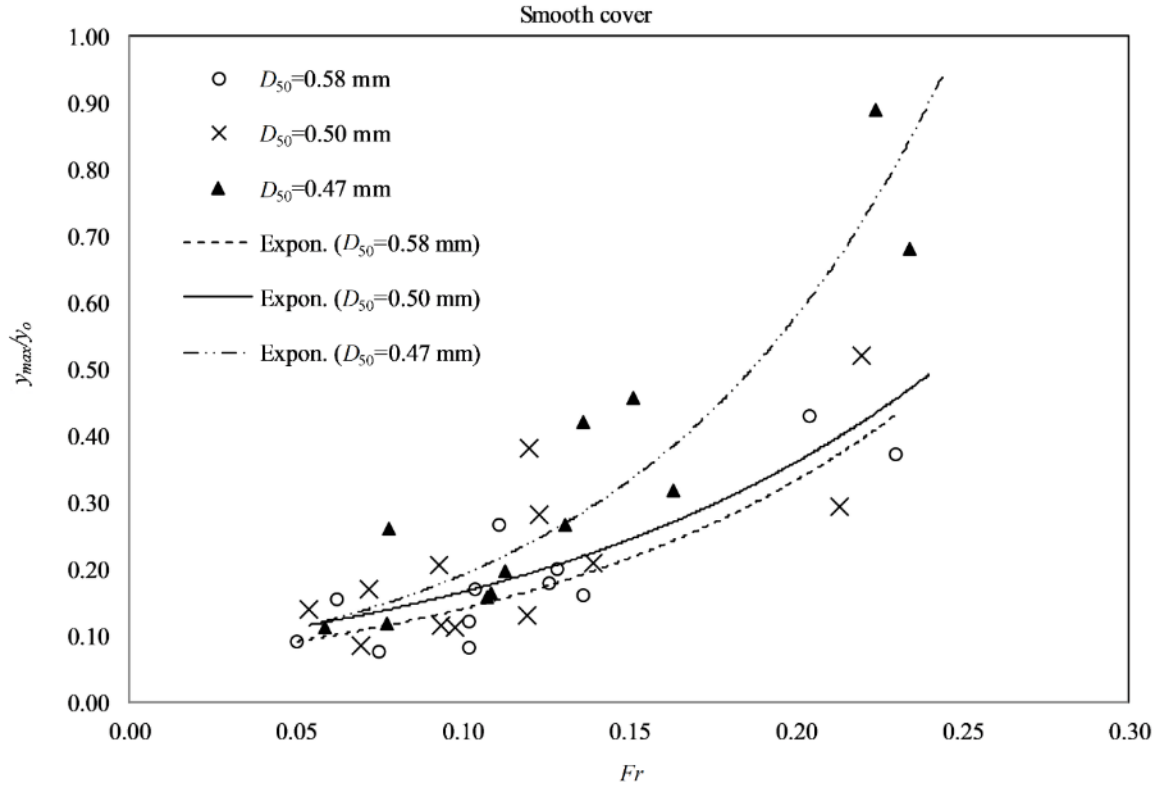

Figure 3–10b: Dependence of the relative MSD (y_{max}/y_0) on flow Froude number (Fr) and grain size of sediment (D_{50}) under smooth covered flow conditions

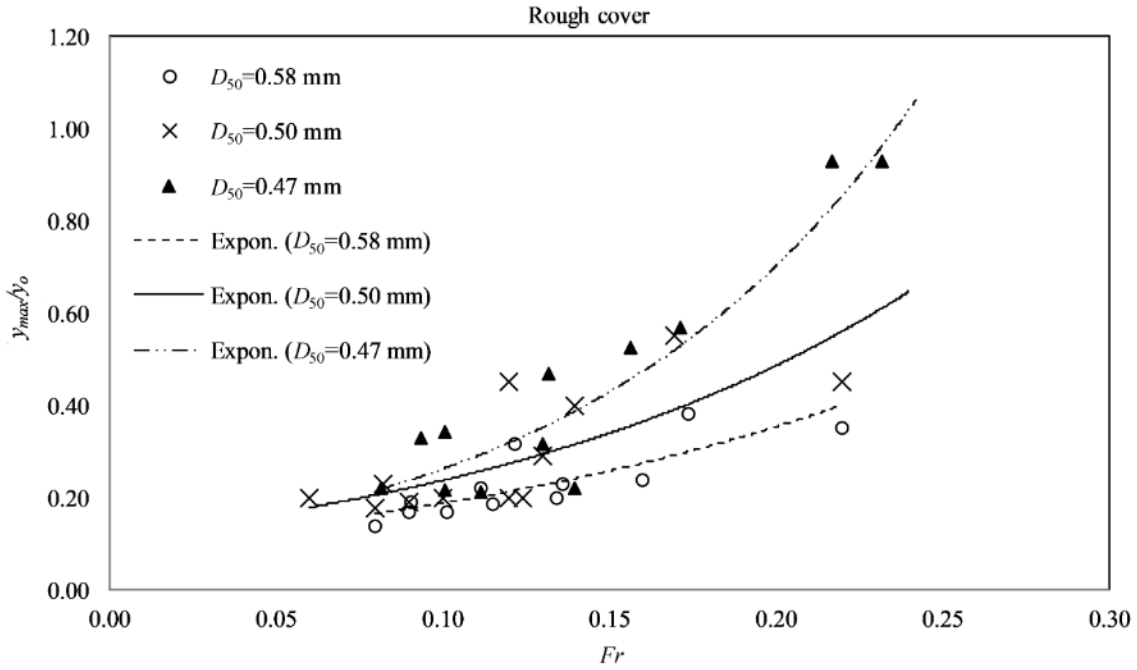

Figure 3–10c: Dependence of the relative MSD (y_{max}/y_0) on flow Froude number (Fr) and grain size of sediment (D_{50}) under rough covered flow conditions

To develop suitable equations for determining the relative *MSD* around the side-by-side piers under covered flows, the impact of the roughness of the model ice cover must be examined. As mentioned earlier, the presence of ice cover changes the velocity field and turbulence characteristics. For concrete with trowel finish, the roughness coefficient is suggested by Mays (1999) to be 0.013. Therefore, due to a relatively smooth concrete-like surface of the Styrofoam panel, the roughness of the modeled smooth ice-cover is suggested to be 0.013. In terms of the rough ice-covered flow condition, Li (2012) reviewed several methods for calculating the Manning's coefficient for ice cover, the following equation can be used depending on the size of the small cubes:

$$\frac{n_i}{k_S^{1/6}} = \frac{(8g)^{-1/2}(R/K_S)^{1/6}}{0.867\ln(12R/K_S)} \qquad (3\text{-}1\text{-}9)$$

Where, K_s is the average roughness height of the ice cover underside and R is the hydraulic radius. By using Eq. 3-1-9, a Manning's coefficient of 0.021 was estimated as the rough ice cover roughness

coefficient. This value also agrees with findings of Carey (1966), Hains et al. Zabilansky (2004), and Wu et al. (2014b). Since the D_{50} values of the three sands used in this study are known, the simple equation proposed by Hager (1999) is used for determining the roughness coefficient of the channel bed:

$$n_b = 0.039 D_{50}^{1/6} \tag{3-1-10}$$

The Hager (1999) equation is the revised form of the Strickler (1923) equation for calculating Manning's roughness coefficient for streambeds composed of cobbles and small boulders: $n=0.039D_{50}^{1/6}$. Therefore, the roughness coefficient of sand bed, n_b, is estimated as 0.0109 for D_{50} = 0.47 mm, 0.0110 for D_{50} = 0.050 mm, and 0.0113 for D_{50} = 0.58 mm. Eventually, Eqs. 3-1-11 and 3-1-12 are proposed for calculating the relative *MSD* under covered flow and open channel flow conditions, respectively:

$$\frac{y_{max}}{y_0} = 5.96\left(\frac{D_{50}}{y_0}\right)^{-0.070}\left(\frac{G}{D}\right)^{-0.256}\left(\frac{n_i}{n_b}\right)^{0.546}(Fr)^{1.677} \quad \text{with } R^2 = 0.90 \tag{3-1-11}$$

$$\frac{y_{max}}{y_0} = 1.45\left(\frac{D_{50}}{y_0}\right)^{-0.314}\left(\frac{G}{D}\right)^{-0.372}(Fr)^{1.739} \quad \text{with } R^2 = 0.92 \tag{3-1-12}$$

Figures 3-11 and 3-12 show comparisons of the calculated relative *MSD* to those of observed under open channel flow and covered flow conditions, respectively. Of note, Eq. 3-1-11 and Figure 3-12 are results for both smooth covered and rough covered flow conditions. From Eqs. 3-1-11 and 3-1-12, it is obvious that the Froude number of the approaching flow is the most influential factor since its index is much higher than those for the other variables. This means that as the Froude number increases, the relative *MSD* around bridge piers increases accordingly. In other words, regardless of

the flow cover and the size of sediment, the higher the flow velocity and the shallower the flow depth, the greater the relative *MSD* will be. As Sui et al. (2010) indicated, the formation of a stable ice cover effectively doubles the wetted perimeter compared to open channel conditions, thus, altering the hydraulics of an open channel by imposing an extra boundary to the flow, causing the velocity profile to shift towards the smoother boundary (channel bed) and adding to the flow resistance. This significant change in the velocity profile, increases the effect of the Froude number under ice-covered flow conditions compared to that for open channel flow conditions. Therefore, under nearly the same Froude number, the maximum scour depth under the rough covered flow condition is greater than that under the smooth covered condition. The turbulent horseshoe vortex and roughness of flow cover are related to each other. Therefore, the positive index of the roughness ratio implies that as the model ice cover gets rougher, the turbulent horseshoe vortex around the bridge piers gets stronger which will eventually lead to a larger scour depth. The negative index for *G/D* implies that as the space between the piers decreases, the maximum scour depth increases which is in good agreement with results of Hannah (1978) and Ataie-Ashtiani and Beheshti (2006).

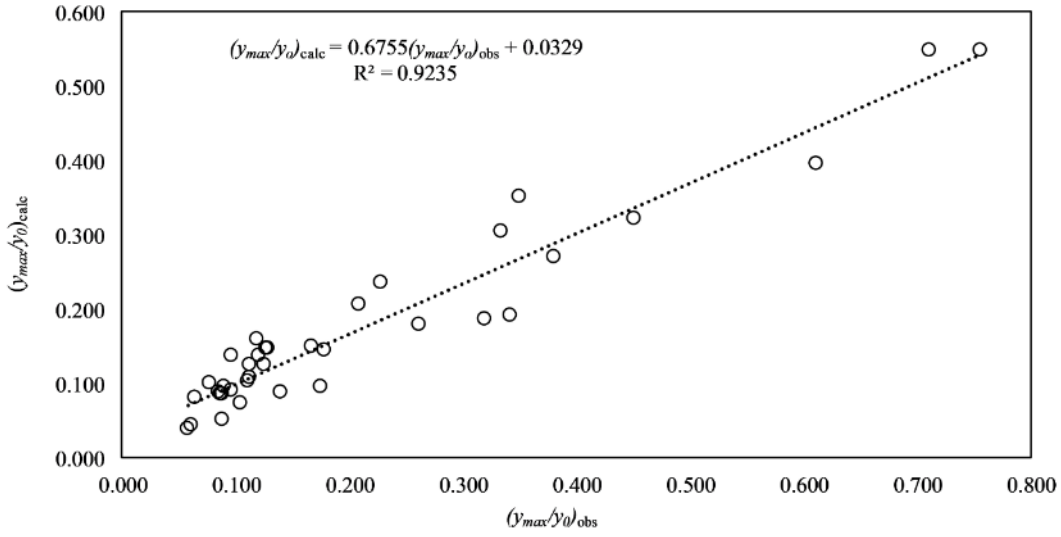

Figure 3–11: Comparison of calculated relative MSD (y_{max}/y_0) to those observed under open channel flow conditions.

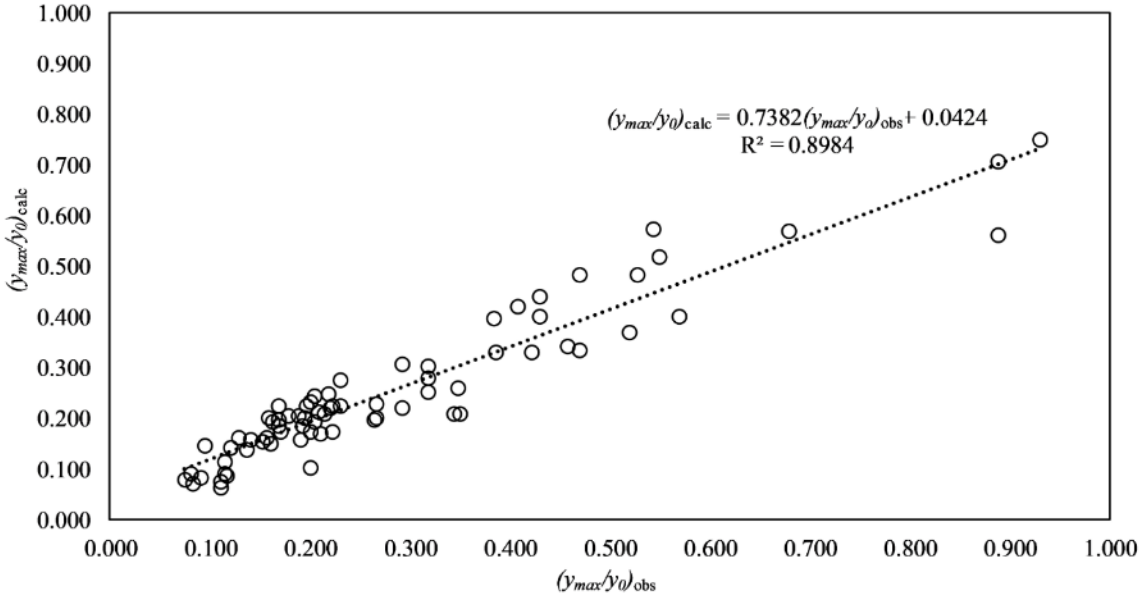

Figure 3–12: Comparison of calculated maximum scour depth (y_{max}/y_0) to those observed under covered flow conditions.

- **Sensitivity analysis:**

In order to see the rate of change of relative MSD to each of the parameters in Eq. 3-1-11, sensitivity analysis has been done. In this regard, the following graph has been obtained by keeping a particular parameter changing from -20% to +20% and keeping the other parameters constant. According to Fig. 3-13, the relative MSD is the most sensible to Fr number as it shows the highest Mean value of Error. According to Fig. 3-13, if Froude number decreases up to 20 percent while the other parameters are kept constant, the relative MSD would decrease up to -31 percent which is very significant. The next parameter which relative MSD is most sensible to is the roughness coefficient. For instance, if 20 percent is added to the roughness of the ice surface the relative MSD would increase up to 10.75 percent. This result states the importance of ice cover roughness coefficient on the rate of change relative MSD. The bridge pier spacing (G/D) is the next sensible parameter. For the present study, if bridge pier spacing increases up to 20 percent, the relative MSD decreases up to 4.3 percent. The

ratio of D_{50}/y_o shows the least amount of sensitivity to the relative MSD. According to Fig. 3-13, if D_{50}/y_o increases up to 20 percent, the relative MSD decrease just up to 1 percent.

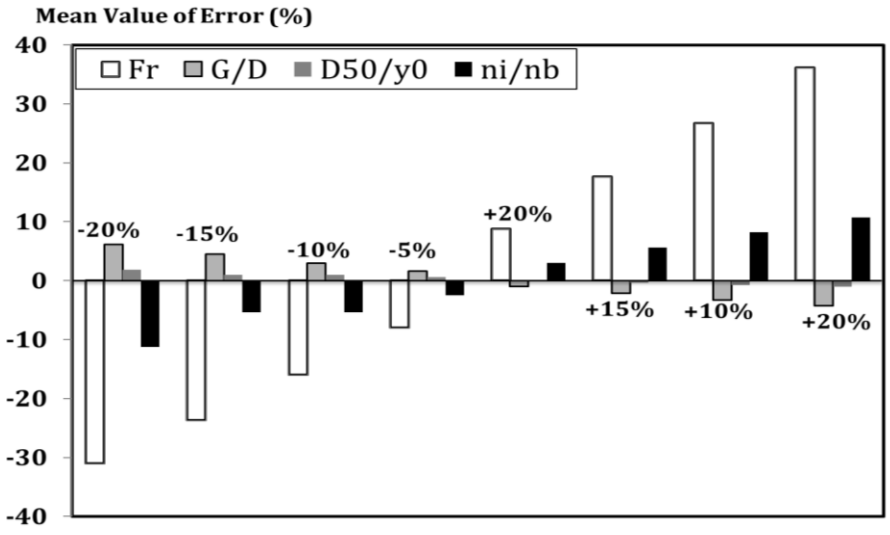

Figure 3–13: Sensitivity analysis of dimensionless parameters of Eq. 3-1-11

3.1.3. Conclusions

In the current study, 108 experiments were done in a large-scale flume with non-uniform sediment to investigate the local scour process around four pairs of side-by-side cylindrical bridge piers under open channel, smooth covered, and rough covered flow conditions. The following conclusions can be drawn from the current study.

1) The pier Reynolds number (Re_b) decreases with the increase in the pier spacing ratio (G/D), which implies that the strength of the horseshoe vortices decreases as the spacing distance between the side-by-side piers increases. The results showed that, under the same flow condition (velocity and flow depth), the lowest pier Reynolds Number (Re_b) occurred under open channel flow conditions, and the highest pier Reynolds Number (Re_b) occurred under rough covered flow conditions. Further, it was observed that the influence of ice cover on pier Reynolds Number fades away as the pier spacing distance increases regardless of flow cover. Also, for the same bridge pier spacing ratio (G/D) and

for the same sediment, the relative *MSD* under open channel flow conditions is the lowest and reaches the maximum under the rough covered flow conditions. This implies that the impact of the pier spacing ratio under the rough ice-covered flow condition is clearly intensified compared to those under both open channel and smooth covered flow conditions. In other words, the smaller the pier size (D) and the larger the pier spacing (G), the weaker the horseshoe vortices around the side-by-side bridge piers.

2) Under the same flow conditions, the effect of flow Froude number on the scour process is stronger than that of pier size. Regardless of ice cover and pier size, the maximum scour depth increases with flow Froude number, especially for finer sand beds. In other words, the local scour depth around bridge piers for a coarse sand bed is less than that for a finer sand bed. The results of this experimental study allow the impacts of ice cover, flow Froude number, and pier spacing distance on local scour around bridge piers to be prioritized. Overall, one can say that the deepest scour hole occurs around closely spaced large side-by-side piers under rough covered flow conditions which have higher Froude numbers. The results also indicate that, regardless of the roughness of the model ice cover and the grain size of sediment, the maximum scour depths always occurred at the upstream front face of the bridge piers. Also, the amount of sediment transported to the downstream side of the bridge pier to form the deposition mound is greatest under rough covered flow conditions. The results indicate that the impact of pier spacing on scour depth under covered flow conditions is similar to that under open channel conditions, however, the scouring process under covered flow conditions is more intense. It was found that the most extreme scour depth around side-by-side bridge piers occurs under rough covered flow conditions with the higher Froude number and smaller bridge pier spacing.

3) Using data collected from the current experiments, empirical equations for predicting the relative *MSD* (y_{max}/y_0) under both channel flow and covered flow conditions have been developed. Among

all the dimensionless parameters, flow Froude number was the most influential factor which had a positive relation with the relative *MSD* (y_{max}/y_0). The impact of the Froude number is most distinct under rough covered flow conditions with smaller pier spacing ratios. Namely, for nearly the same Froude number, the largest scour depth occurs under rough covered flow conditions with smaller pier spacing. This means that under rough covered flow conditions, the maximum velocity is located closer to channel bed. Thus, the shear stress increases, and the horseshoe vortexes are intensified due to the smaller pier spacing ratio. Both the roughness of the ice cover and the pier spacing ratio are two major factors leading to the most critical local scour pattern.

4) Sensitivity analysis was done for Eq. 3-1-11 and it was concluded that the relative *MSD* is most sensible to *Fr,* n_i/n_b*, G/D and* D_{50}/y_0, respectively.

- **Notation:**

A: Constant of the linear regression equation

B: Constant of the linear regression equation

D: Pier width (m)

D_{50}: Median particle diameter (mm)

Fr: Flow Froude number

g: Acceleration due to gravity (m/s^2)

G: Bridge spacing (m)

K_s: Average roughness height (m)

MSD: Relative maximum scour depth defined as y_{max}/y_0

MAE: Mean Absolute Error

n: and the number of datasets

n_i: Ice cover roughness

n_b: Channel bed roughness

R: Hydraulic radius (m)

R^2: Coefficient of determination

Re_b: Pier Reynold number

$RMSE$: Root Mean Square Error

U: Average approach velocity (m/s)

U_c= Critical velocity for incipient motion of the particle size D_{50}

W: channel width (m)

y_{max}: Maximum scour depth (m)

y_0: Approach flow depth (m)

α: Theil's coefficient

ρ_s: Density of the sediment (kg/m^3)

ρ_w: Density of water (kg/m^3)

ψ: Dimensionless variable

e_i: Error in the predicted scour depth

v: The kinematic viscosity (m^2/s)

τ_{cr}: Critical shear stress (Pa)

θ: Temperature (degrees)

3.1.4. Reference

Ackermann, N. L., Shen, H. T., & Olsson, P. (2002). Local scour around circular piers under ice covers". *Proceedings, International Conference. 16th IAHR International Symposium on Ice*, IAHR, Dunedin, New Zealand.

Ataie-Ashtiani, B., & Beheshti, A. A. (2006). Experimental investigation of clear-water local scour at pile groups. *Journal of Hydraulic Engineering*, *132*(10), 1100-1104.

Breusers, H.N.C., & Raudkivi, A.J. (1991). Scouring, *Hydraulic Structures Design Manual*, No. 2, I.A.H.R., Balkema, 143pp.

Briaud, J. L., Gardoni, P., & Yao, C. (2006). Bridge scour. *Geotechnical News*, *24*(3), September, BiTech Publishers Ltd.

Carey, K. (1966). Observed configuration and computed roughness of the underside of river ice, St Croix River. Wisconsin. Professional Paper 550-B.Ph.D. U.S. Geological Survey: B192–B198.

Cea, L., Puertas, J., & Pena, L. (2007). Velocity measurements on highly turbulent free surface flow using ADV. *Experiments in fluids*, *42*(3), 333-348.

Chiew, Y. M. (1984). Local scour at bridge piers (Ph.D. dissertation), Department of Civil Engineering, University of Auckland, New Zealand.

Ettema, R. (1980). *Scour at bridge piers*, Report No. 216, Department of Civil Engineering, University of Auckland, New Zealand.

Ettema, R., Melville, B. W., & Constantinescu, G. (2011). *Evaluation of bridge scour research: Pier scour processes and predictions*. Washington, DC: Transportation Research Board of the National Academies.

Hafez, Y. I. (2016). Mathematical modeling of local scour at slender and wide bridge piers. *Journal of Fluids, 2016*, 4035253.

Hager, W. (1999). *Wastewater Hydraulics: Theory and Practice*. Springer: Berlin, New York.

Hains, D., Zabilansky, L.J., & Weisman, R.N. (2004). An experimental study of ice effects on scour at bridge piers. *Cold Regions Engineering and Construction Conference and Expo*, 16–19 May 2004, Edmonton, Alberta, Canada.

Hannah, C. R. (1978). Scour at pile groups. *Research Report No. 28-3*, Civil Engineering Department, University of Canterbury, Christchurch, New Zealand.

Heller, V. (2011). Scale effects in physical hydraulic engineering models." *Journal of Hydraulic Research, 49*(3), 293-306.

Hirshfield, F. (2015). The impact of ice conditions on local scour around bridge piers, Ph.D. dissertation, Environmental Engineering Program, University of Northern British Colombia, Prince George, B.C., Canada

Hopkins, G. R., Vance, R. W., & Kasraie, B. (1980). *Scour around bridge piers*, FHWA-RD-79-103 U.S. Department of Transportation, Federal Highway Administration, Offices of Research and Development, Environmental Division.

Li, S. S. (2012). Estimates of the Manning's coefficient for ice-covered rivers. *Proceedings of the Institution of Civil Engineers-Water Management, 165*(9), 495-505.

Mays, L. W. (Ed.). (1999). *Hydraulic design handbook*. New York: McGraw-Hill Professional Publishing.

Melville, B. W. (1997). Pier and abutment scour: Integrated approach. *Journal of Hydraulic Engineering, 123*(2), 125-136.

Melville, B. W. & Sutherland, A. J. (1988). Design method for local scour at bridge piers. *Journal of Hydraulic Engineering, 114*(10), 1210-1226.

Melville, B. W. & Coleman, S. E. (2000). Bridge scour. Highlands Ranch, Colo, U.S.: Water Resources Publications.

Richardson, E. V., Simons, D. B. & Lagasse, P. F. (2001). *River engineering for highway encroachments-Highways in the river environment. Federal Highway Administration, Hydraulic Series No. 6*, Washington, DC.

Sheppard, D. M., Odeh, M., & Glasser, T. (2004). Large scale clear-water local pier scour experiments. *Journal of Hydraulic Engineering*, *130*(10), 957-963.

Sheppard, D. M., Melville, B. & Demir, H. (2013). Evaluation of existing equations for local scour at bridge piers. *Journal of Hydraulic Engineering*, *140*(1), 14-23.

Storey, J. D. & Tibshirani, R. (2003). Statistical significance for genomewide studies. *Proceedings of the National Academy of Sciences, 100*(16), 9440-9445.

Strickler, A. (1923). *Beiträge zur Frage der Geschwindigkeitsformel und der Rauhigkeitszahlen für Ströme, Kanäle und geschlossene Leitungen: mit... Tab*. Im Selbstverlag.

Sui, J., Faruque, M.A.A., & Balachandar, R. (2008). Influence of channel width and tailwater depth on local scour caused by square jets. *Journal of Hydro-Environment Research*, 2, 39 - 45.

Sui, J., Faruque, M.A.A. & Balachandar, R. (2009). Local scour caused by submerged square jets under ice cover. *Journal of Hydraulic Engineering, 135* (4), 316-319.

Sui, J., Wang, J., He, Y. & Krol, F. (2010). Velocity profiles and incipient motion of frazil particles under ice cover. *International Journal of Sediment Research, 25*(1), 39-51.

Yanmaz, A. M. (2002). Dynamic reliability in bridge pier scouring. *Turkish Journal of Engineering and Environmental Sciences, 26*(4), 367-376.

Yang, Q. (2005). *Numerical investigations of scale effects on local scour around a bridge pier. (Ph.D. dissertation)*, Department of Civil and Environmental Engineering, Florida State University, Tallahassee, FL, U.S.

Wang, J., Sui, J. & Karney, B. (2008). Incipient motion of non-cohesive sediment under ice cover–an experimental study*". Journal of Hydrodynamics, 20*(1), 117-124.

Wardhana, K., & Hadipriono, F. C. (2003). Analysis of recent bridge failures in the United States. *Journal of performance of constructed facilities, 17*(3), 144-150.

Wiberg, P. L., & Smith, J. D. (1987). Calculations of the critical shear stress for motion of uniform and heterogeneous sediments. *Water Resources Research*, *23*(8), 1471-1480

Williams, P., Balachandar, R., & Bolisetti, T. (2013). *Evaluation of local bridge pier scour depth estimation methods.* Proceedings., 24th Canadian Congress of Applied Mechanics (CANCAM), University of Saskatchewan, Saskatoon, Canada.

Wu, P., Balachandar, R. & Sui, J. (2015a). Local scour around bridge piers under ice-covered conditions. *Journal of Hydraulic Engineering, 142*(1), 04015038.

Wu, P., Hirshfield, F., & Sui, J. Y. (2015b). Local scour around bridge abutments under ice covered condition–an experimental study. *International Journal of Sediment Research*, *30*(1), 39-47.

Wu, P., Hirshfield, F. & Sui, J. (2014a). Armor layer analysis of local scour around bridge abutment under ice covered condition, *River Research and Applications*, *31*(6), 736-746.

Wu, P., Hirshfield, F. Sui, J., Wang, J., & Chen, P. P. (2014b). Impacts of ice cover on local scour around semi-circular bridge abutment. *Journal of Hydrodynamics, 26*(1), 10-18.

Zabilansky, L. J., & K. D. White, (2005). Ice cover effects on scour in narrow rivers. *Ice Engineering*, U.S. Army Cold Regions Research and Engineering Laboratory (CRREL), TN-05-3. (Available at http://www.crrel.usace.army.mil/library/technicalnotes/TN05-3.pdf.

3.2. Impact of armour layer on the depth of scour hole around side-by-side bridge piers under ice-covered and open channel conditions

Bed scour may be a natural occurrence or due to manmade changes to a river. Depending on the intensity of approaching flow for sediment transport, local scour process around bridge piers is classified as either clear-water scour or live bed scour. Clear-water scour occurs when there is no movement of the bed material in the upstream flow while live-bed scour occurs when the scour hole is consistently supplied with sediments by the upstream flow (Richardson and Davis, 2001). Local scour around bridge pier is a process of scouring as the result of installation of artificial obstacles such as weirs, abutments and piers in rivers (Richardson et al, 1993). More specifically, flow contraction in rivers caused by installation of hydraulic constructions such as bridge piers and abutments can lead to substantial local alteration of the flow patterns and significant increase of shear stress. As the result of increased shear stress around the hydraulic structures which is itself direct consequence of increased turbulence, flow velocities and the complex flow structures (downwelling, upwelling, horseshoe vortices) causes increased sediment entrainment at the river bed which eventually results in development of local scour holes (Török et al, 2014). The main feature of the flow around a pier is the system of vortices which develop around the pier. These vortex systems have been discussed by many researchers (Melville and Raudkivi, 1977; Raudkivi and Ettema, 1983; Melville and Sutherland, 1988; Kothyari, 1992, to mention only a few). One of the phenomena associated with characteristics of flow in the vicinity of bridge piers is the development of armour layer. Bed armouring process typically occurs in streams with non-uniform bed materials. This phenomenon occurs mainly due to selective erosion process in which the bed shear stress of finer sediment particles exceeds the associated

critical shear stress for movement. As a consequence, finer sediment particles are transported and leave coarser grains behind. Through this process, the coarser grains get more exposed to the flow while the remaining finer grains get hidden among larger ones (Mao et al, 2011). Armour layer is also partially due to the reduced exposure of the flow with those sediments inside the scour hole zone (Sui et al., 2010). For the same bed sediments, Dey and Raika (2007) found that the scour depth around bridge piers with an armour layer is less than that without armour layer. Froehlich (1995) stated that the thickness of the natural armour layer is up to one to three times the particle grain size of armour layer. Raudkivil and Ettema, (1985) found that due to the local flow structure around a pier, local scour may either develop through the armour layer and into the finer, more erodible sediment, or it may trigger a more extensive localized type of scour caused by the erosion of the armour layer itself. Sui et al (2010) studied clear-water scour around semi-elliptical abutments with armoured beds. The results showed that for any bed material having the same grain size, with the increase in the particle size of armour-layer, scour depth will decrease. Török and Baranya (2014) investigated armour layer development in a scour hole around a single groin in laboratory. The main goal of their research was to study bed morphology, sediment transport, bed composition and hydrodynamics under conditions when bed armour development is expected. Guo (2012) studied the relevant scour mechanism of clear water scour around piers and proposed a scour depth equation. Zhang et al. (2012) studied bed morphology and grain size characteristics around a spur dyke. It was found that the mean grain size and the geometric standard deviation of the bed sediment are two important parameters in characterizing the changes of the bed morphologies and the bed compositions around the spur dyke. Kothyari et al. (1992) concluded that an increase in the geometric standard

deviation of sediment gradation (σ_g) would lead to a decrease in scour depth because of the armouring effect on the bed. The presence of ice cover imposes a solid boundary to flow. The velocity profile under ice-covered condition, is totally different compared to open channel flow. Under ice-covered condition, the maximum velocity occurs between channel bed and the bottom of the ice cover and is dependent on the relative roughness of these two boundaries (Sui et al., 2010). The velocity drops to zero at each boundary due to the no-slip boundary condition, resulting in a parabola-shaped profile (Zabilansky et al., 2006). The presence of ice cover has been found to increase local scour depth around bridge piers by 10%~35% (Hains and Zabilansky, 2004). Based on experiments in laboratory, Wu et al. (2014) claimed that with increase in ice cover roughness, scour depth around bridge abutments increased, correspondingly. The impact of ice on sediment transport in a stream is typically most significant during ice formation and breakup (Ettema and Kempema 2012; Sui et al, 2000). Ice cover can either increase or decrease bed load and suspended sediment transport depending on the type of ice cover (Ettema and Kempema 2012; Sui et al, 2000). Ettema et al. (2000) proposed a method for estimating sediment transport rate in ice-covered alluvial channels. Wu et al (2014) investigated the impact of ice cover on local scour around bridge abutment. Results show that with increase in densimetric Froude number, there is a corresponding increase in the scour depth. Results also showed that with increase in grain size of the armour layer, the maximum scour depth decreases and with increase in ice cover roughness, the maximum scour depth increases correspondingly (Wu et al, 2014). Up to date, research work regarding the impact of ice cover on local scour in the vicinity of bridge piers is limited. In present study, three non-uniform sediments and two types of ice cover are used to study the development of armour layer in the scour hole around four pairs of bridge piers

as well as to investigate the impact of ice cover and armour layer on the maximum scour depth under ice covered conditions.

3.2.1. Experiment setup

Experiments were carried out in a large-scale flume at the Quesnel River Research Centre of the University of Northern British Columbia. The flume is 38.2 m long, 2 m wide and 1.3 m deep, as showed in Figure 3-14a. The longitudinal slope of the channel bed was 0.2 percent. A holding tank with a volume of 90 m^3 was located at the upstream of the flume to keep a constant discharge during each experimental run. To create different velocities, three valves were connected to adjust the amount of water into the flume. Two sand boxes were filled with natural non-uniform sediment. Theses sand boxes were spaced 10.2 m away from each other and were 0.30 m deep and 5.6 m and 5.8 m in length, respectively. Three types of non-uniform sediments with different gain sizes were used in this experimental study. The natural non-uniform sediments had median grain sizes of 0.50 mm, 0.47 mm and 0.58 mm and the geometric standard deviation (σ_g) of 2.61, 2.53 and 1.89, respectively. According to Dey and Barbhuiya, (2004), sediments used in this study can be treated as non-uniform since σ_g is larger than 1.84. Four pairs of bridge piers with different diameters of 60 mm, 90 mm, 110 mm and 170 mm were used. Inside each sand box, a pair of bridge piers was placed symmetrically to the center line of flume. The distance from the centre line of each pier to the flume center is 0.25 m, as illustrated in Figure 3-14b. Water level in the flume was controlled by adjusting the tailgate. In front of the first sand box, a SonTek incorporated 2D Flow Meter was installed to measure flow velocities and water depth during experiment runs. A staff gauge was also installed in the middle of each sand box to manually verify water depth. Velocity fields in scour holes were measured using a 10-MHZ Acoustic Doppler

Velocimeter (ADV). The ADV is a high-precision instrument that can be used to measure 3D flow velocity in a wide range of environments including laboratories, rivers, estuaries, and the ocean (Cea and Pena, 2007). Styrofoam panels which were used to model ice cover, had covered the entire surface of flume. In present study, two types of model ice cover were used, namely smooth cover and rough cover. As showed in Figure 3-15, the smooth cover was the surface of the original Styrofoam panels while the rough cover was made by attaching small Styrofoam cubes to the bottom of the smooth cover. The dimensions of Styrofoam cubes were 25 mm × 25 mm × 25 mm and were spaced 35 mm apart. A total of 108 flume experiments were completed under both open channel and ice-covered flow conditions. In terms of different boundary conditions (open channel, smooth covered and rough covered flow conditions), for each sediment type and each boundary condition, 12 experiments were done. Experimental runs were taken under clear-water scour conditions. After 24 hours, the flume was gradually drained, and the scour and deposition pattern around the piers was measured. To accurately read the scour depth at different locations and to draw scour hole contours, the outside perimeter of each bridge pier was equally divided and labeled as the reference points. The measurement of scour hole was subject to an error of +/- 0.3 mm. After each experiment, sand samples within the scour hole which represent armour layer were collected. The samples were taken from the top layer of 5 mm of the armour layer in each scour hole. The sampling process is based on the sampling methodology for collecting armour samples proposed by Bunte and Abt (2001). The collected sand samples were eventually sieved and the mediums grain size of armour layer (D_{50}) were calculated. The scour contours were also plotted by using Surfer 13, Golden Software. In present study, 108 Experiments (36 experiments for each sediment type) were conducted under open

channel, smooth covered and rough covered conditions. For each sediment type, 12 experiments were done for open flow condition, 12 experiments for smooth ice-covered flow condition and 12 experiments for rough ice-covered flow condition, respectively. Flow depth in the flume were controlled by adjusting downstream tailgate. The flow depth ranges from 90 mm to 280 mm. The flow velocity ranges between 0.7 m/s and 2.709 m/s.

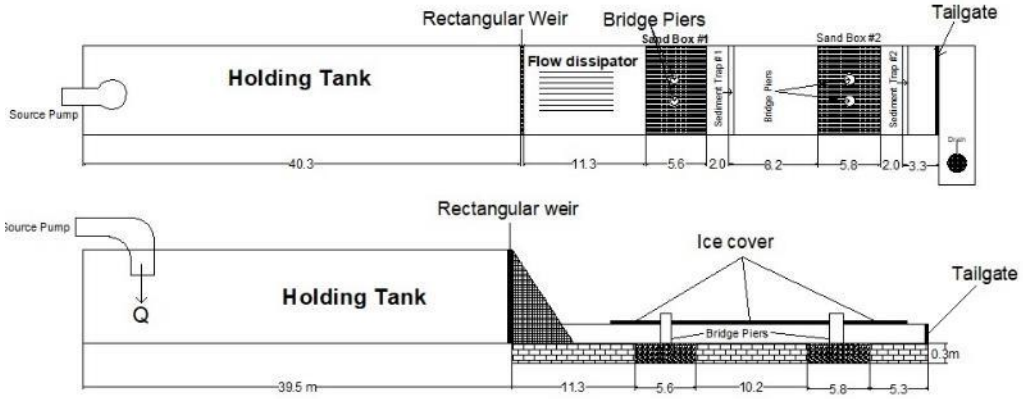

Figure 3–14a: Plan view and vertical view of experiment flume

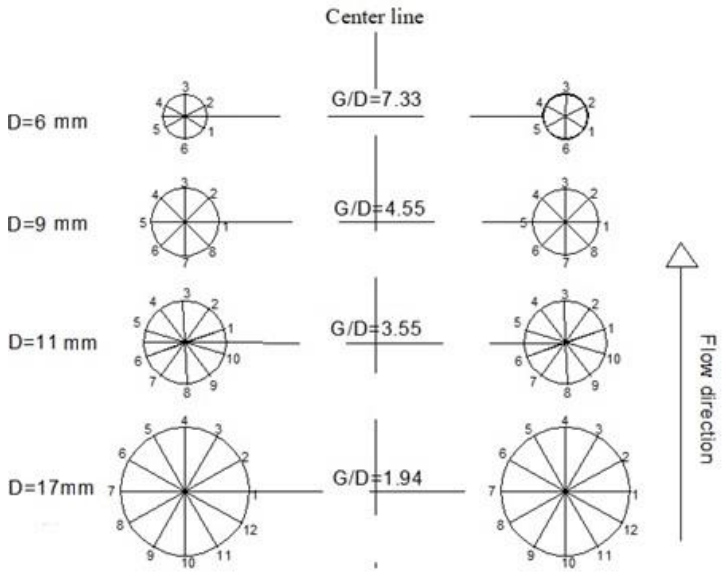

Figure 3-14b: The spacing ratio and measuring points around the circular bridge piers

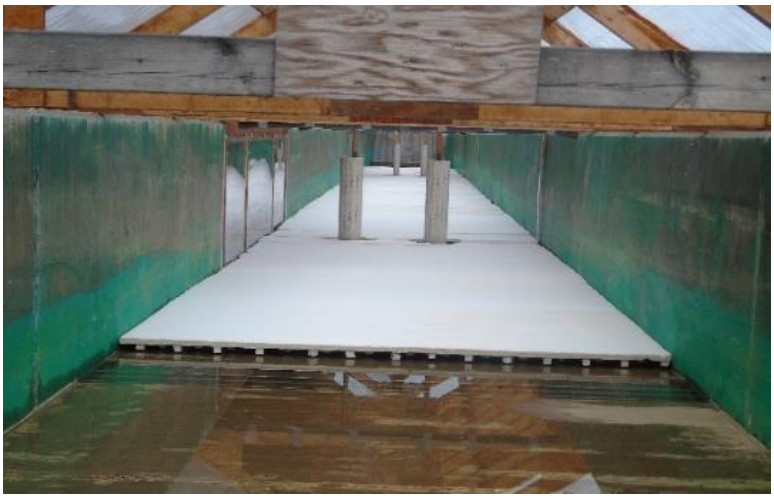

Figure 3-15: Rough model ice cover on water surface

3.2.2 Results and discussion

- **Scour patterns and bed morphology**

Figure 3-16 shows the scour morphology and developed armour layer around the 17-cm-pier. Results indicate that the geometry of the scour holes under open flow condition is approximately similar to that under ice-covered flow condition. As shown in Figure 3-16, the armour layer covers the scour holes around bridge pier. At the downstream of bridge pier, a deposition ridge was developed.

Figure 3-16: Armour layer developed around the 17-cm-pier

Figure 3-17 shows the scour contours and bed morphology around the 11-cm-pier under smooth covered flow condition for the finest and the coarsest sediments. Under the same flow condition and ice-covered condition, the maximum scour depth occurs in channel bed with the finest sediment (D_{50}=0.47 mm). Due to the horseshoe vortex system, the maximum depth of sour hole is located at the upstream face of the piers, and the scour hole extends along the sides of the piers towards the downstream face of the pier where the wake vortex exists. This scouring process around bridge piers is substantially due to the merging of the locally enhanced flow at the sides of the pier with the turbulent horseshoe vortices in front of the piers. Besides, sediment deposition ridge, which is developed at the downstream of the piers, travels further downstream as vortex shedding occurs. Under the same flow condition and ice-covered condition, as the sediment gets coarser, the turbulence of flow between the piers slightly decreases. Thus, with respect to Figure 3-17, a slight deposition which is caused by the jet-like flow has developed between piers, especially for channel bed with sediment of D_{50}=0.47 mm.

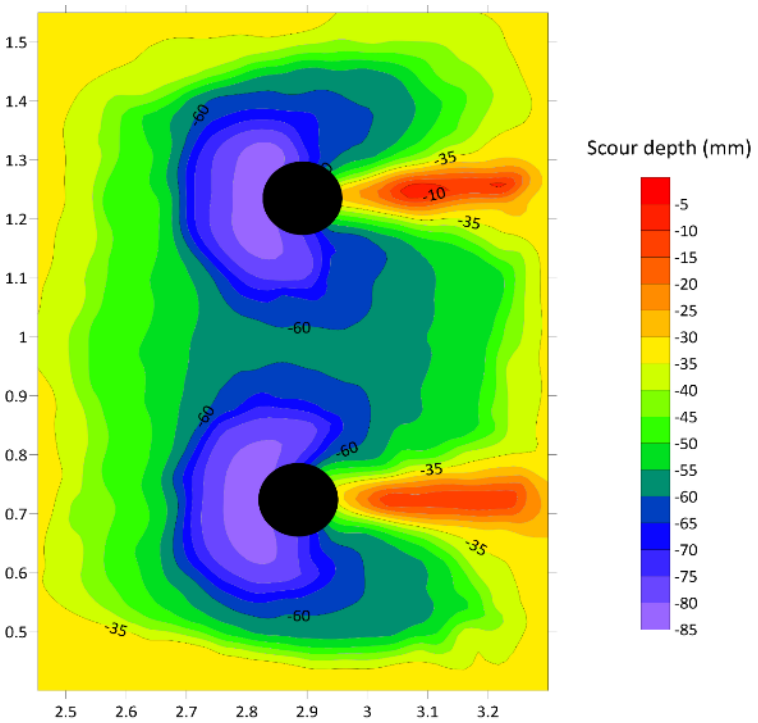

Figure 3–17a: Scour morphology and the deposition ridge around the 11-cm-pier under smooth ice-covered condition for D_{50}=0.47 mm

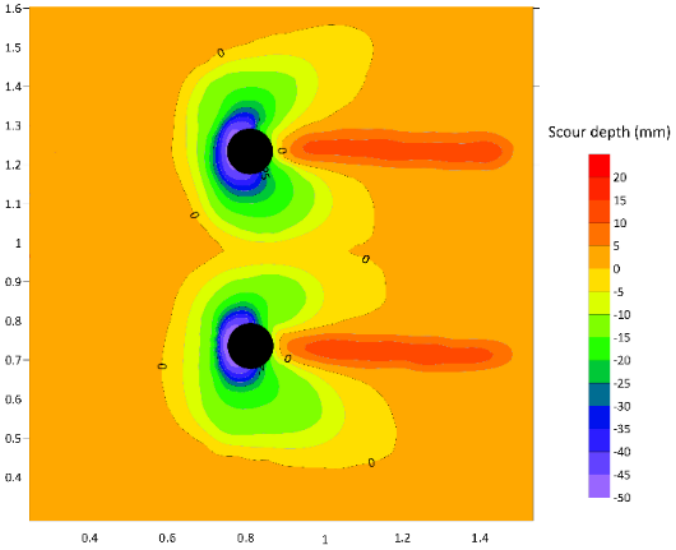

Figure 3–17b: Scour morphology and the deposition ridge around the 11-cm-pier under smooth ice-covered condition for D_{50}=0.58 mm

Figure 3-18 shows the variation in scour depth elevation for sediment of D_{50}=0.58 mm under conditions of open channel, smooth ice-covered and rough ice-covered flows. The following results are obtained from the Figure 3-18:

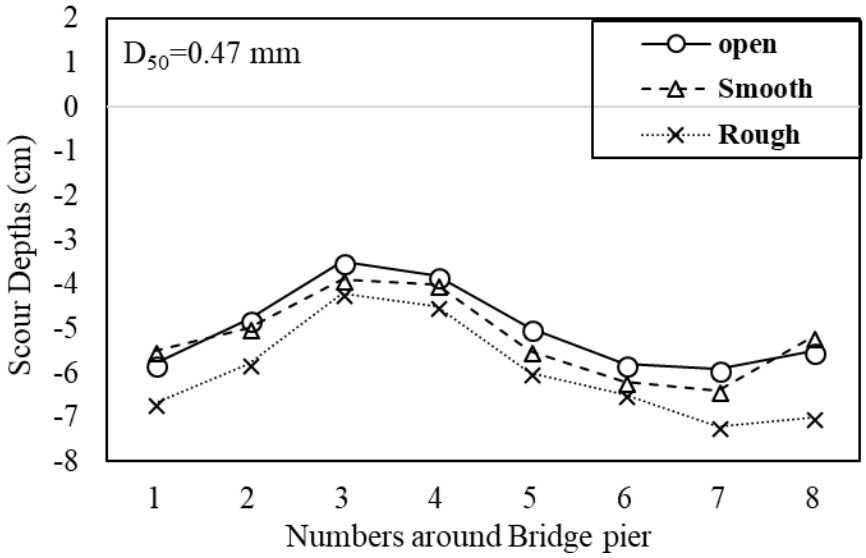

Figure 3–18: Scour profiles around the 9-cm-pier under ice-covered and open channel flow condition for D_{50}=0.47 mm

Under the same boundary condition (either covered flow or open flow), the maximum scour depth is located at the upstream nose of the pier (at point 9 of the 11-cm-pier as showed in Figure 3-14b). The primary horseshoe vortex which is stronger at the front face of pier is responsible for this. As confirmed by Muzzammil and Gangadhariah (2003), the primary horseshoe vortex which generates in front of a pier is the main reason for scour over the entire scouring process. Results showed that the interaction between the primary horseshoe vortex and the finer sediment is more intense than that of coarser sediment. Also, the lowest scour hole is located at point 4 which is behind the pier as showed in Figure 3-18a. Figure 3-18b shows that, for the same sediment (such as D_{50}=0.47 mm), the deepest scour hole has occurred under rough ice-covered flow condition. Besides, regardless of flow cover, the maximum scour depth is located at the upstream face, namely, location point 7 for the 9-cm-pier, similar to that of the 11-cm-pier. According to Sui et al. (2010), the existence of an ice cover on water surface doubles the wetted perimeter compared to that under open flow condition and alters the hydraulics of an open channel by imposing an extra boundary to the

flow. As a consequence, the maximum flow velocity is shifted towards the channel bed. The velocity profile is significant changed (comparing to that under open flow condition). Thus, the strength of primary horseshoe vortexes under ice-covered flow condition is amplified, this leads to more intense scour depths. Under covered flow condition, the roughness of ice cover has significant impacts on velocity field and flow characteristics, namely, the rougher the ice cover, the more effects on velocity field and flow characteristics. For channel bed with the same sediment, the rough ice cover will lead to a deeper scour hole comparing to that of smooth ice-cover.

Figure 3-19a shows the pattern of scour hole and deposition ridge around the 11-cm pier under rough covered flow condition (D_{50}=0.58 mm), while Figure 3-19b shows scour depths around the 9-cm-pier under different boundary conditions for D_{50}=0.47 mm. Results indicate that, regardless of the roughness of ice cover and grain size of sediment, the maximum scour depths always occur at the upstream front face of bridge piers. It has been observed from experiments that the horseshoe vortex shifts the maximum downflow velocity closer to the pier in the scour hole. Besides, under covered condition, the strength of this downflow jet is intensified. The eroded sand particles are carried around the pier by the combined action of accelerating flow and the spiral motion of the horseshoe vortex. As clearly showed in Figure 3-19a, the deposition ridge has been formed downstream of the pier. Melville and Coleman (2000) stated that the wake-vortex system acts like a vacuum cleaner sucking up stream bed material and carrying the sediment moved by the horseshoe vortex system and by the downward flow to the downstream of the pier. However, wake vortices are normally not as strong as the horseshoe vortices and therefore, they are not able to carry the same amount of

sediment load as that carried by the horseshoe vortex. Hereby, sediment deposition occurs downstream of bridge piers in the form of deposition mound as shown in Figure 3-19a.

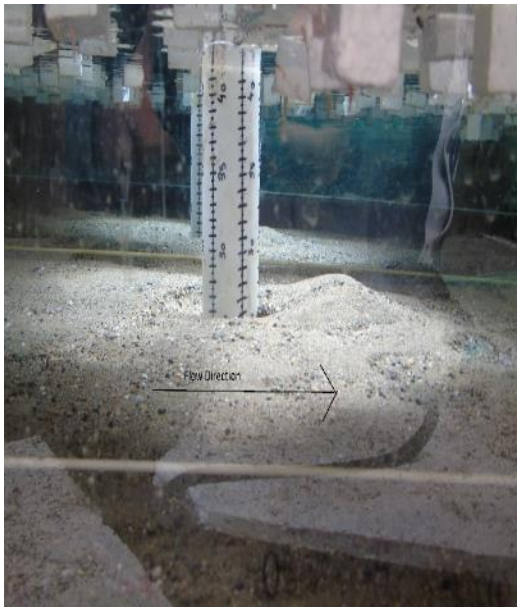

Figure 3–19a: A view of the scour pattern and deposition ridge around the 11-cm pier under rough ice-covered condition (D_{50}=0.58 mm)

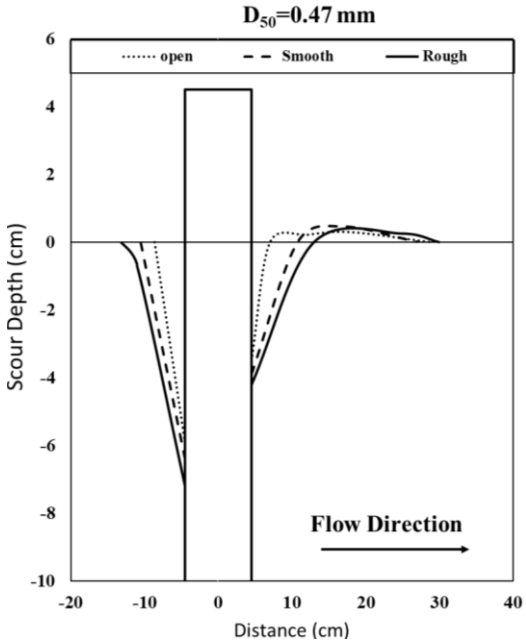

Figure 3–19b: Cross sections of scour and deposition ridge around the 9-cm-piers under open channel, smooth and rough covered flow conditions (D_{50}=0.47 mm)

- **Scour area and Scour Volume**

Accurate determination of scour volume and scour area is important in practical decision-making for the control of local scour and safe design of countermeasures. However, there is very limited research work for examining the scour volume and scour area under ice-covered flow condition. Wu et al (2014) found that there was a linear correlation between scour depth and volume of scour hole around bridge abutments under ice covered condition. Khwairakpam et al. (2012) developed two formulae to estimate scour volume and scour area around a vertical pier under clear water condition in terms of approach flow depth and pier diameter. Figure 3-20 gives the relationship between scour volume (V) and scour area (A) in terms of grain size of sediment. These relationships can be described as follows:

Under open flow condition:

$$V = 0.229\,A^{1.256} \tag{3-2-1}$$

Under ice-covered flow condition:

$$V = 0.465\,A^{1.158} \tag{3-2-2}$$

In which V is volume of scour hole (cm^3) and A is surface area of scour hole. The following results are obtained from the scour volume and scour area analysis.

(a) In terms of grain size of sediment, under the same flow condition, the finest sediment (D_{50} = 0.47 mm) yielded the largest scour volume and scour area and the impact of ice cover on scour volume and scour area is more significant for finer sediment type. On the other hand, under the same flow conditions, the coarsest sediment (namely, D_{50} = 0.58 mm) yielded the smallest scour volume and scour area.

(b) In terms of flow cover, results indicated that the flow under ice-covered condition led to larger amount of scour volume and scour area. It was found that, the maximum amount of scour volume and scour area occurred under rough covered flow condition. Also, under the same flow condition, intense scouring process around bridge piers with smaller pier spacing has been observed, especially in channel bed with the finest sediment.

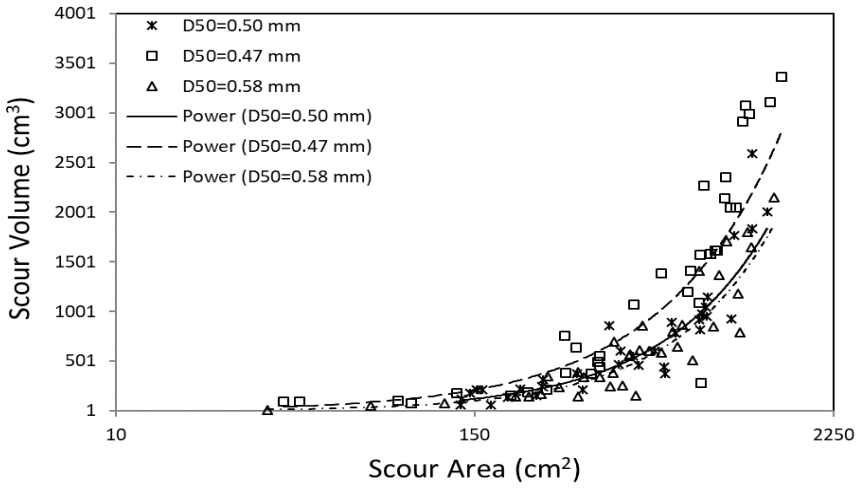

Figure 3–20: Relationship between scour volume and scour area

- **Grain size analysis of armour layer**

Sieve analyses (ASTM D422-63) were performed to obtain the grain size distribution of the three non-uniform sediments. The grain size distribution curves for these three non-uniform sediments used in this experimental study are displayed in Figure 3-21. Sieve analyses revealed that the material collected was almost exclusively coarser than 0.075 mm (#200 sieve). The sediments were classified according to the unified soil classification system (ASTM D2487-11). All three sediments were classed as poorly-graded sands (SP).

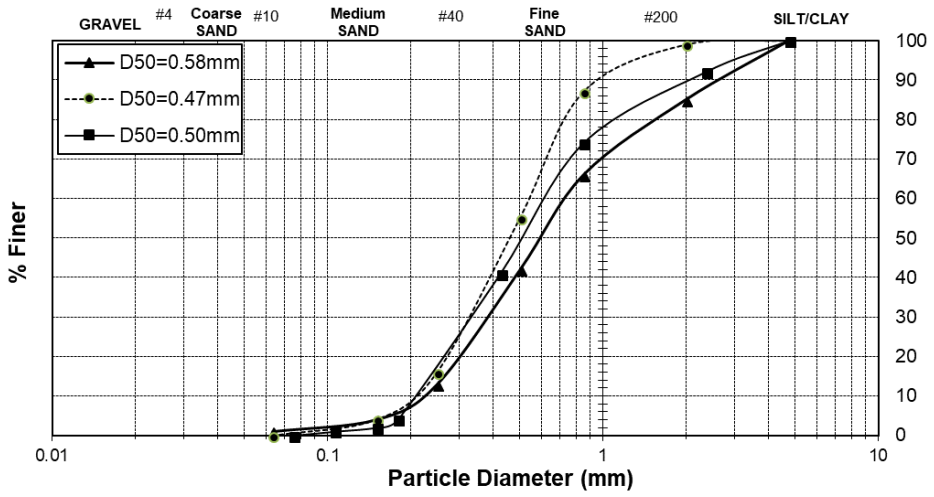

Figure 3–21: Grain size distribution curves of three non-uniform sands used in this study

As the experiments initiated, the armour layer evolution gradually started to develop inside the scour hole. The first sign of armour layer development was inside the scour hole at the upstream face of the pier where the downflow and horseshoe vortex exists and in which the armour layer was denser. The armour layer then extended to the sides and downstream of the pier where the armour layer particles were more separated from each other and it eventually disintegrates at the end of the deposition ridge. Results showed that the armour layer which was formed on the deposition ridges was composed of finer sediment particles compared to those of armour layer formed inside the scour holes. The maximum depth of scour hole remained quite constant once the armour layer was formed which is due to the slope stability caused by formation of the armour layer. The samples of armour layer developed within the scour hole were collected for each experimental run and the D_{50} of the armour layers were extracted from armour layer grain size distribution graphs (described as D_{50A}). Figure 3-22 displays the distribution curves of grain sizes of armour layer in scour hole around the 11-cm-pier for D_{50}=0.50 mm compared to those of the original sands and deposition ridge under rough covered flow condition.

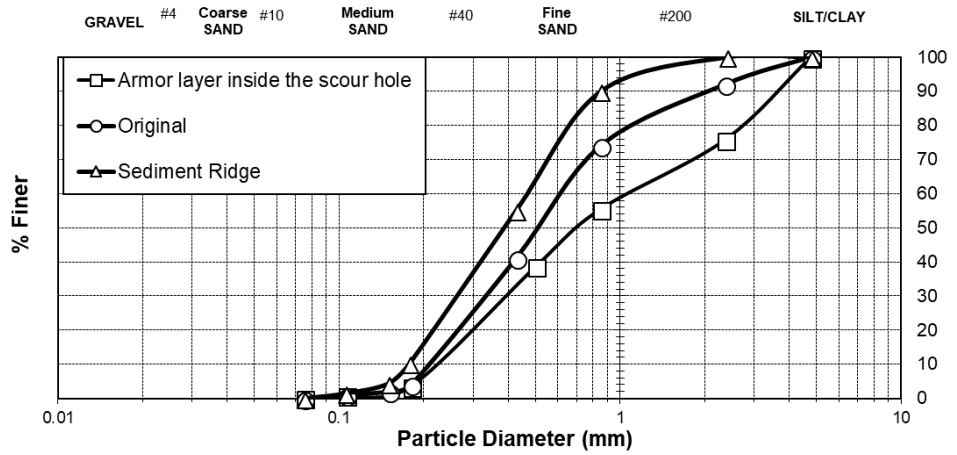

Figure 3–22: Grain size distribution curves of the armour layer in scour hole around the 11-cm-pier, original sand and deposition ridge for sand bed of D_{50}=0.50 mm under rough covered condition

Table 3-2 shows the grain size characteristics of samples of armour layers in scour holes around the 11-cm-pier compared to those of correspondingly deposition ridges for three sands under rough covered flow condition. One can see from Table 3-2, the armour layer generated in sand bed of D_{50}=0.58 mm is coarser than that in sand beds of D_{50}=0.47 mm and D_{50}=0.50 mm. To better distinguish the difference in grain size distributions between the samples of armour layers in scour holes and the samples of the associate deposition ridges, the grain size distributions are separately displayed in Figures 3-23(a-b). Results indicate that the armour layer generated in sand bed of D_{50}=0.58 mm is the coarsest comparing to those of D_{50}=0.47 mm and D_{50}=0.50 mm. Regarding the deposition ridge in sand bed of D_{50}=0.58 mm, the deposition ridge is covered by coarsest sand particles comparing to those of D_{50}=0.47 mm and D_{50}=0.50 mm. With decrease in D_{50} of the original sand, the grain size of the armour layer decreases correspondingly. These results are in good agreement with findings of Wu et al (2015) who investigated the armour layer in scour holes around square and semi-circular abutments.

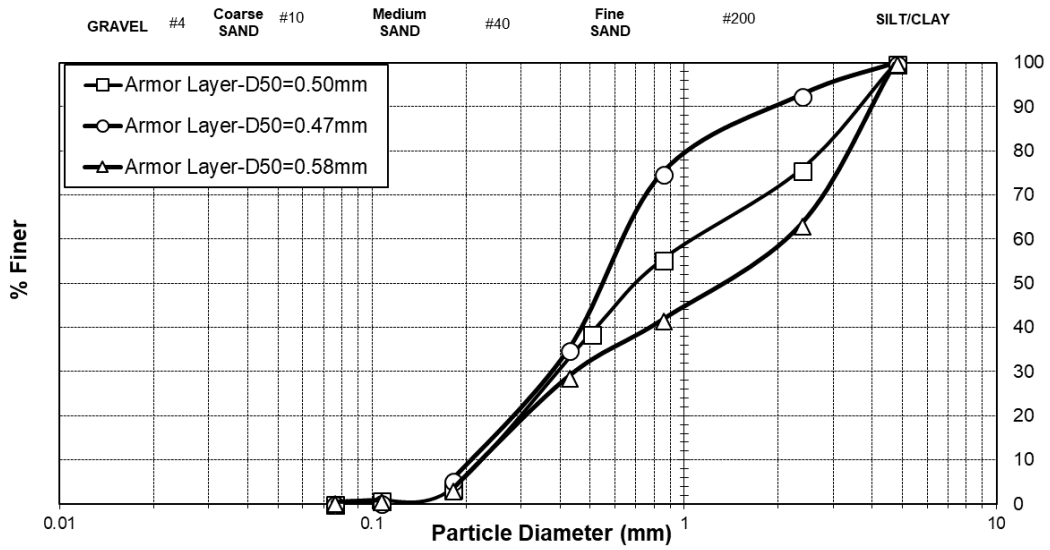

Figure 3–23a: Grain size distributions of armour layer samples in scour hole generated from three sands around the 11-cm-pier

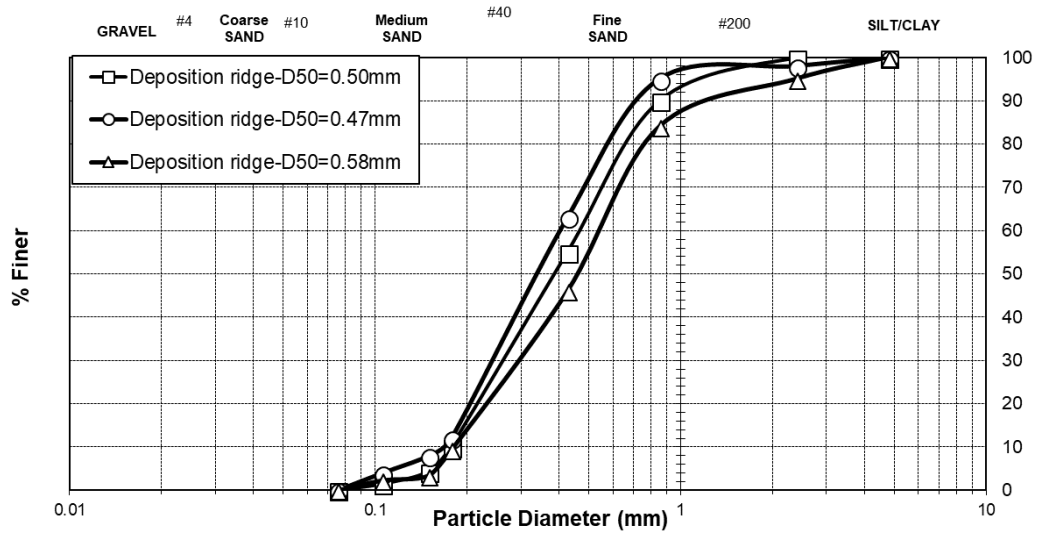

Figure 3–23b: Grain size distributions of samples of deposition ridge generated from three sands downstream of around the 11-cm-pier

Table 3-2: Grain size characteristics of samples of armour layer in scour hole around the 11-cm-pier under rough covered flow condition compared to those of associated deposition ridge

	D_{10} (mm)	D_{16} (mm)	D_{30} (mm)	D_{50} (mm)	D_{60} (mm)	D_{84} (mm)	D_{90} (mm)	Geometric standard deviation (σg)	Uniformity coefficient ($C_{U)}$	Coefficient of curvature (C_c)
Composition of armour layer (D_{XA})										
Sample 1, for D_{50}=0.50mm	0.22	0.28	0.40	0.70	1.10	3.30	3.80	3.43	5.00	0.66
Sample 2, for D_{50}=0.47mm	0.21	0.26	0.38	0.55	0.62	1.40	2.10	2.32	2.95	1.11
Sample 3, for D_{50}=0.58mm	0.23	0.28	0.39	1.40	2.10	3.80	4.00	3.68	9.13	0.31
Composition of deposition ridge (D_{XR})										
Sample 1, for D_{50}=0.50mm	0.18	0.21	0.27	0.40	0.48	0.75	0.88	1.89	2.67	0.84
Sample 2, for D_{50}=0.47mm	0.17	0.19	0.24	0.34	0.40	0.63	0.72	1.82	2.35	0.85
Sample 3, for D_{50}=0.58mm	0.18	0.21	0.30	0.47	0.53	0.90	1.30	2.07	2.94	0.94

- **Determination of scour depth with influence of armour layer:**

Considering a bridge pier in a river whose flow is assumed to be steady and uniform, Breusers et al (1977) pointed out that following parameters may influence the scouring phenomenon as follows: 1) variables characterizing the fluid such as acceleration due to gravity (g) and density of fluid (ρ_w); 2) variables characterizing the bed material such as sediment density (ρ_s), median grain size of the bed material (D_{50B}) and median grain size of sediment particles of the armor layer; 3) variables characterizing the flow such as depth of approaching flow (y_0) and the mean velocity of approaching flow (U); 4) variables characterizing the bridge pier and channel geometry such as pier shape and size and channel width. In addition to above-mentioned parameters, in the present study, the effect of ice cover roughness is an important parameter which must be considered. Therefore, conceptually at least, with influence of armour layer in scour hole around bridge pier, the maximum scour depth of scour hole may be evaluated by means of a general formula for computation:

$$y_{\max} = f\left(U, g, D_{50A}, D_{50B}, n_b, n_i, D, B, y_0, \rho_w, \rho_s\right) \quad (3\text{-}2\text{-}3)$$

In which, y_{max} is the maximum depth of scour hole around bridge pier; D_{50A} is the median grain size of armour layer; n_b is the Manning roughness coefficient of channel bed; n_i is Manning roughness coefficient of ice cover; D is the diameter of bridge pier; B is the channel width; ρ_w and ρ_s are the density of water and sediment, respectively, with $\Delta\rho = \rho_s - \rho_w$. Through dimensional analysis by means of Buckingham π theories, the maximum depth of scour hole can be expressed as follows

$$\frac{y_{\max}}{D_{50A}} = f\left(\frac{U}{\sqrt{\left(\Delta\rho/\rho_w\right) g D_{50A}}}, \frac{D_{50A}}{D_{50B}}, \frac{n_i}{n_b}, \frac{D_{50A}}{y_0}, \frac{D_{50A}}{B}, \frac{D_{50A}}{D}\right) \quad (3\text{-}2\text{-}4)$$

The term $Fr_0 = \dfrac{U}{\sqrt{\left(\Delta\rho/\rho_w\right) g D_{50A}}}$ is called densimetric Froude number and is a criterion of hydraulic conditions for assessment of the incipient motion of bed material (Aguirre-Pe, 2003). It is a term that describes the incipient motion of the sediment articles. The larger the densiometric Froude number, the larger shear stress is needed to transport the sediment particles. Eq. 3-2-4 can be also expressed as follows:

$$\frac{y_{\max}}{D_{50A}} = A\left(Fr_0\right)^a \left(\frac{D_{50A}}{D_{50B}}\right)^b \left(\frac{n_i}{n_b}\right)^c \left(\frac{D_{50A}}{y_0}\right)^d \left(\frac{D_{50A}}{B}\right)^e \left(\frac{D_{50A}}{D}\right)^f \quad (3\text{-}2\text{-}5)$$

Since the values of D_{50A}/B is truly tiny, the term D_{50A}/B can be neglected from Eq. 3-2-5. Besides, the term (D_{50A}/y_0) can be also ignored from Eq. 3-2-5 due to its weak correlation with (y_{max}/D_{50A}). Therefore, the following parameters have been used to assess the relative maximum scour depth (MSD) of scour hole (y_{max}/D_{50A}) around bridge pier.

$$\frac{y_{\max}}{D_{50A}} = A\left(\frac{D_{50A}}{D_{50B}}\right)^a \left(\frac{D_{50A}}{D}\right)^b \left(\frac{n_i}{n_b}\right)^c \left(Fr_0\right)^d \quad (3\text{-}2\text{-}6)$$

In the case of open channel flow condition, the ratio of roughness coefficient of ice cover to roughness coefficient of channel bed would be omitted from Eq. 3-2-6. Each of the independent dimensionless variables of Eq. 3-2-6 were assessed separately to study their impact on the local scour around bridge piers.

- **Variation of relative MSD (y_{max}/D_{50A}) with densimetric Froude number (Fr_0):**

Figure 3-24 illustrates the variation of relative MSD with densimetric Froude number (Fr_0). With increase in Fr_0, the relative MSD increases correspondingly. Besides, under the same Fr_0, the values of the relative MSD under ice-covered conditions are larger than those under open flow condition. On the other hand, with the same values of relative MSD, the larger value of densimetric Froude number is needed to initiate sediment transportation for the open channel flow condition which means that a lower values of shear stress is needed to initiate motion for sediment transportation under ice-covered flow conditions.

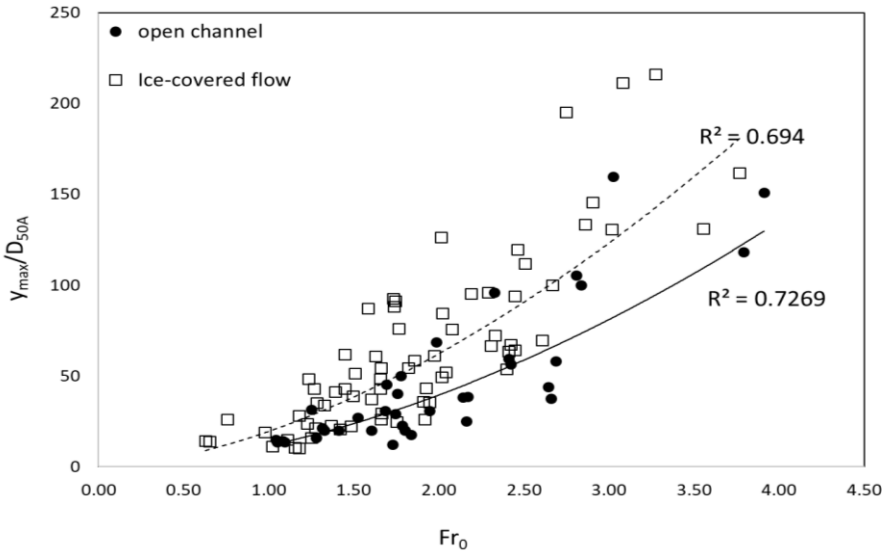

Figure 3–24: Relation between the relative MSD (y_{max}/D_{50A}) with densimetric Froude number (Fr_0)

- **Variation of relative MSD (y_{max}/D_{50A}) with the grain size of armour layer (D_{50A}/D_{50B}):**

Figure 3-25a illustrates the variation of relative MSD (y_{max}/D_{50A}) against ratio of grain size of armour layer (D_{50A}/D_{50B}) distinguished by different pier sizes. Regardless of size of bridge pier, as the grain size of armour layer (D_{50A}/D_{50B}) increases, the relative MSD of scour hole decreases and vice versa. From Figure 3-25b, one can see that the variation of relative MSD (y_{max}/D_{50A}) against ratio of (D_{50A}/D_{50B}) distinguished by different covered conditions. Regardless of flow cover, the relative MSD (y_{max}/D_{50A}) decreases as the grain size of armour layer (D_{50A}/D_{50B}) increases. Under rough covered condition, the relative MSD (y_{max}/D_{50A}) showed a sharper descending trend with the grain size of armour layer (D_{50A}/D_{50B}) compared to those of under both smooth covered and open flow conditions. Also, under smooth covered flow condition, the relative MSD (y_{max}/D_{50A}) showed a sharper descending trend with the grain size of armour layer (D_{50A}/D_{50B}) compared to those of under open flow condition. The reason for this is due to strong turbulent flows and different velocity fields close to channel bed which are caused by ice cover, and it get more intensified under rough covered flow condition. Similar results were also reported by Dey and Raikar (2007).

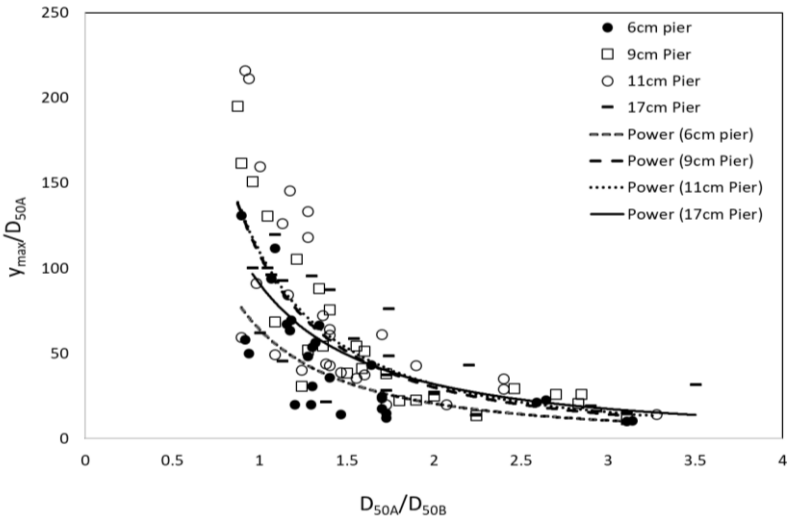

Figure 3–25a: Variation of relative MSD (y_{max}/D_{50A}) with (D_{50A}/D_{50B}) distinguished by pier size

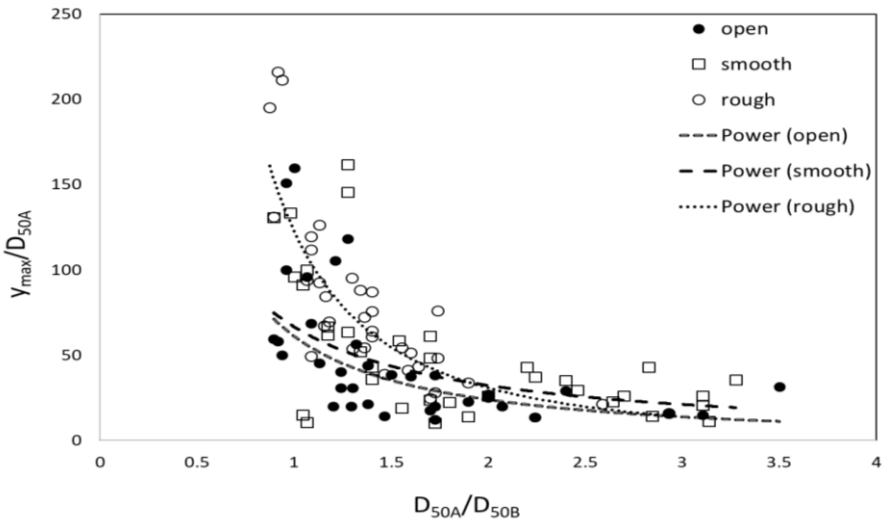

Figure 3–25b: Variation of relative MSD (y_{max}/D_{50A}) with (D_{50A}/D_{50B}) distinguished by different covered conditions

- **Variation of relative MSD (y_{max}/D_{50A}) with the pier spacing (D_{50A}/D):**

Figure 3-26 illustrates the variation of relative MSD (y_{max}/D_{50A}) with ratio of the pier spacing (D_{50A}/D) distinguished by different covered conditions. Regardless of flow cover, the relative MSD (y_{max}/D_{50A}) decreases with increase in ratio of the pier spacing (D_{50A}/D). Under rough covered condition, the relative MSD (y_{max}/D_{50A}) showed a sharper descending trend with the pier spacing (D_{50A}/D) compared to those of under both smooth covered and open flow conditions. Besides, under the same values of (D_{50A}/D), the rough ice-covered flow has resulted in largest relative MSD.

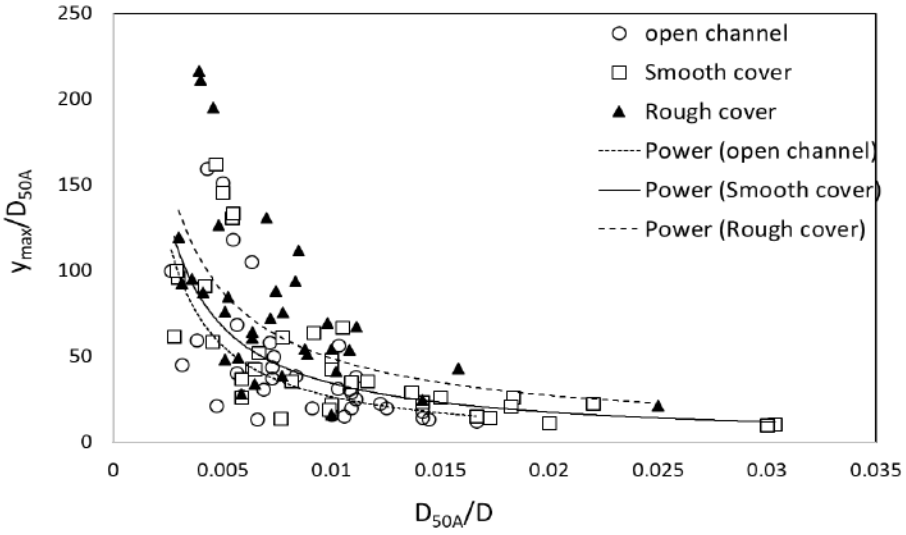

Figure 3–26: Variation of relative MSD (y_{max}/D_{50A}) with the ratio of pier spacing (D_{50A}/D) distinguished by different covered conditions

- **Variation of relative MSD (y_{max}/D_{50A}) with roughness of ice cover (n_i/n_b):**

As pointed out by Mays (1999), due to a relatively smooth concrete-like surface of the Styrofoam panel, the roughness of the model smooth ice-cover was assumed to be 0.013. In terms of model rough ice-cover, Li (2012) reviewed several methods for calculating the Manning's coefficient for ice cover, the following equation can be used depending on the size of the small cubes:

$$\frac{n_i}{k_s^{1/6}} = \frac{(8g)^{-1/2}(R/K_s)^{1/6}}{0.867\ln(12R/K_s)} \qquad (3\text{-}2\text{-}7)$$

In which, *Ks* is the average roughness height of the ice cover underside and R is the hydraulic radius. By using Eq. 3-2-7, a Manning's coefficient of 0.021 was determined as the roughness coefficient of model rough ice cover. This value also agrees with result of Hains and Zabilansky (2004). To calculate channel bed roughness coefficient for non-uniform sand bed, the following equation proposed by Hager (1999) was used:

$$n_b = 0.039 D_{50}^{1/6} \qquad (3\text{-}2\text{-}8)$$

Therefore, the roughness coefficient of sand bed n_b is determined as 0.0109 for sand bed of D_{50}=0.47 mm, 0.0110 for sand bed of D_{50}=0.050 mm, and 0.0113 for sand bed of D_{50}=0.58 mm, respectively. Results indicate that with increase in n_i/n_b, the relative MSD (y_{max}/D_{50A}) increases correspondingly. Following Eq. 3-2-9 and 3-2-10 are developed to predict the relative MSD (y_{max}/D_{50A}) under ice-covered condition and open flow condition, respectively.

Open flow condition:

$$\frac{y_{\max}}{D_{50A}} = 1.433\left(Fr_0\right)^{1.289}\left(\frac{D_{50A}}{D_{50B}}\right)^{-0.190}\left(\frac{D_{50A}}{D}\right)^{-0.488} \qquad R^2=0.85 \qquad (3\text{-}2\text{-}9)$$

Ice-covered flow condition:

$$\frac{y_{\max}}{D_{50A}} = 47.190\left(Fr_0\right)^{0.892}\left(\frac{D_{50A}}{D_{50B}}\right)^{-0.652}\left(\frac{D_{50A}}{D}\right)^{-0.367}\left(\frac{n_i}{n_b}\right)^{0.484} \qquad R^2=0.88 \qquad (3\text{-}2\text{-}10)$$

According to Eq. 3-2-9 and Eq. 3-2-10, the most significant variable is the densimetric Froude number since this variable has the largest power comparing to all other variables. Figure 3-27 showed the comparison of calculated relative MSD (y_{max}/D_{50A}) to those observed under open flow condition, and Figure 3-28 show the comparison of calculated relative MSD (y_{max}/D_{50A}) to those observed under ice-covered flow condition. As showed in Figures 3-27 and 3-28, the calculated relative MSD (y_{max}/D_{50A}) agreed well with those observed under both open flow condition and ice-covered condition. To better specify the correlation of different dimensionless variables of Equation 10 with each other and their impact on the relative MSD (y_{max}/D_{50A}), different combination of those dimensionless variables are generated in Table 3-3. As one can see from Table 3-3 the densimetric Froude number is the most dominant parameter since its individual R^2 coefficient is 0.784. The next dominant term is ratio of grain size of armour layer (D_{50A}/D_{50B}) with R^2 coefficient of 0.694. With respect

to combination of two terms, the combination of (D_{50A}/D_{50B}) and (Fr_0) is the most accurate one with R^2 equal to 0.787. With respect to combination of three terms, the combination of (n_i/n_b); (D_{50A}/D); (Fr_0) is the most accurate with R^2 equal to 0.857.

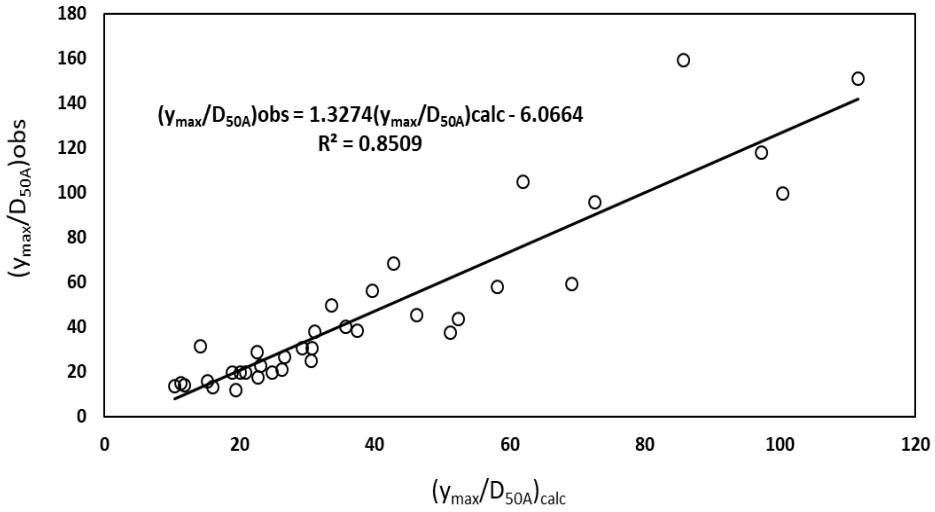

Figure 3–27: Comparison of calculated relative MSD (y_{max}/D_{50A}) to those observed under open flow condition

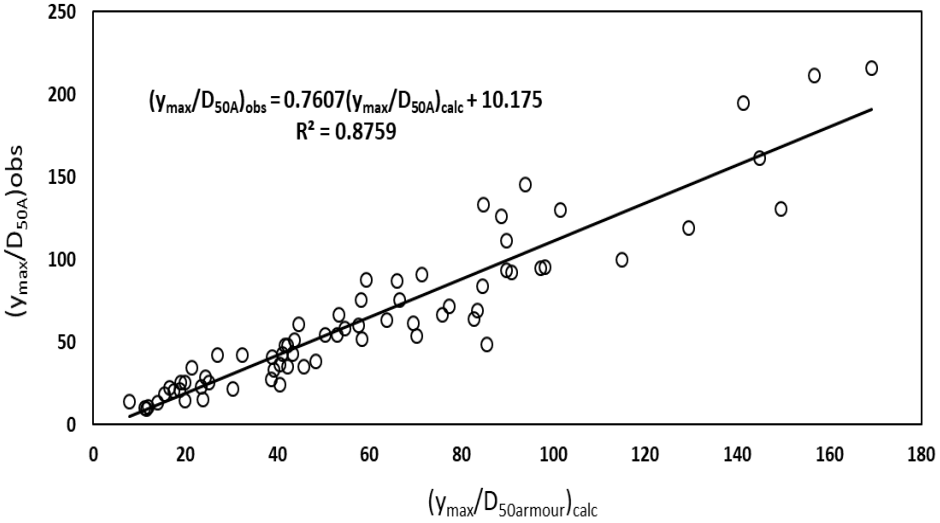

Figure 3–28: Comparison of calculated relative MSD (y_{max}/D_{50A}) to those observed under ice-covered flow condition

Table 3-3: Different combinations of dimensionless variables

y_{max}/D_{50A}= f ()	R^2	Equation
(D_{50A}/D_{50B}); (n_i/n_b); (D_{50A}/D); (Fr_0)	0.890	$47.190(D_{50A}/D_{50B})^{-0.652}(n_i/n_b)^{0.484}(D_{50A}/D)^{-0.367}(Fr_0)^{0.892}$
(n_i/n_b); (D_{50A}/D); (Fr_0)	0.857	$21.573(n_i/n_b)^{0.613}(D_{50A}/D)^{-0.555}(Fr_0)^{1.13}$
(D_{50A}/D_{50B}); (D_{50A}/D); (Fr_0)	0.856	$7.948(D_{50A}/D_{50B})^{-0.772}(D_{50A}/D)^{-0.32}(Fr_0)^{0.889}$
(D_{50A}/D_{50B}); (n_i/n_b); (Fr_0)	0.806	$47.215(D_{50A}/D_{50B})^{-1.132}(n_i/n_b)^{0.008}(Fr_0)^{0.859}$
(D_{50A}/D_{50B}); (Fr_0)	0.787	$45.658(D_{50A}/D_{50B})^{-1.132}(Fr_0)^{0.859}$
(D_{50A}/D_{50B}); (n_i/n_b); (D_{50A}/D)	0.756	$7.948(D_{50A}/D_{50B})^{-1.329}(n_i/n_b)^{0.313}(D_{50A}/D)^{-0.370}$
(D_{50A}/D_{50B}); (D_{50}/D)	0.748	$26.245(D_{50A}/D_{50B})^{-1.577}(D_{50A}/D)^{-0.252}$
(D_{50A}/D_{50B}); (n_i/n_b)	0.742	$841.012(D_{50A}/D_{50B})^{-1.776}(n_i/n_b)^{0.533}$
(Fr_0)	0.784	$19.345(Fr_0)^{1.6851}$
(D_{50A}/D_{50B})	0.694	$110.9(D_{50A}/D_{50B})^{-1.83}$
(D_{50}/D)	0.568	$0.4123(D_{50A}/D)^{-0.992}$
(n_i/n_b)	0.137	$5617.1(n_i/n_b)^{1.1492}$

3.2.3. Conclusions

In present study, to investigate the impact of armour layer and ice cover on scour depth around bridge piers, three non-uniform sediments and four pairs of model piers were used to conduct 108 experiments in a large-scale flume under both open flow condition and ice-covered flow condition. Following conclusions can be drawn from the present study.

1) Although the scour depth under ice-covered flow condition was larger comparing to that under open flow condition, the geometry of the scour holes under open flow condition is similar to that under ice-covered flow condition. Results showed that, regardless of flow cover, the maximum scour depth decreases with increase in the grain size of armour layer. Also, although the maximum depth of scour hole around largest pier was deepest, the grain size distribution of armor layer in scour hole around larger piers did not show a significant difference from those around smaller piers.

2) Under the same flow condition and same covered condition, the maximum scour depth occurs in channel bed with the finest sediment. Due to the horseshoe vortex system, maximum scour depth is located at the upstream face of the piers and extends along the sides of the piers towards the rear side of the pier where wake vortex exists. Due to effect of ice cover, the horseshoe vortex shifts the maximum downflow velocity closer to the pier in the scour hole. Thus, the strength of downflow gets more intensified which leads to a larger and wider deposition ridge downstream of the pier.

3) Under the same flow condition, both scour volume and scour area of scour hole in the finest sand bed are largest comparing to those in channel bed with coarser sands. With respect to the impact of ice cover, it was found that both scour volume and scour area of scour hole under rough covered flow condition are largest comparing to those under both smooth covered condition and open flow condition.

4) Based on data collected in laboratory, two formulae have been developed to predict the relative MSD (y_{max}/D_{50A}) under both open flow condition and ice-covered condition. Following dimensionless variables are considered in the proposed formulae for determining the relative MSD (y_{max}/D_{50A}): densimetric Froude number (Fr_0), grain size of armour layer (D_{50A}/D_{50B}), pier spacing (D_{50A}/D), and roughness of ice cover (n_i/n_b). Results showed that the calculated relative MSD (y_{max}/D_{50A}) agreed well with those observed under both open flow condition and ice-covered condition.

5) Results showed with increase in densimetric Froude number (Fr_0), the relative MSD increases correspondingly. Besides, under the same Fr_0, the values of the relative MSD under ice-covered conditions are larger than those under open flow condition. Results also indicate that, under ice-covered flow condition, a smaller value of densimetric Froude number is

needed to initiate movement of sediment comparing to that under open flow condition which can be justified by the higher flow velocity near channel bed under ice-covered flow conditions and its impact on the threshold of sediment motion.

3.2.4. Reference

Aguirre-Pe J., Olivero M. L., and Moncada A. T. (2003), Particle densimetric Froude number for estimating sediment transport. Journal Hydraul. Eng., Vol. 129, No. 6, pp. 428–437

Bunte, K., and Abt, S. R. (2001). Sampling surface and subsurface particle-size distributions in wadable gravel-and cobble-bed streams for analyses in sediment transport, hydraulics, and streambed monitoring. Gen. Tech. Rep. RMRS-GTR-74. Fort Collins, CO: US Department of Agriculture, Forest Service, Rocky Mountain Research Station. 428 p., 74.

Breusers, H. N. C., Nicollet, G., and Shen, H. W. (1977). Local scour around cylindrical piers. *Journal of Hydraulic Research*, *15*(3), 211-252.

Cea, L., Puertas, J., and Pena, L. (2007). Velocity measurements on highly turbulent free surface flow using ADV. Experiments in fluids, 42(3), 333-348.

Dey, S., and Raikar, R. (2007). Clear-water scour at piers in sand beds with an armor layer of gravels. Journal of Hydraulic Engineering, 133, 703-711.

Dey, S., and Barbhuiya, A. K. (2004). Clear-water scour at abutments in thinly armored beds. Journal of hydraulic engineering, 130(7), 622-634.

Ettema, R., Braileanu, F., and Muste, M. (2000). Method for estimating sediment transport in ice-covered channels. Journal of Cold Regions Engineering, 14(3), 130-144.

Ettema, R., and Kempema, E. W. (2012). River Ice Effects on Gravel Bed Channels. Gravel-Bed Rivers: Processes, Tools, Environments, 523-540.

Froehlich, D.C. (1995). Armor limited clear water construction scour at bridge, Journal of Hydraulic Engineering, ASCE 121: 490–493.

Guo, J. (2012). Pier scour in clear water for sediment mixtures. Journal of Hydraulic Research 50(1): 18–27.

Hager, W. (1999). “Wastewater Hydraulics: Theory and Practice.” Springer: Berlin, New York.

Hains, D., Zabilansky, L.J. and Weisman, R.N. (2004) An experimental study of ice effects on scour at bridge piers. Cold Regions Engineering and Construction Conference and Expo, (16–19 May 2004, Edmonton, Alberta).

Kothyari, U. C., Garde, R. C. J., and Ranga Raju, K. G. (1992). Temporal variation of scour around circular bridge piers. Journal of Hydraulic Engineering, 118(8), 1091-1106.

Khwairakpam, P., Ray, S. S., Das, S., Das, R., and Mazumdar, A. (2012). “Scour hole characteristics around a vertical pier under clear water scour conditions”. ARPN J. Eng. Appl. Sci, 7(6), 649-654.

Li, S. S. (2012). Estimates of the Manning's coefficient for ice-covered rivers. In Proceedings of the Institution of Civil Engineers-Water Management (Vol. 165, No. 9, pp. 495-505). Thomas Telford Ltd.

Mays, L. W. (Ed.). (1999). Hydraulic design handbook. McGraw-Hill Professional Publishing

Melville, B. W., and Raudkivi, A. J. (1977). Flow characteristics in local scour at bridge piers. Journal of Hydraulic Research, 15(4), 373-380.

Melville, B. W., and Sutherland, A. J. (1988). Design method for local scour at bridge piers. Journal of Hydraulic Engineering, 114(10), 1210-1226.

Mao L., Cooper, J. and Frostick, L. (2011). Grain size and topographical differences between static and mobile armour layers. Earth surface Processes and Landforms, 36(10), 1321-1334.

Melville, B. W. and Coleman, S. E. (2000). Bridge scour. Water Resources Publication.

Muzzammil, M., and Gangadhariah, T. (2003). The mean characteristics of horseshoe vortex at a cylindrical pier. Journal of Hydraulic Research, 41(3), 285-297.

Richardson, E., and Davis, S. (2001). Evaluating scour at bridges, 4th edition. Publication No. FHWA NHI 01-001. p380.

Richardson, E. V., Harrison, L. J., Richardson, J. R., and Davis, S. R. (1993). Evaluating scour at bridges (No. HEC 18 (2nd edition)).

Raudkivi, A. J., and Ettema, R. (1983). Clear-water scour at cylindrical piers. Journal of Hydraulic Engineering, 109(3), 338-350.

Sui, J., Wang, D., and Karney, B. (2000). Sediment concentration and deformation of riverbed in a frazil jammed river reach, Canadian Journal of Civil Engineering, 27(6): 1120-1129.

Sui, J., Wang, J., Yun, H. E., and Krol, F. (2010). Velocity profiles and incipient motion of frazil particles under ice cover. International Journal of Sediment Research, 25(1), 39-51.

Török, G. T., Baranya, S., Rüther, N., and Spiller, S. (2014). Laboratory analysis of armor layer development in a local scour around a groin. In Proceedings of the International Conference on Fluvial Hydraulics River Flow, Lausanne EPFL, Lausanne, Switzerland (pp. 3-5).

Wu, P., Hirshfield, F., Sui, J., Wang, J., and Chen, P. P. (2014). “Impacts of ice cover on local scour around semi-circular bridge abutment. Journal of Hydrodynamics”, 26(1), 10-18.

Wu, P., Hirshfield, F., and Sui, J. (2015). Armour layer analysis of local scour around bridge abutments under ice cover. River research and applications, 31(6), 736-746.

Zhang, H., Nakagawa, H., and Mizutani, H. (2012). Bed morphology and grain size characteristics around a spur dyke. International Journal of Sediment Research, 27(2), 141-157.

Zabilansky, L. J., Hains, D. B., and Remus, J. I. (2006). Increased bed erosion due to ice. In Current Practices in Cold Regions Engineering (pp. 1-12).

3.3. Effects of ice cover on the incipient motion of bed material and shear stress around side-by-side bridge piers

An alluvial river bed is likely to experience continuous changes over time. In one case, flowing water erodes, moves and gradually collects sediment in the river, modifying its bed elevation and slightly changing its boundaries. Changes in bed elevation could be resulted from either natural processes or human activities which lead to alteration of the river bed or river geometry (Chiew, 1987). Placement of bridge piers inside the river is one of the most common engineering practices in which the bridge pier is in direct contact with the flowing water. The main issue associated with the interaction of flowing water and the bridge pier is the scouring process which occurs around the bridge piers and is known as local scour. According to Shen et al (1969), local scour is the abrupt decrease in bed elevation near a pier due to erosion of bed material by the local flow structure caused by the pier. Overlooking the local scour phenomenon in the bridge pier design might possibly result in either a huge financial cost or a high casualty rate. According to Briaud et al (2006), 1502 bridges collapsed due to bridge scour between 1966 and 2005 in the United States, with an average rate of one bridge collapse every 10 days. Wardhana and Hadipriono (2003) studied 500 cases of bridge structure failures between 1989 and 2000 in the United States and stated that the most common causes of bridge failures were due to floods and scouring process. Due to its inherent importance, local scour has been studied extensively by many researchers (such as: Ettema, et al, 2011; Graf and Istiarto, 2002; Kothyari, 1992; Melville and Raudkivi, 1977; Melville and Sutherland, 1988; Raudkivi and Ettema, 1983; Yanmaz and Altimbilek, 1991). Melville and Raudkivi (1977) investigated the flow patterns, distributed turbulence intensity and boundary shear stresses in the scour zone. The main results concerned the flow patterns in vertical and horizontal planes, the turbulence intensity and the bed shear stress distribution.

A significant limitation of Melville and Raudkivi's work was that the bed sediments had a uniform grain size which is not an appropriate representative of bed material in natural rivers; this is also the case in most of the experimental studies. Also, most of the reported studies regarding the maximum scour depth around bridge piers have been done in small-scale laboratory flumes under open flow condition. This can result in tremendous conservative results. Up to date, research work regarding local scour around bridge pier under ice-covered flow condition is very limited, primarily due to the difficulties in obtaining field data from ice-covered rivers. Ice cover presence adds a level of complexity to hydraulic processes in rivers, and sometimes extremely influences river characteristics such as hydrodynamics and morphology (Ettema and Zabilansky, 2004). When ice floes move discretely and freely (for example, in the case of low surface concentrations of ice pans during freeze-up), the resistance effect caused by flowing ice is slight and water levels do not modify greatly (Wang, et al, 2008). In practice, ice cover appears quite often in rivers in the cold regions during the winter. From the hydraulics point of view, the presence of an ice cover increases the wetted perimeter by adding an additional boundary to the water surface.

Under ice-covered flow conditions, the flow is highly sensitive to the friction parameter (Hoque, 2009). Ackermann et al (2002) did a laboratory investigation on the effect of ice cover on local scour around circular bridge piers. Their results showed that for equivalent averaged flow velocities, the existence of an ice cover could increase the local scour depth scour by 25% to 35 % from the free surface condition. Bacuta and Dargahi (1986) carried out laboratory tests in a flume with a simulated ice cover for clear-water conditions. They found the extent of scour is larger for ice-covered flows. Besides, the appearance of an ice cover in river changes the velocity profile (Sui et al., 2010a). Under ice-covered flow

condition, the upper portion of the flow is mainly affected by the ice cover resistance while the lower portion of flow is primarily influenced by the channel bed resistance (Sui et al., 2010a). The maximum flow velocity under ice cover is located somewhere between the channel bed and ice cover depending on the ratio of the ice resistance coefficient to the bed resistance coefficient (Crance and Frothingham, 2008). According to Wang et al. (2008), it is expected that as the ice resistance increases, the maximum flow velocity will move closer to the channel bed. Since ice cover imposes an additional solid boundary on the flow, the incipient motion of sediment under ice-covered flow condition is different from that under open channel flow condition. Wang et al. (2008) also studied the impacts of flow velocity and water depth on the incipient motion of bed material under ice-covered condition. It was found that the deeper the flow depth under ice cover, the higher the flow velocity needed for the incipient motion of bed material. One of the main objectives of the studies on local scour process is to help river engineers to predict the incipient motion of bed material. On the other side, the development of an armour layer in the scour hole around bridge piers is associated with incipient motion of sediment particles. Bed armouring process typically occurs in streams with non-uniform bed materials. This phenomenon occurs mainly due to selective erosion process in which the bed shear stress of finer sediment particles exceeds the associated critical shear stress for movement. Consequently, finer sediment particles are transported and leave coarser grains behind. Through this process, the coarser grains get more exposed to the flow while the remaining finer grains get hidden among larger ones (Mao et al, 2011). Armour layer is also partially due to the reduced exposure of the flow with those sediments inside the scour hole zone (Sui et al., 2010b). For the same bed sediments, Dey and Raika (2007) found that the scour depth around bridge piers with an armour layer

is less than that without armour layer. Froehlich (1995) stated that the thickness of the natural armour-layer is up to one to three times the particle grain size of armour-layer. Raudkivil and Ettema, (1983) found that due to the local flow structure around a pier, local scour may either develop through the armour layer and into the finer, more erodible sediment, or it may trigger a more extensive localized type of scour caused by the erosion of the armour layer itself. Sui et al (2010b) studied clear-water scour around semi-elliptical abutments with armoured beds. The results showed that for any bed material having the same grain size, with increase in the particle size of armour-layer, scour depth will decrease. In terms of hydraulic engineering design, determination of the critical condition for incipient motion of sediment and the sediment transport rate is highly crucial. To study the incipient motion of sediment particle, the Shields diagram (Shields 1936) is widely accepted. It is a graph of boundary shear stress non-dimensionalized by the submerged specific weight and the mean size of the sediment particle which is called the Shields parameter, Shields criterion, Shields number or dimensionless shear stress (τ_c*) against the boundary Reynolds number (Re*) (Miller, et al., 1977). According to Shields (1936), the critical conditions in which sediment is on the verge of becoming entrained can be determined by relating the critical Shields value (τ_c*) and the shear Reynolds number (Re*). The boundary shear Reynolds number is defined as follows:

$$\mathrm{Re}^* = \frac{U^* D_i}{\nu} \qquad (3\text{-}3\text{-}1)$$

Where, D_i *is* the grain size diameter, v is the kinetic viscosity of fluid, and U* is shear velocity. In this study, since the applied bed materials are composed of non-uniform natural sediment, the particle grain size is not constant. Therefore, the median grain size of non-uniform sand (D_{50}) is used to represent the particle size for calculating the critical shear Reynolds number. The shear velocity (U*) in Eq. 3-3-1 can be determined as follows:

$$U^* = \sqrt{gRS} \tag{3-3-2}$$

Where, S is the channel slope, R is the hydraulic radius and g is the gravitational acceleration. The dimensionless shear stress is used to calculate the initiation of sediment motion in a fluid flow (Madsen, 1991). The critical dimensionless shear stress (τ_c*) is defined as follows:

$$t_c^* = \frac{r U_c^{*2}}{(r_s - r) g D_{50}} = \frac{t}{(r_s - r) g D_{50}} \tag{3-3-3}$$

In which, ρ_s and ρ are the mass density of sediment and water, respectively, and U^*c is the critical shear velocity that initializes the motion of the particles. In general, the theoretical prediction of the critical condition for incipient motion is based on a force or momentum balance between the destabilizing hydrodynamic drag (F_D) and lift forces (F_L) against the resisting gravitational (W) and frictional forces (F_R). Sediment particle will be moved if the applied forces overcome the resistance force. At the threshold of movement, the applied forces are just in balance with the resisting force (Chang, 1988). In other words, a sediment particle is at a state of incipient motion when the following conditions have been satisfied:

$$\begin{aligned} F_D &= F_R \sin\alpha \\ W &= F_L + F_R \cos\alpha \end{aligned} \tag{3-3-4}$$

The submerged weight of the particle can be given by:

$$W = \frac{\pi d^3}{6}(\rho_s - \rho)g \tag{3-3-5}$$

Where d is sediment size in the armor layer. Apart from geometric details such as bed slope, particle exposure and pocket geometry, accurate prediction of incipient motion requires precise knowledge of the hydrodynamic drag (F_D) and lift forces (F_L) acting on the particle. By using Yang's criteria (2003) for incipient motion, the drag force can be expressed as:

$$F_D = C_D \frac{\pi d^2}{4} \frac{\rho}{2} V_s^2 \tag{3-3-6}$$

where, C_D is the drag coefficient at velocity V_s, and V_s is the local velocity at a distance of "s" above the bed. The lift force acting on the particle can be obtained as:

$$F_L = C_L \frac{\pi d^2}{4} \frac{\rho}{2} V_s^2 \tag{3-3-7}$$

Where C_L is the lift coefficient at velocity V_s. Meyer-Peter and Mueller (1948) proposed the following equation to calculate the sediment size in the armor layer.

$$d = \frac{SH}{K_1 (n / D_{90}^{1/6})^{3/2}} \tag{3-3-8}$$

where, d is the grain size in the armor layer; S is the channel slope; H is the mean flow depth; K_1 is the constant number equal to 0.058 when H is in meters; n is the channel bottom roughness or Manning's roughness, and D_{90} is the bed material size where 90% of the material is finer. To calculate the critical bed shear velocity in Eq. 3-3-3, Eq. 3-3-9 which is developed based on the "Law of wall method" can be used. The Law of wall method was originally proposed by von Kármán (von Kármán 1930) and supposed that the velocity profile in the lower portion of an open channel flow has a logarithmic distribution (Barenblatt and Chorin, 1997).

$$U_c^* = \frac{\bar{u}\, k}{Ln\left(z / z_0\right)} \tag{3-3-9}$$

In which, $\bar{u}$ is the average cross-section flow velocity, k is the Von Karman's constant which is supposed to be 0.4, z represents the distance from channel bed which is supposed to be depth of water, and z_0 is the roughness height which is supposed to be D_{50} of the sediment particles. Due to the presence of U_c^* in both axes of the Shields diagram, Madsen

and Grant (1977) introduced a new variable rather than the shear Reynolds number in the horizontal axis of the Shields diagram which is called the sediment-fluid parameter (S^*). The sediment-fluid parameter (S^*) can be calculated from the following equation:

$$S^* = \frac{D_{50}}{4\nu}\sqrt{(SG-1)gD_{50}} \tag{3-3-10}$$

In which, SG represents the specific weight of sediment.

Of note, since an additional boundary is added to the water surface for the case of ice-covered flow condition, hydraulic radius (R) is different from that of the open channel condition. Therefore, an empirical equation introduced by (Tang and Davar 1985) which is for hydraulic radius estimation, has been adopted for various covered conditions including open water to completely covered flow regimes. The equation can be stated as follows for rectangular channels:

$$R = \frac{y_0\, w}{2y_0 + w\left(1 + a/100\right)} \tag{3-3-11}$$

Where, y_0 is the flow depth, w is the channel width, and a is the percentage of the cover. In an ice-covered channel, the stream flow cross section can be split into two parts: the lower part dominated by the bed and the upper part dominated by the ice cover (Larsen, 1969). Ashton (1986) stated that ice cover presence increases the total channel hydraulic resistance due to the extra resistance of the upper boundary layer induced by the ice cover. The location of maximum velocity defines the interface between the upper ice zone and lower bed zone. In the current study, since the channel-bed and sidewalls have inhomogeneous roughness, the channel becomes a composite channel. Presence of an ice cover complicates the exact estimation of the resistance to flow as it causes the flow regime to change from open water flow to partially covered and finally to the fully covered flow. Several researchers have tried

to estimate flow resistance directly using field observations. Some researchers have provided empirical or semi-empirical methods in composite resistance estimations (Shen and Yapa, 1986; Smith and Ettema, 1997; Davar et al., 1998; Beltaos, 2009). In this paper the method presented by Larsen (1969) is employed. The Larsen method can be written as follows:

$$n_c = \frac{0.63\, n_b \left(y_i / y_b + 1\right)^{5/3}}{\left(n_b / n_i\right)\left(y_i / y_b\right)^{5/3} + 1} \qquad (3\text{-}3\text{-}12)$$

Where, y_i and y_b are the total depths of the ice and bed zones, respectively; n_c, n_b and n_i are the Manning roughness coefficients for total cross section, upper ice-cover (*i*) and lower bed (*b*) boundary layers, respectively. In terms of n_i of smooth ice-covered flow, as pointed out by Mays (1999), due to a relatively smooth concrete-like surface of the Styrofoam panel, the roughness of the model smooth ice-cover was assumed to be 0.013. In terms of n_i of rough ice-cover, Li (2012) proposed the following equation which can be used depending on the size of the small cubes:

$$\frac{n_i}{K_S^{1/6}} = \frac{(8g)^{-1/2}\left(R/K_S\right)^{1/6}}{0.867 \ln\left(12R/K_S\right)} \qquad (3\text{-}3\text{-}13)$$

In which, *Ks* is the average roughness height of the ice cover underside and R is the hydraulic radius.

The transportation process of uniform sediment has been broadly studied and the mechanism of sediment transport has been well discussed (Aguirre-Pe et al, 2003; Montgomery and Buffington, 1997; Schvidchenko and Pender, 2000; Yalin and Karahan, 1979). However, the knowledge for estimating the non-uniform sediment transport is still limited. Moreover, results of laboratory experiments using uniform sediment is not an appropriate representative of natural river systems since bed materials in natural riverbeds are non-uniform and

composed of sediment particles with different grain-size. During the movement process of non-uniform sediment, the coarse grains are easier to be entrained than the same particle size of uniform sediment, because they have higher probabilities to be exposed to the flow. On the other hand, the finer grain tends to be hidden beneath the coarse grains (Huang et al, 2015). One of the earliest researches regarding the calculation of the bed load transport rate in a non-uniform riverbed was done by Einstein (1950). In his proposed bed-load function, he used a comprehensive hiding factor to represent the interaction effects between the coarse particles and the fine particles. Ever since, several researchers have developed formulae to determine the incipient motion of non-uniform sediment mixtures (Andrews, 1983; Dey and Debnath, 2000; Egiazaroff, 1965; Kuhnle, 1993; Nakagawa et al, 1982; Patel and Ranga Raju, 1999; Xu et al., 2008). For instance, Xu et al (2008) studied the incipient velocity of non-uniform sediment. As pointed out by Xu et al (2008), the incipient velocity for the coarse particles of the non-uniform sediment is less than that for same particle size of uniform sediment, and the incipient velocity for the finer particles of the non-uniform sediment is greater than that for the same particle size of uniform sediment.

The primary objective of this study is to investigate the features of the incipient motion of three non-uniform sediments under ice-covered conditions by comparing to those of under open channel flow conditions, and to identify the effects of flow roughness caused by ice cover on the incipient motion of non-uniform sediment

3.3.1. Experimental setup

Experiments were carried out in a large-scale flume at the Quesnel River Research Centre of the University of Northern British Columbia. The flume is 38.2 m long, 2 m wide and 1.3 m deep, as shown in Figure 3-29a. The longitudinal slope of the channel bed is 0.2 percent. A

holding tank with a volume of 90 m^3 is located at the upstream of the flume to keep a constant discharge during each experimental run. To create different velocities, three valves are connected to adjust the amount of water into the flume. Two sand boxes are filled with natural non-uniform sediment. Theses sand boxes are spaced 10.2 m away from each other and are 0.30 m deep and 5.6 m and 5.8 m in length, respectively. Three types of non-uniform sediments with different gain sizes are used in this experimental study. The median grain sizes of three natural non-uniform sediments are 0.50 mm, 0.47 mm and 0.58 mm with the geometric standard deviation (σ_g) of 2.61, 2.53 and 1.89, respectively. According to Dey and Barbhuiya (2004), sediments used in this study can be treated as non-uniform since σ_g is larger than 1.84. Most of the studies on local scour have been limited to only single piers under open flow condition and provide detailed information around single piers. However, practically, due to geotechnical and economic reasons, bridge designs are often constructed in complex piers or pier group arrangements in which the direct application of the results derived from local scour around single piers may be problematic and not applicable. In this study, four pairs of bridge piers with different diameters of 60 mm, 90 mm, 110 mm and 170 mm have been used. Of note, that the piers are vertical, non-sloping. Inside each sand box, a pair of bridge piers was placed symmetrically to the center line of the flume. The distance from the center line of each pier to the flume center is 0.25 m, as illustrated in Figure 3-29b. In order to avoid the bed material from initial erosion, the water depths were increased gradually and when the water overflowed from the top of the tailgate, the volumetric discharge was increased to the desired amount. Flow velocity ranges from 0.07 m/s to 0.27 m/s. In front of the first sand box, a SonTek incorporated 2D Flow Meter was installed to measure flow velocities, flow discharge and water depth during each experiment run. A staff

gauge was also installed in the middle of each sand box to manually verify water depth. Velocity fields in scour holes were measured using a 10-MHZ Acoustic Doppler Velocimeter (ADV). The ADV is a high-precision instrument that can be used to measure 3D flow velocity in a wide range of environments including laboratories, rivers, estuaries, and the ocean (Cea et al., 2007). The Styrofoam panels which were used to model ice cover, had covered the entire surface of flume. Figure 3-30a shows the entire experimental model with the ice cover and Figure 3-30b shows the ADV measurement around the scour hole. In the current study, two types of model ice cover were used, namely smooth cover and rough cover. The smooth cover was the surface of the original Styrofoam panels while the rough cover was made by attaching small Styrofoam cubes to the bottom of the smooth cover. The dimensions of Styrofoam cubes were 25 mm × 25 mm × 25 mm and spaced 35 mm apart. Since the flow in the rivers is normally subcritical flow, especially when the water surface is covered by ice, it does not have a very high velocity value in which live-bed scour occurs. Therefore, it was decided to do the experiments under clear water conditions. Each experiment run lasted 24 hours. Afterward, the flume was gradually drained, and the scour and deposition pattern around the piers was measured using manual calipers. To accurately read the scour depths at different locations and to draw the scour hole contours, the outside perimeter of each bridge pier was equally divided and labeled as the reference points. The scour contours were plotted by using Surfer 13 (Golden Software). The measurement of the scour hole was subject to an error of +/-0.3 mm. After each experiment, sand samples within the scour hole which represent the composition of the armour layer were collected. The samples were taken from the top layer of 5 mm of the armour layer in each scour hole. The sampling process is followed the sampling methodology for collecting armour samples

proposed by Bunte and Abt (2001). The collected sand samples were eventually sieved and the mediums grain size of the armour layer (D_{50}) were determined. In total, 108 experiments were done, namely, 36 experiments for each sediment type. For each sediment type, 12 experiments were done under open flow condition, 12 experiments under smooth ice-covered flow condition and 12 experiments under rough ice-covered flow condition, respectively. Table 3-3 shows the experimental values obtained regarding incipient motion of sediment particles for D_{50}=0.50 mm. Of note, in the current study, the motion of the sediment was observed through the transparent window of the flume. The layers of sediment could easily be moved when the critical value was reached. It was observed from the transparent window that the sediment particles were moved by saltation (bouncing) and by traction (being pushed along by the force of the flow).

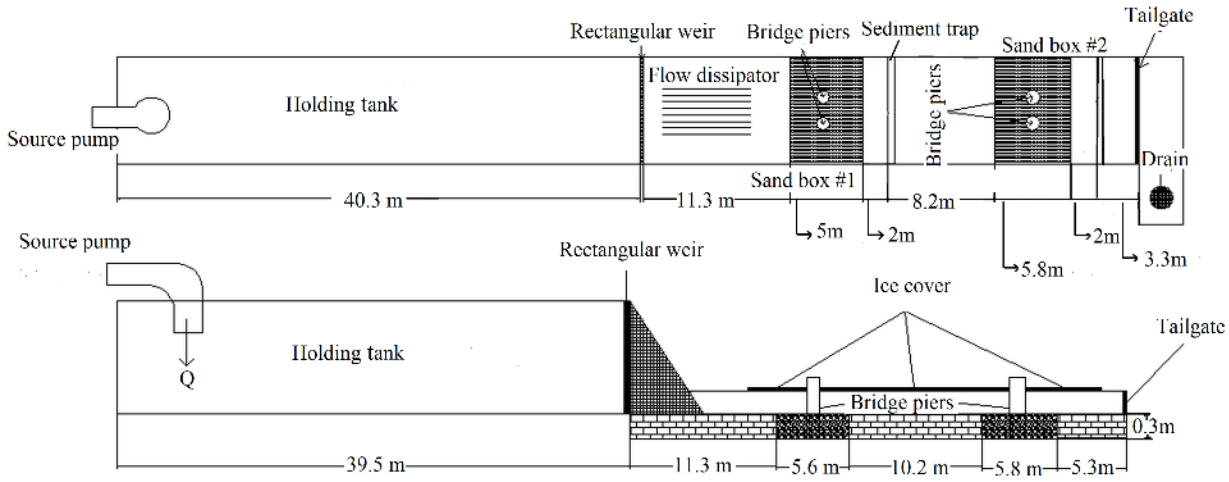

Figure 3-29a: Plan view and vertical view of experiment flume

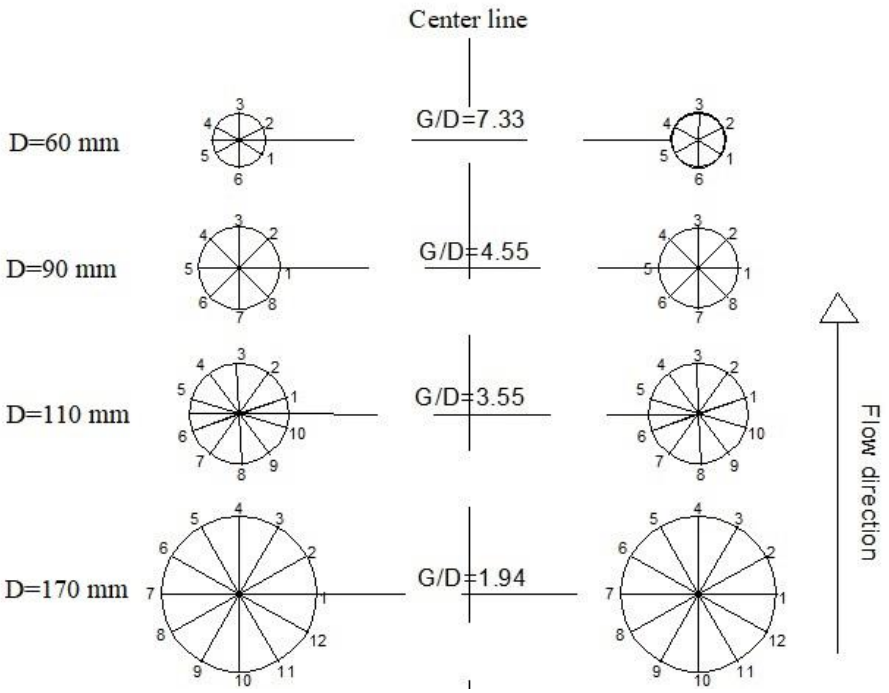

Figure 3-29b: The spacing ratio and measuring points around the circular bridge piers

Figure 3-30a: Downstream view of the entire experimental model with the ice cover

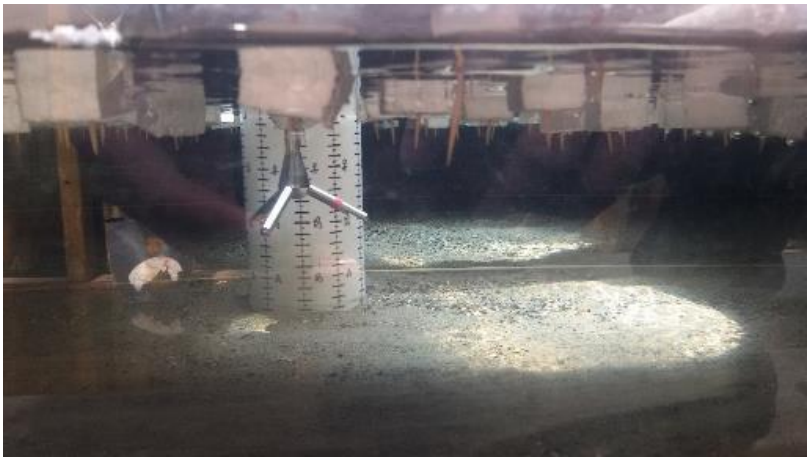

Figure 3-30b: The ADV measurement around the bridge piers under rough ice-covered condition

3.3.2. Results and discussions

- **Effect of pier spacing distance on the scour patterns**

Multiple bridge piers have become more common in recent years in bridge design for geotechnical and economic reasons. These types of pier not only can significantly reduce construction costs but also are more practical and efficient (Ataie-Ashtiani & Beheshti, 2006). However, the mechanisms of the scouring process around pier groups are much more complex. According to Hannah (1978), if the pier spacing ratio is 0.25, the maximum scour depth around side-by-side piers is about 50% more than that around a single pier and for G/D < 0.25, the two side-by-side piers can be assumed to act as a single bridge pier (where G represents the bridge spacing distance and D represents the pier diameter). Ataie-Ashtiani and Beheshti (2006) investigated local scour for different pier arrangements and with different bridge pier spacings. It was found that with an increase in the pier spacing distance between two piers, scour depth is reduced. To the authors' knowledge, all reported research regarding local scour around pier groups has been done under open channel flow conditions (Ataie-Ashtiani & Beheshti, 2013; Hannah, 1978; Melville & Coleman, 2000). As pointed out by Ettema et al. (2011), the impact of ice cover on bridge pier scour is still unknown and

needs further investigation. In this regard, a more in-depth study has been done here to investigate the impact of ice cover on local scour around four pairs of side-by-side bridge piers under different sediment compositions and flow conditions. Figure 3-31a shows the ratio of the maximum scour depth to the depth of approaching flow (y_{max}/y_0, termed as relative MSD) against the ratio of pier spacing distance to pier diameter (G/D, termed as bridge pier spacing ratio) for D_{50} = 0.50 mm. Of note, the maximum scour depth between left hand side and the right-hand side bridge piers were more or less identical. In Fig. 3-31a, the Froude number ranges from 0.072 to 0.270 and G/D ranges from 3.54 to 7.33. As indicates in Figure 3-31a, the relative MSD decreases with the increase in G/D. Also, for the same bridge pier spacing ratio (G/D) and for the same sediment, the relative MSD under open channel flow conditions is the lowest, and the relative MSD under the rough covered flow reaches the highest. Figure 3-31b shows the changes of the pier Reynold number (Re_b) with the pier spacing ratio (G/D) for D_{50} = 0.50 mm. The pier Reynolds number is defined as:

$$\mathrm{Re}_b = \frac{UD}{\nu} \tag{3-3-14}$$

Where, U is the average velocity of the approaching flow and v is the kinematic viscosity. As shown in Figure 3-31b, the pier Reynold number (Re_b) decreases with the increases in G/D. Hopkins et al. (1980) stated that the strength of the horseshoe vortex system is a function of the pier Reynolds number (Re_b). Therefore, it can be concluded that the strength of horseshoe vortices, which is a function of Re_b, decreases with the increase in the pier spacing ratio. Namely, the smaller the pier size (D) and the larger the pier spacing (G), the weaker the horseshoe vortices around bridge piers, which will result in shallower scour

depths around the pier group. According to Figure 3-31b, under the same flow condition (velocity and flow depth), the lowest pier Reynolds number (Re_b) occurred under the open channel flow conditions, and the highest pier Reynolds number (Re_b) occurred under rough covered flow condition. However, with an increase in the pier spacing ratio, the pier Reynolds number under rough covered flow conditions, gets closer to those of the smooth covered and open channel flow conditions, implying that the influence of ice cover on pier Reynolds number diminishes as the pier spacing distance increases.

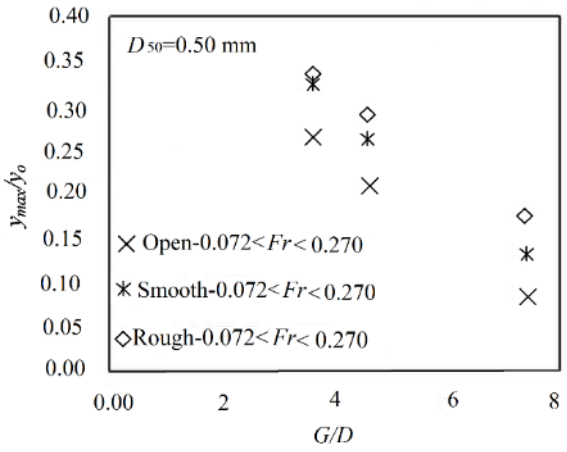

Figure 3–31a: Relative MSD (y_{max}/y_0) against pier spacing (G/D) under open channel, smooth, and rough covered flow conditions (D_{50} = 0.50 mm).

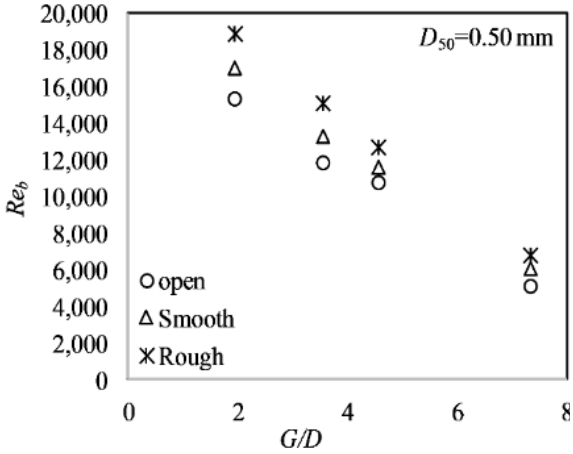

Figure 3–31b: Variation of pier spacing (G/D) with respect to pier Reynolds number (Re_b).

- **Shear stress vs. sediment-fluid parameter for the incipient motion of sediment**

To the authors' knowledge, shear stress against sediment-fluid parameter for the incipient motion of sediment under ice-covered flow conditions have not been studied. This information will give a better insight to the hydraulic engineers in terms of sediment incipient motion under ice-covered condition. In Figure 3-32, the relationship between [$S^*(U/U^*)$] and the dimensionless shear stress (τ^*) is given for channel bed for those three non-uniform sediments. Of note, U is the mean velocity of approaching flow (m/s); U^* is the shear velocity

(m/s) and S^* is the sediment-fluid parameter. For each type of the sediment, the sediment-fluid parameter (S^*) is unique and the dimensionless shear stress increases with the increase in [$S^*(U/U^*)$] correspondingly. Also, for all three sands, the larger the [$S^*(U/U^*)$], the greater the dimensionless shear stress for the incipient motion of bed material. For the same [$S^*(U/U^*)$], the finer the sediment, the higher the dimensionless shear stress. Of note, Eq. 3-3-3 in conjunction with Eq. 3-3-9 are used to calculate the dimensionless shear stress.

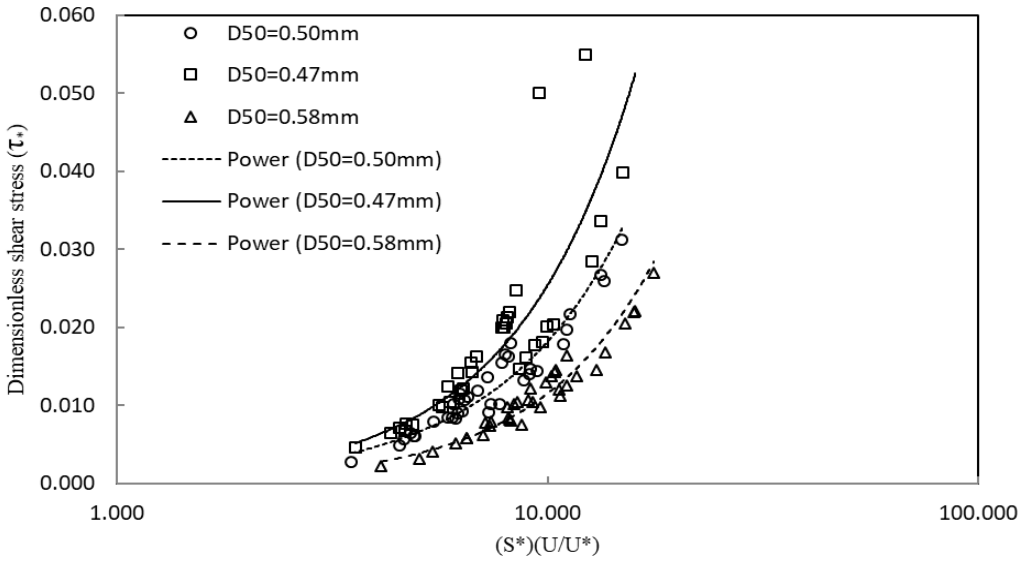

Figure 3-32: Dimensionless shear stress (τ*) vs S*(*U/U**)

- **Dimensionless shear stress (τ*) vs. shear Reynolds number (Re*) for the incipient motion of sediment**

The relationship between the dimensionless shear Reynolds number and the dimensionless shear stress for the incipient motion of the coarsest sediment (D_{50}=0.58 mm) and that of the finest sediment (D_{50}=0.47 mm) under both open flow and rough ice-covered flow conditions have been shown in Figure 3-33. From Figure 3-33, the following results can be drawn:

1) With the increase in the dimensionless shear Reynolds number, the dimensionless shear stress increases correspondingly. For all three sands, the larger the dimensionless shear Reynolds number, the greater the dimensionless shear stress for the incipient motion of bed

material. However, for the same dimensionless shear stress, the dimensionless shear Reynolds number for the finer sediment is lower for the incipient motion of sediment particles.

2) In terms of the impacts of ice cover on the incipient motion of bed material, for the same grain size of sediment, the dimensionless shear stress is lower under rough ice- covered flow condition, implying that the threshold of the dimensionless shear stress for the incipient motion of bed material under rough ice-covered flow condition is lower than that under open flow conditions.

Of note, Wang et al (2008) also studied dimensionless shear stress (τ^*) against shear Reynolds number (Re^*) for the incipient motion of sediment under ice-covered condition. Their result showed that for bed material of same grain size, the larger the shear Reynolds number, the greater the dimensionless shear stress for the incipient motion of bed material. For the same dimensionless shear stress, the finer the particle, the lower the shear Reynolds number for the incipient motion of sediment.

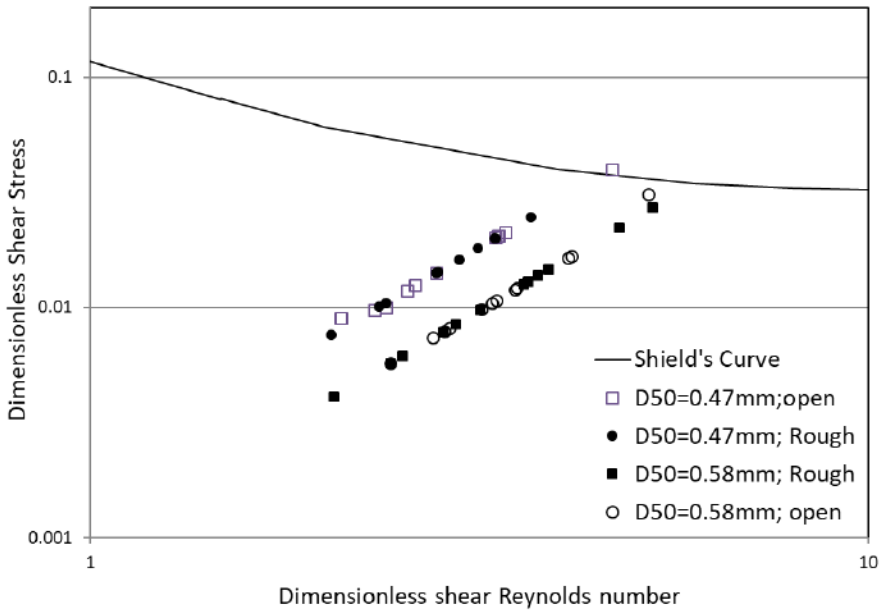

Figure 3-33: Dimensionless shear stress (τ*) vs. shear Reynolds number (Re*) for the incipient motion of the finest sediment (D_{50}=0.47 mm) and the coarsest sediment (D_{50}=0.58 mm) under open and rough ice-covered flow conditions

- **Shear stress vs. densimetric Froude number for incipient motion of bed material**

Aside from the Shields parameter which is used to describe the incipient motion of the sediment particles, the densimetric Froude number is another important variable used to describe hydraulic condition of bed material (Aguirre-Pe et al., 2003). The densimetric flow Froude number is defined as follows:

$$Fr_0 = \frac{U}{\sqrt{g D_{50}\left(\rho_s - \rho\right)/\rho}} \qquad (3\text{-}3\text{-}15)$$

In which, U represents the mean velocity of the approaching flow. Since the distribution of flow velocity under ice covered condition is different from that of under open channel condition, the boundary conditions of flow significantly affect the incipient motion of bed material. The relationship between the densimetric Froude number and the dimensionless shear stress is shown in Figure 3-34a and Figure 3-34b. The main reason for presenting Figure 3-34 is to show how the dimensionless shear stress and the densimetric Froude

number correlate to each other under different cover conditions (open flow or free cover, smooth covered and rough covered conditions) and different grain size of bed materials. Following results can be observed from Figure 3-34

1) The dimensionless shear stress increases with the increase in the densimetric Froude number. As showed in Figure 3-34a, for the same densimetric Froude number, a lower dimensionless shear stress can initiate motion of the finest sediment type (D_{50}=0.47 mm). Besides, under the same dimensionless shear stress, the densimetric Froude number for the coarser sediment (D_{50}=0.58 mm) is lower. In other words, a larger particle requires more kinetic energy to be moved. Namely, the larger the particle, the more densimetric Froude number is needed for the incipient motion of bed material. This result is in good agreement with the study of Wang et al (2008).

3) With the same dimensionless shear stress for the incipient motion of bed material, the values of the densimetric Froude number under open flow condition are slightly smaller than that under ice-covered flow condition which is more distinct for higher values. The reason for this is that under ice-covered condition, both the bed roughness and ice cover roughness affect both the flow velocity distribution and the densnimetric Froude number. Wang et al (2008) also stated that for the same bed material, the more the roughness coefficient of ice cover, the less the densimetric Froude number for incipient motion of bed material, since a larger roughness coefficient of ice cover leads to an increased near-bed velocity. And thus, it can move larger particles.

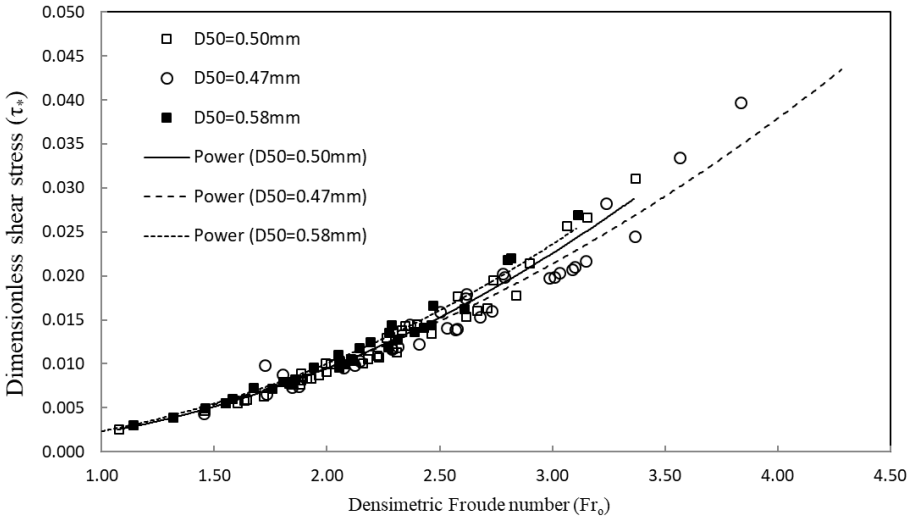

Figure 3-34a: Variation of the dimensionless shear stress against the densimetric Froude number classified by particle grain size

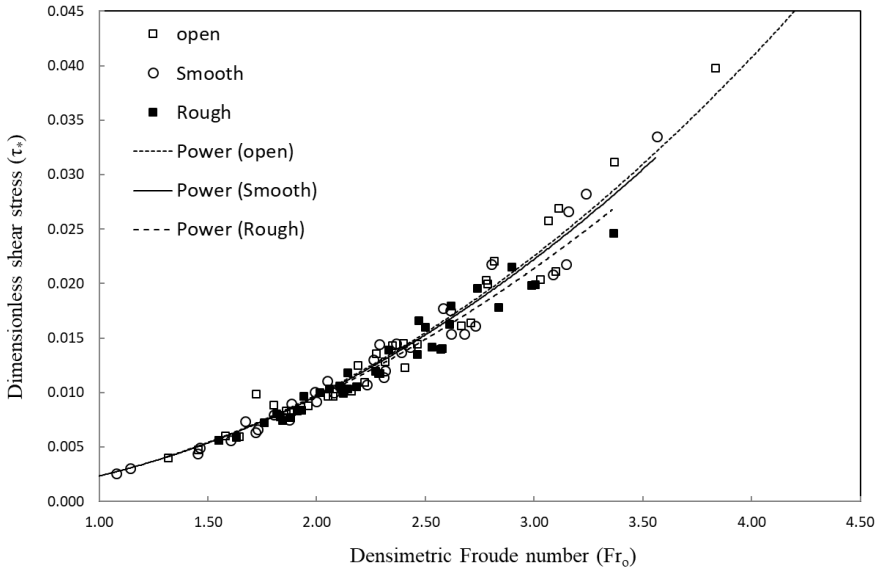

Figure 3-34b: Variation of the dimensionless shear stress against the densimetric Froude number classified by cover conditions for flow

- **Shear Reynolds number vs. densimetric Froude number for the incipient motion of bed material**

To the authors' knowledge, shear Reynolds number against the densimetric Froude number for the incipient motion of sediment under ice-covered flow conditions have not been studied. Results of present study will give a better insight to the hydraulic engineers in terms of

understanding the incipient motion of sediment under ice-covered condition. The variation of the densimetric Froude number against the shear Reynolds number is shown in Figure 3-35. Results indicate that the dimensionless shear Reynolds number increases with the increase in the densimetric Froude number, correspondingly. For the same densimetric Froude number, the dimensionless shear Reynolds number for the coarser sand (D_{50}=0.58mm) is higher. In other words, the larger the grain size of sediment, the higher the dimensionless shear Reynolds number for the incipient motion of bed material.

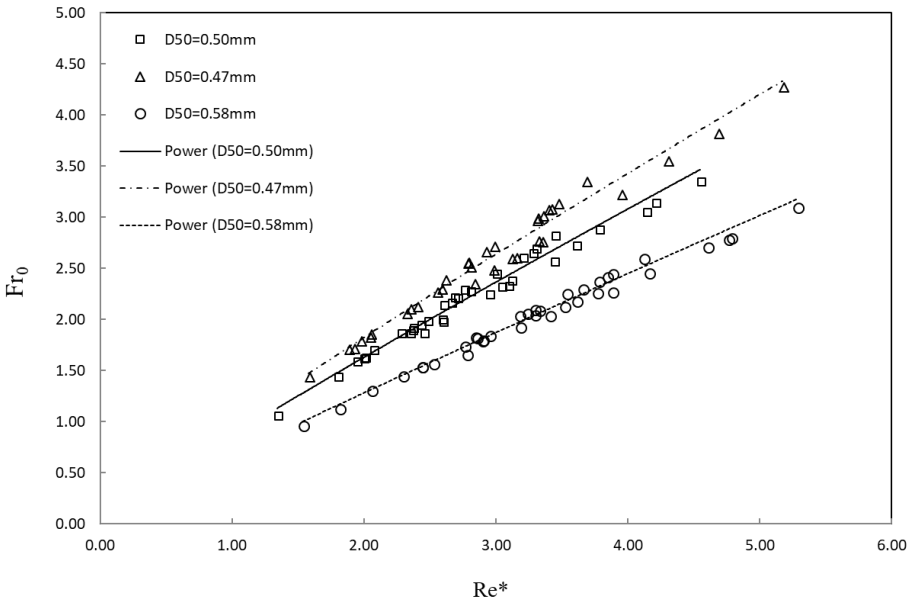

Figure 3-35: Variation of the densimetric Froude number against the dimensionless shear Reynolds number classified by particle grain size

- **Shear stress vs. dimensionless transport-stage parameter for the incipient motion of bed material**

To the authors' knowledge, the shear stress against the dimensionless transport-stage parameter for the incipient motion of sediment under ice-covered flow conditions have not been investigated. Van Rijn (1984) found that the movement of bed load material is a function of the dimensionless transport-stage parameter which is defined as follows:

$$T = \frac{(U^*)^2 - (U_c^*)^2}{(U_c^*)^2} \qquad (3\text{-}3\text{-}16)$$

Figure 3-36 shows the relationship between the dimensionless shear stress (τ_*) and the dimensionless transport-stage parameter (T). The following results have been drawn:

1) With the increase in the dimensionless shear stress, the dimensionless transport-stage parameter (T) decreases. The decreasing trend of T-value is very sharp when τ_*>0.01. For τ_*<0.01, T-value gradually decreases, and nearly approaches a constant when the scour hole reaches the equilibrium condition at which the armour layer is completely formed and prevents the scour hole from further scouring. In other word, the rate of sediment erosion is faster at the beginning. During the scouring process, an armour layer is gradually developed. This results in the decrease in the rate of sediment erosion until the scour hole reaches equilibrium condition.

2) With the same dimensionless transport-stage parameter, the dimensionless shear stress for the finer the sand is larger. As discussed earlier, sediment particle will get moved when the shear stress acting on it is greater than the resistance of the particle to movement. The greater dimensionless shear stress, the greater the capacity for sediment transport. The resistance of the particle against movement and entrainment is highly dependent on the particle size. Therefore, for finer particles in non-uniform sediment, high dimensionless shear stress values lead to greater sediment transport. On the other hand, for the coarser sediment with the same transport-stage parameter as of the finer sediment, the dimensionless shear stress is smaller, implying that the sediment transport capacity for the coarse sediment is lower. Of note, the difference between results for finer sand and those for coarser sand is not so obvious, since the grain sizes of these 3 sands are not so different.

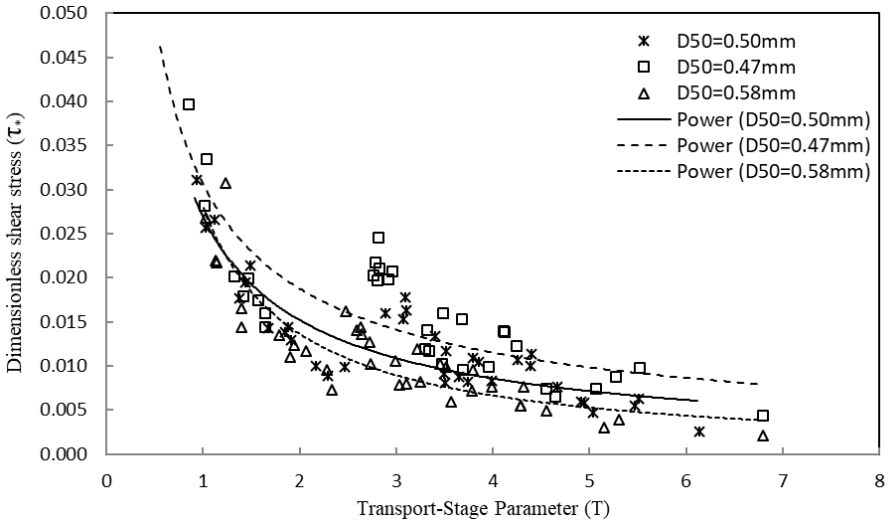

Figure 3-36: Variation of the dimensionless shear stress against the dimensionless transport-stage parameter classified by particle grain size

- **Scour hole velocity profile**

Scour hole velocity profiles were measured for approaching flow depths range from 0.18 m to 0.28 m. For shallow flow depths (less than 0.10 m), scour hole velocity measurements were unable to be conducted due to limitations of the ADV in shallow water. Since the ADV must be located 10 cm from the probe head, the velocity profile does not fully cover up to the water surface. In order to gain an entire velocity profile, it is recommended to use the Sontek's 16 MHz micro ADV that can be used to measure flow velocity 0.05 m from the probe head. Of note, since the ADV functions on the principal of a Doppler shift, the velocity values close to the bed are representative of both sediment and water mixture velocity. Even though clear water scour was achieved, it is impossible to achieve water velocity measurements within 10 mmm of the bed. This was also noted by Muste et al. (2000). Velocity measurements were performed one hour before the end of the experimental run, at which the scour hole was fully developed and stabilized based on the visual observation. Of note, the rate of change of scouring around the bridge pier was too small as it gets closer to the equilibrium scour depth (24 hours). The ADV measures velocity in x, y and z directions.

Therefore, the streamwise velocity component (U_x) is the component of scour hole velocity in the direction of the flow, the span-wise velocity component (U_y) is the component of scour hole velocity in the lateral direction and the velocity component (U_z) is the component of scour hole velocity in the vertical direction. Figure 3-37 shows just U_x scour hole velocity component profile at the upstream face of the 60-mm pier for the finest sand of D_{50}=0.47 mm under both ice-covered and open channel flow conditions. Since the location of maximum flow velocity was important, only U_x is shown in Figure 3-37. In order to be able to generalize the velocity profiles and to compare different velocity profiles under different flow conditions, the depth of flow on the vertical axis has been non-dimensionalized by ratio of vertical distance of the location of ADV measurement from bed (z) to the approaching flow depth (y_0). The streamwise scour hole velocity component (U_x) is also non-dimensionalized divided by the approaching flow velocity (U). Of note, a SonTek incorporated 2D Flow Meter was installed at the upstream of the first sand box to measure flow velocities and water depth. Results showed that, the streamwise velocity distribution follows a reverse C-shaped profile which begins from the scour hole up to the water surface. The same pattern was also reported by Kumar and Kothyari (2011). In terms of velocity magnitude, the streamwise velocity in the scour hole under rough covered condition is generally greater than those under both smooth covered and open flow conditions. Regardless of the cover conditions of flow, the magnitude of velocity is the least in the scour hole. Also, the values of the velocity component are mostly negative within the scour hole which is an indication of the reversal flow happening due to the presence of the horseshoe vortex which is strongest at the pier face. On the other hand, the location of the maximum

velocity is closer to the bed under rough covered flow condition than that under smooth covered flow condition.

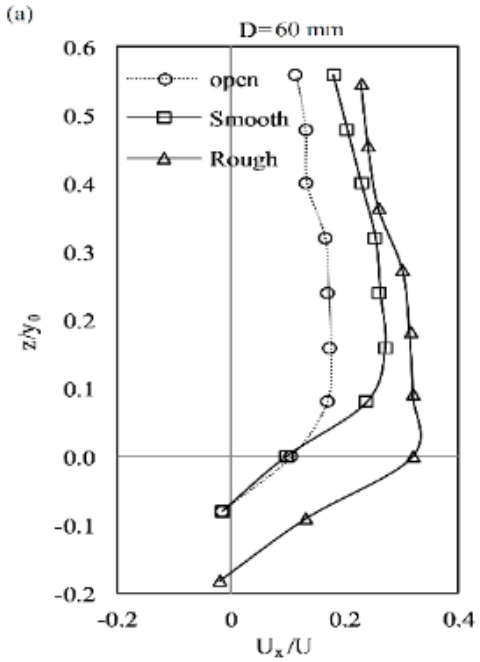

Figure 3-37: Ux velocity component profile in the scour hole under both ice-covered and open channel flow conditions at the upstream face of the 6-cm pier for D_{50}=0.47mm

- **Variation of the relative maximum scour depth with the near-bed velocity distribution**

To better illustrate the impacts of the near-bed velocity on the relative maximum scour depth (MSD) under ice-covered condition, the variation of the relative MSD (y_{max}/y_0) with U^*/U^*c under different conditions is given in Figure 3-38. Of note, by near-bed we refer to the ratio of shear velocity (U^*) over critical shear velocity (Uc^*) that initializes the motion of the particles. Shear velocity is usually applied to motion near the bed where the shearing stress is often assumed to be independent of height and approximately proportional to the square of the mean velocity. As outlined by Melville and Coleman (2000), the maximum scour depth occurs when $U^*/U^*c = 1$. Of note, results for sand of D_{50}=0.50 mm are not included in Figure 3-38 since they are not obviously different from those of the finest sand.

1) For the same sediment, with increase in U^*/U^*_c, the relative MSD (y_{max}/y_0) decreases. For y_{max}/y_0<0.20, the trend of decrease in U^*/U^*_C is very sharp, indicating the early state of scouring. For y_{max}/y_0>0.20, the scouring process gradually decreases during the experiment run, indicating the weaker horseshoe vortex and wake vortex and, consequently, a decrease in the bed shear stress. When the bed shear stress becomes less than the critical shear stress, the scour depth will reach to the equilibrium state at which the sediment particles may not be transported or moved into suspension. The reason is due to the decrease in scour rate when the scour hole reaches the equilibrium condition at which the armour layer is completely formed and prevents the scour hole from further scouring.

2) Regardless of the flow cover conditions, with the same U^*/U^*_c -values, the finer the sediment, the larger the relative MSD (y_{max}/y_0) of the scour hole. In other words, due to a lower threshold of sediment motion for the finest sediment type, under the same U^*/U^*_c, a scour hole with a larger MSD has developed.

3) Regarding the impact of ice cover on the (y_{max}/y_0) ~ (U^*/U^*c) relationship, with the same U^*/U^*c values, the relative MSD (y_{max}/y_0) is greater under rough covered flow condition. On the other side, for the same relative MSD, under the rough ice-covered flow condition, the U^*/U^*c -value is greater than that of under smooth covered condition, implying that the near-bed velocity is higher under rough ice-covered flow condition.

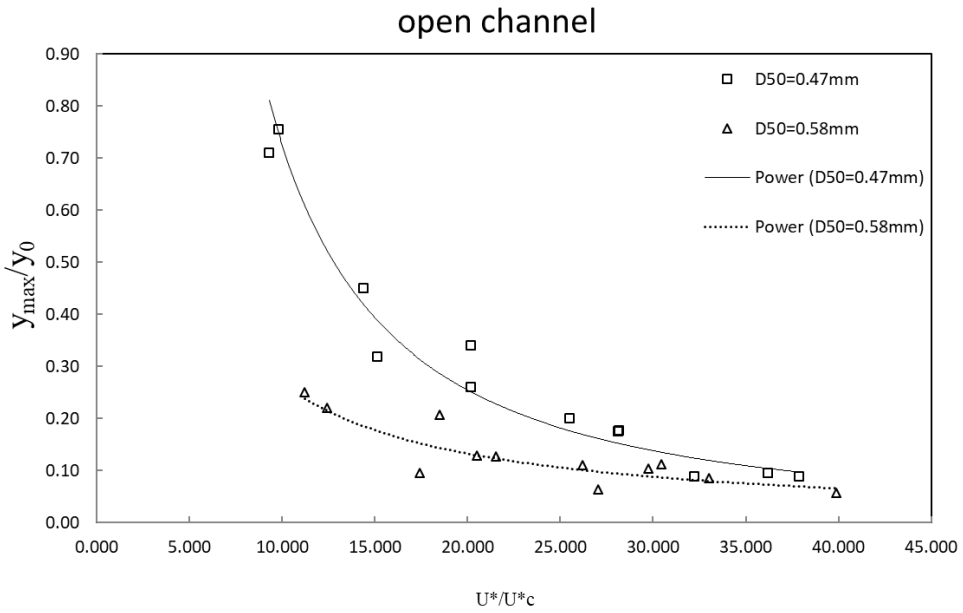

Figure 3-38a: Variation of the relative MSD with U*/U*c classified by particle grain size for open flow condition

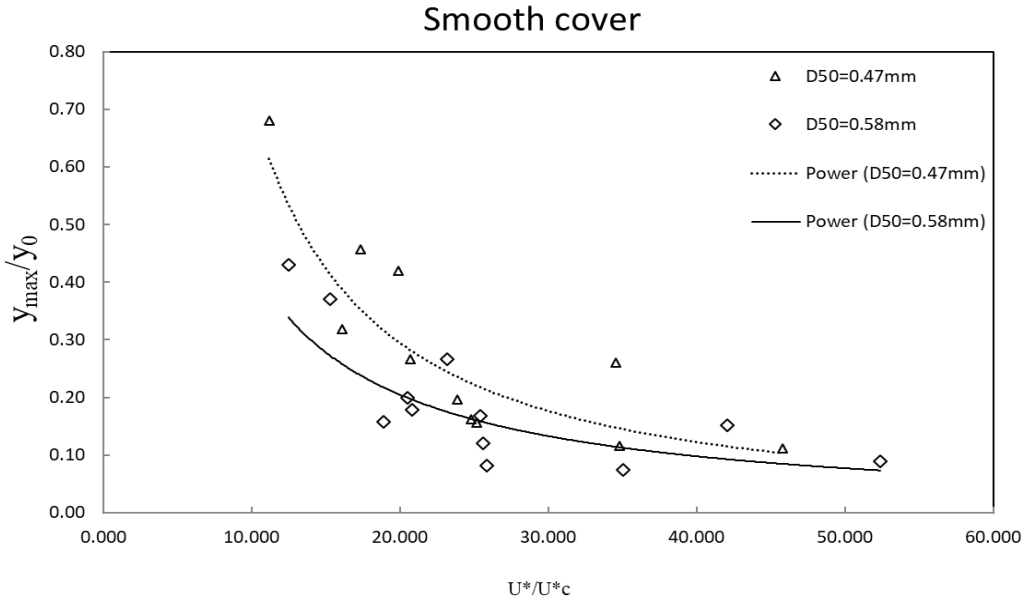

Figure 3-38b: Variation of the relative MSD with U*/U*c classified by particle grain size for smooth covered flow condition

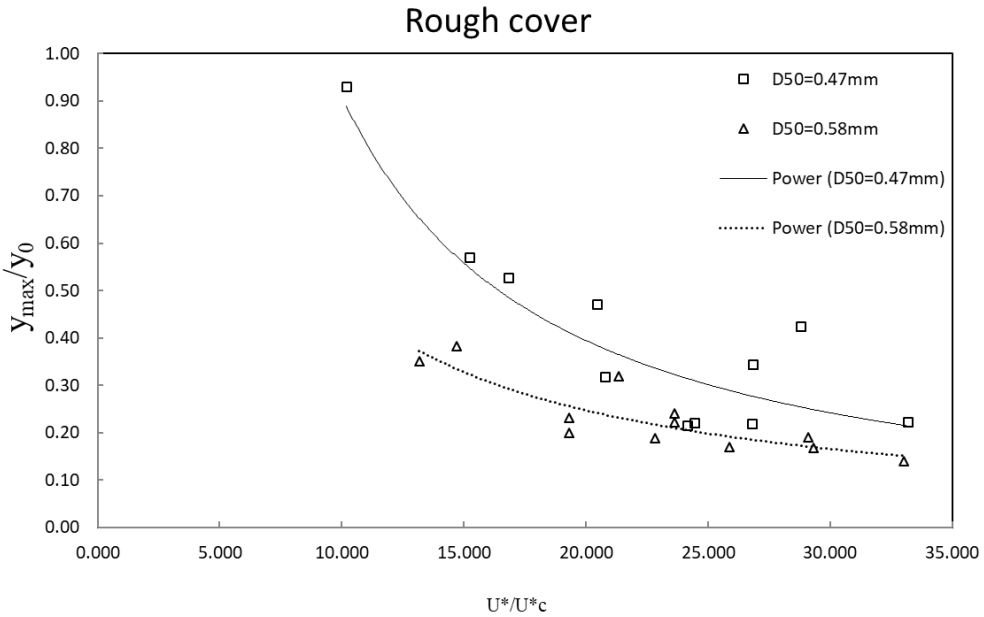

Figure 3-38c: Variation of the relative MSD with U*/U*c classified by particle grain size for rough covered flow condition

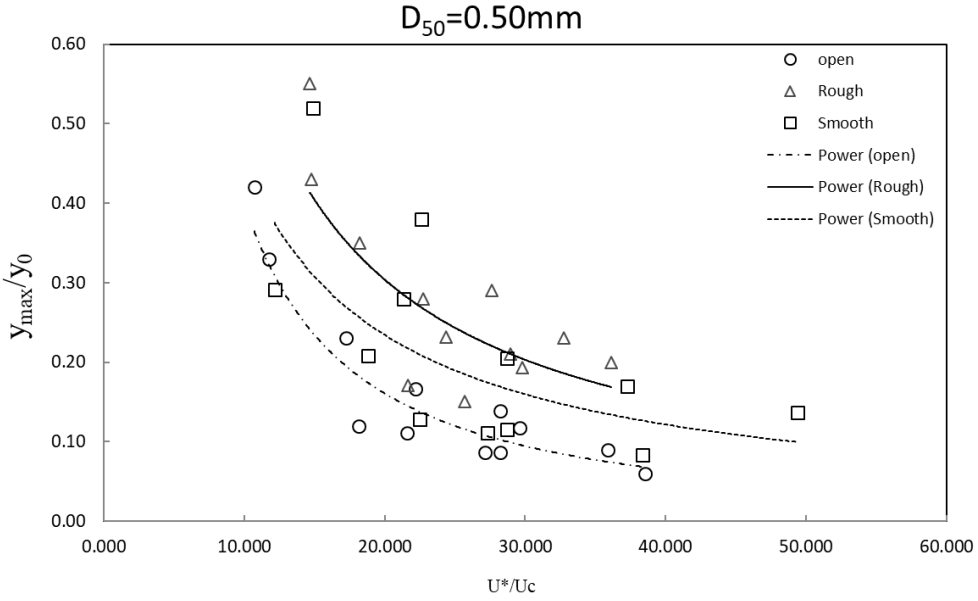

Figure 3-38d: Variation of the relative MSD with U*/U*c classified by flow cover conditions for sediment of D_{50}=0.50 mm

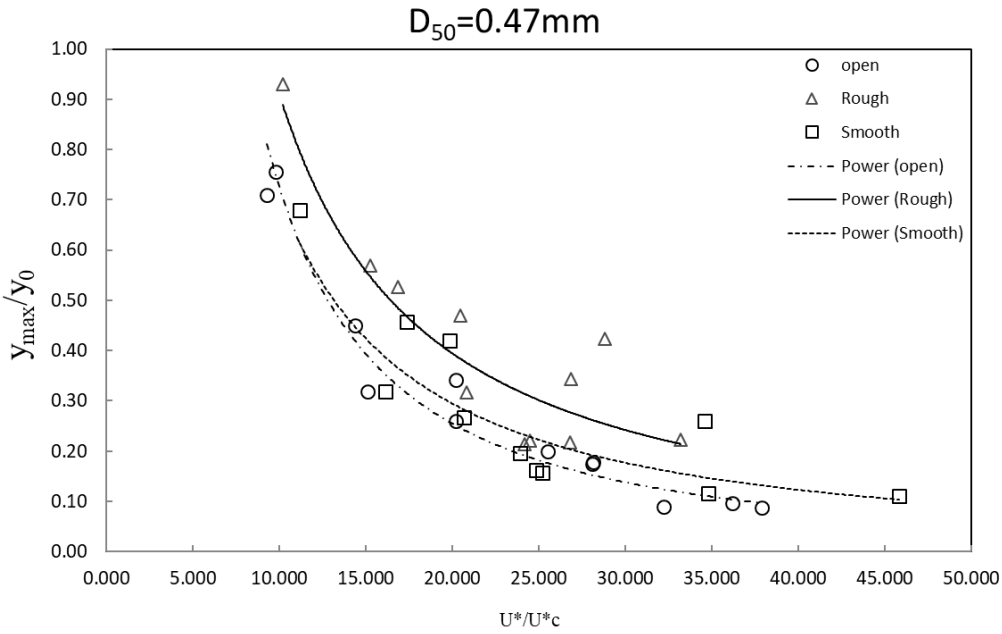

Figure 3-38e: Variation of the relative MSD with U*/U*c classified by flow cover conditions for sediment of D_{50}=0.47 mm

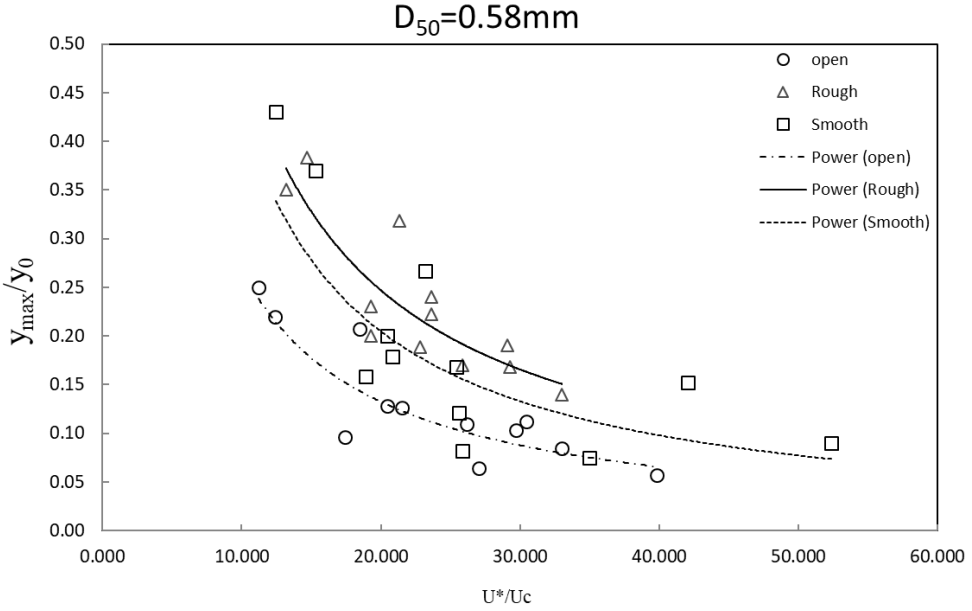

Figure 3-38f: Variation of the relative MSD with U*/U*c classified by flow cover conditions for sediment of D_{50}=0.58 mm

A relationship between (y_{max}/y_0), (U^*/U^*_c) and (D_{50}/y_0) has been established, as shown in Figure 3-39:

$$\frac{y_{max}}{y_0} = 2.514\left(\frac{U^*}{U_c}\right)^{-1.955}\left(\frac{D_{50}}{y_0}\right)^{-0.577} \quad (3\text{-}3\text{-}17)$$

According to Eq. 3-3-17, for the same D_{50}/y_0–value, the higher the U^*/U^*_c –value, the lower the relative MSD. Similarly, for the same the U^*/U^*_c –value, the more the D_{50}/y_0–value, the less the relative MSD, indicating that the relative MSD decreases as the grain size of bed material gets coarser.

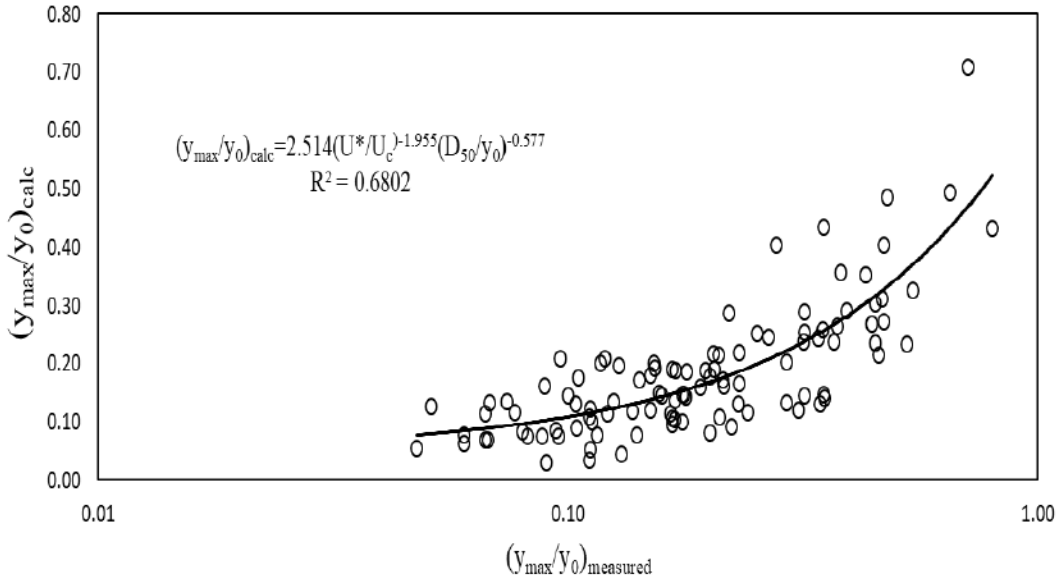

Figure 3-39: Variation of the relative measured MSD against calculated MSD

3.3.3. Conclusions

There is a paucity of information in terms of maximum scour depth characteristics and incipient motion of sediment particles around bridge piers under ice-covered flow conditions due to measurement restraint. In the present study, a series of large scale-flume experiments have been conducted by using three non-uniform sediments and four pairs of side-by-side bridge piers of different diameters under different ice-covered conditions to investigate the effects of ice cover on the incipient motion of bed material and shear stress around bridge piers. The obtained results can contribute to design of bridge piers in cold regions by considering the impact of ice. Following conclusions have been drawn:

1) It is found the presence of ice cover can result in a deeper maximum scour depth compared to that under open flow condition, and consequently, the required flow velocity for incipient motion of sediment particles under ice-covered conditions decreases with the increase in the relative roughness coefficient of ice cover.

2) The pier Reynolds number (Re_b) decreases with the increase in the pier spacing ratio (G/D), implying that the strength of the horseshoe vortices decreases as the spacing distance increases. Results showed that, under the same flow condition (velocity and flow depth), the least pier Reynolds Number (Re_b) occurred under open channel flow conditions, and the highest pier Reynolds Number (Re_b) occurred under rough covered flow conditions. Further, it was observed that the influence of ice cover on pier Reynolds Number fades away as the pier spacing distance increases regardless of flow cover. Also, for the same bridge pier spacing ratio (G/D) and the same sediment, the relative *MSD* under open channel flow conditions is the lowest and the maximum under the rough covered flow conditions, respectively. This implies that the impact of the pier spacing ratio under the rough ice-covered flow condition is clearly intensified compared to those under both open channel and smooth covered flow conditions. In other words, the smaller the pier size (D) and the larger the pier spacing (G), the weaker the horseshoe vortices around the side-by-side bridge piers.

3) The larger the sediment-fluid parameter, the greater the dimensionless shear stress for incipient motion of bed material. In other word, with the increase in the sediment-fluid parameter, the dimensionless shear stress increases correspondingly. However, for the same sediment-fluid parameter, a higher dimensionless shear stress is resulted in channel bed with finer sediment. Meanwhile, for the same dimensionless shear stress, the finer sediment has a

lower sediment-fluid value while the coarser sediment has a greater sediment-fluid parameter value for the incipient motion of bed material.

4) The dimensionless shear stress increases with the increase in the densimetric Froude number. For the same densimetric Froude number, the dimensionless shear stress is for the finest sediment type (D_{50}=0.47 mm) is the least. It is also found that the dimensionless shear Reynolds number increases with the increase in densimetric Froude number. With the same densimetric Froude number, the dimensionless shear Reynolds number for the coarser sand (D_{50}=0.58 mm) is higher.

5) For the same relative MSD, the U^*/U_c –value under the rough ice-covered flow condition is more than that under smooth covered condition, implying that the near-bed velocity is higher under rough ice-covered flow condition than that under smooth covered condition.

6) For the streamwise velocity component (U_x), it can be described as a reverse C-shaped profile shape which begins from the scour hole up to the water surface. In terms of velocity magnitude, the streamwise velocity in the scour hole under rough covered condition is generally greater than those under both smooth covered and open flow conditions. Regardless of the cover conditions of flow, the magnitude of velocity is the least in the scour hole. Moreover, the location of the maximum velocity is closer to the bed under rough covered flow condition than that under smooth covered flow condition.

7) In terms of the effects of rough ice cover vs those of smooth ice cover, the MSD under rough ice-covered flow condition was deeper. The location of the maximum velocity was closer to the bed under rough covered flow condition than that under smooth covered flow condition. For the same bed material, the dimensionless shear stress for incipient motion of sediment increases with the shear Reynolds number as the ice cover becomes rougher. The

results are in good agreement with the result of Ackermann et al., (2002) in which they stated that the rough cover gave slightly larger scour depths than the smooth cover.

Notation:

a	Percentage of the cover
D_{50}	50^{th} percentile particle diameter (m)
D_{90}	The bed material size where 90% of the material is finer.
D_i	Grain size diameter (m)
D	The diameter of the bridge pier (m)
d	Sediment size in the armor layer (m)
Fr_0	Densimetric Froude number
g	Gravitational acceleration (m/s^2)
k	Von Karman's constant
Ks	The average roughness height (m)
Re_*	The boundary shear Reynolds number
R	Hydraulic radius (m)
S	Channel slope
S^*	The sediment-fluid parameter
S. G	Specific weight of the sediment
T	Dimensionless transport-stage parameter
U	Mean approach flow velocity (m/s)
U*	Shear velocity (m/s)
U^*_c	Critical shear velocity (m/s)
U_x	Scour hole velocity component in x-direction (m/s)
U_y	Scour hole velocity component in y-direction (m/s)
U_z	Scour hole velocity component in z-direction (m/s)
$\bar{u}$	Average cross-sectional velocity (m/s)
y_{max}	Relative maximum scour depth (MSD) (m)
y_0	The depth of approaching flow (m)
w	Cross-section width (m)
z	Distance from channel bed (m)
z_0	Roughness height (m)
ρ_s	Mass density of sediment (kg/m^3)
ρ	Mass density of water (kg/m^3)
ν	Kinetic viscosity of fluid (m^2/s)
τ	Shear stress (Pa)
τ_{c*}	Dimensionless shear stress, critical Shields value
Re*	Shear Reynolds number
Re_b	The pier Reynolds number

MSD	Relative maximum scour depth
y_i	The total depths of the ice (m)
y_b	The total depths of the bed zone (m)
n	The channel bottom roughness or Manning's roughness
n_c	Manning roughness coefficients for total cross section
n_b	Manning roughness coefficients for upper ice-cover
n_i	Manning roughness coefficients for the lower bed boundary layers
W	Resisting gravitational (N)
F_R	Frictional forces (N)
F_L	Lift force (N)
α	Scour angle
C_D	Drag coefficient at velocity Vs
C_L	Lift coefficient at velocity Vs
V_s	The local velocity at a distance s above the bed.
H	The mean flow depth (m)
K_1	The constant number equal to 0.058
s	Distance above the bed associated with Vs (m)

3.3.4. References:

Ackermann, N. L., Shen, H. T., Olsson, P. (2002). Local scour around circular piers under ice covers. Proc. Int. Conf. 16th IAHR International Symposium on Ice, IAHR, Dunedin, New Zealand

Aguirre-Pe, J., Olivero, M. I. A. L., Moncada, A. T. (2003). Particle densimetric Froude number for estimating sediment transport. Journal of Hydraulic Engineering, 129(6): 428-437.

Andrews, E. D. (1983). Entrapment of gravel from naturally sorted riverbed material. Geol. Soc. Am. Bull.94: 1225–1231

Ashton, G. D. (1986). *River and lake ice engineering*. Water Resources Publication.

Ataie-Ashtiani, B., & Beheshti, A. A. (2006). Experimental investigation of clear-water local scour at pile groups. *Journal of Hydraulic Engineering*, *132*(10), 1100-1104.

Batuca, D. and Dargahi, B. Some experimental results on local scour around cylindrical piers for open and covered flow. In Third International Symposium on River Sedimentation, University of Mississippi (1986).

Barenblatt, G. I., Chorin, A. J. (1997). Scaling laws and zero viscosity limits for wall-bounded shear flows and for local structure in developed turbulence. Commun. Pure Appl. Math, 50(4).

Beheshti, A. A., Ataie-Ashtiani, B., & Khanjani, M. J. (2013). Discussion of "Clear-Water Local Scour around Pile Groups in Shallow-Water Flow" by Ata Amini, Bruce W. Melville, Thamer M. Ali, and Abdul H. Ghazali. *Journal of Hydraulic Engineering*, *139*(6), 679-680.

Beltaos, S. (2009), River flow abstraction due to hydraulic storage at freezeup, *Can. J. Civ. Eng.*, 36(3), 519–523.

Briaud, J. L., Gardoni, P., Yao, C. (2006). "Bridge Scour". Geotechnical News, Vol. 24, No.3, September, BiTech Publishers Ltd.

Bunte, K., Abt, S. R. (2001). Sampling surface and subsurface particle-size distributions in wadable gravel-and cobble-bed streams for analyses in sediment transport, hydraulics, and streambed monitoring. Gen. Tech. Rep. RMRS-GTR-74. Fort Collins, CO: US Department of Agriculture, Forest Service, Rocky Mountain Research Station. 428 p., 74.

Cea, L., Puertas, J., & Pena, L. (2007). Velocity measurements on highly turbulent free surface flow using ADV. Experiments in fluids, *42*(3): 333-348.

Chiew, Y. M., Melville, B. W. (1987). Local scour around bridge piers. Journal of Hydraulic Research, *25*(1): 15-26.

Chang, H.H. (1988). Fluvial processes in river engineering. Krieger Publishing, Malabar, Florida, 432 pp

Crance, M. J., & Frothingham, K. M. (2008). The impact of ice cover roughness on stream hydrology. In 65 th Eastern snow conference, Fairlee (Lake Morey), Vermont (p. 149).

Davar, K. S., S. Beltaos, and B. Pratte (1998), A primer on hydraulics of ice-covered rivers, Canadian Committee on River Ice Processes and Environment

Dey, S., Barbhuiya, A. K. (2004). Clear-water scour at abutments in thinly armored beds. Journal of hydraulic engineering, 130(7): 622-634.

Dey S, Debnath K 2000 Influence of stream-wise bed slope on sediment threshold under stream flow. J. Irrig. Drain. Eng., Am. Soc. Civil Eng. 126: 255–263

Dey, S., and Raikar, R. 2007. Clear-water scour at piers in sand beds with an armor layer of gravels. Journal of Hydraulic Engineering, 133, 703-711.

Einstein, H. A. (1950). The bed-load function for sediment transportation in open channel flows (Vol. 1026). Washington DC: US Department of Agriculture.

Egiazaroff, J. V. (1965). Calculation of non-uniform sediment concentrations. J. Hydraul. Div., Am. Soc. Civil Eng. 91: 225–247

Ettema, R., Melville, B. W. and Constantinescu, G. (2011). "Evaluation of bridge scour research: Pier scour processes and predictions". Transportation Research Board of the National Academies, Washington, DC.

Ettema, R., & Zabilansky, L. (2004). Ice influences on channel stability: Insights from Missouri's Fort Peck reach. *Journal of Hydraulic Engineering*, *130*(4), 279-292.

Froehlich, D.C. (1995). Armor limited clear water construction scour at bridge, Journal of Hydraulic Engineering, ASCE 121: 490–493

Graf, W. H., & Istiarto, I. (2002). Flow pattern in the scour hole around a cylinder. Journal of Hydraulic Research, 40(1): 13-20.

Hannah, C. R. (1978). Scour at pile groups. Research Report No. 28-3, Civil Engineering Department, University of Canterbury, Christchurch, New Zealand.

Hopkins, G. R., Vance, R. W., & Kasraie, B. (1980). Scour around bridge piers, FHWA-RD-79-103 U.S. Department of Transportation, Federal Highway Administration, Offices of Research and Development, Environmental Division.

Hoque, M. (2009). Hydraulic analysis of ice-covered river flow. Master thesis, Concordia University.

Huang, T., Lu, Y., Lu, Y., (2015). Incipient motion and bed load transport of non-uniform sediment. E-Proceedings of the 36th IAHR World Congress, The Haque, the Netherlands

Karman, T. V. (1930). Mechanische Ähnlichkeit und Turbulenz, nach Ges. Wiss. Gottingen. Math. Physik. Klasse.

Kothyari, U. C., Garde, R. C. J., Ranga Raju, K. G. (1992). Temporal variation of scour around circular bridge piers. Journal of Hydraulic Engineering, 118(8): 1091-1106.

Kuhnle R A 1993 Incipient motion of sand-gravel sediment mixtures. J. Hydraul. Eng., Am. Soc. Civil Eng. 119: 1400–1415

Kumar, A., & Kothyari, U. C. (2011). Three-dimensional flow characteristics within the scour hole around circular uniform and compound piers. Journal of Hydraulic Engineering, 138(5), 420-429

Larsen, P. A. (1969), Head losses caused by an ice cover on open channels, J. Boston Soc. Civ. Eng., 56(1), 45–67

Lee, H., & Balachandar, S. (2012). Critical shear stress for incipient motion of a particle on a rough bed. *Journal of Geophysical Research: Earth Surface*, *117*(F1).

Li, S. S. (2012). Estimates of the Manning's coefficient for ice-covered rivers. In Proceedings of the Institution of Civil Engineers-Water Management (Vol. 165, No. 9, pp. 495-505). Thomas Telford Ltd

Madsen, O. S., & Grant, W. D. (1977). Quantitative description of sediment transport by waves. In Coastal Engineering 1976 (pp. 1092-1112).

Madsen, O. S. (1991, July). Mechanics of cohesionless sediment transport in coastal waters. In Coastal sediments (pp. 15-27). ASCE.

Mao L., Cooper, J. and Frostick, L. (2011). Grain size and topographical differences between static and mobile armour layers. Earth surface Processes and Landforms, 36(10), 1321-1334

Mays, L. W. (Ed.). (1999). Hydraulic design handbook. McGraw-Hill Professional Publishing

Meyer-Peter, E., & Müller, R. (1948). Formulas for bed-load transport. In *IAHSR 2nd meeting, Stockholm, appendix 2*. IAHR.

Melville, B. W. & Coleman, S. E. (2000). Bridge scour. Highlands Ranch, Colo, U.S.: Water Resources Publications.

Melville, B. W., Raudkivi, A. J. (1977). Flow characteristics in local scour at bridge piers. Journal of Hydraulic Research, 15(4): 373-380.

Melville, B. W. and Sutherland, A. J. (1988). "Design method for local scour at bridge piers". Journal of Hydraulic Engineering, 114(10): 1210-1226.

Miller, M. C., McCave, I. N., & Komar, P. (1977). Threshold of sediment motion under unidirectional currents. Sedimentology, 24(4): 507-527.

Montgomery, D. R., Buffington, J. M. (1997). Channel-reach morphology in mountain drainage basins. Geological Society of America Bulletin, 109(5): 596-611.

Muste, M., Braileanu, F., and Ettema, R. 2000. Flow and sediment transport measurements in a simulated ice-covered channel. Water Resources Research, 36(9), 2711-2720.

Nakagawa, H, Tsujimoto, T, Nakano, S. (1982) Characteristics of sediment motion for respective grain sizes of sand mixtures. Bull. No. 286, Disaster Prevention Research Institution, Kyoto University

Patel, P. L, Ranga Raju, K. G. (1999). Critical tractive stress of nonuniform sediments. J. Hydraul. Res. 37:39–58

Raudkivi, A. J., Ettema, R. (1983). Clear-water scour at cylindrical piers. Journal of Hydraulic Engineering, 109(3): 338-350.

Schvidchenko, A. B., Pender, G. (2000). Flume study of the effect of relative depth on the incipient motion of coarse uniform sediments. Water Resources Research, 36: 19–628.

Shields A 1936 Application of similarity principles and turbulence research to bed-load movement. Mitteilunger der Preussischen Versuchsanstalt fuer Wasserbau und Schiffbau 26: 5–24

Shen, H., Schneider, V. R., Karaki, S. (1969). "Local scour around bridge piers Journal of the Hydraulics Division, 95(6): 1919–1940

Shen, H. T., and P. D. Yapa (1986), Flow resistance of river ice cover, *J. Hydraul. Eng.*, 112(2), 142–156

Smith, B. T., and R. Ettema (1997), Flow resistance in ice-covered alluvial channels, *J. Hydraul. Eng.*, 123(7), 592–599.

Sui, J., Wang, J., He, Y. and Krol, F. (2010a). Velocity profiles and incipient motion of frazil particles under ice cover. International Journal of Sediment Research, 25(1): 39-51.

Sui, J., Afzalimehr, H., Samani, A., and Maherani, M. (2010b), Clear-water scour around semi-elliptical abutments with armored beds, International Journal of Sediment Research 25 (3): P. 233-245, 2010.

Van Rijn, L. C. (1984). Sediment pick-up functions. Journal of Hydraulic engineering, 110(10): 1494-1502.

Wang, J., Sui, J. Y., Karney, B. W. (2008). Incipient motion of non-cohesive sediment under ice cover-an experimental study. Journal of Hydrodynamics, 20(1), 117.doi:10.1016/ S1001-6058(08) 60036-0

Wardhana, K., Hadipriono, F. C. (2003). "Analysis of recent bridge failures in the United States". Journal of performance of constructed facilities, 17(3): 144-150

Xu, H., Lu, J., Liu, X. 2008.Non-uniform sediment incipient velocity. International Journal of Sediment Research 23(1): 69–75.

Yanmaz, A. M., Altinbilek, H. D. G. A. (1991). Study of time-dependent local scour around bridge piers. Journal of Hydraulic Engineering, 117(10): 1247-1268.

Yang, C. T. (2003). Sediment transport, theory and practice. Krieger publishing company, Krieger Drive, Malabar, Florida.

Yalin, M. S., Karahan, E. (1979). Inception of sediment transport. Journal of the hydraulics division, 105(11): 1433-1443.

3.4. Scour patterns and velocity profiles around side-by-side bridge piers under ice-covered flow

Bridges constructed with elements within the boundaries of rivers are potentially exposed to scour around their foundations. If the depth of scour exceeds a critical value, instability and vulnerability caused by the scour will threaten the bridge foundation, which might possibly lead to critical issues such as bridge collapse, significant transport disruption and in an extreme case, human casualty. Melville & Coleman (2000) studied 31 cases of bridge failures due to scour in New Zealand and concluded that on average one major bridge failure each year can be attributed to scour occurring around the bridge foundations. Wardhana & Hadipriono (2003) studied 500 cases of bridge structure failures in the United States between 1989 and 2000 and stated that the most common cause of bridge failure was due to either floods or scour. Sutherland (1986), in conjunction with National Roads Board of New Zealand, determined that of the 108 bridge failures recorded between 1960 and 1984, 29 could be attributed to abutment scour. Local scour around bridge foundations has been the focal point of many studies (Melville & Sutherland, 1988; Ahmed & Rajaratnam, 1998; Melville & Chiew, 1999; Graf & Istiarto, 2002; Dey & Raikar, 2007; Ettema et al, 2011; Sheppard et al. 2013; Wu & Balachandar, 2018; Williams et al., 2018; Williams et al., 2017; Wu & Balachandar, 2016; Wu et al., 2015a, 2015b, 2014a, 2014b). Important to understanding bridge pier scour is to better comprehend the the velocity distribution in the vicinity of bridge piers. The flow field at piers has been documented in literature (Dey et al., 1995; Graf & Istiarto, 2002; Unger and Hager, 2007; Beheshti & Ataie-Ashtiani; 2009 and Kumar and Kothyari; 2012).

Graf and Istiarto (2002) performed an experimental study of the flow pattern in the upstream and downstream plane of a cylinder positioned vertically in a scour hole. Detailed measurements were obtained by using an acoustic-Doppler velocity profiler (ADVP) in and around the scour hole. The results indicated that in the upstream reach of the cylinder, a vortex system was detected which was a rather strong one (horseshoe vortex) and was positioned at the foot of the cylinder. Another but weaker vortex (not so visible) was probably due to the change in the slope of the bottom leading into the scour hole. Besides, in the downstream reach of the cylinder, there existed a flow reversal towards the water surface. In their study, the results indicated that the turbulent kinetic energy was very strong at the foot of the cylinder on the upstream side and in the wake behind the cylinder. Unger and Hager (2007) investigated the temporal evolution of the vertical deflected flow at the pier front and the horseshoe vortex inside the scour hole as it formed. Their work provided novel insight into the complex two-phase flow around circular bridge piers placed in loose sediment. A three-dimensional turbulent flow field around a complex bridge pier placed on a rough fixed bed was experimentally investigated by Beheshti & Ataie-Ashtiani, (2009). Comparison of flow patterns with the observed scour map revealed that the scour patterns at the upstream and sides of the pier correlate well with the contracted flow below the pile cap. A flow field analysis around side-by-side piers with and without a scour hole was carried out by Ataie-Ashtiani and Aslani-Kordkandi, (2012). They found that the streamwise velocity increased between the two piers. As a result, the maximum depth of scour hole was approximately 15% greater than in the single-pier case. Kumar and Kothyari (2012) performed their study on flow patterns and turbulence characteristics within a developing (transient stage) scour hole around circular uniform and compound piers with measurements obtained using an acoustic

Doppler velocimeter (ADV). According to their study, the measurements of velocity, turbulence intensities, and Reynolds shear stress made around each of the pier at different vertical planes exhibited almost similar profiles along the flow depth. However, at certain locations close to the pier, a significant change occurred in the vertical profile of the flow parameters. Besides, the observations made in the upstream planes revealed that within the scoured region, the bed shear stress was much smaller compared with the bed shear stress of the approach flow.

Due to the difficulty of making velocity measurements under ice-covered conditions, nearly all the studies regarding velocity distribution around bridge piers have been carried out using open channel flow conditions. The number of studies on the flow field around both bridge abutments and bridge pier under ice-covered condition is limited. Wu et al. (2015a, 2015b, 2014a, 2014b) studied the effect of relative bed coarseness, flow shallowness, and pier Froude number on local scour around a bridge pier and reported that the scour depth under covered conditions is larger compared to that under open channel flow conditions. It has been found the presence of an ice cover alters the hydraulics of the channel by imposing an extra boundary to the water surface (Sui et al., 2010). Under ice-covered flow conditions, the velocity drops to zero at each boundary (ice-covered water surface and the bed) due to the no-slip boundary condition, resulting in a parabolic-shaped profile (Ettema, et al. 2000; Zabilansky et al., 2006). In addition, the maximum velocity occurs between the bed and the bottom of the ice cover and is dependent on the relative roughness of the two boundaries (Wang et al., 2008). Sui et al., 2010 showed that the upper flow is mainly influenced by the ice cover resistance while the lower flow is primarily impacted by the channel bed resistance. Wang et al. (2008) stated that the location of maximum velocity depends on the relative

magnitudes of the ice and bed resistance coefficients. According to Wang et al. (2008), it is expected that as the ice resistance increases, the maximum flow velocity will move closer to the channel bed. In terms of local scour depth, the severity of the local scour in the vicinity of a bridge's foundation gets more intense during the freezing period at which the water surface is covered by ice. The presence of ice has been found to increase local clear-water scour depth at bridge piers by 10%–35% (Hains & Zabilansky, 2004). In terms of transverse flow distributions and velocities of secondary currents, ice cover can impact flows in an existing thalweg, altering the position of the thalweg and changing the morphology of the stream which in an extreme case will lead to bank and bed erosion (Beltaos et al., 2007). Zabilansky et al. (2006) performed a series of flume experiments under smooth and rough ice cover conditions and found that the maximum velocity for rough ice cover was 20 percent greater than for smooth ice cover. This statement was confirmed by Muste et al. (2000) who found that the measured maximum velocity under smooth cover is located roughly at $0.8y_0$, while maximum velocity under rough cover is approximately located at $0.6y_0$, where y_0 represents the approaching flow depth.

In the current study, a series of large-scale flume experiments were conducted to examine scour hole patterns along with scour hole velocity profile measurements around four side-by-side bridge piers under ice-covered and open channel flow conditions. The main objective of this study is to gain a better understanding of the flow field and velocity distribution around bridge piers under different flow cover and to focus on their associated distinctive flow field characteristics.

3.4.1. Methodology

Experiments were carried out in a large-scale flume at the Quesnel River Research Centre of the University of Northern British Columbia, Canada. The flume was 38.2 m long, 2 m wide and 1.3 m deep. Figure 3-40 shows a plan view and a side view of the experiment flume. The longitudinal slope of the flume was 0.2 percent. A holding tank with a volume of 90 m^3 was located at the upstream end of the flume to maintain a constant discharge during the experimental runs. To create different velocities, three input valves were connected to control the inlet volume discharge. Water level in the flume was controlled by the downstream tailgate. Two types of tailgate configurations (one-tailgate and two-tailgate configurations) were incorporated to produce a wide range of main channel approaching velocities. The range of flow depth was from 0.09 m to 0.137 m for one-tailgate configuration and from 0.165 m to 0.28 m for two-tailgate configuration. For the case of two-tailgate configuration, two pumps were employed for the lowest flow discharge while three pumps were employed to create the highest flow discharge. At the end of the holding tank and upstream of the main flume, water overflowed from a rectangular weir into the flume. Two sand boxes were constructed in the flume. Both had a depth of 0.3 m and were 10.2 m apart. The length of the sand boxes were 5.6 m and 5.8 m, respectively. Three natural, non-uniform sediments with median grain sizes of 0.47 mm, 0.50 mm and 0.58 mm were used. Side-by-side cylindrical bridge piers with diameters of 60 mm, 90 mm, 110 mm and 170 mm were used. The distance between the center of left pier and the center of the right pier was 0.50 m. Figure 3-41 shows the piers and the space ratio (G/D) in which G is the distance from the outside to outside of the piers and D is the pier diameter. The geometric channel aspect ratio (channel width/flow depth) of the current experiments ranged from 7.14 to 22.2. Of note, Roussinova et al. (2006)

declared that velocity dip would not be significant when the geometric channel aspect ratio (channel width/ flow depth) is greater than five as secondary flow effects are minimal. The bridge pier spacing ratio G/D ranged from 1.94 to 7.33 (Figure 3-41). In front of the first sand box, a 2D Flow Meter (SonTek Inc.) was installed to measure flow velocities and water depth. A staff gauge was also installed in the middle of each sand box to manually verify water depth. Styrofoam panels were used as ice cover across the entire surface of flume. Both smooth and rough ice cover were simulated. The smooth cover was the smooth surface of the original Styrofoam panels while the rough cover was made by attaching small Styrofoam cubes to the bottom of the smooth cover. The dimensions of Styrofoam cubes were 25 mm × 25 mm × 25 mm and they were spaced 35 mm apart. The velocity field in the scour holes were measured using a 10-MHZ acoustic Doppler velocimeter (ADV). The sampling volume of the 10-MHz ADV is 100 mm from the sensor head. In a standard configuration, the sampling volume is approximately a cylinder of water with a diameter of 6 mm and a height of 9 mm. In the current study, the ADV measured the scour hole velocity profiles at approaching flow depths within 0.18-0.28 m range for four sets of bridge piers (60 mm, 90 mm 110 mm and 170 mm) under the two-tailgate flume configurations for the highest and lowest levels of discharge. Scour hole velocity measurements for shallow flow depths (one-tailgate flume configuration) were inaccessible due to the limitations of the ADV in measuring shallow flow depths. Velocity measurements were performed at one hour before the end of the experimental run (total test time = 24 hours) at which point the scour hole was fully developed and stabilized. For the purposes of these experiments, the streamwise velocity component, $U_{x,}$ is the component in the direction of the flow, the span-wise velocity component is denoted as U_y, and the velocity component, U_z, is the component in the vertical

direction. Of note, a negative value of U_z means the velocity vector is directed downwards. To develop the three-dimensional velocity profiles, measurements were obtained at each point for 120 seconds. Of note, for velocity values very close to the channel bed, the presence of sediment affected the ADV velocity measurement, therefore, the velocity values are representative of sediment and water velocity as previous noted by Muste et al. (2000). The scour hole flow field was measured at 20 mm increments from the bottom of scour hole in front of the bridge pier up to free surface for each experimental run. In the ice-covered experiments, a part of the Styrofoam was cut to allow for the ADV to be positioned inside the flow for flow field measurements. Further, since the ADV measuring volume is located 100 mm from the probe head, the velocity profile for each channel condition is not up to the water surface. After the experiments were completed, collected data were analyzed to filter out for velocity spikes. Signal strengths and correlations are used principally to judge the quality and accuracy of the velocity data (Fugate & Friedrichs, 2002). In the current study, data quality was defined based on signal-to-noise ratio amplitudes (SNR≥ 15) and correlation coefficient scores (≥ 70). In terms of uncertainty in velocity measurements, at a sampling rate of 25Hz and an SNR above 15, uncertainty due to Doppler noise can be estimated as 1% of the maximum velocity range (Sontek, 1997). In total, 108 experiments (36 experiments for each sediment type) were conducted under open channel, smooth covered, and rough covered conditions. In terms of different boundary conditions (open channel, smooth, and rough covered flows), for each sediment type and each boundary condition, 12 experiments were carried out. In the preliminary stage of the experiments, local scour around bridge piers was carefully observed for any changes in the scour depths. It was observed that after approximately a period of 6 hours, no significant change in scour depth was observed and

scour hole equilibrium depth was achieved. The experiment was continued for 24 hours and again no obvious change in scour depth was observed. For the 110-mm bridge pier under open channel and ice-covered flow condition for the highest discharge, the experimental time was extended to 38 hours and there was not any significant change in scour depth between 24 hr. and 38 hr. experiments. Further, according to Wu et al. (2014a), who did a series of experiments regarding local scour around a semi-circular bridge abutment, the time for development of equilibrium scour depth was 24 hr. Based on the current experimental results and the results of Wu et al. (2014a), the experimental run time of 24 hr. was chosen. After 24 hours, the flume was gradually drained, and the scour and deposition pattern around the piers was measured. To accurately read the scour depth at different locations and to draw scour hole contours, the outside perimeter of each bridge pier was divided between 6 and 12 labeled segments based on the diameter of the cylinder (Figure 3-41).The measurement of scour hole was subject to an error of +/-0.3 mm. Of note, the maximum scour depth between left hand side and the right-hand side bridge piers were more or less identical. Of note, since an additional boundary is added to the flow for the case of ice-covered flow condition, hydraulic radius (R) is calculated from the following equation:

$$R = \frac{A}{P} = \frac{Wy_0}{2(y_0 + W)} = \frac{y_0}{(y_0 + 2)} \qquad (3\text{-}4\text{-}1)$$

Where W is the width of the channel.

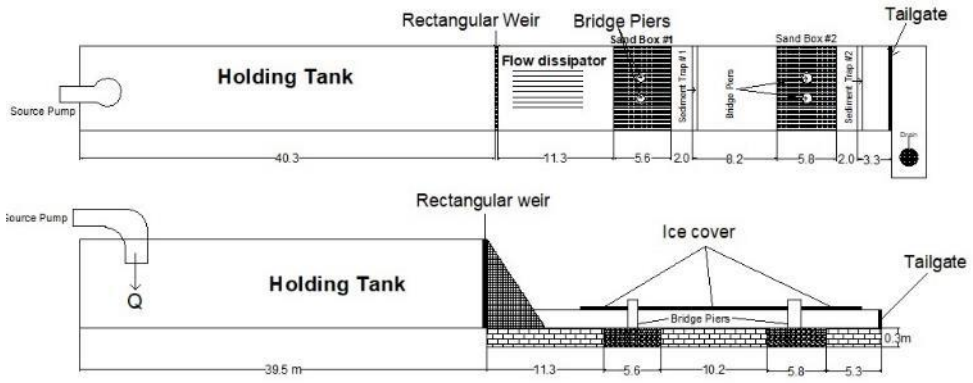

Figure 3-40: Plan view and vertical view of experiment flume (Dimensions in m)

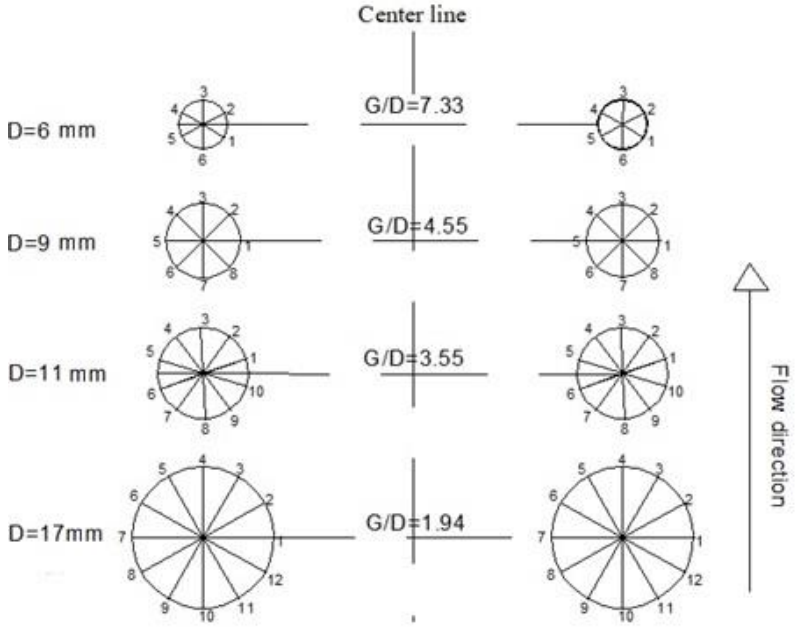

Figure 3-41: The spacing ratio and measuring points around the circular bridge piers

3.4.2. Results and discussions

- **Local Scour pattern around bridge piers**

Figure 3-42a shows scour depth around the 110 mm bridge pier and Figure 3-42b compares the scour and depositional pattern upstream and downstream of the pier for D_{50} = 0.47 mm under open and rough flow conditions for the highest flow discharge, respectively. Figure 3-42 (a-b) also compares the scour depth with that of Hirshfield (2015) in which local scour around 110-mm single bridge pier under open and rough ice cover conditions for D_{50}=0.47 mm is reported. According to Figure 3-42a, regardless of flow cover and number of piers, the maximum scour depth occurred at point 8 which is at the pier face where the horseshoe vortex and down-flow velocity coexist and are the strongest. The least amount of scour occurred near point 3 which is diametrically opposed to point 8 behind the pier. Further, regardless of flow cover, it is obvious that the scour depth is deeper for the side-by-side pier compared to the single bridge pier in the study of Hirshfield (2015). Besides, according to Figure 3-42b, sediment ridges have been developed downstream of the side-by-side bridge pier under all the flow cover conditions. Sediment ridges downstream of the pier, as noted in the present study, were not reported by Hirshfield (2015) for the single bridge pier. The reason is due to confining effects of the side-by-side bridge pier compared to the singular bridge pier which has resulted in greater scour depth and developed sediment ridge at the downstream side of the bridge pier. According to Hodi (2009), as blockage ratio increases, larger amount of discrepancies will be developed in both scour depth and bed geometry. In the present study, regardless of flume cover and sediment grain size, the maximum scour depths were always located at the upstream face of the pier. According to Williams (2018), the scour commences in the region of the highest velocity in the vicinity of the separating

streamline. The horseshoe vortex which forms at the pier face shifts the maximum downflow velocity closer to the pier in the scour hole. The downflow acts as a vertical jet to erode a groove in front of the pier. The eroded sand particles are carried around the pier by the combined action of accelerating flow and the spiral motion of the horseshoe vortex (Hafez, 2016). Melville and Coleman (2000) report a wake-vortex system which occurs behind the pier, acts like a vacuum cleaner sucking up bed material and carrying the sediment moved by the horseshoe vortex system and by the downward flow to downstream of the pier. However, wake-vortices are not normally as strong as the horseshoe vortex and therefore, are not able to carry the same sediment load as the horseshoe vortex does. Therefore, sediment deposition is likely to occur downstream of the pier in the form of sediment ridge which is clearly shown in Figure 3-42b. The scour pattern around the 110-mm bridge pier under highest flow discharge viewed from the top for D_{50}= 0.47 mm was mapped into Surfer 13 plotting software (Golden Software, 1999) as shown in Figure 3-43 (a-c) for open, smooth, and rough flow cover, respectively. According to Figure 3-43, the deepest location of scour depth around the pier is clearly at the face of bridge pier and the location of deposition ridge is downstream of the pier which is densest and most widely spread for the rough ice-covered flow condition. The same pattern was observed for the other bridge piers regardless of sediment type and bridge pier diameter. It was experimentally noted by Qadar (1981) that the maximum value of scour depth should certainly be a function of the initial vortex strength. Therefore, the deepest scour depth, which is the result of a stronger vortex, should occur under the highest approach velocity and rougher ice cover type as observed in these experiments.

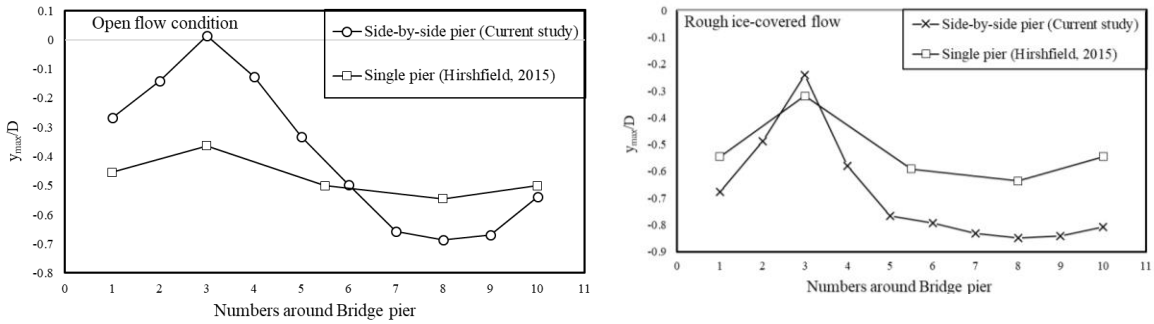

Fig. 3-42a: Scour depth around the 110-mm bridge pier for D_{50}= 0.47 mm type sediment under a) open flow and b) rough covered flow conditions using the highest flow discharge

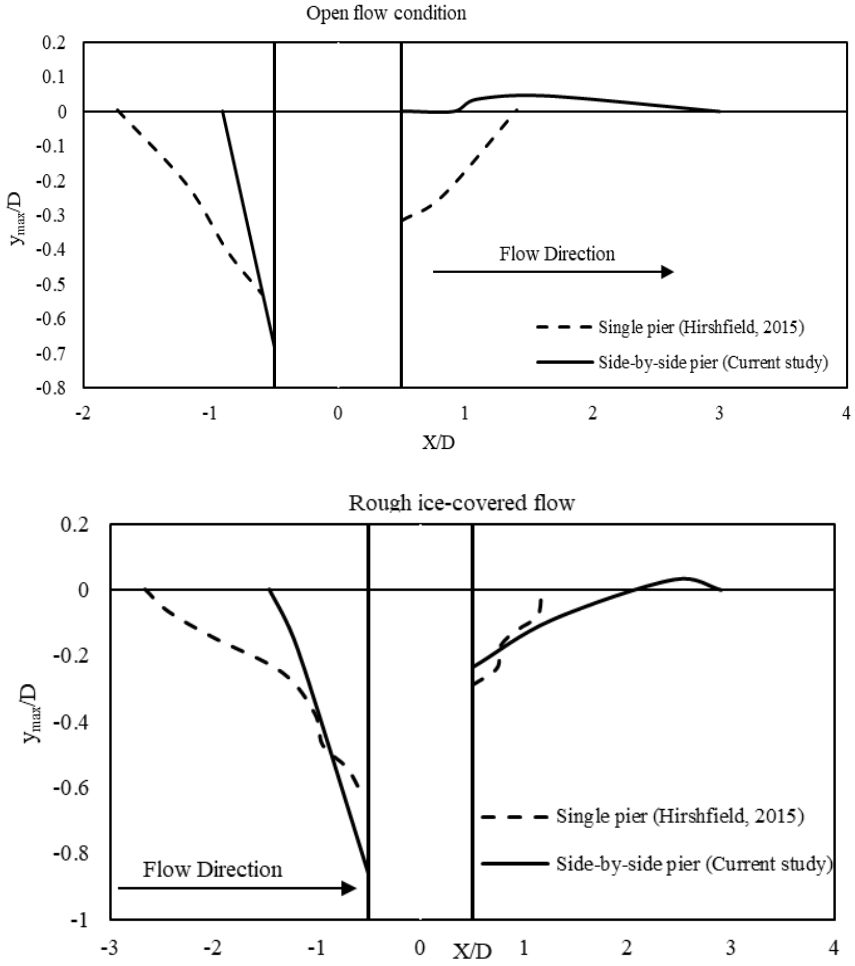

Figure 3-42b: Cross-section of scour and depositional pattern at the upstream and downstream of the 110-mm bridge pier under a) open flow condition and b) rough covered flow conditions for D_{50}=0.47 mm

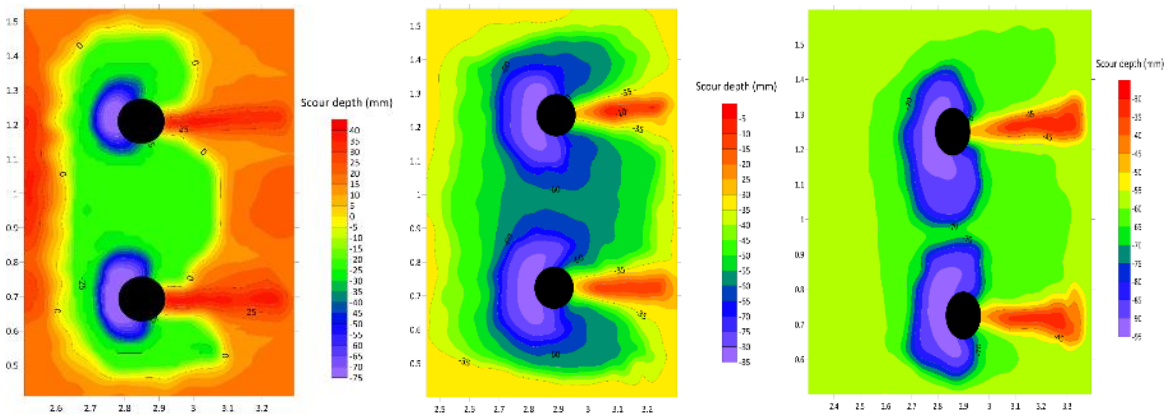

Figure 3-43: a) Scour pattern around the 110-mm bridge pier for D_{50}=0.47 mm type under open for the highest flow discharge; b) Scour pattern around the 110-mm bridge pier for D_{50}= 0.47 mm type under smooth for the highest flow discharge; c) scour patterns around the 110-mm bridge pier for D_{50}= 0.47 mm type under rough for the highest flow discharge

- **Flow velocity profiles**

Scour hole velocity profiles for the streamwise (U_x) vertical (U_z) velocity components under open, smooth and rough ice cover for all the pier size separately and under D_{50}=0.47 mm for the lowest discharge is presented in Figure 3-44. Figure 3-45 shows scour hole velocity profiles for the streamwise (U_x) and vertical (U_z) velocity components distinguished by flow cover for all the pier size under D_{50}= 0.47 mm for the lowest discharge. Figure 3-46 shows the vertical velocity distribution for the lowest discharge for the 90-mm bridge pier under rough ice-covered condition for the three D_{50}s. Of note, regardless of pier size, since the lateral (y) velocity profiles, does not exhibit any meaningful pattern in the flow and constantly changes between positive and negative values along the entire profile, they are not presented. In order to be able to generalize the velocity profiles and to compare different velocity profiles under different flow cover, the depth of flow on the vertical axis has been non-dimensionalized by taking the ratio of vertical distance from bed (z) to approach flow depth (y_0). The streamwise scour hole velocity component (U_x) and the vertical scour hole velocity component (U_z) are also non-dimensionalized by the approaching flow velocity (U).

Of note, the ADV location for the velocity measurement of all the experiments was set at 10 mm upstream of the pier face where the maximum scour depth occurred. The following outcome can be concluded from Figure 3-44 to Figure 3-46:

1) For the streamwise velocity distribution is a reverse C-shaped profile which begins from the scour hole up to the water surface. The same pattern was also reported by Hirshfield (2015) and Kumar and Kothyari (2011). In terms of velocity magnitude, the streamwise velocity for rough cover is generally greater than the scour hole velocity for smooth and open channel conditions. As expected, the magnitude of velocity is smallest in the scour hole and is the highest at the water surface. Furthermore, regardless of flow cover, pier size and sediment type, the values of the velocity component are mostly negative within the scour hole which is an indication of reversal flow happening due to the presence of horseshoe vortex which is strongest at the pier face. Moreover, for the 90-mm and 110-mm bridge piers, which were placed in the first sand box and were exposed to nearly the same flow depth and approaching flow velocity, the average value of U_x is higher for the 110-mm pier under all flow cover conditions. Similarly, for the 60 mm and 170 mm bridge piers which were placed in the second sand box and were exposed to nearly the same flow depth and approaching flow velocity, the average value of U_x is higher for the 170-mm pier under all flow cover conditions. In other words, the results indicate the strength and intensity of the horseshoe vortex increased with pier size.

2) Within the scour hole upstream of the pier, the most significant feature is the appearance of down-flow velocities in the vertical direction due to obstruction of the flow by the pier and is represented by negative values of U_z. Therefore, the vertical velocity distribution (U_z) is highly significant in terms of scour hole development. In terms of flow

cover, it is obvious that the value of U_z is the largest under rough ice cover. According to Tison (1961), the downward velocity originates from the horizontal curvature of the streamline in front of the pier and the reduction of velocity near the bed by friction. Downward velocity intensifies the horseshoe vortex at the pier face and can effectively speed up the process of scour hole development, which in an extreme case, leads to bridge failure. Generally, considering the absolute value of U_z, the value of U_z diminishes from the channel bed toward the scour hole. From the channel bed toward the free surface, U_z values tend to move toward zero and the positive direction which implies that downflow velocity vectors are changing their direction and diminishing as they get closer to free surface which causes the velocity profile to have a parabolic shaped profile.

3) Under the same flow cover and flow condition, the larger pier yielded the larger values of the streamwise and vertical (U_x, U_z) velocity. However, these values are larger under rough ice-covered flow conditions. The larger scour hole velocity under rough ice cover justifies the findings of greater pier scour depth
4) The vertical velocity distribution exhibits the same pattern for the three sands as seen in Figure 3-46. According to the figure, the finest sediment (D_{50}= 0.47 mm), has a greater velocity magnitude and, consequently, a deeper scour depth. Besides, the location of maximum velocity under the finest sediment is closer to the bed which has resulted in stronger horseshoes vortices.

Table 3-4 represents the location of maximum velocity based on z/y_0 for different flow cover. Of note, the velocity profiles were measured before the cylinder inside the scour hole in the upstream region. According to Table 3-4, the location of maximum velocity is closer to the bed which is in good agreement with the findings of Zabilansky et al. (2006) and Muste et

al. (2000). Figure 3-47a shows vertical velocity component (U_z) for the 60- and 170-mm bridge piers (bridges in the second sand box) from the scour hole up to the maximum velocity point under open, smooth and rough-covered flow covers, while Figure 3-47b shows U_z of the 90- and 110-mm bridge piers (bridges in the first sand box) from the scour hole up to the maximum velocity point under open, smooth and rough-covered flow covers. As mentioned before, the location of maximum velocity is expected to depend on the relative magnitudes of the ice and bed resistance coefficients and the rougher the ice cover, the closer the location of the maximum velocity to the channel bed. Therefore, the magnitude of vertical velocity is generally higher near the channel bed under rough flow cover compared to open channel flow cover. According to Figures 3-47(a-b), location of the maximum velocity is closer to the bed under ice-covered condition which is in good agreement with the previous findings. Since there was not any significant change from the maximum location of the vertical component of velocity (U_z) up to the free surface, a general linear relationship is developed for all the bridge piers under open channel and ice-covered flow conditions in Figure 3-47c which reads as follows:

$$z / y_0 = 0.5816(Uz / U) + 0.5503 \qquad (3\text{-}4\text{-}2)$$

Of note, due to the limitations of ADV in measuring the full vertical velocity profile, there is no data in the upper portions of the depth. Resultant of the three average velocity components is calculated for the lowest discharge of D_{50}= 0.47 mm from the Eq. 3 and are presented in Figure 3-48. The results indicate regardless of flow discharge and pier size, the resultant velocity is highest for rough cover. For the 90-mm pier and 110-mm pier which were placed in the first sand box and were under nearly the same flow condition, the larger pier has resulted in larger values of resultant velocity component which implies that the

strength and intensity of horseshoe vortex increases with pier size. The same trend can be seen for the 60-mm piers and 170-mm piers which were placed in the second sand box.

$$U_R = \sqrt{\left(\overline{u}\right)^2 + \left(\overline{v}\right)^2 + \left(\overline{w}\right)^2} \tag{3-4-3}$$

in which $\overline{u}$, $\overline{v}$ and $\overline{w}$ are average velocity components in XYZ coordinates and U_R is the total velocity or the resultant of the three average velocity components. Of note, $\overline{u}$, $\overline{v}$ and $\overline{w}$ are time-averaged velocities calculated by taking their averages from instantaneous velocity values in their associated direction as follows:

$$\overline{u} = \frac{1}{n}\sum_{i=1}^{n} u_i; \qquad \overline{v} = \frac{1}{n}\sum_{i=1}^{n} v_i; \qquad \overline{w} = \frac{1}{n}\sum_{i=1}^{n} w_i \tag{3-4-4}$$

$$u' = u - \overline{u}; \qquad v' = v - \overline{v}; \qquad w' = w - \overline{w} \tag{3-4-5}$$

in which, n is the number of time series data, u_i, v_i and w_i are instantaneous flow velocities in XYZ coordinate system and u', v', w' are velocity fluctuations in XYZ coordinate system, respectively.

Table 3-4: Location of maximum velocity based on (z/y_0) values according to flow cover

Flow cover	Stage of maximum velocity (z/y_0)
Open channel	0.25
Smooth cover	0.15
Rough cover	0.10

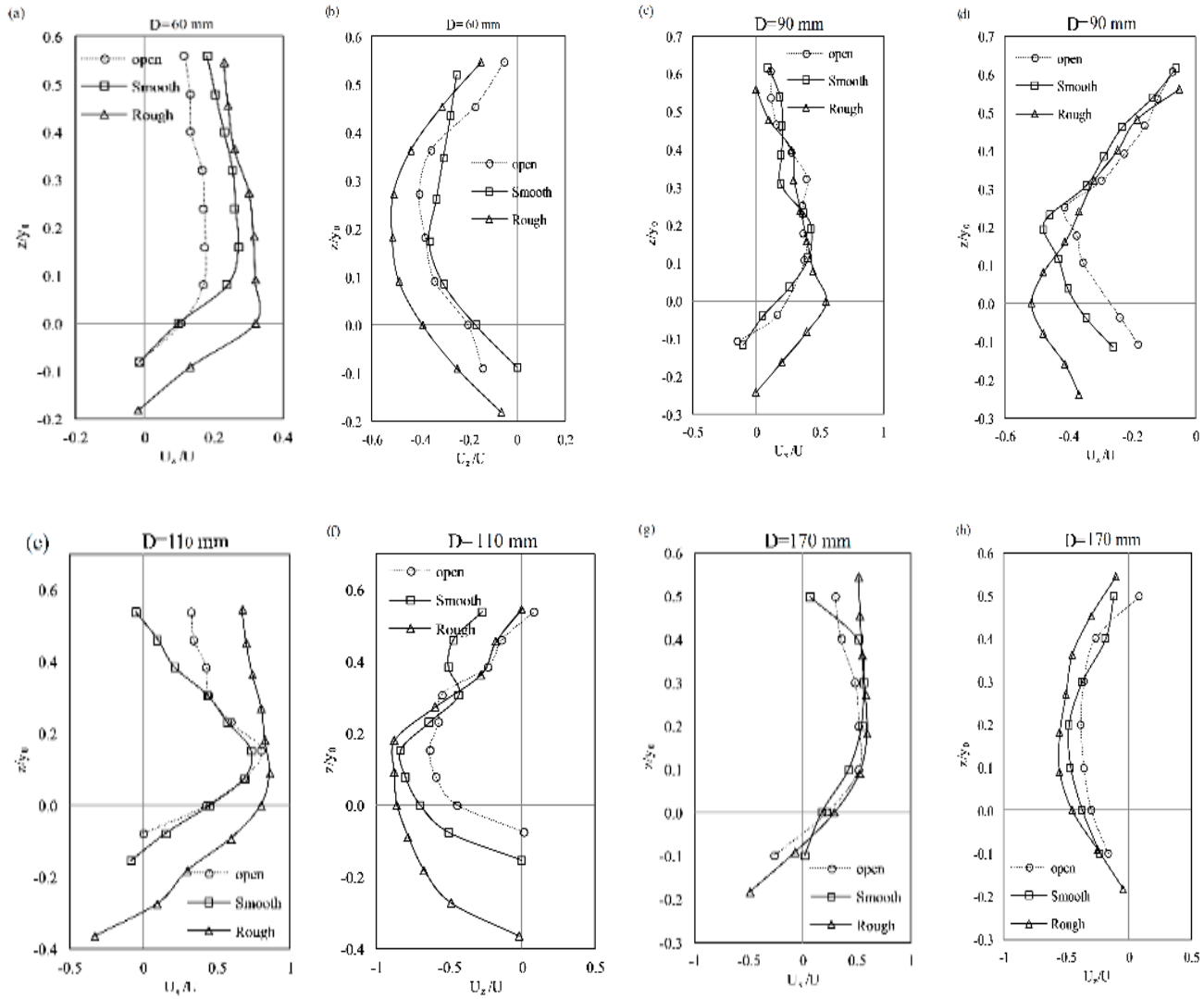

Figure 3-44: Scour hole velocity profiles for the streamwise (U_x) and vertical (U_z) velocity components under open, smooth and rough ice-cover distinguished by the pier size and under D_{50}= 0.47 mm for the lowest discharge

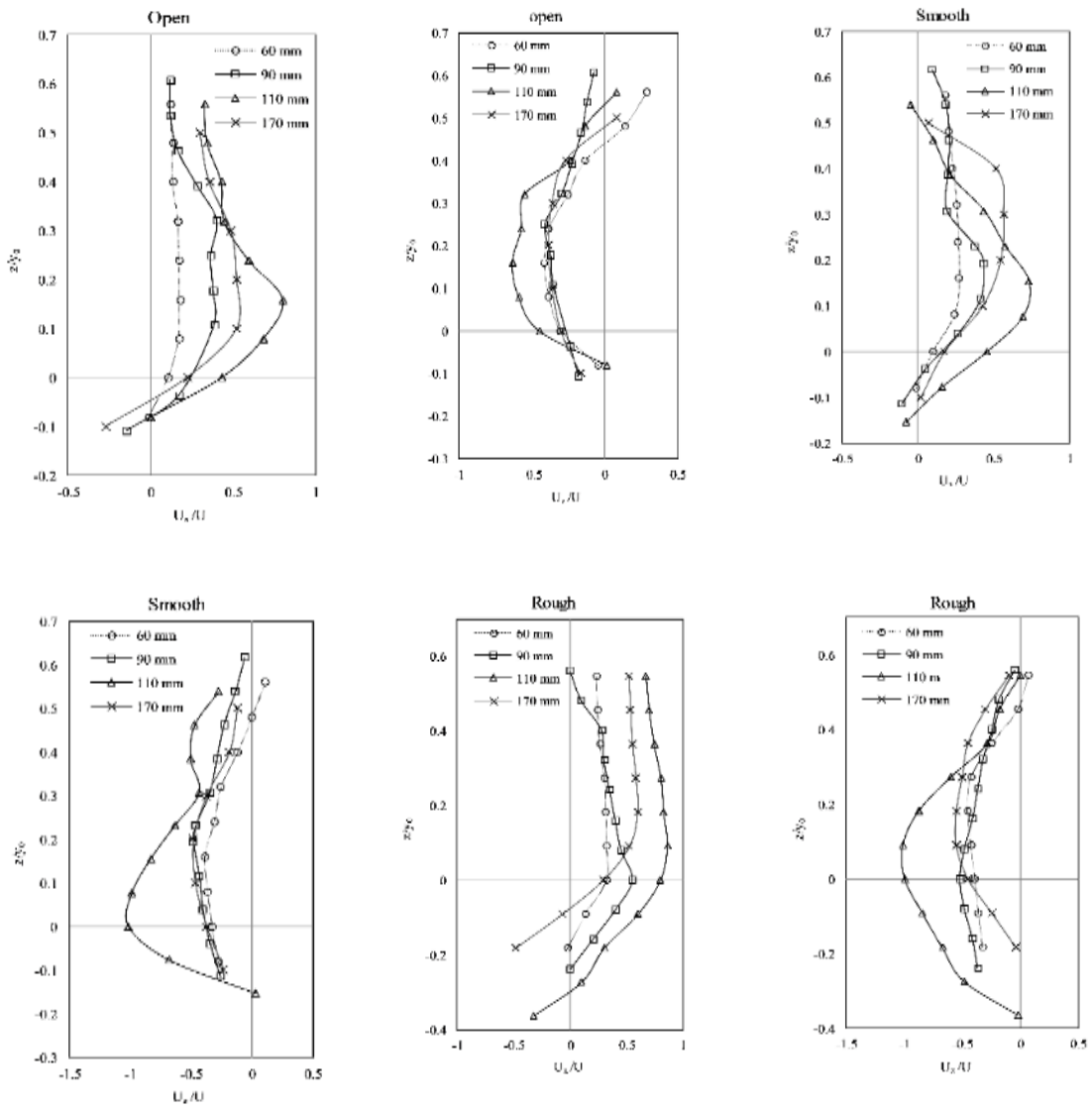

Figure 3-45: Scour hole velocity profiles for the streamwise (Ux) and vertical (Uz) velocity components distinguished by flow cover for all the pier size and under D_{50}= 0.47mm for the lowest discharge

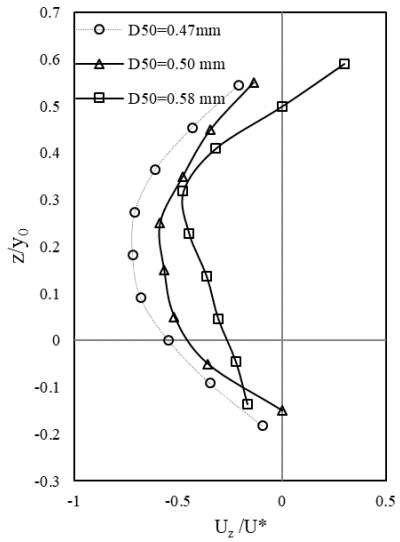

Figure 3-46: The vertical velocity distribution for the lowest discharge for the 90-mm bridge pier under rough ice-covered condition for the three values of D_{50}

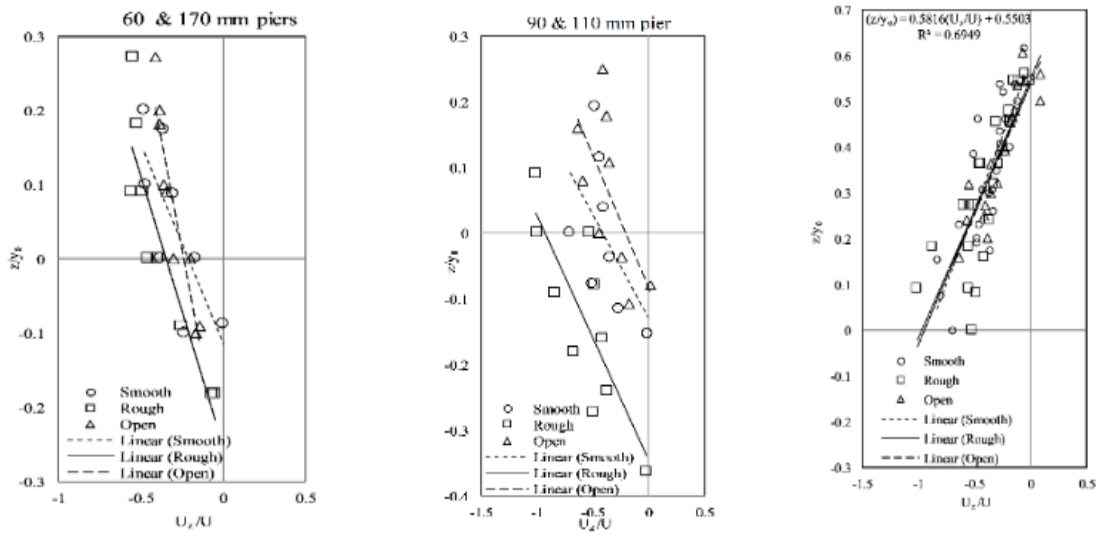

Figure 3-47: a) Vertical velocity component (U_z) of the 60- and 170-mm bridge piers from the scour hole up to the maximum velocity locale under open, smooth and rough-covered flow covers; **b)** Vertical velocity component (Uz) of the 90- and 110-mm bridge piers from the scour hole up to the maximum velocity locale under open, smooth and rough-covered flow covers; **c)** Vertical velocity component (U_z) of all the bridge piers from the maximum velocity locale toward the free surface under open, smooth and rough-covered flow covers

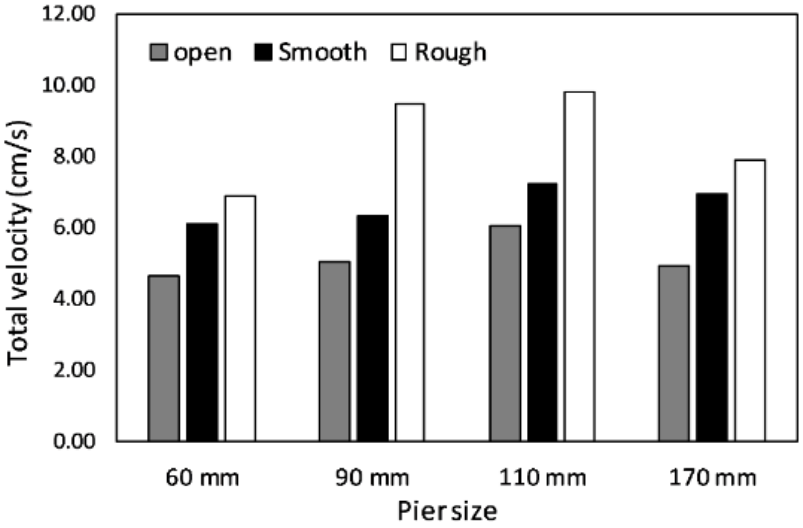

Figure 3-48: Scour hole velocity profiles for the resultant of the three average velocity components under open, smooth and rough ice cover for D_{50}= 0.47 mm for the lowest discharge.

- **Turbulence intensities and turbulent kinetic energy (TKE)**

In terms of ice-covered flow condition, the formation of a stable ice cover almost doubles the wetted perimeter compared to open channel conditions, alters the hydraulics of an open channel by imposing an extra boundary to the flow, causing velocity profile to be shifted towards the smoother boundary (channel bed) and adding up to the flow resistance. Since near-bed velocity is higher under ice-covered conditions, a higher shear stress is exerted on the river bed (Sui et al., 2010; Wang et al., 2008). As the near bed velocity increases, the kinetic energy exerted on the bed increases correspondingly. An increase in kinetic energy affects the capacity of flow in terms of sediment transport rate. To determine turbulence intensities along with turbulent kinetic energy, the root-mean-square of the turbulent velocity fluctuations about the mean velocity are calculated as shown in Eqs. (6) to (8). The RMS values are equal to the standard deviation of the individual velocity measurements in x, y and z directions, respectively. RMSs are considered as a measure of the violence of turbulent fluctuations yielding the spread of velocities around the mean velocity and they are calculated as follows (Wilcox and Wohl, 2007).

$$RMS[u'] = \sqrt{\frac{1}{n}\sum_{i=1}^{n}(u-\bar{u})^2} = \sqrt{\frac{1}{n}\sum_{i=1}^{n}u'^2} = \sqrt{\overline{u'^2}} \quad (3\text{-}4\text{-}6)$$

$$RMS[v'] = \sqrt{\frac{1}{n}\sum_{i=1}^{n}(v-\bar{v})^2} = \sqrt{\frac{1}{n}\sum_{i=1}^{n}v'^2} = \sqrt{\overline{v'^2}} \quad (3\text{-}4\text{-}7)$$

$$RMS[w'] = \sqrt{\frac{1}{n}\sum_{i=1}^{n}(w-\bar{w})^2} = \sqrt{\frac{1}{n}\sum_{i=1}^{n}w'^2} = \sqrt{\overline{w'^2}} \quad (3\text{-}4\text{-}8)$$

Where, RMS [u'] is the Root-mean-square of the velocity fluctuations in streamwise direction; RMS [v'] is the Root-mean-square of the velocity fluctuations in lateral direction and RMS [w'] is the Root-mean-square of the velocity fluctuations in vertical direction. The root mean squares of the streamwise, cross-stream, and vertical velocities ($RMS_{u'}$, $RMS_{v'}$, $RMS_{w'}$) for each time series were used to estimate TKE. RMS [u'], RMS [v'], RMS [w'] are also called turbulent intensities for the streamwise (x), lateral (y) and vertical (z) directions, respectively. Figure 3-49 and Figure 3-50 show the turbulent intensity values non-dimensionalized by the shear velocity for the streamwise (x) and vertical (z) flow velocity components. Of note, turbulent energy is the mean kinetic energy per unit mass and has the unit of J/kg in SI unit. Since fluctuations for the lateral direction measurements did not display any meaningful patterns, the lateral turbulent component (y) is not presented. The same unstructured turbulent intensities pattern was also observed by other studies such as Muste et al., (2000) and Robert and Tran, (2012). Turbulent kinetic energy (TKE) which is defined as the mean energy per unit mass of turbulent eddies is calculated as follows (Clifford and French, 1993):

$$TKE = \frac{1}{2}(RMS_{u'}^2 + RMS_{v'}^2 + RMS_{w'}^2) \quad (3\text{-}4\text{-}9)$$

Figure 3-51 shows TKE values for all the piers for D_{50}=47 mm for the lowest discharge. Analysis of TKE values shows a pattern similar to the turbulent intensity. The following observations can be obtained from Figure 3-49 to Figure 3-51:

1) Regardless of flow cover, the streamwise and vertical turbulent intensities are highest just over the channel bed and diminishes towards the flow surface. According to Muste et al. (2000), observing the highest value of turbulent intensity near the bed is due to the highest rate of sediment movement near the bed. Muste et al. (2000) also concluded the turbulent intensities are relevant to sediment transport as the strength of the turbulence will affect sediment suspension.

2) The streamwise turbulent intensity and the vertical turbulent intensity for the rough flow conditions are greater than those for open channel and smooth ice-covered flow conditions. As the turbulent intensity in both the streamwise and vertical direction are higher under the rough ice-covered flow conditions, there is more potential for sediment transport due to the higher kinetic energy than in the open channel and smooth ice-covered flow conditions.

3) Regardless of pier size, the vertical turbulent intensities are less than the streamwise turbulent intensities which indicates the turbulence is primarily related to fluctuations in the streamwise velocity. The same argument was also presented by Muste et al., (2000).

4) Similar to the observations made for the velocity profile**,** for the 90 mm and 110 mm bridge piers in the first sand box, exposed to nearly the same flow depth and approaching flow velocity, the streamwise and vertical turbulent intensities are higher for 110 mm than 90 mm pier under all forms of flow cover. Similar results were obtained for the 60 mm and 170 mm bridge piers in the second sand box with the 170 mm pier having higher values than the 60 mm pier under all flow cover conditions. The results show the turbulent intensity

increases with pier size. The above statement can also be generalized for TKE. Therefore, it can also be concluded that, under nearly the same flow condition, the maximum value of turbulence kinetic energy occurs at a larger diameter pier.

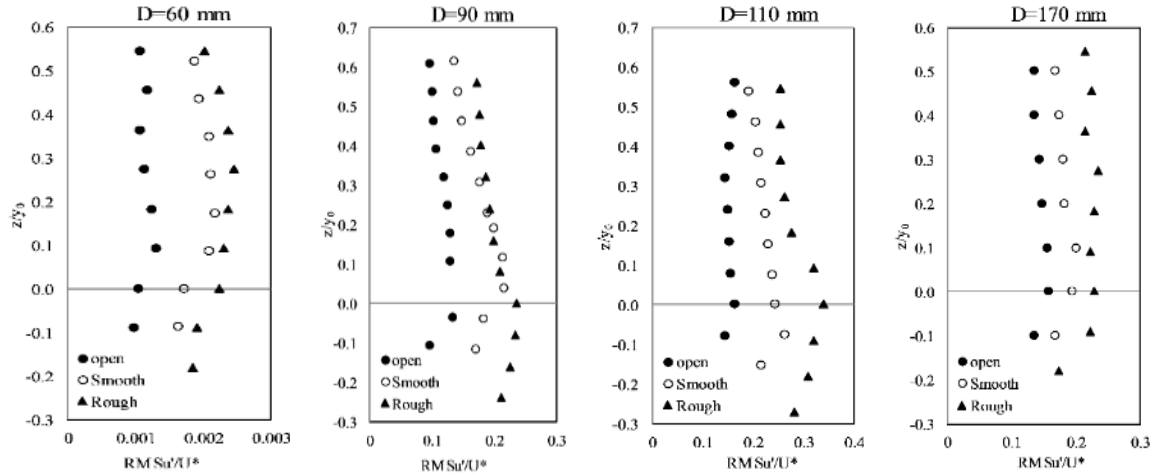

Figure 3-49: Distribution of the turbulent intensity values at the upstream of the piers non-dimensionalized by the shear velocity for the streamwise (x) flow velocity component

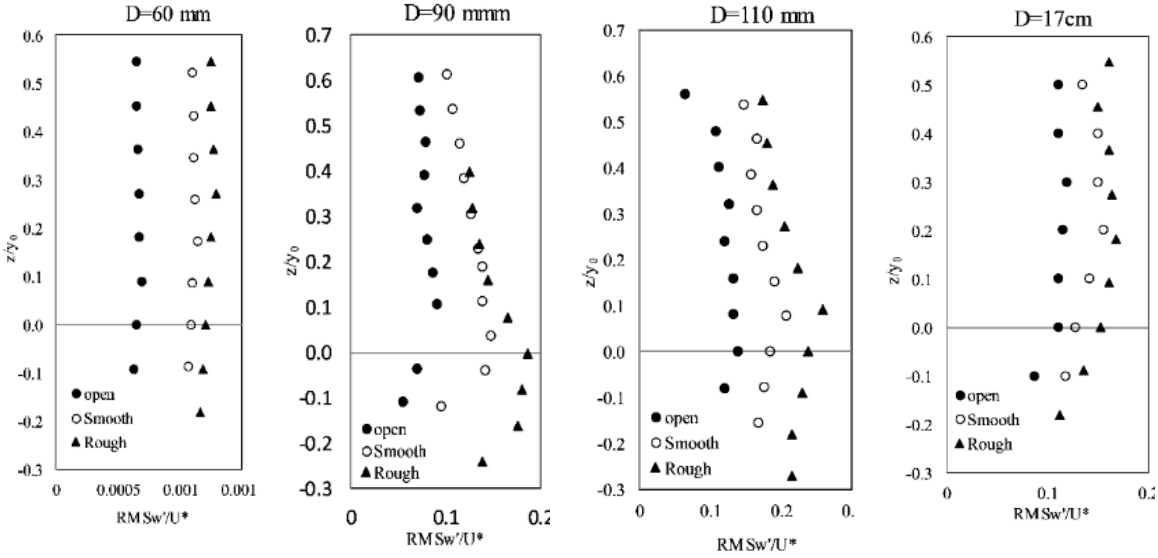

Figure 3-50: Distribution of the turbulent intensity values at the upstream of the piers non-dimensionalized by the shear velocity for the vertical (z) flow velocity component

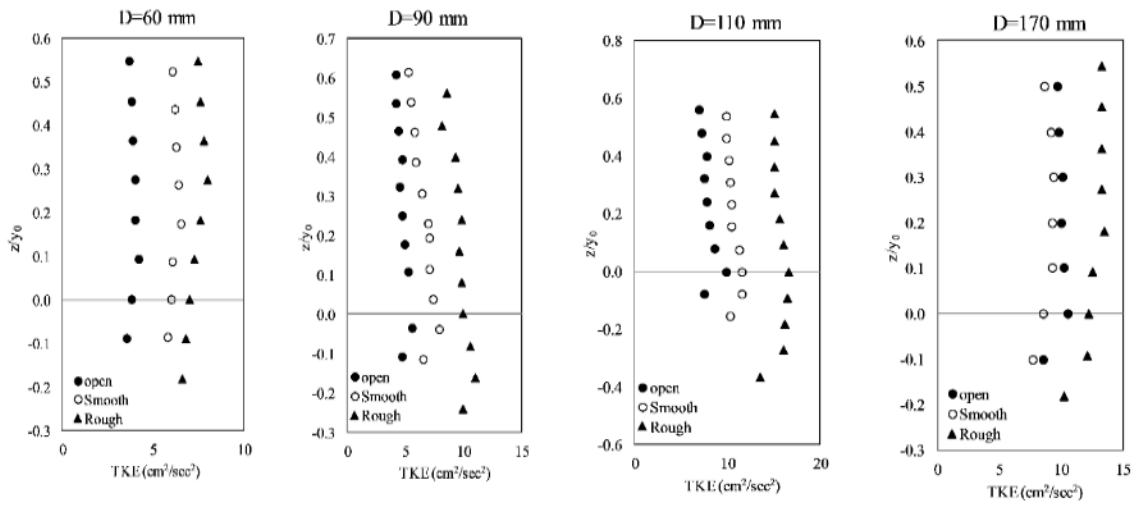

Figure 3-51: Distributions of the turbulent kinetic energy at the upstream of the piers

3.4 Quadrant analysis and Reynolds stresses

The Reynolds shear stress is associated with the balance of mean linear momentum and is important in examining turbulent flows and sediment transport. The component of Reynolds stress for constant density in x-z plane, which has the dimensions of velocity squared, is defined as:

$$t_{xz} = u'w' \qquad (3\text{-}4\text{-}10)$$

Where τ_{xz} is the shear stress in x-z plane, u' represents fluctuation (turbulence) of velocity in x direction and w' represents fluctuation (turbulence) of velocity in z direction. Quadrant analysis, first introduced by Lu and Willmarth (1973), is used to investigate the structure of the Reynolds shear stress in a turbulent boundary layer. In the current study, this analysis is applied to the 60-mm pier to examine the contribution of each quadrant to the Reynolds shear stress. In quadrant analysis, there are four quadrants (i = 1 to 4) in the u' –w' plane: (i) i = 1 represents the outward motion (u'>0 and w'>0); (ii) i = 2 represents ejection (u'<0 and w'>0); (iii) i = 3 represents the inward motion (u'<0 and w'<0); and (iv) i = 4 represents sweep (u'>0 and w'<0) (Afzalimehr et al., 2016). Because of limited space, Figure 3-52 only shows the

percentage of velocity fluctuation components (u' and w') from each quadrant (i = 1, 2, 3 and 4) at the upstream face of 0.06 m bridge pier. Of note, the percentage is defined as ($u'w'/U^{*2}$) *100 in which U* is shear velocity. Similar trends were observed for the other bridge piers sizes. In general, only outward motion and ejection have been observed and sweeps and inward motion do not contribute to the Reynolds stress distribution. Between the outward motion and ejection, outward motion is the most frequently occurring event while ejection has occurred at the upper portion of the flow near the free surface and inside the upper portion of the scour hole. In terms of the maximum point of Reynolds shear stress values for the ice-covered flow conditions, the values reached to their maximum closer to the channel bed in compared to open channel flow conditions. Regardless of flow cover, values of Reynolds shear stress gradually become smaller towards the free surface of the flow. Regardless of sediment type, the values of Reynolds shear stress follow the same pattern for open channel, smooth and rough covered flow conditions.

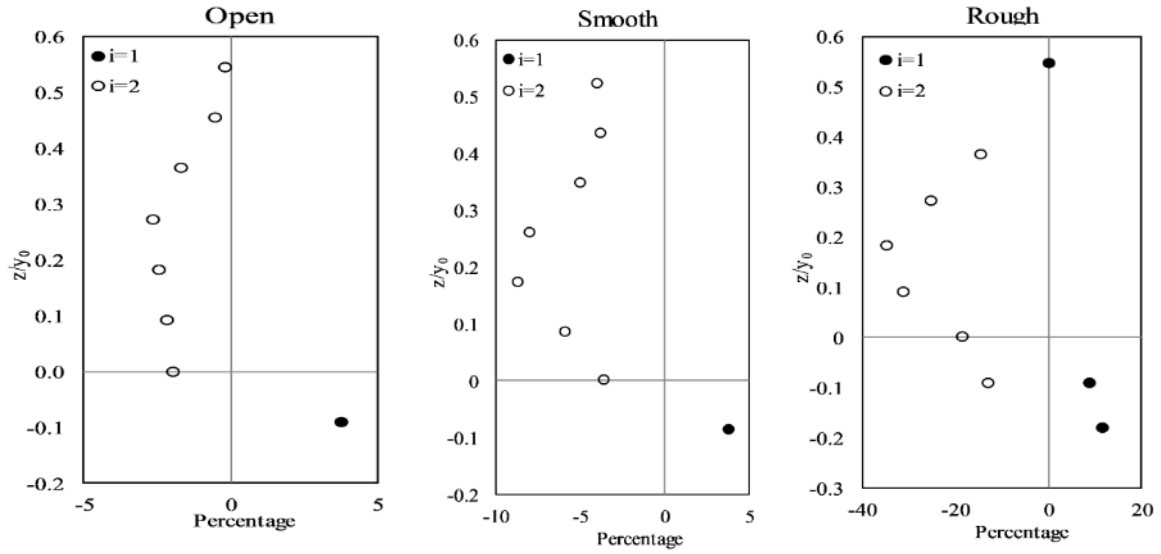

Figure 3-52: Percentage of velocity fluctuation components (u' and w') from each quadrant (i = 1, 2, 3 and 4) at the upstream of 60 mm pier for D50= 0.47 mm

3.4.3. Conclusions

In this paper, the three-dimensional velocity measurements along with scour hole development patterns around paired bridge piers were investigated under open channel, smooth, and rough ice-covered flow conditions with a non-uniform bed. A total of 108 experiments incorporating four side-by-side bridge piers with 60 mm, 90 mm, 110 mm and 17 mm diameter, respectively, were performed. The following is the summary of the milestones from this study:

1) In terms of scour hole pattern, regardless of sediment type and flow cover, the deepest point in each scour hole is clearly at the front face of bridge piers and the deposition mound is located downstream of bridge piers. Under the rough covered flow conditions, both the maximum scour depth and maximum deposition height are clearly greater than for open channel flow. The results indicate under the rough covered flow condition more sediment deposition develops at the downstream side of bridge piers and the deposition mound is wider spread than those under open flow.

2) For the streamwise velocity component (U_x), there is a logarithmic pattern which begins from the scour hole up to the water surface (or simulated ice-cover). In terms of velocity magnitude, the streamwise velocity for rough cover is generally greater than the scour hole velocity for smooth and open channel conditions. Regardless of sediment type, the rough ice cover resulted in a larger maximum velocity compared to the smooth ice cover.

3) The vertical velocity distribution (U_z), which is a representative of the strength of downfall velocity, is the greatest under rough ice cover. Generally, considering the absolute value of U_z, the values of U_z diminish from the channel bed toward the scour hole and from the channel bed toward the free surface. They tend to move toward right which implies

downflow velocity vectors are diminishing as they get closer to free surface which results in the velocity profile having a parabola-shaped profile pattern.

4) There is no significant difference in velocity field for the different sediment types and different types of sediment. Different types of armor layer and sediment ridge development were observed which are the result of differences in critical shear stress in the sediment particles.

5) Regardless of flow cover, the streamwise turbulent intensity along with the vertical turbulent intensity are highest just over the channel bed and diminishes towards the flow surface. The streamwise turbulent intensity, the vertical turbulent intensity and turbulence kinetic energy for the rough flow conditions are greater than those for open channel and smooth ice-covered flow conditions.

6) Under nearly the same flow conditions, the maximum value of turbulence kinetic energy and turbulent intensity occurs at the largest diameter pier.

7) Quadrant analysis revealed only outward motion and ejection have been observed at the upstream face of the pier while sweeps and inward motion do not contribute to the Reynolds stress distribution. Among outward motion and ejection, outward motion is the most frequently occurring event while ejection has only occurred at the upper portion of the flow near the free surface and within the upper reaches of the scour hole.

Notations:

D_{50}: 50^{th} percentile particle diameter (mm)
U_z: Vertical velocity component (m/s)
G: Bridge spacing (m)
D: Pier width (mm)
U_x: The streamwise velocity component (m/s)
U_y: The span-wise velocity component (m/s)
y_{max}: Maximum scour depth (mm)
y_0: Approach flow depth (mm)
U: Average approach velocity (m/s)
U^*= Shear velocity (m/s)
ɵ: Flow temperature (degree)
S: longitudinal slope of the channel
R: Hydraulic radius (m)
W: width of the channel (m)
Q: Volumetric flow discharge (m^3/s)
z: The vertical distance from bed (m)
TKE: turbulent kinetic energy (J/kg)
U_R: The resultant of the three average velocity components (m/s)
$\overline{u}$: Average velocity components (Time-averaged velocities) in x-direction (m/s)
$\overline{v}$: Average velocity components (Time-averaged velocities) in y-direction (m/s)
$\overline{w}$: Average velocity components (Time-averaged velocities) z-direction (m/s)
u_i: Instantaneous flow velocity in in x-direction (m/s)
v_i: Instantaneous flow velocity in y-direction (m/s)
w_i: Instantaneous flow velocity z-direction (m/s)
u': Velocity fluctuations in x-direction (m/s)
v': Velocity fluctuations in y-direction (m/s)
w': Velocity fluctuations in z-direction (m/s)
RMS [u']: Root-mean-square of the velocity fluctuations in streamwise direction (m/s)
RMS [v']: Root-mean-square of the velocity fluctuations in lateral direction (m/s)
RMS [w']: Root-mean-square of the velocity fluctuations in vertical direction (m/s)
τ_{xz}: Shear stress in x-z plane (m^2/s^2)
n: Number of time series data
i: Number of quadrants

3.4.4. References

Ahmed, F., & Rajaratnam, N. (1998). Flow around bridge piers. Journal of Hydraulic Engineering, 124(3), 288-300.

Afzalimehr, H., Moradian, M., Gallichand, J., & Sui, J. (2016). Effect of adverse pressure gradient and different vegetated banks on flow. *River Research and Applications*, *32*(5), 1059-1070.

Ataie-Ashtiani, B., & Aslani-Kordkandi, A. (2012). Flow field around side-by-side piers with and without a scour hole. European Journal of Mechanics-B/Fluids, 36, 152-166.

Beheshti, A. A., & Ataie-Ashtiani, B. (2009). Experimental study of three-dimensional flow field around a complex bridge pier. Journal of engineering mechanics, 136(2), 143-154.

Beltaos, S. (2007). River ice breakup processes: recent advances and future directions. Canadian Journal of Civil Engineering, 34(6), 703-716.

Blanckaert, K., & Lemmin, U. (2006). Means of noise reduction in acoustic turbulence measurements. Journal of hydraulic Research, 44(1), 3-17.

Chanson, H. (2008). Acoustic Doppler velocimetry (ADV) in the field and in laboratory: practical experiences. In International Meeting on Measurements and Hydraulics of Sewers IMMHS'08, Summer School GEMCEA/LCPC (pp. 49-66). Department of Civil Engineering at The University of Queensland.

Clifford, N. & French, J. 1993. Monitoring and modelling turbulent flows: historical and contemporary perspectives. In Turbulence: Perspectives on flow and sediment transport, (Eds. Clifford N., French, J., and Hardistry, J). Wiley: Chichester, 1-34.

Dey, S., Bose, S. K., & Sastry, G. L. (1995). Clear water scour at circular piers: a model. Journal of Hydraulic Engineering, 121(12), 869-876.

Dey, S. & Raikar, R. 2007. Clear-water scour at piers in sand beds with an armor layer of gravels. Journal of Hydraulic Engineering, 133, 703-711.

Ettema, R., Melville, B. W., & Constantinescu, G. (2011). Evaluation of bridge scour research: Pier scour processes and predictions. Washington, DC: Transportation Research Board of the National Academies.

Ettema, R., Braileanu, F., & Muste, M. (2000). Method for estimating sediment transport in ice-covered channels. Journal of Cold Regions Engineering, 14(3), 130-144.

Fugate, D. C., & Friedrichs, C. T. (2002). Determining concentration and fall velocity of estuarine particle populations using ADV, OBS and LISST. Continental Shelf Research, 22(11-13), 1867-1886.

Soltani-Gerdefaramarzi, S., Afzalimehr, H., Chiew, Y. M., & Gallichand, J. (2014). Effect of jet injection on flow structure in local pier scour. British Journal of Applied Science & Technology, 4(3), 477.

Golden Software, Inc, 1999. Surfer User's Guide: Contouring and 3D Surface Mapping for Scientists and Engineers. 809, 14th Street, Golden, CO 80401-1866.

Graf, W. & Istiarto, W. 2002. Flow pattern in the scour hole around a cylinder. Journal of Hydraulic Research, 40(1), 13-20.

Hafez, Y. I. (2016). Mathematical Modeling of Local Scour at Slender and Wide Bridge Piers. Journal of Fluids, 2016.

Hains D.B. & Zabilansky L. 2004. Laboratory test of scour under ice: data and preliminary results. Cold Regions Research and Engineering Laboratory, ERDC/CRREL TR-04-09: Hanover, NH, USA.

Hirshfield, F. (2015). The Impact of Ice Conditions on Local Scour around Bridge Piers (Doctoral dissertation, Doctoral Dissertation, University of Northern British Columbia).

Hodi, B. 2009. Effect of blockage and densimetric froude number on circular bridge pier scour. M.A.Sc. Thesis, Department of Civil and Environmental Engineering, Faculty of Engineering, University of Windsor, Windsor, Ont

Jay Lacey, R. W., & Roy, A. G. (2008). Fine-scale characterization of the turbulent shear layer of an instream pebble cluster. Journal of Hydraulic Engineering, 134(7), 925-936.

Kothyari, U. C., & Kumar, A. (2012). Temporal variation of scour around circular compound piers. Journal of Hydraulic Engineering, 138(11), 945-957.

Kumar, A., & Kothyari, U. C. (2011). Three-dimensional flow characteristics within the scour hole around circular uniform and compound piers. Journal of Hydraulic Engineering, 138(5), 420-429

Lu, S. S., & Willmarth, W. W. (1973). Measurements of the structure of the Reynolds stress in a turbulent boundary layer. *Journal of Fluid Mechanics*, *60*(3), 481-511.

Liu, H., Li, M., Zhou, J. G., & Burrows, R. (2010). Bridge afflux predictions using the Lattice Boltzmann method. *Procedia Environmental Sciences*, *2*, 1881-1893.

Melville, B. W., & Sutherland, A. J. (1988). Design method for local scour at bridge piers. Journal of Hydraulic Engineering, 114(10), 1210-1226.

Melville, B. W., & Chiew, Y. M. (1999). Time scale for local scour at bridge piers. Journal of Hydraulic Engineering, 125(1), 59-65.

Melville, B. W., & Coleman, S. E. (2000). Bridge scour. Water Resources Publication.

Muste, M., Braileanu, F., and Ettema, R. 2000. Flow and sediment transport measurements in a simulated ice-covered channel. Water Resources Research, 36(9), 2711-2720.

Ömer, K. (2011). Distribution of turbulence statistics in open-channel flow. International Journal of Physical Sciences 6 (14):3426–36.

Qadar, A. (1981, September). The vortex scour mechanism at bridge piers. In Institution of Civil Engineers, Proceedings, Pt2 (Vol. 71).

Roussinova, V., Biswas, N., and Balachandar, R. (2006). Revisiting turbulence in smooth uniform open channel flow. Journal of Hydraulic Research, 46 (Extra Issue1), 36-48.

Robert, A. & Tran, T. 2012. Mean and turbulent flow fields in a simulated ice-covered channel with a gravel bed: some laboratory observations. *Earth surface processes and landforms*, 37, 951-956.

Sontek, A. D. V. (1997). Operation manual, firmware version 4.0. Sontek, San Diego.

Sontek Inc. (2001). ADV operation manual, 1st Ed., Sontek Inc., San Diego

Sheppard, D. M., Odeh, M., & Glasser, T. (2004). Large scale clear-water local pier scour experiments. Journal of Hydraulic Engineering, 130(10), 957-963.

Sheppard, D. M., Melville, B., & Demir, H. (2013). Evaluation of existing equations for local scour at bridge piers. Journal of Hydraulic Engineering, 140(1), 14-23.

Sutherland, A. J. (1986). Reports on bridge failure. RRU Occasional Paper, National Roads Board, Wellington, New Zealand

Sui, J., Wang, J., He, Y. & Krol, F. 2010. Velocity profiles and incipient motion of frazil particles under ice cover. International Journal of Sediment Research, 25(1), 39-51.

Unger, J., & Hager, W. H. (2007). Down-flow and horseshoe vortex characteristics of sediment embedded bridge piers. Experiments in Fluids, 42(1), 1-19.

Wardhana, K., & Hadipriono, F. C. (2003). Analysis of recent bridge failures in the United States. Journal of performance of constructed facilities, 17(3), 144-150.

Wang, J., Sui, J., & Karney, B. 2008. Incipient motion of non-cohesive sediment under ice cover – an experimental study. Journal of Hydrodynamics, 20(1), 117-124.

Wilcox, A.C. & Wohl, E.E. (2007) Field Measurements of Three-Dimensional Hydraulics in a Step-Pool Channel. Geomorphology, 83, 215-231.

Williams, P., Balachandar, R. and Bolisetti, T., 2018, Blockage corrections for pier scour experiments, Canadian Journal of Civil Engineering, doi.org/10.1139/cjce-2017-0563

Williams, P., Bolisetti, T. & Balachandar, R., 2017, Evaluation of governing parameters on pier scour geometry, Canadian Journal of Civil Engineering, NRC Research Press, 44(1) pp. 48-58, DOI:10.1139/cjce-2016-0133.

Wu, P. and Balachandar, R., 2018, Effects of splitter plate on reducing local scour around bridge pier, River Research and Applications, Wiley, In press.

Wu, P. & Balachandar, R., (2016), Local scour around bridge abutments including effects of relative bed coarseness and blockage ratio, Canadian J. of Civil Engineering, Vol. 43 (1), 51-59.

Wu, P., Balachandar, R., & Sui, J., (2015a), Local scour around bridge piers under ice-covered conditions, J. of Hydraulic Engineering, 142(1), Art. No. 04015038, 10.1061/(ASCE)HY.1943-7900.0001063.

Wu, P., Hirshfield, F. & Sui, J., (2015b), "Local scour around bridge abutments under ice covered condition- an experimental study", International Journal of Sediment Research, Vol. 30(2015): P.39-47.

Wu, P., Hirshfield, F. & Sui, J., (2014a), "Further studies of incipient motion and shear stress on local scour around bridge abutments under ice cover", Canadian Journal of Civil Engineering, Vol. 41: P.892-899.

Wu, P., Hirshfield, F. & Sui, J., (2014b), "Armor layer analysis of local scour around bridge abutment under ice covered condition", River Research and Applications, (doi: 10.1002/rra.2771)

Zabilansky, L. J., Hains, D. B., & Remus, J. I. (2006). Increased bed erosion due to ice. In Current Practices in Cold Regions Engineering (pp. 1-12).

3.5. Three-dimensional numerical modeling of local scour around bridge piers under ice-covered flow condition

Piers which are constructed inside the rivers are one of the most frequently used foundation in offshore platforms, bridges, etc. Due to local scour process, the flow pattern around these foundations will be changed and the turbulence will be enhanced, which ultimately leads to the creation of horseshoe vortex in front of the pier, the wake vortex behind the pier, and the contraction of streamlines at the side of the pier (Zhang et al, 2017). The horseshoe vortex is created by the flow of water separating at the upstream face of the bridge pier where the initial scour hole has developed. Wake vortices develop behind a bridge pier and disturb the downstream flow pattern. These vortices are the main causes of local scour creation and they lead to intensified local sediment transport capacity, and the expansion of local scour around the piers. Due to the local scour, the insertion depth of the pier reduces as the scour depth around the pier grows, which is directly associated with the stability of pier foundation. The deeper the depth of local scour around the pier, the more vulnerable pier foundation becomes which leads to bridge collapse in the many case (Zhang et al, 2017). Therefore, it is commonly accepted that the local scour is one of the main causes of pier foundation failure in river and marine environments. Thus, the estimation of riverbed deformation in the vicinity of bridge piers is crucial for the safe design of bridge piers. The development of scour hole around bridge piers is affected by the characteristics of flow pattern near the bed and around the pier. The characteristics of flow pattern around the piers are clearly fully three-dimensional and complex. The tremendous complexity of three-dimensional flow field around a pier is attributed to separation and generation of multiple vortices. It is even more aggravated because of the dynamic interaction between the flow and the moveable bed

throughout the development of a scour hole (Esmaeili, 2009). Therefore, precise prediction of scour patterns around bridge piers mainly depend on the flow field and mechanism of sediment transport in and out of the scour hole. Up to date, many researchers have done experiments to investigate the local scour around bridge piers and develop empirical equations to estimate the maximum scour depth under open channel flow condition (Ettema et al., 2011; Sheppard et al., 2013). In winter, ice cover appears in many rivers in the northern region. The influence of ice cover on a channel involves in complex interactions among the ice cover, fluid flow, and channel geometry. This complex interaction can have a dramatic effect on the sediment transport process (Hains et al., 2004). The formation of a stable ice cover in natural rivers effectively doubles the wetted perimeter compared to open channel conditions and causes the maximum velocity to be lowered towards the channel bed (Sui et al., 2010). The most extreme case of local scour around bridge piers occurs in cold regions where the surface of flow is covered with ice. Zabilansky and White (2005) investigated the impact of ice cover on scour in narrow rivers. It was found that when discharge increases above the freeze-up datum, the pressurized flow condition, combined with the rough underside of the ice, will cause the maximum velocity in the flow to increase and shift closer to the bed. Wu et al (2015) studied the effect of relative bed coarseness, flow shallowness, and pier Froude number on local scour around a bridge pier and reported that the scour depth under covered conditions is larger compared to that under open channel flow conditions. Wu et al (2014) investigated scour morphology around a bridge abutment under ice cover. It was found that, at different locations around the abutment, the sediment sorting process under ice cover was more obvious. Wu et al (2015) studied the impact of ice cover on local scour around bridge abutments.

In recent years, by means of computer science, the numerical method has been widely applied in many fields of science such as hydromechanics. Not only CFD models are timely and monetary efficient and are highly precise, but also, they are free of scaling effect and can be employed for various types of geometry and hydraulic conditions of a specific hydraulic problem (Toombes & Chanson, 2011). Regarding the numerical modelling of local scour around bridge pier, Richardson and Panchang (1998) used a fully 3D hydrodynamic model to simulate the flow pattern at the base of a cylindrical bridge pier within a scour hole. Vasquez and Walsh (2009) applied FLOW-3D to simulate the initial stages of scour development in a complex pier made of a large pile cap and 10 cylindrical piles. Kim et al (2014) studied the local scour around two adjacent cylinders, in which the Large-eddy simulation (LES) was employed to simulate the instantaneous turbulent flow around the cylinders. In their research, the effects of both the longitudinal and transverse spacing distance between cylinders on the flow structure, scour evolution, bed topography, and maximum scour depth were examined in detail. To the authors' knowledge, only few studies have been carried out to compare results of numerical simulation of local scour to those of laboratory experiments, and none of those studies was devoted to investigating this phenomenon under ice-covered condition. In present study, to understand the mechanisms of local scour around side-by-side bridge piers, the velocity vectors, streamline around bridge piers, morphological changes of scour hole and deposition patterns under both open channel flow and ice-covered (smooth-covered and rough-covered) flows conditions have been studied. Further, based on the experimental results, it has been assessed whether it is feasible to use the FLOW-3D numerical model to simulate the flow field and local scour depth pattern around bridge piers. A comparison between the results of numerical simulation of local scour

under different flow covers (open channel flow and the ice-covered flow) and those of laboratory experiments has been presented. The impacts of ice cover on the local scour process around bridge piers have been investigated.

3.5.1 Experiment setup

Experiments were done in a large-scale flume at the Quesnel River Research Centre of the University of Northern British Columbia, Canada. The flume is 38.2 m long, 2 m wide and 1.3 m deep. Figure 3-53 shows a plan and side view of the experimental flume. A holding tank with a volume of 90 m^3 was located at the upstream end of the flume to maintain a constant discharge during the experimental runs. To create different velocities, three input valves are connected to control the inlet volumetric discharge. At the end of the holding tank and upstream of the main flume, water overflows from a rectangular weir into the flume. Two sand boxes were constructed in the flume. Both have a depth of 0.30 m and are 10.2 m spaced apart. The lengths of the sand boxes are 5.6 m and 5.8 m, respectively. In each sand box, a pair of bridge piers was placed. Three natural non-uniform sediment compositions with median grain sizes of 0.50 mm, 0.47 mm, and 0.58 mm were used. Four pairs of cylindrical bridge piers with diameters of 60 mm, 90 mm, 110 mm, and 170 mm were used. Each pier was offset from the centre line by 25 cm, as illustrated in Figure 3-54. The water level in the flume was controlled by the downstream tailgate. In front of the first sand box, a SonTek two-dimensional Flow Meter was installed to measure flow velocities and water depth. A staff gauge was also installed in the middle of each sand box to manually verify the water depth. The velocity fields in the scour holes were measured using a 10-MHz Acoustic Doppler Velocimeter (*ADV*). Styrofoam panels were used to represent ice cover and covered the entire surface of the flume. Two types of model ice cover were used, namely smooth

cover and rough cover. The smooth cover was the smooth surface of the original Styrofoam panels while the rough cover was made by attaching small Styrofoam cubes to the bottom of the smooth cover. The dimensions of Styrofoam cubes were 25 mm × 25 mm × 25 mm and they were spaced 35 mm apart. 108 Experiments (36 experiments for each sediment type) were done under open channel, smooth covered, and rough covered flow conditions. In terms of different boundary conditions (open channel, smooth, and rough covered flows), for each sediment type and each boundary condition, 12 experiments were done. Throughout the calibration stage of the experiments, local scour around bridge piers was carefully watched hourly for any changes in the scour depths. It was observed that after approximately a period of 24 hours, no obvious change in scour depth was observed and scour hole equilibrium depth was achieved. After 24 hours, the flume was gradually drained, and the scour and deposition pattern around the piers was measured.

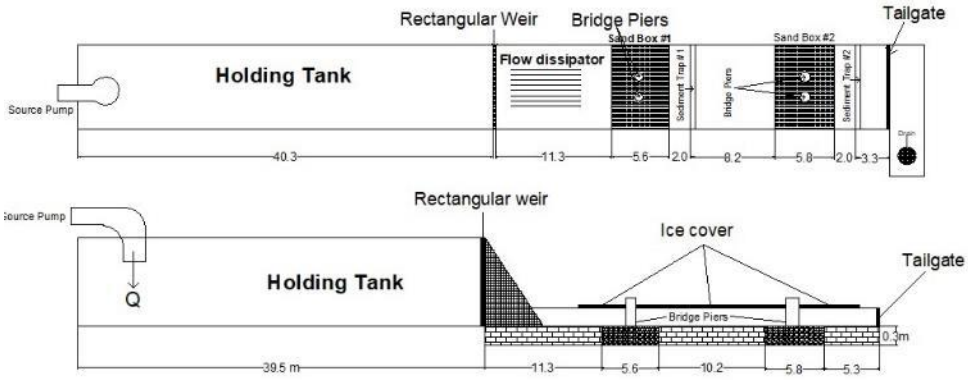

Figure 3-53: Plan view and side view of experiment flume

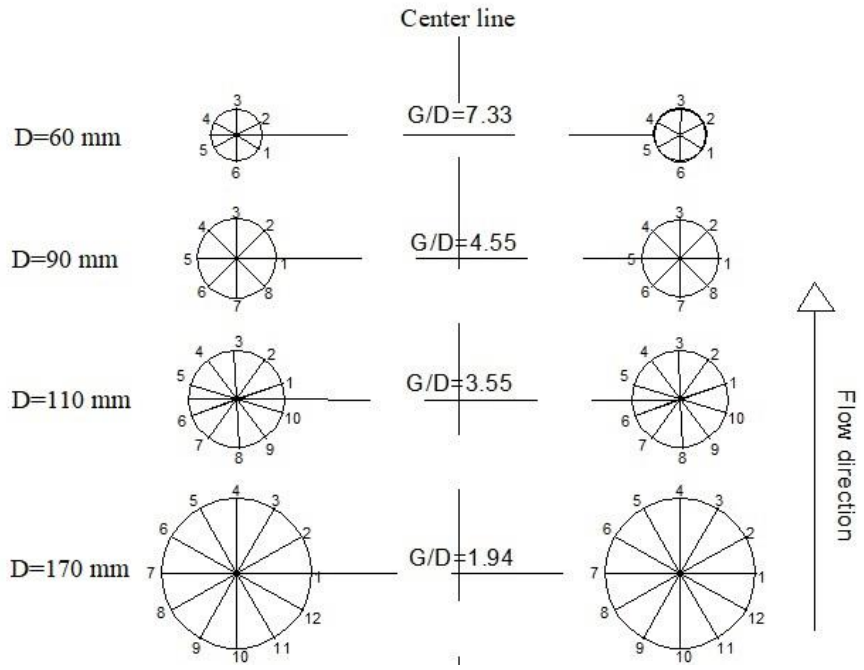

Figure 3-54: The spacing ratio and measuring points around the circular bridge piers

3.5.2 Numerical model

In present study, FLOW-3D which is a widely used computational fluid dynamics (CFD) model has been evaluated. FLOW-3D adopts the volume of fluid (VOF) method (Hirt and Nichols, 1981) to track the free water surface. The Fractional Area/Volume Obstacle Representation (FAVOR) method (Hirt and Sicilian, 1985) is also employed to model complex geometric regions (such as the packed sediment) in fixed rectangular meshes using area fractions (A_i) and volume fractions (V_F) in FLOW-3D. The area fractions (A_i) are defined at each of the six faces as ratios of the particular open area to the total area in each mesh cell and V_F is defined as the ratio of the volume open to fluid to the total cell volume. A_i and V_F associated with the packed sediments are updated at each time step to describe the modifications of the geometry of the packed sediment. The FAVOR method is able to precisely define the geometry by using a smaller number of mesh cells than the finite

difference method (FDM) which can reduce the computation time to a great extend (Flow Science Inc., 2015).

- **Governing equations**

FLOW-3D incorporates various turbulence models, a sediment transport model and an empirical bed erosion model together with VOF (Volume of Fraction) method for calculating the free surface of the fluid without solving the air component (Hirt & Nichols, 1981). The RANS (RAN: Re-Normalisation Group) equations closed with RNG $k-\varepsilon$ turbulence model are adopted as the governing equations for the incompressible viscous fluid motion around the bridge piers. The general governing RANS and continuity equations for Newtonian, incompressible fluid flow, including the FAVOR variables, are given as follows. Note that area fractions (A_i) and volume fractions (V_F) appear in equations.

$$\frac{\partial x}{\partial x_i}\left(u_i A_i\right)=0 \tag{3-5-1}$$

$$\frac{\partial u_i}{\partial t}+\frac{1}{V_F}\left(u_j A_j \frac{\partial u_i}{\partial x_j}\right)=-\frac{1}{\rho}\frac{\partial P}{\partial x_i}+g_i+f_i \tag{3-5-2}$$

Where:

$$f_i=\frac{1}{V_F}\left[\frac{\tau_{b,i}}{r}-\frac{\partial}{\partial x_j}\left(A_j S_{ij}\right)\right] \tag{3-5-3}$$

$$S_{ij}=\left(\mu+\mu_T\right)\left(\frac{\partial u_i}{\partial x_j}+\frac{\partial u_j}{\partial x_i}\right) \tag{3-5-4}$$

Where u_i = velocity component in subscript direction, V_F = volume fraction of fluid in each cell, A_i = fractional area open to flow in subscript direction, p = pressure, ρ = mass density of fluid, t = time, g_i = gravitational force in subscript direction and f_i = diffusion transport term. V_F and A_j (cell face areas) =1, thereby reducing the equations to the basic

incompressible RANS equations. S_{ij}= strain rate tensor, $\tau_{b,i}$ = wall shear stress and ν = kinematic viscosity, ν_T= kinematic eddy viscosity.

- **Sediment scour model**

The sediment scour model in FLOW-3D is fully coupled with the fluid flow (Flow Science Inc, 2015). It simulates all the sediment transport processes of non-cohesive soil including bedload transport, suspended load transport, entrainment and deposition. It allows multiple non-cohesive sediment species with different properties such as grain size, mass density, critical shear stress, angle of repose, and parameters for entrainment and transport. It approximates the motion of the sediment particles by predicting the erosion, advection, and deposition of them. The sediment scour model incorporates four sediment transport mechanisms, which could define the sediment transport processes. The first mechanism of the sediment transport is entrainment and it occurs when the bed shear stress exceeds the critical shear stress, as the result, the sediment particles that are set at the top of the packed bed may be lifted and move into suspension. The second mechanism is suspended load transport in which the sediment particles are carried by the flow current within a certain height above the packed bed. The third mechanism is deposition, which occurs when the ability of flow to carry the suspended sediments decreases because of impact of gravity, buoyancy, and friction and as the result the suspend sediments are deposited where the slowing flow can no longer move them. The last mechanism of the sediment transport is bed-load transport, which includes grains that roll, slide or bounce along the bed in response of the shear stress applied by fluid flow (Zhang, 2017). Therefore, sediment scour model can be used to compute the suspended sediment transport, settling of sediment due to gravity, the entrainment of the sediment due to bed shearing and flow perturbations, bed-load transport,

whereby sediment grains roll, hop or slide along the packed sediment bed (Flow Sciences Inc 2015).

- **Deposition and entrainment**

Deposition is the process that the sediment grains either settle out of suspension onto packed bed due to their weight or come to rest in bed-load transport. Settling and entrainment of grains are opposite processes and often occur at the same time (Flow Sciences Inc 2015). According to Mastbergen and Van Den Berg (2003), the entrainment lift velocity of sediment is computed as:

$$U_{lift,i} = a_i n_s d_*^{0.3} \left(q_i - q_{cr,i}^{'}\right)^{1.5} \sqrt{\frac{\|g\| d_i \left(r_i - r_f\right)}{r_f}} \tag{3-5-5}$$

Where, α_i is the entrainment parameter, whose recommended value is 0.018 (Mastbergen and Van Den Berg, 2003) and n_s is the outward pointing normal to the packed bed interface. $U_{lift,i}$ is used to compute the amount of packed sediment that is converted into suspension, effectively acting as a mass source of suspended sediment at the packed bed interface. θ_i is the local Shields parameter which is calculated based on the local bed shear stress, $\theta_{cr,i}$ is the critical Shields parameter, $\|g\|$ is the magnitude of the acceleration of gravity, d_i is the diameter, ρ_i is the density of the sediment species i, ρ_f is the fluid density and d* is dimensionless diameter of the sediment, which can be computed by:

$$d_{*,i} = d_i \left[\frac{r_f \left(r_i - r_f\right) \|g\|}{m_f^2}\right]^{1/3} \tag{3-5-6}$$

In which, μ_f is the dynamic viscosity of fluid. The local Shields parameter is computed based on the local bed shear stress, τ:

$$q_i = \frac{t}{\|g\| d_i \left(r_i - r_f\right)} \tag{3-5-7}$$

where, τ is calculated using the law of the wall and the quadratic law of bottom shear stress for 3D turbulent flow and shallow water turbulent flow, respectively, with consideration of bed surface roughness (Flow Sciences Inc 2015). The dimensionless critical Shields parameter is computed using the Soulsby-Whitehouse equation (Soulsby & Whitehouse, 1997):

$$\theta_{cr,i} = \frac{0.3}{1+1.2d_i^*} + 0.055\left[1 - \exp\left(-0.02d_i^*\right)\right] \quad (3\text{-}5\text{-}8)$$

Deposition is the process that sediment grains either settle out of suspension on the packed bed due to the weight or come to rest in bedload transport (Flow Sciences Inc 2015). The setting velocity of the sediment is computed as follow (Soulsby, 1997):

$$u_{settling,i} = \frac{v_f}{d_i}\left[\left(10.36^2 + 1.049d_*^3\right)^{0.5} - 10.36\right] \quad (3\text{-}5\text{-}9)$$

Where, v_f is the kinematic viscosity of fluid.

- **Suspended sediment**

Suspended sediment is transported by advection along with the fluid. FLOW-3D assumes there are totally *i* sediment species. The transport equation for each sediment species *i* is:

$$\frac{\partial C_{s,i}}{\partial t} + \nabla \bullet \left(\overline{u}_{s,i} C_{s,i}\right) = \nabla \bullet \nabla \left(D_f C_{s,i}\right) \quad (3\text{-}5\text{-}10)$$

Where, $C_{s,i}$ is the concentration of the suspended sediment, in units of mass per unit volume of species *i*, D_f is the diffusivity; $\overline{u}_{s,i}$ is the suspended sediment velocity. Of note, each sediment species in suspension moves at its own velocity that is different from those of fluid and other species. This is due to difference in inertia and drag force between grains with different mass density. Supposing that there are not strong interactions between each grain, and that the velocity difference between the suspended grains and the fluid-sediment mixture

is primarily the setting velocity of the grains, the sediment velocity of species *i* can be calculated as:

$$u_{s,i} = \overline{u} + u_{settling,i} c_{s,i} \tag{3-5-11}$$

Where, $\overline{u}$ represents the velocity of the fluid-sediment mixture, and $c_{s,i}$ is the volume of suspended sediment species *i* per volume of the fluid-sediment mixture and is computed as follow:

$$c_{s,i} = \frac{C_{s,i}}{\rho_i} \tag{3-5-12}$$

Sediment is entrained by the picking up and re-suspension of packed sediment due to shearing and small eddies at the packed sediment interface. The empirical model used in FLOW-3D is based on method proposed by Mastbergen and Von den Berg (2003). The first step to compute the critical Shields number is the calculation of the dimensionless parameter d^* from Eq. 11. According to Eq. 11, the dimensionless critical Shields parameter is computed using the Soulsby-Whitehouse equation (Soulsby & Whitehouse, 1997):

$$q_{cr,i} = \frac{0.3}{1+1.2d_i^*} + 0.055\left[1 - \exp\left(-0.02d_i^*\right)\right] \tag{3-5-13}$$

- **Bed-load transport**

Bed-load transport is the sediment transport due to rolling or bouncing over the surface of the packed bed of sediment. FLOW-3D considers three equations for volumetric transport rate of sediment per width of bed, namely, models proposed by Meyer-Peter & Muller (1948); Nielsen (1992) and Van Rijn (1984). In the current study, Meyer-Peter & Muller (1948) equation was used. This model predicts the volumetric flow of sediment per unit width over the surface of the packed bed:

$$\Phi_i = \beta_i\left(\theta_i - \theta'_{cr,i}\right)^{1.5} \tag{3-5-14}$$

Where, the typical value of $\beta_i = 8$ (5 and 13 for low and high sediment transport, respectively) (Van Rijn, 1984), ϕ_i is the dimensionless bed-load transport rate and is related to the volumetric bed-load transport rate ($q_{b,i}$) by:

$$q_{b,i} = \Phi_i\left[\left|g\right|\left(\frac{\rho_i - \rho_f}{\rho_f}\right)d_i^3\right]^{\frac{1}{2}} \tag{3-5-15}$$

The bedload transport velocity is proposed by (van Rijn, 1984):

$$u_{bedload,i} = \frac{q_{b,i}}{\delta_i c_{b,i} f_b} \tag{3-5-16}$$

where, f_b is the critical packing fraction of the sediment, $c_{b,i}$ is the volume fraction of species i in the bed material which is used to account for the effect of multiple species, $q_{b,i}$ is the volumetric bed-load transport rate, and δ_i is the bed-load thickness which is calculated by:

$$\frac{\delta_i}{d_i} = 0.3 d_*^{0.7}\left(\frac{\theta_i}{\theta'_{cr,i}} - 1\right)^{0.5} \tag{3-5-17}$$

- **Model setup**

The numerical simulations of local scour around bridge piers in channel with the finest sediment (D_{50}=0.470 mm) and the coarsest sediment (D_{50}=0.580 mm) have been carried out. In total, 72 numerical models have been established to simulate local scour process around four pairs of side-by-side bridge piers under open channel, smooth ice-covered and rough ice-covered flow conditions. Figure 3-54 shows the bridge pier diameters and their associated bridge pier spacing G/D. The scale of the numerical models is set to be 5 m × 2 m × 1 m for all the models and a pair of bridge piers is located at the center of the channel. The computational domain is long enough and provides adequate distance downstream of piers

to ensure there is not any interference between the turbulent flow and the downstream boundary. The thickness of the packed bed equals to 0.30 m. The packed bed is composed of the finest sand and the coarsest sand with D_{50} of 0.470 mm and 0.580 mm respectively, as of the experimental study. The entrainment coefficient, which can be used to scale the scour rate, uses a default value of 0.018 from the data of (Mastbergen and Van Den Berg, 2003). The critical Shields number was calculated using the Soulsby-Whitehouse equation. The bed load coefficient is used to control the rate at which bed load transport occurs at a given shear stress, which is higher than the critical shear stress with a default value of 8.0 (suggested vales ranging from 5.0 for low transport to 13.0 for very high sand transport) (Soulsby, 1997). The angle of repose, which describes the maximum resting angle of the bed, equals to default value of 32 degrees. The other corresponding parameters are the same with the experiment in order to verify the applicability, validity and accuracy of the current numerical models leading to a significant improvement in the case of numerical simulation of sediment transport around bridge piers especially under ice-covered conditions.

- **Meshing**

The computational domain is subdivided into a mesh of fixed rectangular cells using Cartesian coordinates. A multi-block mesh based on hexahedral elements is considered by using three mesh blocks. Fine cells with grid size of 20×20 mm is used for the second mesh block in which bridge piers are present and is from 0.5 m to 4.5 m from the origin. Whereas, to optimize the computational time, 30 mm×30 mm cells are adopted from 0 to 1.5 m and from 4.5 to 5.6 m from the origin for the first and third mesh blocks, respectively. The sensitivity analysis showed that no significant changes were observed in bed scour with using smaller grid although the simulation time with the finer mesh increased in 2.2 times. Total

number of real cells are 1,072,963 in which 35,376 cells are for the first mesh block, 1,000,000 cells are for the second mesh block and 37,587 cells are allocated to the third mesh block.

- **Boundary Conditions**

To simulate flow fields and scour process around bridge piers, it is important that the boundary conditions are preciously given. Figure 3-55 illustrates the boundary conditions for the numerical models under rough ice-covered flow conditions. Because the flow domain is defined as a hexahedral in cartesian coordinates, there are totally six different boundaries on the mesh to be fixed, in addition to the boundary conditions for the pier surface and the ice cover bottom surface. The boundaries of the mesh and their coordinate directions were set as follows: sidewalls y—no slip/wall; top z—symmetry; bottom z—no slip/wall; left x—specific velocity; and right x—outflow. The bridge pier was modeled as a smooth surface with no slip. For the case of smooth ice-covered flow condition, smooth non-floatable ice cover was applied at the same water depth of physical model. However, for the case of rough ice-covered flow condition, in addition to the simulated smooth ice cover, ice cubes which had the dimension of 35 mm × 35 mm × 35 mm were simulated. With this configuration, the flow moves from left to right, parallels with the slip walls, and locates between the no-slip floor and on the sediment bed until it reaches to the outflow boundary.

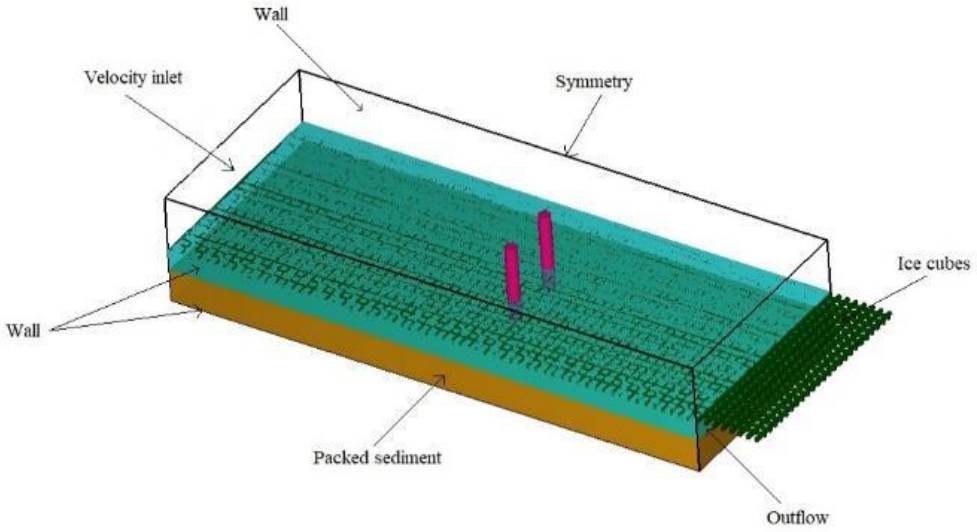

Figure 3-55: The calculation model and boundary conditions for rough ice-covered flow condition

3.5.3. Principal results and discussion

In this section, based on experimental results under different flow and cover conditions (open channel, smooth ice-covered and rough ice-covered flow), the mechanisms of local scour around the side-by-side bridge piers in channel bed with different bed material will be examined. To avoid repetition, simulation results of the maximum depth of scour hole around the 110-mm side-by-side piers have been presented for channel bed with the fine sand.

- **Local scour under open flow condition**

Simulation results of local scour around the 110-mm side-by-side piers under open flow condition show the scour profile, morphological changes, and deposition patterns in the vicinity of the bridge piers. Figure 3-56a illustrates the simulation results around the 110-mm side-by-side piers in channel bed with sand of 0.470 mm after 450 s, compared to those of laboratory experiment (with average approaching velocity of 0.20 m/s and flow depth of 0.253 m) as showed in Figure 3-56b. As shown in Figure 3-56, the maximum scour depth of numerical simulation which occurs at the pier face agrees well with the experimental result. For both numerical simulation and laboratory experiment, the maximum scour depth of 75

mm appears in front of the bridge piers, which is due to the acceleration of the flow at these areas. Of note, the upstream face of the bridge pier is the location where the horseshoe vortex is formed, which is mainly caused by the down flow in front of the pier. The horseshoe vortex along with the acceleration of the flow at the sides of the pier increase the bed shear stress, which will ultimately lead to development of local scour around the bridge piers. As illustrated in Figure 3-57, the simulated scour depths around the bridge pier are compared to those of experiment for channel bed with both coarse and fine sand. Of note, point "8" in Figure 3-57 is the apex of the pier face facing upstream. Figure 3-58a shows two-dimensional velocity field at the *x*-*y* plan at the water depth of z= 0.326 m at the last second of simulation time, and Figure 3-58b shows the distribution of turbulent energy (mean kinetic energy per unit mass) at the cross section of the bridge piers under open channel flow condition. One can see from Figure 3-58b, the turbulent energy which is associated with eddies of flow increases from the channel bed toward water surface and reaches the maximum around the sides of bridge piers. Due to the flow being impeded in front of bridge pier, flow velocity decrease at this location which is clearly seen in Figure 3-58a. Figure 3-59 illustrates flow streamlines around the right-hand side bridge pier at the initial stage of the development of the scour hole (t=22.25 s) and at the final stage (t=445 s). The streamlines in Figure 3-59 clearly show how the obstruction caused by bridge pier leads flow velocity to separate at the pier face. Besides, the acceleration of the flow at the sides of bridge pier, and the existence of the wake vortex at the back of bridge pier can been clearly seen in Figure 3-59. By comparing Figure 3-59a to Figure 3-59b, one can see that the scouring process gradually declines over the course of time which will cause the horseshoe vortex and the wake vortex to become weaker and, consequently, the bed shear stress decrease. When the bed shear stress

becomes less than the critical shear stress, the scour depth will reach to the equilibrium state at which the sediment particles may not be transported or moved into suspension any more.

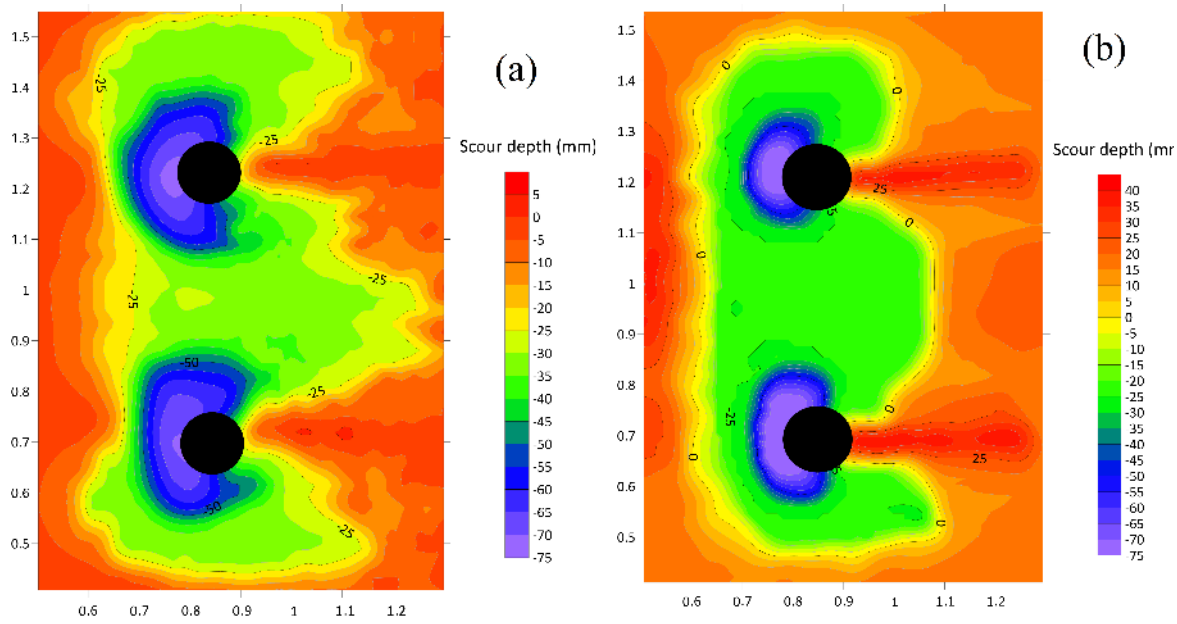

Figure 3-56: (a) Simulated bed elevation contours around the 110-mm bridge piers in channel bed with fine sediment at t=450 s under open channel condition; (b) Laboratory measured bed elevation contours around 110-mm bridge piers in channel bed with fine sediment under open channel condition

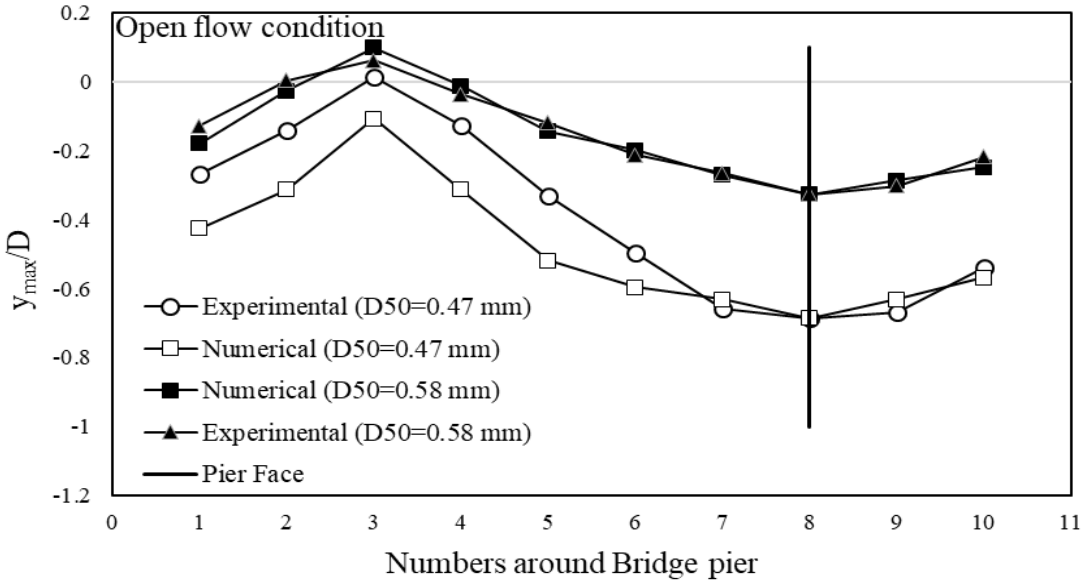

Figure 3-57: Simulated scour depths compared to those of experiments around the 110-mm bridge piers in channel bed under open channel flow condition

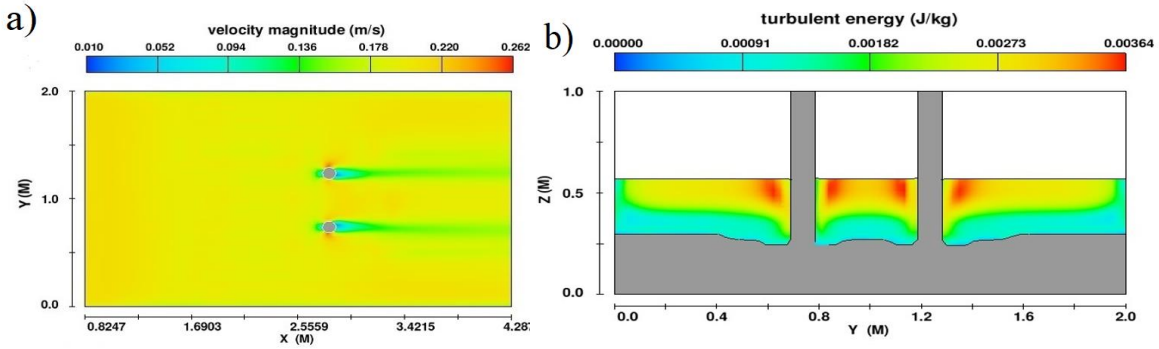

Figure 3-58: (a): Flow field at the plane z= 0.326 m at the end of simulation time, and (b): The distribution of turbulent energy at the cross section of the bridge pier under open channel flow condition

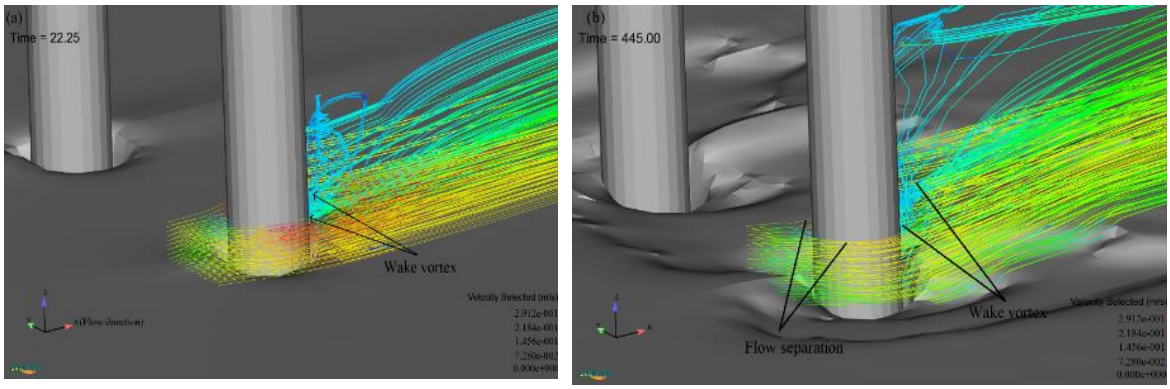

Figure 3-59: (a) Flow streamlines around the 110-mm bridge pier: (a) at initial stage (t= 22.25 s) and (b) at the last second of simulation (t= 445 s)

- **Local scour under ice-covered flow conditions**

The appearance of an ice cover in a river changes the velocity profile, with the ice cover acting as a flow boundary that increases the wetted perimeter and the composite roughness. The presence of ice cover tends to shift the velocity maximum closer to the bed, and lead to

more erosion (Sui et al., 2010). The maximum velocity occurs between the bed and the bottom of the ice cover in a region depends on the relative roughness of the two boundaries. The velocity drops to zero at each boundary due to the no-slip boundary condition, leading to a parabola-shaped profile. The rougher the ice cover, the further the maximum velocity shifts towards the bed in order to reduce energy, causing more scour (Sui et al., 2010). Therefore, a lower average velocity threshold is needed to reach to the critical shear stress for bed deformation in an ice-covered flow as compared to an open-water flow (Beltaos, 2011). As pointed out by Hains and Zabilansky (2004), the presence of ice has resulted in increase in local scour depth at bridge piers by 10%–35%. In this section, results of numerical simulation of flow under ice-covered condition will be presented with comparison to those of experiments in laboratory. In present study, since the local scour patterns around the side-by-side bridge piers in channel bed with the coarse sediment are similar to those of in channel bed with the fine sediment, to avoid repetition, only the results for channel bed with fine sand is presented in this paper.

- **Local scour under smooth ice-covered flow condition**

Simulated results of local scour patterns around the 110-mm side-by-side bridge piers under smooth-covered flow condition will be described by the scour depth, morphological changes, and deposition patterns. Figure 3-60a illustrates simulated bed elevation contours around the 110-mm bridge piers in channel bed with fine sediment and Figure 3-60b illustrates those of laboratory experiment (with an average approaching velocity of 0.20 m/s corresponding to a water depth of 0.255 m). One can see from Figures 3-60 (a-b), results of the numerical simulation agree well with those of experimental study. The maximum scour depth appears at the upstream pier face (point “8”) with a scour depth of 85 mm. However, results of

simulated scour depth show more irregular distributed comparing to those of experiments. The difference between the simulated scour pattern and that of experiments is due to the fact whether the ice cover floats freely. In laboratory experiments, model ice cover floated freely on water surface. However, in the numerical simulation, ice cover had to be considered as rigid due to the restriction in numerical model for simulating the ice-covered flow. In the case of a non-moving ice cover, the restraint on the cross-sectional area causes increased velocity and sediment transport capacity with any increase in scour (Zabilansky, 1996). If an ice cover floats freely, the drop-in flow can reduce the transport of both suspended and bed-load sediment compared to non-moving ice cover (Ettema and Kempema, 2012). Figure 3-61 shows the comparison between the simulated scour depths and those of experiments around the bridge pier in channel bed with both coarse and fine sands. As results showed in Figure 3-61, for both numerical simulation and laboratory experiment, the maximum scour depth occurred at the upstream apex of the pier face (point 8). However, the simulated scour depth is slightly deeper than that of laboratory experiment. Figure 3-62a shows the simulated two-dimensional velocity field at the *x*-*y* plan at the water depth of z= 0.326 m at the last second of numerical simulation under smooth covered condition. Since the flow in front of the bridge pier is impeded, flow velocity decreases clearly in front of bridge piers, as showed in Figure 3-62. Figure 3-62b shows the distribution of turbulent energy at the cross section where the bridge piers are located under smooth covered condition. Obviously, the turbulent energy is higher near the bridge piers.

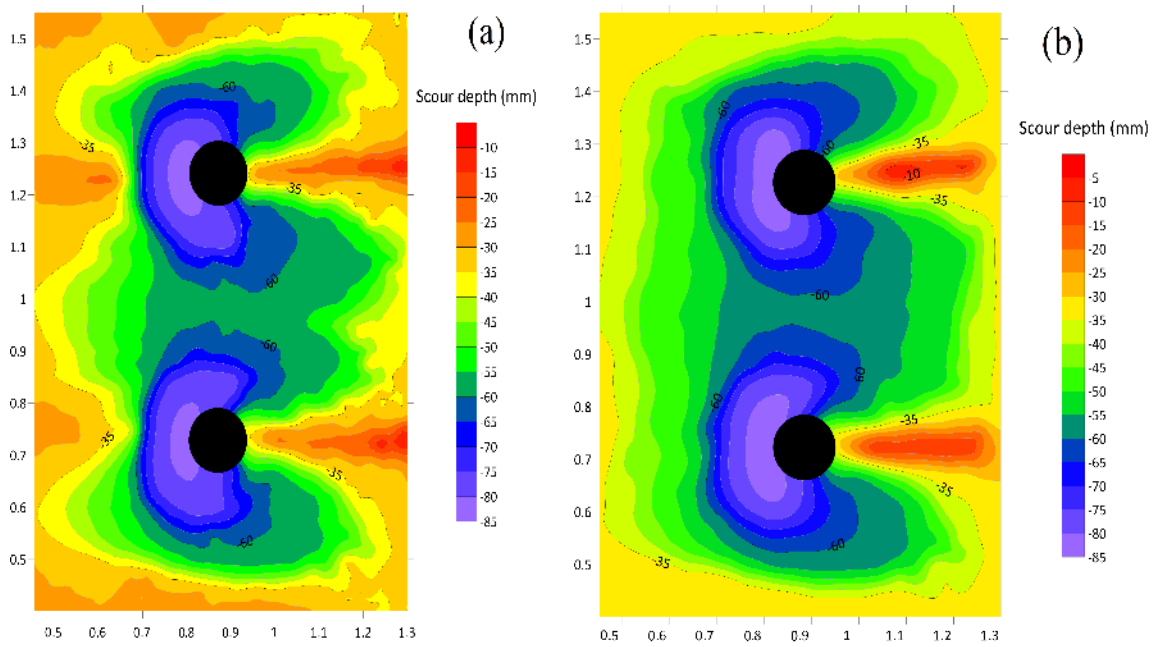

Figure 3-60: (a) Simulated bed elevation contours around 110-mm bridge piers in channel bed with fine sediment at t=450 s under smooth-ice-covered condition; (b) Laboratory measured bed elevation contours around 110-mm bridge piers in channel bed with fine sediment under smooth-ice-covered condition

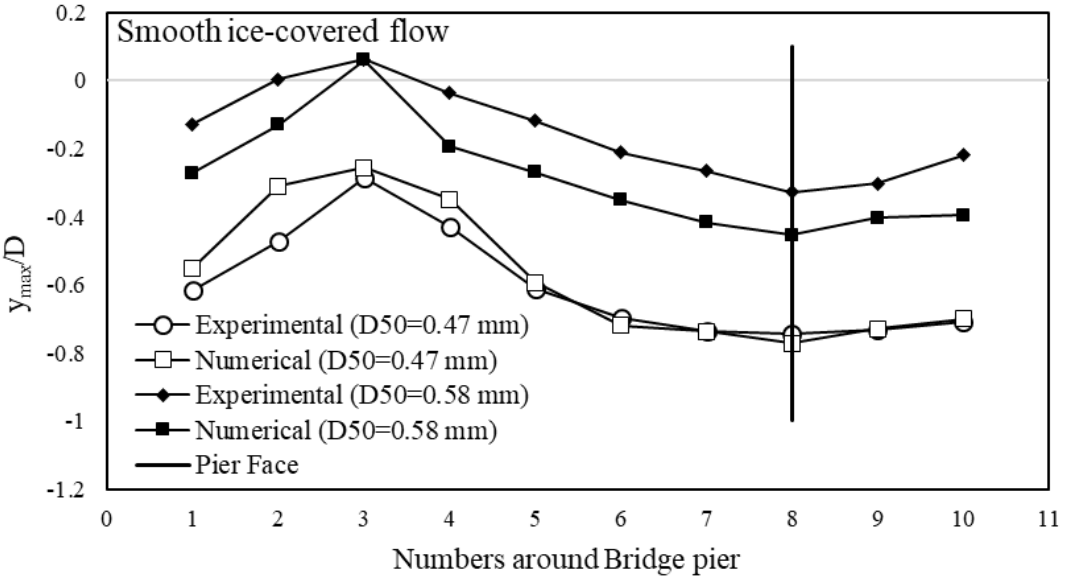

Figure 3-61: Simulated scour depths compared to those of experiments around the 110-mm bridge piers in channel bed under smooth ice-covered condition

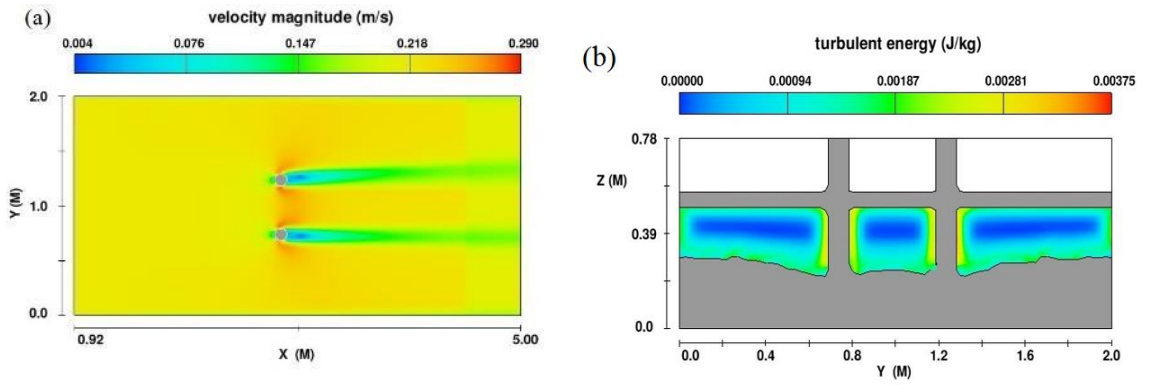

Figure 3-62: (a): Flow field at the plane z= 0.326 m at the end of simulation time, and (b): The distribution of turbulent energy at the cross section of the bridge pier under the smooth-covered flow condition

○ Local scour under rough ice-covered flow condition

Figure 3-63a illustrates simulated bed elevation contours around the 110-mm bridge piers in channel bed with fine sediment compared to those of laboratory experiment as showed in Figure 3-63b (with an average approaching flow velocity of 0.19 m/s corresponding to a water depth of 0.220 m). For both laboratory experiments and numerical simulation, the maximum scour depth around the bridge piers reaches a value of 95 mm. However, with respect to the numerical simulation, the simulated scour field around bridge piers is more widely spread. The difference between the simulated scour patterns and those of experiments based on whether the ice cover floats freely. In laboratory experiments, model ice cover floated freely on water surface. However, in the numerical simulation, ice cover had to be considered as rigid due to the restriction of the numerical model in simulating the ice-covered flow. Besides, the local scour process in the vicinity of the bridge piers is an extremely complex phenomenon and is related to many factors such as the flow velocity, water depth, grain size distribution of sediment, critical shield stress for each type of sediment. Under rough ice-covered flow condition, the zone of maximum flow velocity is closer to channel bed comparing to that under the smooth covered condition (Sui, et al., 2010). In addition to

forcing the maximum of the velocity profile closer to the bed, erosion may even act as a relief, and the erosion provides a balance between the increased shear stress and the depth of the bed (Hains, 2004). This leads to the difference between the scour depths under smooth covered condition and those under rough ice-covered condition. This is also the reason for more irregular distribution in the scour-deposition patterns of channel bed under rough covered condition comparing to that under both smooth ice-covered and open channel flow conditions. Similarly, flow under smooth ice-covered flow condition also resulted in more irregular distribution in scour pattern around bridge piers comparing to that under open channel flow condition. Figure 3-64 shows the difference between the simulated scour depths around the bridge pier and those of laboratory experiments. As shown in Figure 3-64, similar to the results under both open channel and smooth ice-covered flow conditions, the deepest scour depth under rough covered flow condition also occurs at point "8" - the apex of the pier face facing upstream. Figure 3-65a shows the simulated two-dimensional velocity field at the *x*-*y* plan for z= 0.326 m at the last second of numerical simulation under rough covered flow condition. Since the flow in front of the bridge pier is impeded, flow velocity decreases clearly in front of bridge piers, as showed in Figure 3-65. Figure 3-65b shows the distribution of turbulent energy at the cross section where the bridge piers are located under rough covered condition. Clearly, the turbulent energy is higher near the bridge piers. The comparison between the simulated scour depths around bridge piers and those of measured in laboratory experiments are presented in Figure 3-66. As indicated in Figure 3-66, the simulated maximum scour depths around bridge piers agree well with those of laboratory experiments. Based on both simulated and measured results in laboratory, following

relationship have been derived between the simulated maximum scour depth (MSD) and those of laboratory experiments:

a) channel bed with coarse sand: $MSD_{Num} = 0.9786 MSD_{Exp} + 5.4573$ (3-5-18)

b) channel bed with fine sand: $MSD_{Num} = 0.9885 MSD_{Exp} + 5.286$ (3-5-19)

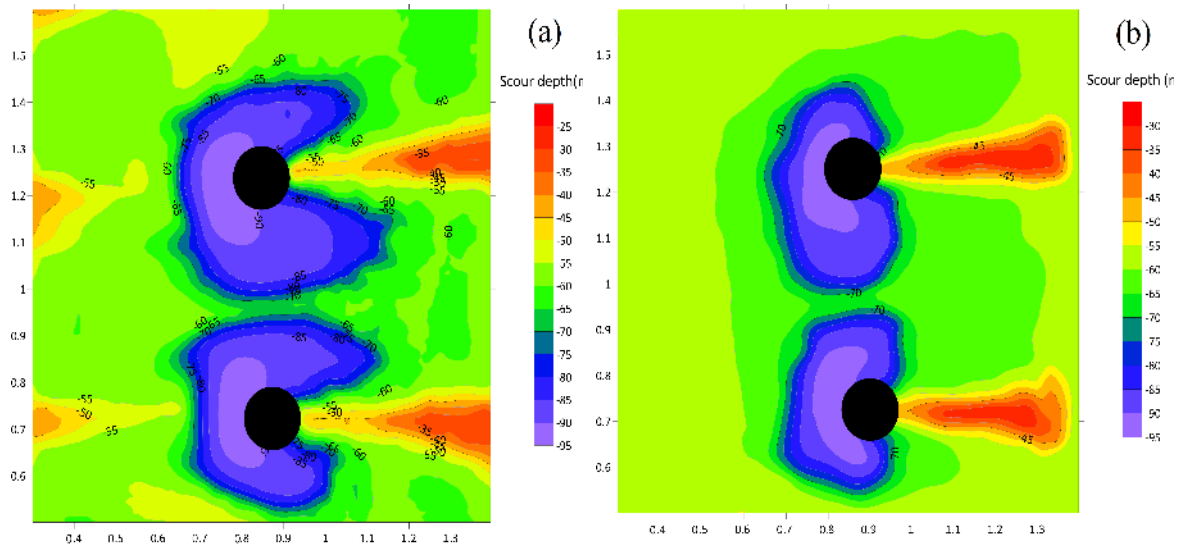

Figure 3-63: (a) Simulated bed elevation contours around 110-mm bridge piers in channel bed with fine sediment under rough-ice-covered condition; (b) Laboratory measured bed elevation contours around 110-mm bridge piers in channel bed with fine sediment under rough-ice-covered condition

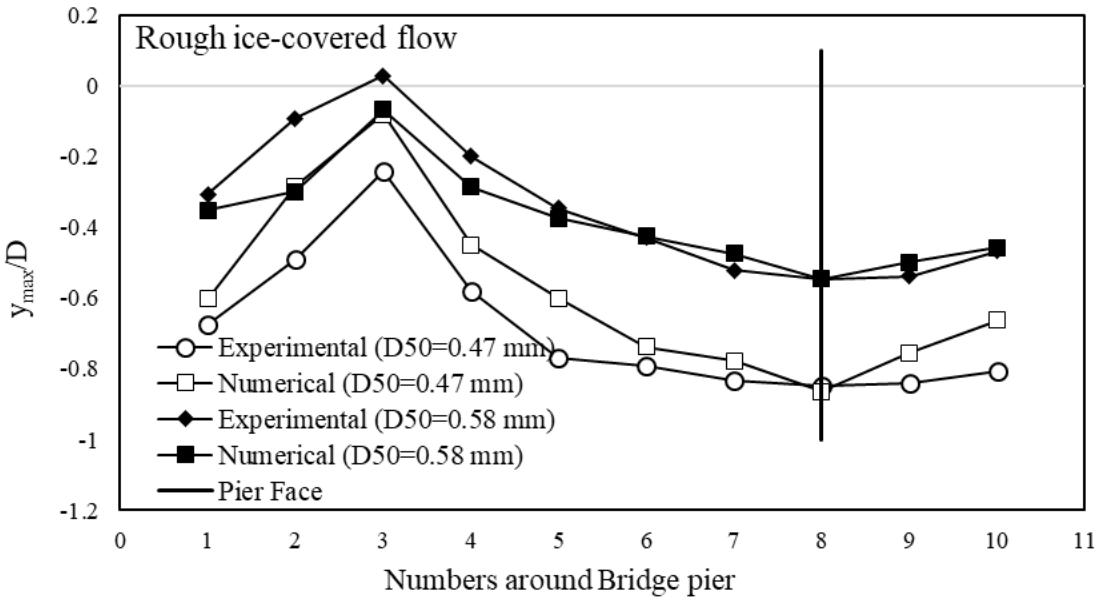

Figure 3-64: Simulated scour depths compared to those of experiments around the 110-mm bridge piers in channel bed under rough ice-covered condition

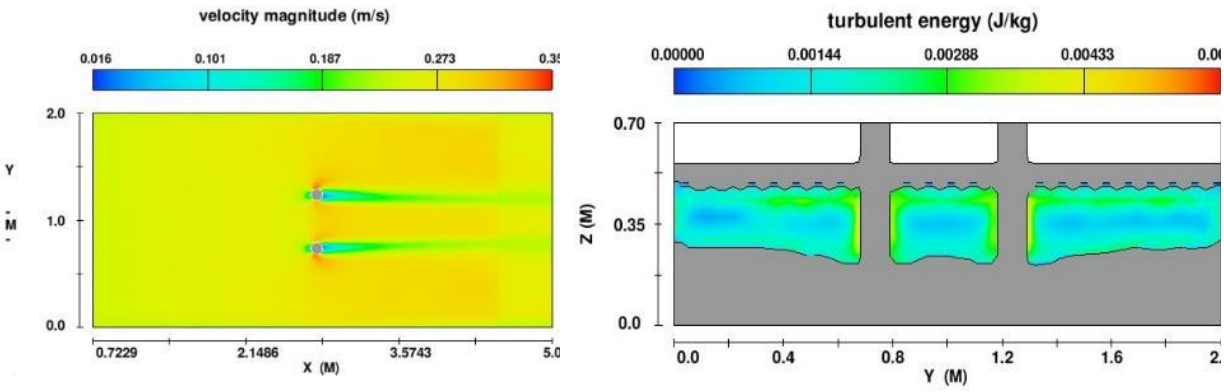

Figure 3-65: (a) Flow field at the plane z= 0.326 m at the end of simulation time, and (b): The distribution of turbulent energy at the cross section of the bridge pier for the rough-covered flow condition

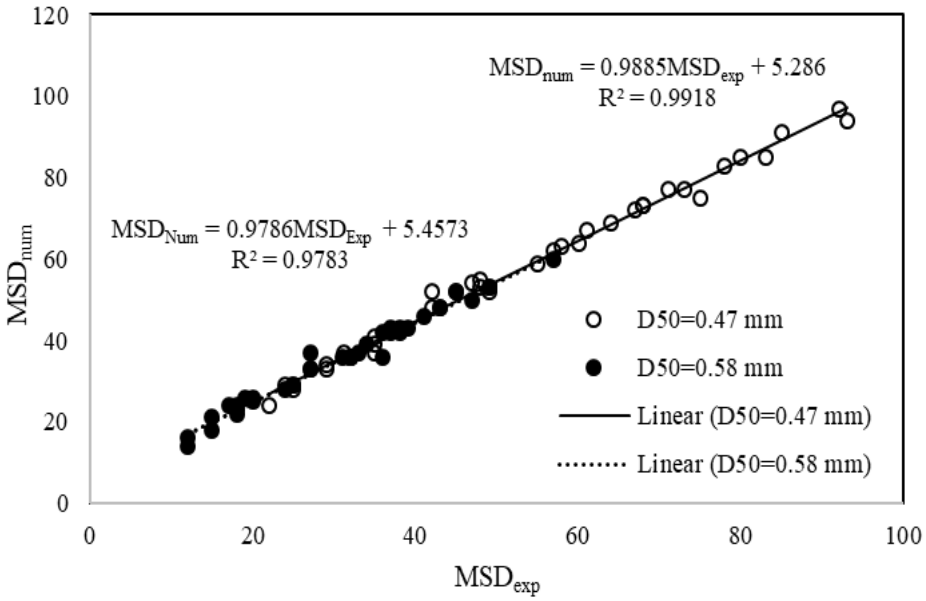

Figure 3-66: Comparison of the simulated maximum scour depths (MSD) to those of laboratory experiments

3.5.4. Conclusions

In this study, three-dimensional numerical models have been established to simulate the local scour around the side-by-side bride piers under both smooth and rough ice-covered flow conditions by comparing to those under open channel flow condition. Following conclusions have been obtained:

1) The RNG k-ε turbulence model and the sediment scour model adopted in this research were successful to simulate flow fields and the local scour process around bridge piers under both open ice-covered conditions.
2) On the upstream side of the bridge piers, the horseshoe vortex together with the acceleration of the flow around the bridge piers resulted in a high bed shear stress, which is the main factor that induces local scour around bridge piers. On the downstream side of the bridge pier, the wake vortex together with the gravity force and bed friction, resulted in the sediment deposition downstream of the bridge piers.
3) Results of both numerical simulations and experimental studies showed that the maximum scour depth and turbulent energy around bridge piers under rough ice cover condition were highest, comparing to those under both open channel and smooth covered flow conditions. The reason for this difference is that, under rough ice-covered flow condition, the zone of maximum flow velocity is closer to channel bed comparing to that under the smooth covered condition. In addition to forcing the maximum of the velocity profile closer to the bed, erosion may even act as a relief, and the erosion provides a balance between the increased shear stress and the depth of the bed.
4) The simulated scour range under ice-covered flow conditions were more widely spread and more irregular distributed. The main reason for the difference between the simulated scour depths and those of measured in laboratory experiment is due to the fact whether or not the ice cover floats freely. In laboratory experiments, model ice cover floats freely on water surface. However, in the numerical simulation, ice cover had to be considered as rigid due to the restriction of the numerical model in simulating the floating ice.

3.5.5. Reference

Beltaos, S., T. Carter, and T. Prowse. (2011). Morphology and Genesis of Deep Scour Holes in the Mackenzie Delta. *Canadian Journal of Civil Engineering* 386:638–649.

Ettema, R., and E. W. Kempema. (2012). River-Ice Effects on Gravel-Bed Channels. In *Gravel-Bed Rivers: Processes, Tools, Environments*, ed. M. Church, P. Biron, and A. Roy, 523–540. Chichester, UK: Wiley-Blackwell

Ettema, R., Melville, B. W., & Constantinescu, G. (2011). *Evaluation of bridge scour research: Pier scour processes and predictions*. Washington, DC: Transportation Research Board of the National Academies.

Flow Sciences Inc. (2015). FLOW-3D User's Manual Version 11.1. Santa Fe, New Mexico.

Hains, D., and L. Zabilansky. (2004). *Laboratory Test of Scour under Ice: Data and Preliminary Results*. ERDC/CRREL TR-04-9. Hanover, NH: U.S. Army Engineer Research and Development Center.

Hains, D., Zabilansky, L.J., & Weisman, R.N. (2004). An experimental study of ice effects on scour at bridge piers. *Cold Regions Engineering and Construction Conference and Expo*, 16–19 May 2004, Edmonton, Alberta, Canada

Hirt, C.W., Nichols, B.D., (1981). Volume of fluid (VOF) method for the dynamics of free boundaries. J. Comput. Phys. 39, 201–225.

Hirt, C.W., Sicilian, J.M., (1985). A porosity technique for the definition of obstacles in rectangular cell meshes, In: Proceedings of the International Conference on Numerical Ship Hydrodynamics, 4th. Washington,D.C., pp. 1–19.

Kim, H.S., Nabi, M., Kimura, I., Shimizu, Y. (2014). Numerical investigation of local scour at two adjacent cylinders. Adv. Water Resour. 70, 131–147. http://dx.doi.org/ 10.1016/j.advwatres.2014.04.018.

Launder, B. E., and Spalding, D. B., (1974). The Numerical Computation of Turbulent Flows, Computer Methods in Applied Mechanics and Engineering, Vol. 3, pp. 269-289

Mastbergen, D.R., Von den Berg, J.H., (2003). Breaching in fine sands and the generation of sustained turbidity currents in submarine canyons. Sedimentology 50, 625–637.

Richardson, J. E., & Panchang, V. G. Three-dimensional simulation of scour-inducing flow at bridge piers. *Journal of Hydraulic Engineering*, 1998, *124*(5): 530-540.

Soulsby, R. L., & Whitehouse, R. J. S. (1997). Threshold of sediment motion in coastal environments. In Pacific Coasts and Ports' 97: Proceedings of the 13th Australasian Coastal

and Ocean Engineering Conference and the 6th Australasian Port and Harbour Conference; Volume 1 (p. 145). Centre for Advanced Engineering, University of Canterbury.

Soulsby, R., (1997). Dynamics of Marine Sands. Thomas Telford Publishing. http://dx.doi.org/10.1680/doms.25844.

Sui, J., Wang, J., He, Y. & Krol, F. (2010). Velocity profiles and incipient motion of frazil particles under ice cover. *International Journal of Sediment Research, 25*(1), 39-51.

Sheppard, D. M., Melville, B. & Demir, H. (2013). Evaluation of existing equations for local scour at bridge piers. *Journal of Hydraulic Engineering*, *140*(1), 14-23.

Toombes, L., & Chanson, H. (2011, January). Numerical limitations of hydraulic models. In *34th IAHR World Congress, 33rd Hydrology and Water Resources Symposium and 10th Conference on Hydraulics in Water Engineering* (pp. 2322-2329). Engineers Australia.

Van Rijn, L. (1984). Sediment transport, Part I: bed load transport. J. Hydraul. Eng. 110, 1431–1456.

Vasquez, J. A., & Walsh, B. W. (2009, August). CFD simulation of local scour in complex piers under tidal flow. In *33rd IAHR Congress: Water Engineering for a Sustainable Environment*.

Wu, P., Hirshfield, F., Sui, J. Y. Local scour around bridge abutments under ice covered condition–an experimental study. *International Journal of Sediment Research*, 2015, *30*(1): 39-47.

Wu, P., Balachandar, R., Sui, J. Local scour around bridge piers under ice-covered conditions. *Journal of Hydraulic Engineering, 2015, 142*(1).

Yakhot, V., Orszag, S.A., (1986). Renormalization group analysis of turbulence. I. Basic theory. J. Sci. Comput. 1, 3–51. http://dx.doi.org/10.1007/BF01061452

Zabilansky, L. J., & K. D. White, (2005). Ice cover effects on scour in narrow rivers. *Ice Engineering*, U.S. Army Cold Regions Research and Engineering Laboratory (CRREL), TN-05-3.

Zhang, Q., Zhou, X. L., & Wang, J. H. (2017). Numerical investigation of local scour around three adjacent piles with different arrangements under current. *Ocean Engineering*, *142*, 625-638.

4. GENERAL CONCLUSIONS

Experiments have been done in a large-scale flume to study the effect of ice cover roughness and non-uniform sediments on the local scour around four pairs of side-by-side bridge piers. It was found that existence of ice cover on the water surface affects bed morphology, maximum scour depth, armor layer, vertical velocity distribution, scour volume and scour area. The general conclusions are as follows:

1) The pier Reynolds number (Re_b) decreases with the increase in the pier spacing ratio (G/D), which implies that the strength of the horseshoe vortices decreases as the spacing distance between the side-by-side piers increases. The results showed that, under the same flow condition (velocity and flow depth), the lowest pier Reynolds Number (Re_b) occurred under open channel flow conditions, and the highest pier Reynolds Number (Re_b) occurred under rough covered flow conditions. Further, it was observed that the influence of ice cover on pier Reynolds Number fades away as the pier spacing distance increases regardless of flow cover. Also, for the same bridge pier spacing ratio (G/D) and for the same sediment, the relative MSD under open channel flow conditions is the lowest and reaches the maximum under the rough covered flow conditions. This implies that the impact of the pier spacing ratio under the rough ice-covered flow condition is clearly intensified compared to those under both open channel and smooth covered flow conditions. In other words, the smaller the pier size (D) and the larger the pier spacing (G), the weaker the horseshoe vortices around the side-by-side bridge piers.

2) Under the same flow conditions, the effect of flow Froude number on the scour process is stronger than that of pier size. Regardless of ice cover and pier size, the maximum scour depth increases with flow Froude number, especially for finer sand beds. In other words, the local scour depth around bridge piers for a coarse sand bed is less than that for a finer sand

bed. The results of this experimental study allow the impacts of ice cover, flow Froude number, and pier spacing distance on local scour around bridge piers to be prioritized. Overall, one can say that the deepest scour hole occurs around closely spaced large side-by-side piers under rough covered flow conditions which have higher Froude numbers. The results also indicate that, regardless of the roughness of the model ice cover and the grain size of sediment, the maximum scour depths always occurred at the upstream front face of the bridge piers. Also, the amount of sediment transported to the downstream side of the bridge pier to form the deposition mound is greatest under rough covered flow conditions. The results indicate that the impact of pier spacing on scour depth under covered flow conditions is similar to that under open channel conditions, however, the scouring process under covered flow conditions is more intense. It was found that the most extreme scour depth around side-by-side bridge piers occurs under rough covered flow conditions with the higher Froude number and smaller bridge pier spacing.

3) Using data collected from the current experiments, empirical equations for predicting the relative *MSD* (y_{max}/y_0) under both channel flow and covered flow conditions have been developed. Among all the dimensionless parameters, flow Froude number was the most influential factor which had a positive relation with the relative *MSD* (y_{max}/y_0). The impact of the Froude number is most distinct under rough covered flow conditions with smaller pier spacing ratios. Namely, for nearly the same Froude number, the largest scour depth occurs under rough covered flow conditions with smaller pier spacing. This means that under rough covered flow conditions, the maximum velocity is located closer to channel bed. Thus, the shear stress increases, and the horseshoe vortexes are intensified due to the smaller pier

spacing ratio. Both the roughness of the ice cover and the pier spacing ratio are two major factors leading to the most critical local scour pattern.

4) Sensitivity analysis was done, and it was concluded that the relative MSD is most sensible to Fr, n_i/n_b, G/D and D_{50}/y_0, respectively.

5) Although the scour depth under ice-covered flow condition was larger comparing to that under open flow condition, the geometry of the scour holes under open flow condition is similar to that under ice-covered flow condition. Results showed that, regardless of flow cover, the maximum scour depth decreases with increase in the grain size of armour layer. Also, although the maximum depth of scour hole around largest pier was deepest, the grain size distribution of armor layer in scour hole around larger piers did not show a significant difference from those around smaller piers.

6) Under the same flow condition and same covered condition, the maximum scour depth occurs in channel bed with the finest sediment. Due to the horseshoe vortex system, maximum scour depth is located at the upstream face of the piers and extends along the sides of the piers towards the rear side of the pier where wake vortex exists. Due to effect of ice cover, the horseshoe vortex shifts the maximum downflow velocity closer to the pier in the scour hole. Thus, the strength of downflow gets more intensified which leads to a larger and wider deposition ridge downstream of the pier.

7) Under the same flow condition, both scour volume and scour area of scour hole in the finest sand bed are largest comparing to those in channel bed with coarser sands. With respect to the impact of ice cover, it was found that both scour volume and scour area of scour hole under rough covered flow condition are largest comparing to those under both smooth covered condition and open flow condition.

8) Based on data collected in laboratory, two formulae have been developed to predict the relative MSD (y_{max}/D_{50A}) under both open flow condition and ice-covered condition. Following dimensionless variables are considered in the proposed formulae for determining the relative MSD (y_{max}/D_{50A}): densimetric Froude number (Fr_0), grain size of armour layer (D_{50A}/D_{50B}), pier spacing (D_{50A}/D), and roughness of ice cover (n_i/n_b). Results showed that the calculated relative MSD (y_{max}/D_{50A}) agreed well with those observed under both open flow condition and ice-covered condition.

9) Results showed with increase in densimetric Froude number (Fr_0), the relative MSD increases correspondingly. Besides, under the same Fr_0, the values of the relative MSD under ice-covered conditions are larger than those under open flow condition. Results also indicate that, under ice-covered flow condition, a smaller value of densimetric Froude number is needed to initiate movement of sediment comparing to that under open flow condition which can be justified by the higher flow velocity near channel bed under ice-covered flow conditions and its impact on the threshold of sediment motion.

10) It is found the presence of ice cover can result in a deeper maximum scour depth compared to that under open flow condition, and consequently, the required flow velocity for incipient motion of sediment particles under ice-covered conditions decreases with the increase in the relative roughness coefficient of ice cover.

11) The larger the sediment-fluid parameter, the greater the dimensionless shear stress for incipient motion of bed material. In other word, with the increase in the sediment-fluid parameter, the dimensionless shear stress increases correspondingly. However, for the same sediment-fluid parameter, a higher dimensionless shear stress is resulted in channel bed with finer sediment. Meanwhile, for the same dimensionless shear stress, the finer sediment has a

lower sediment-fluid value while the coarser sediment has a greater sediment-fluid parameter value for the incipient motion of bed material.

12) The dimensionless shear stress increases with the increase in the densimetric Froude number. For the same densimetric Froude number, the dimensionless shear stress is for the finest sediment type (D_{50}=0.47 mm) is the least. It is also found that the dimensionless shear Reynolds number increases with the increase in densimetric Froude number. With the same densimetric Froude number, the dimensionless shear Reynolds number for the coarser sand (D_{50}=0.58 mm) is higher.

13) For the same relative MSD, the U^*/U_c –value under the rough ice-covered flow condition is more than that under smooth covered condition, implying that the near-bed velocity is higher under rough ice-covered flow condition than that under smooth covered condition.

14) For the streamwise velocity component (U_x), it can be described as a reverse C-shaped profile shape which begins from the scour hole up to the water surface. In terms of velocity magnitude, the streamwise velocity in the scour hole under rough covered condition is generally greater than those under both smooth covered and open flow conditions. Regardless of the cover conditions of flow, the magnitude of velocity is the least in the scour hole. Moreover, the location of the maximum velocity is closer to the bed under rough covered flow condition than that under smooth covered flow condition.

15) In terms of the effects of rough ice cover vs those of smooth ice cover, the MSD under rough ice-covered flow condition was deeper. The location of the maximum velocity was closer to the bed under rough covered flow condition than that under smooth covered flow condition. For the same bed material, the dimensionless shear stress for incipient motion of

sediment increases with the shear Reynolds number as the ice cover becomes rougher. The results are in good agreement with the result of Ackermann et al (2002). in which they stated that the rough cover gave slightly larger scour depths than the smooth cover.

16) In terms of scour hole pattern, regardless of sediment type and flow cover, the deepest point in each scour hole is clearly at the front face of bridge piers and the deposition mound is located downstream of bridge piers. Under the rough covered flow conditions, both the maximum scour depth and maximum deposition height are clearly greater than for open channel flow. The results indicate under the rough covered flow condition more sediment deposition develops at the downstream side of bridge piers and the deposition mound is wider spread than those under open flow.

17) For the streamwise velocity component (U_x), there is a logarithmic pattern which begins from the scour hole up to the water surface (or simulated ice-cover). In terms of velocity magnitude, the streamwise velocity for rough cover is generally greater than the scour hole velocity for smooth and open channel conditions. Regardless of sediment type, the rough ice cover resulted in a larger maximum velocity compared to the smooth ice cover.

18) The vertical velocity distribution (U_z), which is a representative of the strength of downfall velocity, is the greatest under rough ice cover. Generally, considering the absolute value of U_z, the values of U_z diminish from the channel bed toward the scour hole and from the channel bed toward the free surface. They tend to move toward right which implies downflow velocity vectors are diminishing as they get closer to free surface which results in the velocity profile having a parabola-shaped profile pattern.

19) There is no significant difference in velocity field for the different sediment types and different types of sediment. Different types of armor layer and sediment ridge development were observed which are the result of differences in critical shear stress for the sediment particles.

20) Regardless of flow cover, the streamwise turbulent intensity along with the vertical turbulent intensity are highest just over the channel bed and diminishes towards the flow surface. The streamwise turbulent intensity, the vertical turbulent intensity and turbulence kinetic energy for the rough flow conditions are greater than those for open channel and smooth ice-covered flow conditions.

21) Under nearly the same flow conditions, the maximum value of turbulence kinetic energy and turbulent intensity occurs at the largest diameter pier.

22) In terms of grain size of sediment, under the same flow condition, the finest sediment size of D_{50} = 0.47 mm yielded the largest scour volume and scour area. The impact of ice cover on local scour volume and area is more significant for finer sediment type. On the other hand, under the same flow conditions, the coarsest sediment of D_{50} = 0.58 mm yielded the smallest scour volume and scour area.

23) In terms of flow cover, it was found that the rough ice-covered flow has led to the maximum amount of scour volume and scour area. Besides, under the same flow condition, the flow turbulence caused by high velocities and lower flow depths occurring around bridge piers with smaller pier spacing is more significant for finer sediment. It was also found that, regardless of whether or not the flow is covered, the scour volume decreases with the increase in bed sediment size.

24) The RNG k−ε turbulence model and the sediment scour model adopted in this research were quite successful to simulate flow field and the local scour around bridge piers.

25) On the upstream side of the pier, the horseshoe vortex along with the acceleration of the flow around the bridge piers resulted in high bed shear stress, which is the main factor that induces local scour around bridge piers. On the downstream side of the pier, the wake vortex, along with the gravity force and bed friction, resulted in the sediment deposition downstream of the piers.

26) In both the numerical and experimental studies, the maximum scour depth and turbulent energy which were achieved under rough ice cover condition were highest. The reason is due to more pressurized flow under rough ice-covered flow condition. Pressurized flow causes more restriction in flow area which causes more increase in velocity and shift the maximum velocity more closely to the bed. In addition to forcing the maximum of the velocity profile closer to the bed, erosion may even act as a relief of pressurized flow; if discharge rises above freeze-up levels, erosion provides a balance between the increased shear stress and the depth of the bed.

27) The values of maximum scour depth obtained by numerical model under ice-covered flow conditions were more widespread. The main reason for the difference between the numerical and experimental maximum scour depth is due to the fact the type of the ice cover in the experiment was floating ice, however, in the numerical simulation, the type of ice cover is assumed to be rigid due to the restriction of the numerical model in simulating the floating ice.

28) The values of maximum scour depth obtained by numerical model under open channel flow conditions were in good agreement with the experimental value which confirms that the model is accurate enough to predict hydraulic of flow under open channel flow conditions.

The present study would be helpful to engineers and scientists for safe design of the bridge pier structures in cold regions. This investigation on the hydraulics over scoured bed around the bridge piers under ice-covered flow conditions contributes to the field of fluid dynamics and river engineering. It is highly recommended to do more experiments under different pile group arrangements, pier spacing, flow rates, and sediment grain sizes to have a more through perception of local scour phenomenon under ice-covered flow conditions.

APPENDIX I

A.I.1. Effects of ice cover on local scour around bridge piers in non-uniform sand bed

Local scour is considered as one of the major reasons for failure of hydraulic structures especially bridge foundation. Bridge failure may result in the loss of lives and financial costs for reconstruction and restoration. Difficulties in perceiving the clear interaction between the geometries of bridge piers with scouring mechanisms make the prediction of local scour depth around bridge piers difficult. The foremost feature of the flow around bridge foundations is the large-scale eddy structure, or system of vortices (Breusers et al. 1977). The vortex system around bridge piers and abutments removes the erodible bed materials and may result in the failure of bridge foundation. Numerous studies have been conducted with the purpose of predicting scour depth of scour holes, and various equations have been developed (Laursen and Toch, 1956; Liu et al., 1961; Shen et al., 1969; Jain and Fischer, 1980; Raudkivi and Ettema, 1983; Melville and Sutherland, 1988; Froehlich, 1989; Melville, 1992; Abed and Gasser, 1993; Richardson and Richardson, 1994 and Heza et al., 2007, to mention only several). Most of these empirical equations were developed based either on laboratory results or field data. These empirical equations were different from each other in terms of the factors considered in the scour model, parameters used in the equation, laboratory or site conditions, flow condition, grain sizes of bed material, etc. For instance, Raudkivi and Ettema (1983) studied relationship between local scour depth and particle size distribution of bed sediment and developed an equation to estimate the maximum depth of local scour hole. Although numerous studies have been conducted to investigate local scour around bridge foundation, this challenging phenomenon has been remained as one of the main issues in terms of bridge pier design. Local scour process around bridge pier gets more complicated when the water surface is covered ice. In this situation, the presence of ice cover

leads to a different set of geomorphological conditions comparing to those under open flow conditions (Hicks, 2009). The characteristics of flow under ice cover affects the process of sediment transport, traverse and vertical mixing and mean flow velocity (Andre and Thang, 2012). It has been proved that the formation of a stable ice cover effectively doubles the wetted perimeter compared to that under open channel condition, alters the hydraulics of an open channel by imposing an extra boundary to the flow, causing velocity profile to be shifted towards the smoother boundary (channel bed) and adding up to the flow resistance (Sui et al., 2010; Wang et al., 2008). However, up to date, there is still very limited research work regarding local scour around bridge infrastructures under ice covered condition, and this issue is one of the major concerns in bridge foundation design field. Using non-uniform sediments, Wu et al (2013) carried out experiments to investigate scour morphology around bridge abutment under ice cover. It was found that that under ice cover, at different locations of the abutment, the sediment sorting process were observed. Wu et al (2014) assessed the impacts of ice cover on local scour around a semi-circular bridge abutment. It was found that the average scour depth under ice-covered condition was always greater compared to that in open flow condition. The average scour depth under rough ice cover was 35% greater than that under smooth ice cover. Wu et al (2014) studied the incipient motion of bed material and shear stress distribution around bridge abutments under ice-covered condition. They claimed that the average scour angle around a semi-circular abutment is around 10 degrees larger than that around the square abutment. Wu et al (2015) compared the scour profile under an ice-covered condition with previous studies by considering the role of relative bed coarseness, flow shallowness, and pier Froude number. It is found that the scour depth under ice-covered condition is larger compared to that under open flow condition. Besides, the

presence of an ice cover results in a greater scour depth in flow with a shallower flow depth, and with the increase in flow depth, the impact of ice cover decreases. In terms of protection against possible undermining caused by local scour process around bridge infrastructure, riprap is the most commonly employed countermeasure (Lauchlan and Melville, 2001). The most suitable countermeasure for avoiding local scour process around hydraulic structure depends on the relative effectiveness, cost, maintenance, and ability to detect failures (Deng and Cai, 2009). Having an accurate and precise estimation of scour area and scour volume is crucial for the safe design of bridge piers and abutments. Very few studies have thoroughly investigated scour volume and scour area around bridge piers, especially under condition of ice-covered flow. In this case, Wu et al (2014) found that there was a linear correlation between scour depth and volume of scour hole around bridge abutments under ice covered condition. Khwairakpam et al. (2012) developed two equations to estimate scour volume and scour area around a vertical pier under clear water condition in terms of approach flow depth and pier diameter. Hirshfield (2015) found that scour area and volume increase with pier size. The aim of this study is to thoroughly investigate scour volumes and scour areas based on a series of large-scaled flume experiments using non-uniform natural sediment under conditions of open channel and ice-covered flow around four pairs of side-by-side cylindrical bridge piers and to investigate how different scour volume and scour area are under ice-covered flow compared to those of under open flow condition.

Methodologies and experimental Setup

Experiments have been carried out in a large-scale flume at the Quesnel River Research University of Northern British Columbia. The flume is 40-m long, 2-m wide and 1.3-m deep. The longitudinal slope of the flume bottom was 0.2 percent. A holding tank with a volume of nearly 90 m^3 was located at the upstream end of the flume and provides a constant head in the experimental zone. At the end of the holding tank, water overflowed from a rectangular weir into the flume section for experiments. A flow diffuser was placed downstream of the rectangular weir to maintain the flow to be uniform. Two sand boxes with the depth of 0.30 m were spaced 10.2 m. Figure AI-1 shows the experimental setup. Three natural non-uniform sediments were used in this experimental study. The median grain sizes of these sands (D_{50}) were 0.58 mm, 0.50 mm and 0.47 mm, and the geometric standard deviation (σ_g) is 2.61, 2.53 and 1.89, respectively. For all the three sediments, the geometric standard deviation (σ_g) is larger than 1.4 which can be treated as non-uniform sediments (Dey and Barbhuiya, 2004). The first sand box was 5.6-m long and the second sand box was 5.8-m in long. Four pairs of bridge piers with diameter of 60 mmm, 90 mm, 110 mm and 170 mm were used in this experimental study. Bridge piers were made of PVC circular plumbing pipe. A pair of side-by-side bridge piers were placed inside each sand box. The distance between the central lines of these side-by-side bridge piers was 0.50 m, namely, each pier was offset from the centre line by 0.25 m, as illustrated in Figure AI-2. Water depth in the flume was adjusted by adjusting the tailgate. In front of the first sand box, a SonTek Incorporated 2D flow meter was installed to measure the approaching flow velocity and water depth during the experiment. A staff gauge was also installed in the middle of each sand box to manually verify water depth. The scour hole velocity field was measured using a 10-Mhz Acoustic

Droppler Velocimeter (ADV) by SonTek. The ADV is a high-precision instrument used to measure 3D water velocity in a wide range of environments including laboratories, rivers, estuaries, and the ocean (Cea et al, 2007). The Styrofoam panels were used to simulate ice cover. Styrofoam density was 0.026 gr/cm^3 and was floated on water surface during the experimental runs. In the present study, two types of model ice cover were used, namely smooth cover and rough cover. The smooth ice cover was the surface of the original Styrofoam panels while the rough ice cover was made by attaching small Styrofoam cubes to the bottom of the smooth cover. The dimensions of Styrofoam cubes were 25 mm×25 mm× 25 mm and were 35 mm spaced apart. Figure AI-3a shows the local scour around a bridge pier under condition of rough ice-covered flow and Figure AI-3b shows the top view of local scour around the 9-cm-bridge pier in sand bed of for D_{50}=0.50 mm under rough ice-covered condition. Each experimental run lasted 24 hours, and this allowed the local scour process to reach an equilibrium condition. After 24 hours, the flume was gradually drained. The scour depth was manually measured along the outside lines of the circular bridge piers. In terms of scour depth measurement, the outside perimeter of each bridge pier was equally divided into numbered measuring point in order to accurately read the scour depth at different locations to draw scour hole contours, as shown in Figure AI-2. The scour hole around bridge piers were measured at proper increments from numbered measuring point along each bridge pier. In total, 108 Experiments were conducted to investigate scour area and scour volume. For each sediment type, 36 experiments have been carried out under different flow conditions, namely, open channel, smooth ice-covered and rough ice-covered. It should be mentioned that the range of Froude number in the first sand box was higher than the second sand box. This is because of the longitudinal slope of the channel and dissipation of

momentum of flow due to friction. The flow Froude number in the first sand box ranges from 0.072 to 0.240, and in the second sand box ranges from 0.054 to 0.177.

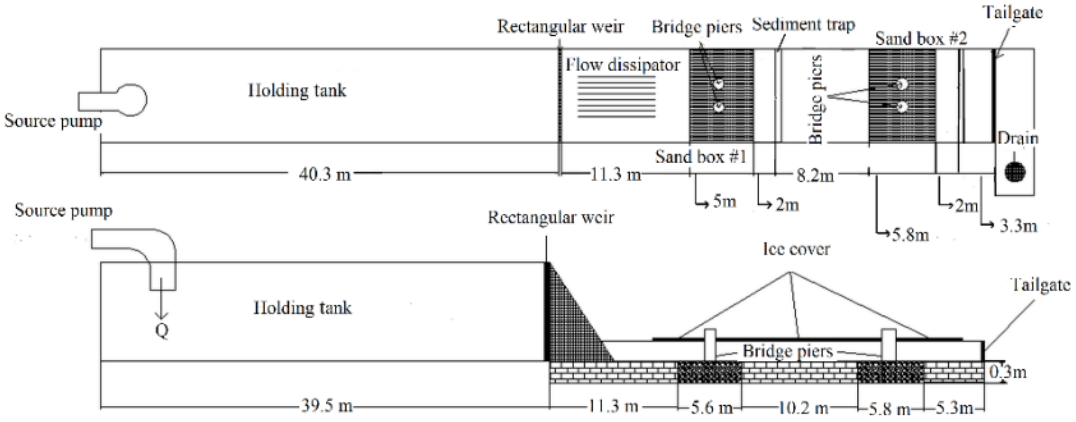

Figure AI-1: Plan view and vertical view of experiment flume

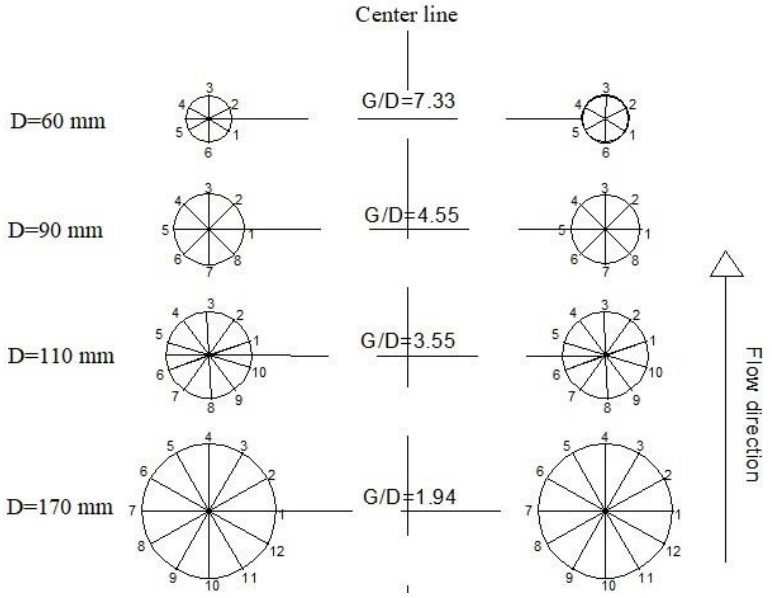

Figure AI-2: Measuring points around the circular bridge pier

Figure AI-3a: Side view of scour hole around the 11-cm-bridge pier under rough ice-covered condition

Figure AI-3b: Top view of the local scour pattern around the 9-cm-bridge pier under rough ice-covered condition (D_{50}=0.50 mm)

Results and discussions

To compute scour hole volume and area for each experimental run, all measured data for scour hole were input into the Surfer 12 which is a surface and contour mapping program. The planar area defined in the Surfer 12 is computed by projecting the cut and fill portions of the surface onto a plane and calculating the area of the projection where positive planar area represents the projection of the cut (map areas where the upper surface is above the lower surface) onto a horizontal plane and negative planar area represents the projection of the fill (map areas where the upper surface is below the lower surface) onto a horizontal plane. In terms of scour volume, the cut and fill volumes section of the grid volume report

display the positive volume (cut) and the negative volume (fill). The cut portion is the volume between the upper and lower surface when the upper surface is above the lower surface while the fill portion is the volume between the upper and lower surfaces when the upper surface is below the lower surface (Yang et al, 2004). For instance, Figure AI-4a and Figure AI-4b display the scour volume and scour area associated with the 17-cm-bridge pier under smooth and rough ice-covered condition for sediment of D_{50}= 0.47 mm, respectively. As Figure AI-4b shows the blue regions are the planar areas which are needed to be filled while the red regions are the planar areas needed to be cut off. Planar area is independent of the depth of scour hole. It should be mentioned that among a pair of piers, the one which shows the highest scour volume and scour area was selected in order to investigate the most critical case in terms of bridge pier design.

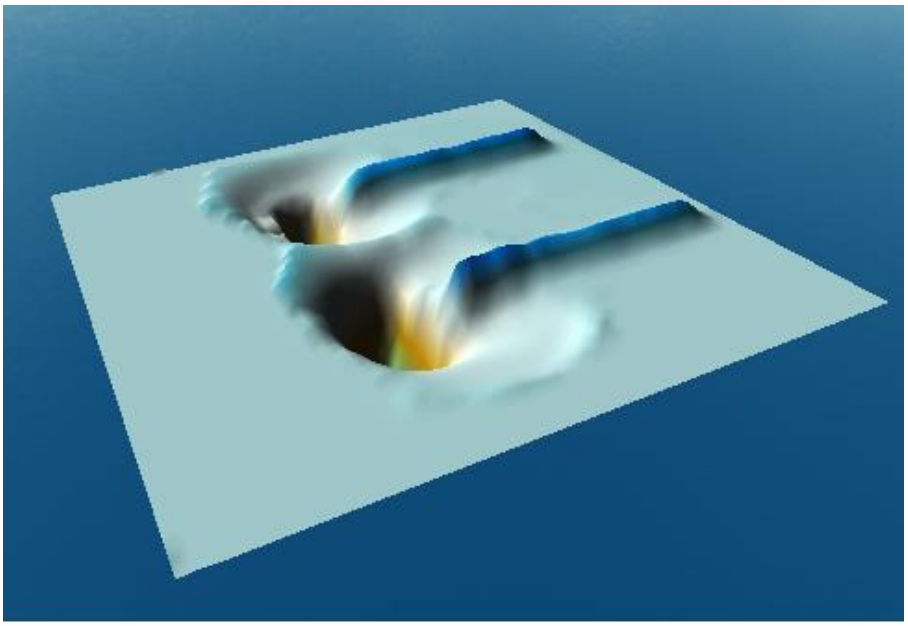

Figure AI-4a: 3-D scour volume view for the 17-cm-bridge pier under rough ice-covered flow condition for sediment of D_{50}=0.47 mm

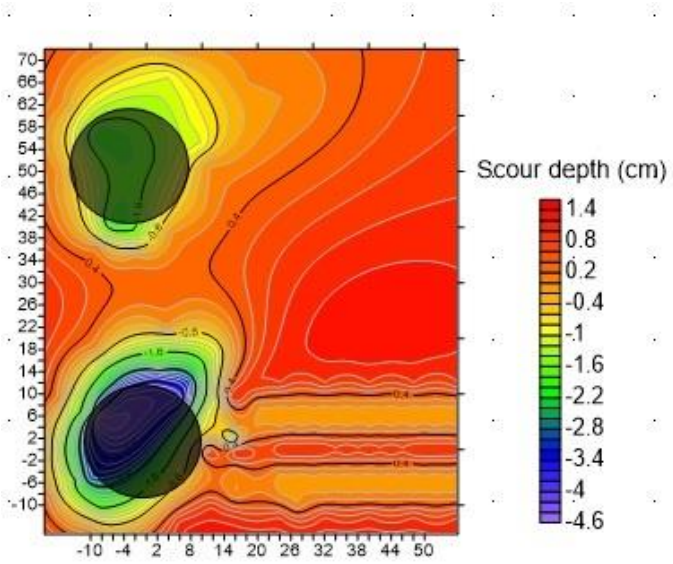

Figure AI-4b: Top view of cut and fill scour area for the 17-cm-bridge pier under smooth ice-covered flow condition for sediment of D_{50}=0.47 mm

Figure AI-5 shows the changes in scour volume with respect to pier size and grain size of sediment under different flow conditions (open channel, smooth ice-covered and rough ice-covered flows). In Figure AI-5, for each type of sediment, the first three experiments, the second three experiments, the third three experiments and the last three experiments are associated with different pier diameters of 6 cm, 9 cm, 11 cm and 17 cm, respectively. One can see from Figure AI-5 that for sediment of D_{50}=0.50 mm, the volumes of scour hole under rough ice-covered condition are the highest and the volumes of scour hole under open flow condition are the lowest. The mean scour volume under open flow, smooth ice-covered and rough ice-covered flow conditions is 459.96 cm^3, 661.81 cm^3 and 1069.24 cm^3, respectively. The difference between the mean scour volume under rough ice-covered flow condition and that under open flow condition is 56.98%, and the difference between the mean scour volume under smooth ice-covered flow condition and that under open flow condition is 35.10 %. These differences indicate that, under nearly the same flow condition with the same bed

material, the presence of rough ice cover and smooth ice cover resulted in an increase in scour volume of 56.98% and 35.10 % compared to those under the open channel flow condition, respectively. The reason for an increase in the scour volume under ice-covered condition compared to that under open flow condition is the modification of flow velocity distribution caused by ice cover. Ice cover imposes an extra solid boundary on water surface, and thus changes velocity distribution and increases turbulent intensity. The maximum flow velocity under ice-covered flow condition is located between channel bed and ice cover, depending on the roughness of ice cover and channel bed. The near bed flow velocity under ice-covered conditions is higher than that under open flow conditions. As the near bed velocity increases, the kinetic energy exerted on the bed material also increases, implying more sediment transport (Sui et al, 2010). In terms of scour volume for sediment of D_{50}=0.47 mm, similar to results for sediment of D_{50}=0.50 mm, the volume of scour hole under rough ice-covered flow condition is the highest and the volume of scour hole under open flow condition is the lowest. Besides, under ice-covered condition, the volume of scour hole for sediment of D_{50}=0.47 mm is significantly increased compared to that for sediment of D_{50}=0.50 mm. This reveals the fact that under the same flow condition, the impact of ice cover on local scour process is significant for finer sediment type. The mean scour volume under open flow, smooth ice-covered and rough ice-covered conditions is 1059.66 cm^3; 1187.77 cm^3 and 1529.95 cm^3, respectively. Namely, under the same flow condition and with the same sand bed, compared to the scour volumes under the open channel flow and smooth-ice-covered flow conditions, the presence of rough ice cover resulted in the increase in the scour volume of 30.72 % and 22.35%, respectively.

In terms of scour volume for sediment of D_{50}=0.58 mm, similar to those of D_{50}=0.50 mm and D_{50}=0.47 mm, the volume of scour hole under rough ice-covered condition is the highest and the volume of scour hole under open channel condition is the lowest. However, the difference between volume of scour hole around same bridge pier in bed sand of D_{50}=0.58 mm and that in bed sand of D_{50}=0.47 mm has relatively decreased. This result shows that, regardless of whether or not the flow is covered, as the grain size of bed sediment increase, the volume of scour hole decrease. For sediment of D_{50}=0.58 mm, the mean scour volume under open flow, smooth ice-covered and rough ice-covered conditions is 392.58 cm^3; 610.72 cm^3 and 965.76 cm^3, respectively. Namely, under the same flow condition and with the same sand bed, compared to the scour volumes under the open channel flow and smooth-ice-covered flow conditions, the presence of rough ice cover resulted in the increase in the scour volume of 36.82 % and 58.1%, respectively. The grain size of sediment plays a key role on the volume of scour hole. For instance, regardless of whether or not the flow is covered, for sediment of D_{50}= 0.47 mm, the mean scour volume around the 11-cm-bridge pier is 2684.5 cm^3 with the highest scour volume of 3366.72 cm^3. However, for sediment of D_{50}= 0.50 mm, the average volume of scour hole around the 11-cm-pier is 1275.5cm^3. It is worth mentioning that there is a tremendous difference of 52.49% between the mean volume of scour hole around the 11-cm-bridge pier for bed sand of D_{50}= 0.47 mm and that for bed sand of D_{50}= 0.50 mm. Results also showed that it takes slightly shorter time for the scour hole to reach the equilibrium state for the finer sediment. In contrast, for the coarser sediment, it takes longer time for the scour hole to reach an equilibrium state.

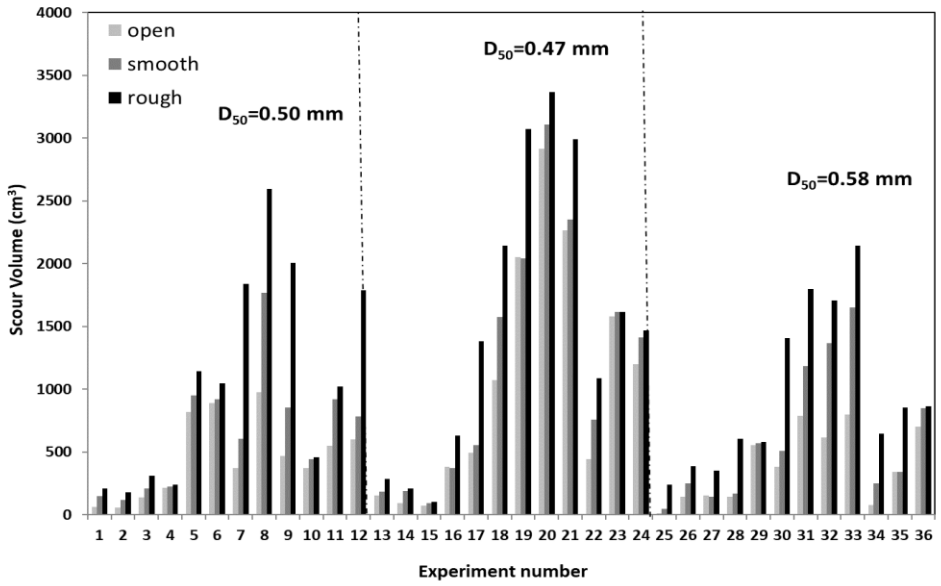

Figure AI-5: Variation of scour volume around bridge pier

Figure AI-6 shows the scour area with respect to sediment types under different flow conditions (open channel, smooth ice-covered and rough ice-covered flows). Similar to Figure AI-6, for each type of sediment, the first three experiments, the second three experiments, the third three experiments and the last three experiments are associated with different pier diameters of 6 cm, 9 cm, 11 cm and 17 cm, respectively. Unlike the volume of scour hole, the scour area is not dominantly highest for flow under rough ice-covered condition comparing to those under smooth ice-covered and open channel flow conditions. In terms of scour area for sediment of D_{50}= 0.47 mm, in most cases, the scour area under rough ice-covered condition is the highest and the scour area under open channel condition is the lowest. However, under the same flow condition and with the same sand bed, compared to the scour area under the smooth-ice-covered flow condition, the presence of rough ice cover didn't result in clearly increase in the scour area. This means that the impact of smooth ice-covered flow on scour area is nearly the same as that of rough ice-covered flow. For

sediment of D_{50}= 0.47 mm, the mean scour areas under open flow, smooth ice-covered and rough ice-covered conditions are 546.09 cm^2; 618.40 cm^2 and 796.77 cm^2, respectively. Namely, under the same flow condition and with the same sand bed, compared to the scour area under the open channel flow and smooth-ice-covered flow conditions, the presence of rough ice cover resulted in the increase in the mean scour area of 31.46 % and 22.39%, respectively. In terms of scour area for sediment of D_{50}= 0.50 mm, the mean scour areas under open flow, smooth ice-covered and rough ice-covered conditions are 443.54 cm^2; 585.44 cm^2 and 714.85 cm^2, respectively. Namely, under the same flow condition and with the same sand bed, compared to the scour area under the open channel flow and smooth-ice-covered flow conditions, the presence of rough ice cover resulted in the increase in the mean scour area of 37.95 % and 18.10 %, respectively. In terms of scour area for sediment of D_{50}= 0.58 mm, in most cases, the scour area under rough ice-covered condition is the highest and the scour area under open channel condition is the lowest. For sediment of D_{50}= 0.58 mm, the mean scour areas under open flow, smooth ice-covered and rough ice-covered conditions are 426.10 cm^2, 607.19 cm^2 and 700.78 cm^2, respectively. Namely, under the same flow condition and with the same sand bed, compared to the scour area under the open channel flow and smooth-ice-covered flow conditions, the presence of rough ice cover resulted in the increase in the mean scour area of 13.40 % and 15.39%, respectively. The grain size of sediment plays a key role on the scour area. For instance, regardless of whether or not the flow is covered, for sediment of D_{50}=0.47 mm, the mean scour area around the 11-cm-bridge pier is 1151.70 cm^2 with the highest scour area of 1524.94 cm^2. However, for sediment of D_{50}=0.50 mm, the average scour area around the 11-cm-pier is 881.47 cm^2 with the highest scour area of 1216.82 cm^2. It is worth mentioning that there is a tremendous difference of

52.49% between the mean scour area around the 11-cm-bridge pier for bed sand of D_{50}=0.47 mm and that for bed sand of D_{50}=0.50 mm.

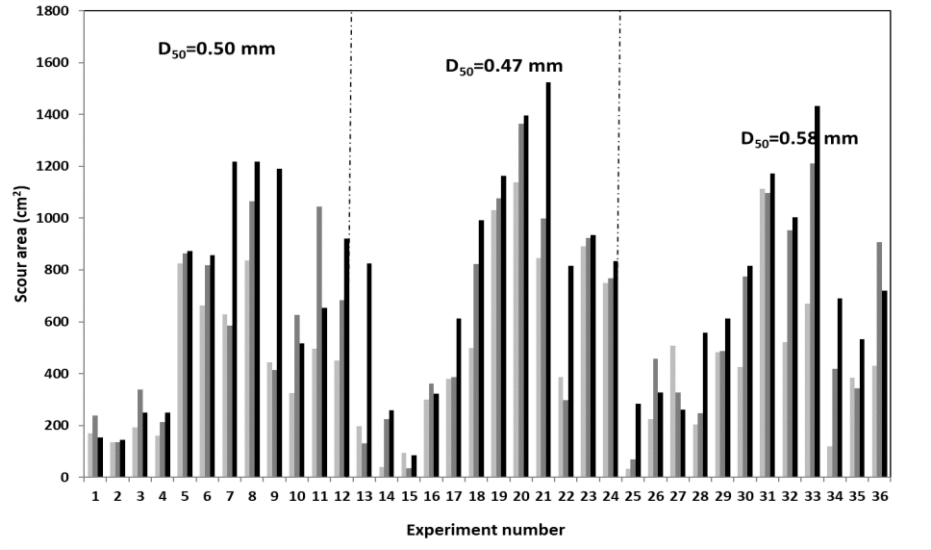

Figure AI-6: Variation of scour area around bridge pier

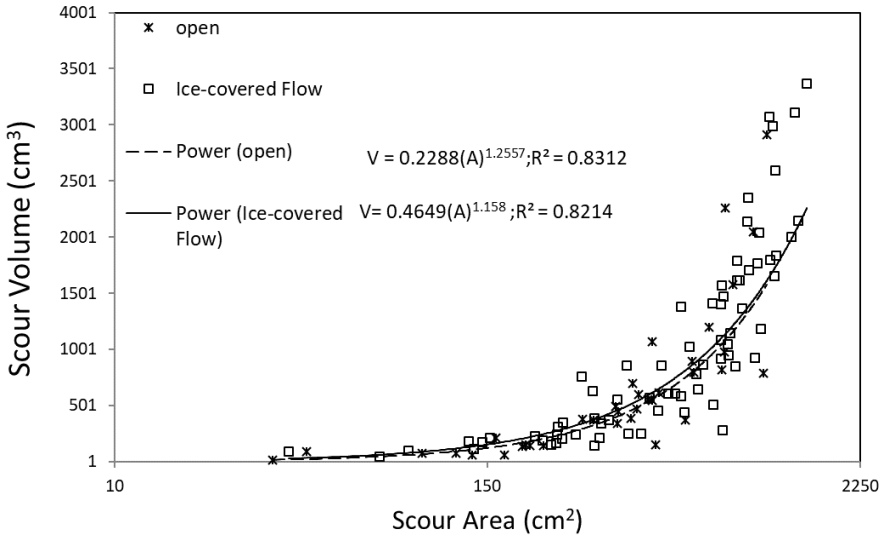

Figure AI-7: Scour volume (V) vs. scour area (A)

Figure AI-7 shows the relationships between scour volume (V) and scour area (A) under condition of both ice-covered flows and open channel flows. These relationships can be described as follows:

Under condition of open channel flow:

$$V = 0.2288(A)^{1.2557} \quad \text{(AI-1)}$$

Under condition of ice-covered flow

$$V = 0.4649(A)^{1.158} \quad \text{(AI-2)}$$

According to Eq. AI-1 and Eq. AI-2, the coefficient factor of regression equation under ice-covered flow is larger than that under open channel flow, implying that the flow under ice-covered condition has led to higher amount of scour volume and scour area. Figure AI-8 gives the relationship between scour volume and scour area in terms of grain size of sediment. One can see from Figure AI-8 that the largest amount of scour volume and scour area occurs in the finest sand of D_{50}= 0.47 mm.

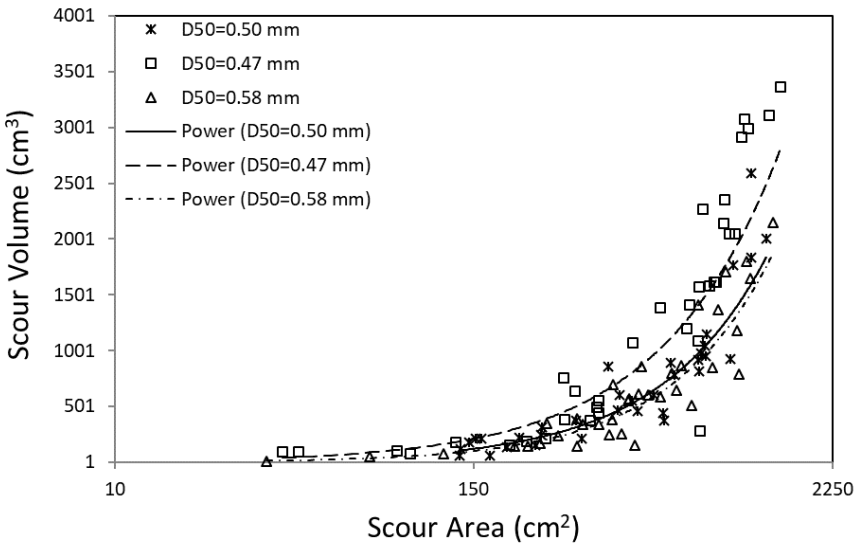

Figure AI-8: Relationship between scour volume and scour area in terms sediment type

Conclusions

In the present study, the main objective was to thoroughly investigate the correlation between scour volume and scour area under conditions of ice-covered and open channel flow in flume with non-uniform sediment. In this study, three natural non-uniform sediment mixtures with

median grain size of 0.58 mm, 0.50 mm and 0.47 mm were used. Besides, two types of artificial ice cover namely rough and smooth ice cover were used to simulate ice-covered flow conditions. Totally, 108 Experiments have been conducted in a large-scaled flume to study scour area, scour volume around four pairs of side-by-side cylindrical bridge piers. The following are the major conclusions of this study:

1) In terms of grain size of sediment, under the same flow condition, the finest sediment size of D_{50} = 0.47 mm yielded the largest scour volume and scour area. The impact of ice cover on local scour volume and area is more significant for finer sediment type. On the other hand, under the same flow conditions, the coarsest sediment of D_{50} = 0.58 mm yielded the smallest scour volume and scour area.

2) In terms of flow cover, it was found that the rough ice-covered flow has led to the maximum amount of scour volume and scour area. Besides, under the same flow condition, the flow turbulence caused by high velocities and lower flow depths occurring around bridge piers with smaller pier spacing is more significant for finer sediment. It was also found that, regardless of whether or not the flow is covered, the scour volume decreases with the increase in bed sediment size.

3) Finally, two empirical equations were developed to predict scour volume and scour area under conditions ice-covered flow and open channel flow.

References

Abed, L., and Gasser, M. M. (1993). Model study of local scour downstream bridge piers. In Hydraulic Engineering (pp. 1738-1743). ASCE.

Andre, R., Thang, T. (2012). Mean and turbulent flow fields in a simulated ice-cover channel with a gravel bed: Some laboratory observations. Journal of Earth Surface Processes and Landforms, 37(9): 951-956.

Barbhuiya, A. K., and Dey, S. (2004). Local scour at abutments: A review. *Sadhana*, *29*(5), 449-476.

Breusers, H.N.C., Nicollet, G. and Shen, H.W.: Local scour around cylindrical piers, Journal of Hydraulic Research, I.A.H.R., Vol.15(3), pp.211-252, 1977

Cea, L., Puertas, J., and Pena, L. (2007). Velocity measurements on highly turbulent free surface flow using ADV. Experiments in fluids, 42(3), 333-348.

Deng, L., and Cai, C. S. (2009). Bridge scour: Prediction, modeling, monitoring, and countermeasures. *Practice periodical on structural design and construction*, *15*(2), 125-134.

Froehlich, D. C. (1989). Local scour at bridge abutments. In Proceedings of the 1989 National Conference on Hydraulic Engineering (pp. 13-18).

Heza, Y. B. M., Soliman, A. M., and Saleh, S. A. (2007). Prediction of the scour hole geometry around exposed bridge circular-pile foundation. Journal of Engineering and Applied Science, 54(4), 375

Hicks, F. (2009). An overview of river ice problems. Journal of Cold Regions Science and Technology, 55(2): 175-185.

Hirshfield, F. (2015). The impact of ice conditions on local scour around bridge piers (Doctoral dissertation, University of Northern British Colombia

Jain, S. C., and Fischer, E. E. (1980). Scour around bridge piers at high flow velocities. Journal of the Hydraulics Division, 106(11), 1827-1842.

Khwairakpam, P., Ray, S. S., Das, S., Das, R., and Mazumdar, A. (2012). Scour hole characteristics around a vertical pier under clear water scour conditions. *ARPN J. Eng. Appl. Sci*, *7*(6), 649-654.

Yang, C. S., Kao, S. P., Lee, F. B., & Hung, P. S. (2004, July). Twelve different interpolation methods: A case study of Surfer 8.0. In Proceedings of the XXth ISPRS Congress (Vol. 35, pp. 778-785).

Lauchlan, C. S., and Melville, B. W. (2001). Riprap protection at bridge piers. *Journal of Hydraulic Engineering*, *127*(5), 412-418.

Laursen, E. M., and Toch, A. (1956). Scour around bridge piers and abutments (Vol. 4). Ames, IA: Iowa Highway Research Board

Liu, H. K., Chang, F. F., and Skinner, M. M. (1961). Effect of bridge constriction on scour and backwater. Civil Engineering Section, Colorado State University

Melville, B. W. (1992). Local scour at bridge abutments. Journal of Hydraulic Engineering, 118(4), 615-631

Melville, B. W., and Sutherland, A. J. (1988). Design method for local scour at bridge piers. Journal of Hydraulic Engineering, 114(10), 1210-1226.

Raudkivi, A. J., and Ettema, R. (1983). Clear-water scour at cylindrical piers. Journal of Hydraulic Engineering, 109(3), 338-350.

Richardson, J. R., and Richardson, E. V. (1994). Practical method for scour prediction at bridge piers. In Hydraulic Engineering (pp. 1-5). ASCE.

Shen, H. W., Schneider, V. R., and Karaki, S. (1966).”Mechanics of Local Scour.” U.S. Department of Commerce, National Bureau of Standards, Institute for Applied Technology, Fort Collins, Colorado.

Sui, J., Wang, J., He, Y., and Krol, F. (2010). Velocity profiles and incipient motion of frazil particles under ice cover. International Journal of Sediment Research, 25(1), 39-51.

Wang, J., Sui, J., and Karney, B. (2008). Incipient motion of non-cohesive sediment under ice cover – an experimental study. Journal of Hydrodynamics, 20(1), 117-124.

Wu, P., Hirshfield, F., and Sui, J. (2013). Scour morphology around bridge abutment with non-uniform sediments under ice cover, Proceedings of 2013 IAHR Congress, Tsinghua University Press, Beijing

Wu, P., Hirshfield, F., Sui, J., Wang, J., and Chen, P. P. (2014). Impacts of ice cover on local scour around semi-circular bridge abutment. Journal of Hydrodynamics, 26(1): 10-18.

Wu, P., Hirshfield, F., and Sui, J. (2014). Further studies of incipient motion and shear stress on local scour around bridge abutment under ice cover. *Canadian Journal of Civil Engineering*, *41*(10), 892-899

Wu, P., Hirshfield, F., and Sui, J. (2015). Local scour around bridge abutments under ice covered conditions-an experimental study. International Journal of Sediment Research, 30(1), 39-47.

A.I.2. Comparison of three commonly used Equations for calculating local scour depth around bridge pier under ice covered flow condition

Scouring can be defined as the process by which the particles of soil or rock around an abutment or pier of a bridge get eroded and removed to a certain depth which is called the scour depth (Warren, 2011). The U.S. Federal Highway Administration (FHWA) has estimated 60% of bridge failure cases in the USA are due to scour and on average, approximately 50 to 60 bridges collapse annually in the USA (FHWA, 1988). Wardhana & Hadipriono (2003) studied 500 failures of bridge structures in the United States between 1989 and 2000 and reported that the most frequent causes of bridge failures were due to floods, scour, and their cumulative impact. The average age of the 500 failed bridges was 52.5 years but ranged from 1 to 157 years old (Brandimarte et al. 2012). Brice & Blodgett (1978) reported that damages to bridges and highways from major regional floods in 1964 and 1972 were equivalent to approximately 100 million US dollars per event. Bridge foundations should be designed to withstand the effects of scour. Bridge damage and failure have huge negative social and economic impacts in terms of reconstruction costs, maintenance and monitoring of existing structures, the disruptions of traffic flow, and in some life-threatening cases, the cost of human lives (Brandimarte et al. 2012). Moreover, a precise prediction of scour depth will not only help to prevent those bridge failures which are the consequence of under-estimation of scour depth but also will efficiently reduce unnecessary construction cost of those bridge piers in which scour depths are over-estimated. To safely design bridges located on waterways under severe flooding conditions, many researchers have developed several laboratory-derived equations for predicting bridge pier scour depth (Liu et al. 1961; Shen et al. 1969;

Jain and Fischer 1980; Melville and Sutherland 1988; Froehlich 1989; Melville 1992; Heza et al. 2007). These equations are mostly empirical formulae which are usually based on regressional analysis of laboratory and/or field scour data. However, they differ from each other in terms of the factors considered in constructing the scour model, parameters used in the equation, laboratory and/or site conditions. Since the number of these equations is relatively large, selection of the best performing equations for a special case is a difficult task. Comparison studies of scour formulae especially for different flow conditions might be helpful to select the one with the best performance. Additionally, many rivers become ice-covered during the winter months. However, the winter season is often overlooked even though most rivers in Canada and northern parts of the United States, Europe, and Asia are annually affected by ice. The relatively smaller number of studies on the scour around bridge pier under ice-covered flow condition is due to the inherent difficulty in collecting field data while ice is present and complications in lab-based measurements as a result of different scales and of temperature effects (Moore and Landrigan, 1999). Ice cover can significantly change the flow field and impact sediment transport in natural rivers. The formation of a stable ice cover effectively doubles the wetted perimeter compared to open channel conditions. This alters the hydraulics of the channel by imposing an extra boundary to the flow, causing the velocity profile to be shifted towards a smoother boundary (channel bed) and adding to the flow resistance (Sui et al. 2010). Furthermore, ice cover can lead to issues such as ice jamming, flooding, restricting the generation of hydro-power, blocking river navigation, and affecting the overall ecosystem balance (Hicks, 2009). One of the latest studies on bridge pier scour under ice-covered flow condition was conducted by Hirshfield (2015). These experiments were conducted in a large-scale flume to study the impact of ice cover roughness

and non-uniformity of sediment on the local scour around a single circular bridge pier under open channel, smooth ice and rough ice-covered conditions. It was concluded turbulence intensity was greater under ice covered than open channel conditions. In addition, it was observed that local pier scour under rough and smooth ice cover was on average 37 and 20 percent greater than open channel scour depth, respectively. Another significant study on local Scour around bridge piers under ice-covered conditions was carried out by Wu et al. (2015). In this study, the scour profile under an ice cover is compared with previous studies by examining the role of relative bed coarseness, flow shallowness, and pier Froude number. It was concluded the scour depth under an ice-covered condition is larger than under open channel flow conditions. Further, the presence of the ice cover becomes more significant with respect to scour at shallower flow depths.

Materials and Methods

Most of the equations for the prediction of bridge pier scouring express the final scour depth as a function of the flow characteristics (mean flow velocity at the approach section, water depth), flow properties (density and viscosity of the fluid), stream bed material properties (mean particle diameter, density) and bridge geometry (shape and dimension of the pier, angle of attack of the flow). In this paper, scour around circular bridge piers will be experimentally examined and subsequently the validity and reliability of three of the more commonly used and cited scour equations developed specifically for open channel flow condition will be investigated to see how accurately they predict scouring around bridge piers under ice-covered flow conditions.

- **HEC-18/Jones Equation**

The most commonly used pier scour equation in the United States is the Colorado State University (CSU) equation proposed by Richardson and Davis (1995) and is recommended by the U.S. Department of Transportation's Hydraulic Engineering (HEC-I8) (1993). It was developed from laboratory data and is recommended for both live-bed and clear-water conditions. The HEC-18/Jones equation is based on the Colorado State University (CSU) equation:

$$y_s / y_0 = 2K_1K_2K_3K_4(b/y_0)^{0.65}Fr^{0.43} \qquad \text{(AI-2-1)}$$

where y_s = scour depth; y_0= the approach flow depth; y_s/y_0 is a dimensionless expression of the relative scour depth with respect to flow depth; K_1 = correction factor for pier nose shape which is unity for circular cylinder; K_2 = correction factor for angle of attack flow which is unity for 90^0; K_3 = correction factor for bed condition which is 1.1 for clear water scour; b = nominal pier width; and Fr = approach flow Froude number. K_4 is a correction factor to account for armoring of the scour hole:

$$K_4 = [1 - 0.89(1 - V_R)^2]^{0.5} \qquad \text{(AI-2-2)}$$

Where V_R is the velocity ratio and is dimensionless:

$$V_R = [\frac{V_0 - V_{i50}}{V_{c90} - V_{i50}}] \qquad \text{(AI-2-2a)}$$

Where V_o is the approach velocity directly upstream from the pier and V_{i50} is the approach velocity, in feet per second, required to initiate scour at the pier for the particle size D_{50}. V_{i50}

is calculated as follows:

$$V_{i50} = 0.645[\frac{D_{50}}{b}]^{0.053} V_{c50} \quad \text{(AI-2-2b)}$$

Where D_{50} is the particle size for which 50 percent of the bed material is finer, in units of feet and Vc_{50} is the critical velocity, in feet per second, for incipient motion of the particle size D_{50}. V_{c50} is defined as follows:

$$V_{c50} = 11.21 y_0^{1/6} D_{50}^{1/3} \quad \text{(AI-2-2c)}$$

While D_{90} is the particle size for which 90 percent of the bed material is finer, in units of feet, and V_{c90} is the critical velocity, in feet per second, for the incipient motion of the particle size as given by:

$$V_{c90} = 11.21 y_0^{1/6} D_{90}^{1/3} \quad \text{(AI-2-2d)}$$

- **Gao's simplified Equation**

Gao's simplified pier scour equation is based on laboratory and field data from China (Gao et al. 1993). This equation has different forms depending upon whether the scour condition is live-bed scour (bed material upstream from bridge is in motion) or clear-water scour (bed material upstream from bridge is not in motion) as discussed in Landers & Mueller (1996). The Gao's simplified equation for clear-water pier scour is defined as [19]:

$$y_s = 1.141 K_s b^{0.6} y_0^{0.15} D_m^{-0.07} (\frac{V_0 - V_{ic}}{V_c - V_{ic}}) \quad \text{(AI-2-3)}$$

where y_s is the depth of pier scour below the ambient bed, in feet; Ks is the simplified pier shape coefficient which is 1.0 for cylinders; b is the width of bridge pier, in feet; y_0 is the

depth of flow directly upstream from the pier, in feet; D_m is the mean particle size of the bed material, in feet (for this study D_{50} was used as D_m); V_o is the approach velocity directly upstream from the pier, in feet per second; and V_c is the critical (incipient motion) velocity, in feet per second, for the D_m-sized particle. V_{ic} is the approach velocity, in feet per second, corresponding to critical velocity at the pier. V_{ic} can be calculated using the following equation:

$$V_{ic} = 0.645(\frac{D_m}{b})^{0.053} V_c \qquad \text{(AI-2-4)}$$

If the density of water is assumed to be 62.4 pounds per cubic foot and the bed material is assumed to have a specific gravity of 2.65, the equation for V_c can be expressed as:

$$V_c = 3.28(\frac{y_0}{D_m})^{0.14}\left(8.85D_m + 6.05E^{-7}\left[\frac{10+0.3048y_0}{(0.3048D_m)^{0.72}}\right]\right)^{0.5} \qquad \text{(AI-2-5)}$$

- **Froehlich Design Equation**

The Froehlich design equation is included as a pier-scour calculation option within the computer model HEC-RAS, Version 3.1 (Brunner, 2002). The Froehlich's (1988) design equation is defined as:

$$y_s = 0.32b\phi Fr_1^{0.2}(\frac{b_e}{b})^{0.62}(\frac{y_0}{b})^{0.46}(\frac{b}{D_{50}})^{0.08} + b \qquad \text{(AI-2-6)}$$

where ϕ is a dimensionless coefficient based on the shape of the pier nose, and is 1.0 for round-nosed piers; Fr_1 is the Froude Number directly upstream from the pier; b_e is the width of the bridge pier projected normal to the approach flow, in feet; b is the width of the bridge pier, in feet; D_{50} is the particle size for which 50 percent of the bed material is finer, in feet

and y_0 is the depth of flow directly upstream from the pier, in feet.

Experiment setup

Experiments were carried out at the Quesnel River Research Centre, Likely, BC, Canada in a large-scale flume. The flume measures 40 m long, 2 m wide and 1.3 m deep. The longitudinal slope of the flume bottom was 0.2 percent. A holding tank with a volume of nearly 90 m^3 was located at the upstream end of the flume and provided a constant head in the experimental zone. Two valves were connected to the holding tank to allow for control of the flow velocity. At the end of the holding tank and upstream of the main flume, water overflowed from a rectangular weir into the flume. Since the flow of water was turbulent while entering the flume, a flow diffuser was placed downstream of the rectangular weir to dissipate the turbulence in the flow of water. Figure AI-9a shows the experimental setup. Two sand boxes with the depth of 0.30 m were filled with a uniform sediment having a median particle size (D_{50}) of 0.47 mm. The first sand box was 5.6 m in length and the second sand box was 5.8 m in length. The distance between the sand boxes was 10.2 m. Four different pairs of bridge piers with diameter of 60 mm, 90 mm, 110 mm and 170 mm were used (Figure AI-9b). Bridge piers were constructed from PVC plumbing pipe and were circular in shape. One pair of bridge piers were in each sand box so two experiments were carried out simultaneously in each experimental run. Each pier was offset from the centre line by 0.25 m, as illustrated in Figure AI-9b. The water depth in the flume was adjusted by the position of the tailgates. In front of the first sand box, a SonTek Incorporated 2D flow meter was installed to measure the approaching flow velocity, water depth, and inflow discharge during the experiment. A staff gauge was also installed in the middle of each sand box to manually verify water depth. The scour hole velocity field was measured using a 10-

Mhz Acoustic Droppler Velocimeter (ADV) by SonTek. In order to simulate ice cover, 13 panels of Styrofoam with dimensions of 1.2 m × 2.4 m (4×8 foot) were used to cover nearly the entire surface of flume. Styrofoam density was 0.026 gr/cm^3 and the Styrofoam was floated on the surface in the flume during the experimental runs. In the present study, two types of model ice cover were used, namely smooth cover and rough cover. The smooth ice cover was the surface of the original Styrofoam panels while the rough ice cover was made by attaching small Styrofoam cubes to the bottom of the smooth cover. The dimensions of Styrofoam cubes were 25 mm×25 mm× 25 mm and were spaced 35 mm apart for the Styrofoam covering panels. 36 experiments were conducted under open channel, smooth and rough ice conditions. Figure AI-10 shows the rough ice-covered flow around a bridge pier in experiment as well as ADV measurement around scour depth. The experimental runs were 24 hours long which allowed the scour hole to reach an equilibrium depth as noted in previous experiments conducted by Hirshfield (2015). After 24 hours, the flume was gradually drained. The scour depth was manually measured along the outside lines of the circular bridge piers

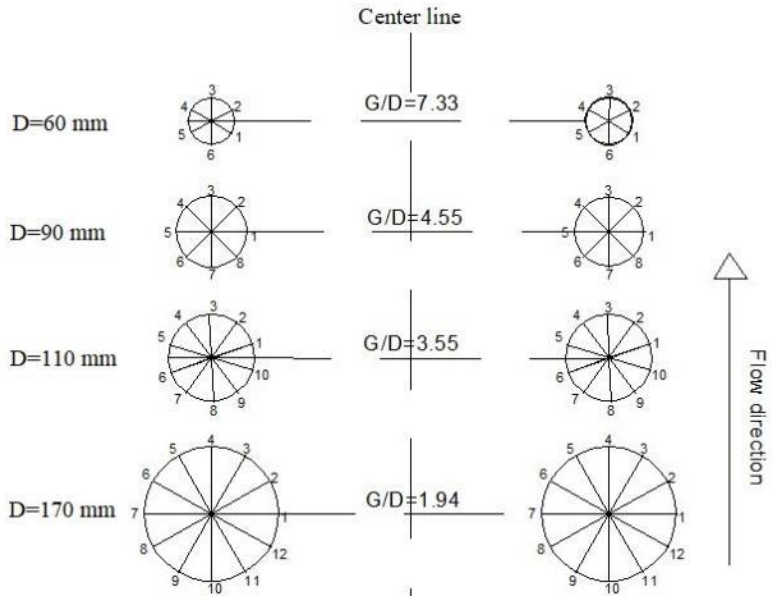

Figure AI-9a: Measuring points around the circular bridge piers

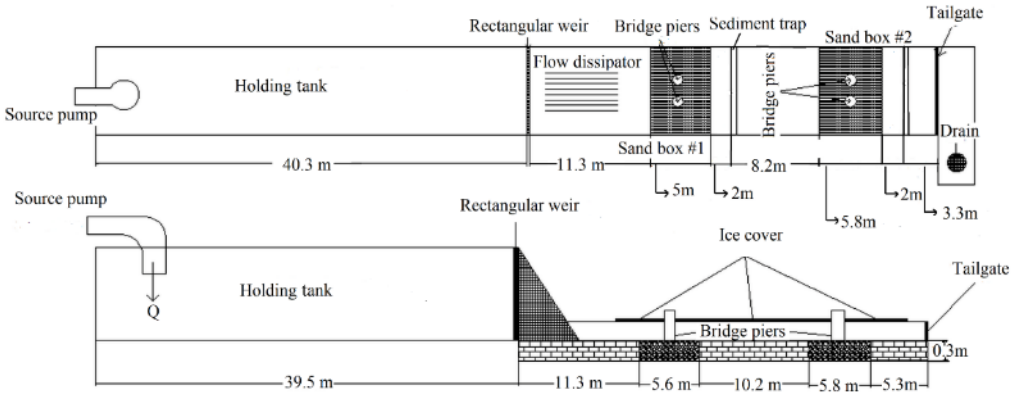

Figure AI-9b: Experimental setup –plan and side views, respectively

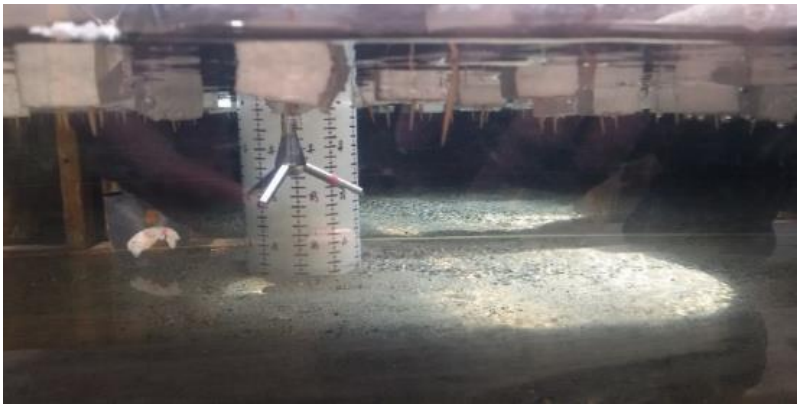

Figure AI-10: 10-Mhz Acoustic Droppler Velocimeter in use to measure the velocity field around bridge piers under rough ice-covered flow conditions

Results and discussion

Maximum scour depths calculated by the above three pier-scour equations were compared to 36 sets of experimental data. In this section, comparisons between the results from each equation and the experimental results are discussed along with an Error analysis including RMSE (Root Mean Squared Error), Index of Agreement (Ia) and MAE (Mean Absolute Error). The Absolute Error (MAE); Root Mean Square Error (RMSE) and Index of Agreement (Ia) are mathematically described by the following equations:

$$MAE = \frac{\sum_{i=1}^{n} |e_i|}{n} \qquad \text{(AI-2-7)}$$

$$RMSE = \sqrt{\frac{\sum_{i=1}^{n} (y_i - x_i)^2}{n}} \qquad \text{(AI-2-8)}$$

$$I_a = 1 - \frac{\sum_{i=1}^{n} (y_i - x_i)^2}{\sum_{i=1}^{n} \left(|x_i - \bar{x}| + |y_i - \bar{x}| \right)^2} \qquad \text{(AI-2-9)}$$

Where x_i is scour depth obtained from experiments and y_i is the corresponding predicted scour depths; $\bar{x}$ is the mean experimental scour depth and n is number of records. Smaller values of MAE and RMSE indicate a more successful prediction. The Index of Agreement (I_a) is a standardized measure of the degree of model prediction error and varies between 0 and 1. A value of 1 indicates a perfect match, while 0 indicates no agreement (Willmot, 1981). Table AI-1 demonstrates the performance of the Gao's simplified equation (SCE), the HEC-18/Jones equation (HJE) and Froehlich Design Equation (FDE) under smooth and rough flow conditions. The measured scour in Table AI-1 stands for the maximum

scour depth between left and right bridge pier. Table AI-2 provides a comparison of the predicted maximum scour depth from the three equations to maximum measured scour depth under smooth and rough ice-covered flow condition. It should be mentioned the residual values are defined as predicted scour depth minus measured scour depth. A negative residual value indicates over-estimated scour depth. From the data provided, it is possible to determine which equation is most useful under various conditions. Evaluation of these equations are important to bridge design especially for the case of flow under ice-covered condition. The scatterplots in Figure AI-11(a-c) compare predicted pier scour depth for each of the three equations to the measured scour depths obtained experimentally under the different flow conditions. Pier-scour depths calculated using the Froehlich design equation exceeded measured scour depths for every measurement of both open channel and ice-covered flows (Figure AI-11a, Table AI-1). Likewise, Pier-scour depths calculated using the HEC-18/Jones equation similarly exceeded measured pier scour for all 36 observations (Figure AI-11b and Table AI-1). However, overestimations were larger for the Froehlich design than for the HEC-18/Jones equation. Overall, the most reliable and accurate equation which has predicted the pier scour depths under open channel and ice-covered flow to a very good extent was Gao's simplified equation. Pier-scour depths calculated using the Gao's simplified equation were smaller than measured scour depths for 6 of the 12 measurements for open channel flow and for 9 of the 12 measurements for smooth ice cover. However, it completely underestimated Pier-scour depths for the rough ice cover flow (Figure AI-11c and Table AI-1). Statistics for calculated and measured pier scour are summarized in Table AI-2. The averages of pier-scour depths for open channel flow calculated from Froehlich equation was 0.46 ft, from the HEC-18/Jones was 0.38 ft,

and from the Gao's simplified equation was 0.15 ft. The average of the measured pier-scour depths was 0.15 ft. This result indicates Gao's simplified equation was entirely successful in predicting the scour depth under open channel conditions. Both the Froehlich and HEC-18/Jones equations resulted in significant over-estimation of the average scour depth. Furthermore, from Table AI-2, the highest index of agreement value (I_a) and the lowest RMSE and MAE values are for the Gao's simplified equation for the case of open channel flow. In terms of smooth ice-covered flow, the averages of pier-scour depths for open channel flow calculated from Froehlich equation was 0.46 ft, from the HEC-18/Jones was 0.37 ft, and from the Gao's simplified equation was 0.13 ft. The actual average measured pier-scour depth was 0.16 ft again indicating Gao's simplified equation provided the best agreement with the measured value and was more successful in predicting the scour depth. Both the Froehlich and HEC-18/Jones equations resulted in the significant over-estimation of the scour depth on average. The highest index of agreement value (0.84) and the lowest RMSE and MAE values were obtained with Gao's simplified equation under the smooth ice-covered flow condition. In terms of rough ice-covered flow, the averages of pier-scour depths for open channel flow calculated from Froehlich equation was 0.46 ft, from the HEC-18/Jones was 0.37 ft, and from the Gao's simplified equation was 0.14 ft. In this case, the rough ice surface increased the average measured pier-scour depths to 0.22 ft which is higher than the average scour depth calculated using Gao's simplified equation. However, the results from Gao's equation were closer to the experimental results than either the Froehlich or the HEC-18/Jones equation might suggest it was more successful in calculating scour depth. Further, the highest index of agreement value (0.78) and the lowest RMSE and MAE values are for

the Gao's simplified equation under rough ice-covered flow condition. Mathematically, Gao's simplified equation is the most successful of the three equations at calculating scour depth, but it does underestimate the extent of scour. In practical terms, this could lead to a false sense of security in practical situations as increased scour depth could lead to premature failure of a pier.

Table AI-1: Comparison of calculated pier scour to measured pier scour from three equations under smooth and rough ice-covered flow condition

Cover	Pier Size (ft.)	Pier Identification	Measured Scour (ft.)	Equations					
				Gao's simplified		Froehlich Design		Hec-18/Jones	
				Calculated scour (ft.)	Residual (ft.)	Calculated scour (ft.)	Residual (ft.)	Calculated scour (ft.)	Residual (ft.)
Smooth	0.197	Right	0.10	0.06	-0.03	0.28	0.19	0.24	0.15
Smooth	0.197	Left	0.11	0.10	-0.01	0.26	0.15	0.25	0.13
Smooth	0.197	Right	0.14	0.10	-0.04	0.29	0.15	0.28	0.14
Smooth	0.295	Left	0.10	0.11	0.01	0.4	0.3	0.33	0.23
Smooth	0.295	Right	0.22	0.19	-0.03	0.38	0.15	0.36	0.14
Smooth	0.295	Left	0.21	0.16	-0.05	0.41	0.2	0.39	0.18
Smooth	0.361	Left	0.14	0.08	-0.06	0.47	0.33	0.33	0.2
Smooth	0.361	Right	0.26	0.19	-0.07	0.45	0.18	0.39	0.13
Smooth	0.361	Left	0.26	0.18	-0.08	0.49	0.23	0.43	0.17
Smooth	0.558	Left	0.10	0.08	-0.02	0.71	0.61	0.42	0.33
Smooth	0.558	Left	0.16	0.17	0.01	0.67	0.51	0.46	0.3
Smooth	0.558	Left	0.16	0.20	0.04	0.72	0.56	0.55	0.39
Rough	0.197	Left	0.15	0.09	-0.06	0.28	0.13	0.27	0.11
Rough	0.197	Right	0.19	0.10	-0.09	0.26	0.07	0.25	0.06
Rough	0.197	Left	0.18	0.14	-0.04	0.3	0.11	0.31	0.13
Rough	0.295	Right	0.31	0.10	-0.21	0.4	0.1	0.32	0.02
Rough	0.295	Right	0.31	0.13	-0.18	0.37	0.07	0.32	0.01
Rough	0.295	Left	0.24	0.15	-0.09	0.41	0.17	0.38	0.14
Rough	0.361	Left	0.22	0.11	-0.11	0.47	0.25	0.36	0.14
Rough	0.361	Right	0.26	0.19	-0.08	0.45	0.18	0.38	0.12
Rough	0.361	Right	0.28	0.17	-0.11	0.49	0.21	0.42	0.15
Rough	0.558	Left	0.16	0.12	-0.05	0.7	0.54	0.46	0.3
Rough	0.558	Left	0.19	0.18	-0.01	0.67	0.48	0.47	0.28
Rough	0.558	Right	0.20	0.18	-0.02	0.73	0.53	0.55	0.35

Table AI-2: Error Values of the three equations with respect to measured data under open, smooth and rough flow

Cover	RMSE (%)			Ia			MAE (%)		
	SCE	HJE	FDE	SCE	HJE	FDE	SCE	HJE	FDE
Open	3.58	24.88	35.5	0.9	0.48	0.34	6.8	23	38
Smooth	4.38	22.33	33.91	0.84	0.56	0.41	14.1	26	25
Rough	10.33	18.21	29.19	0.46	0.78	0.64	15.7	45	39

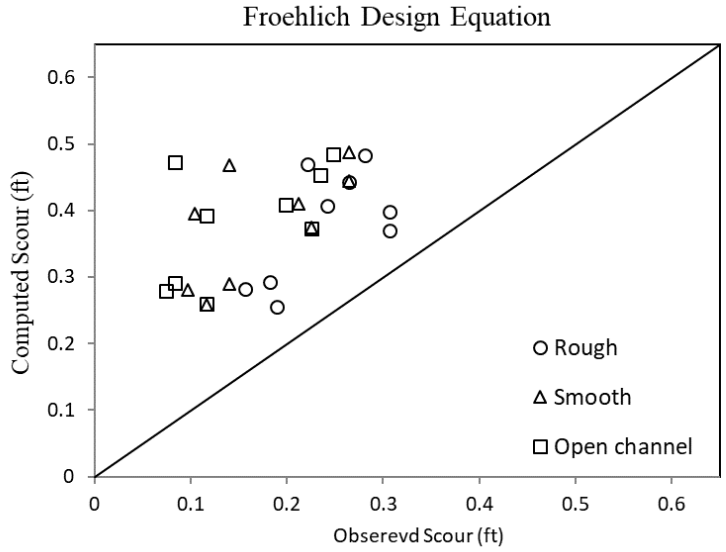

Figure AI-11a: Comparison of calculated to measured pier scour for Froehlich equation under open, smooth and rough flow condition.

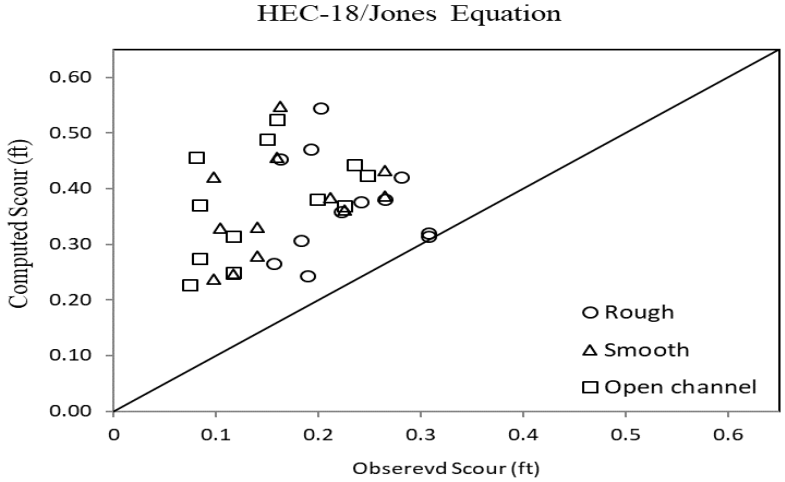

Figure AI-11b: Comparison of calculated to measured pier scour for HEC-18/Jones equation under open, smooth and rough flow condition.

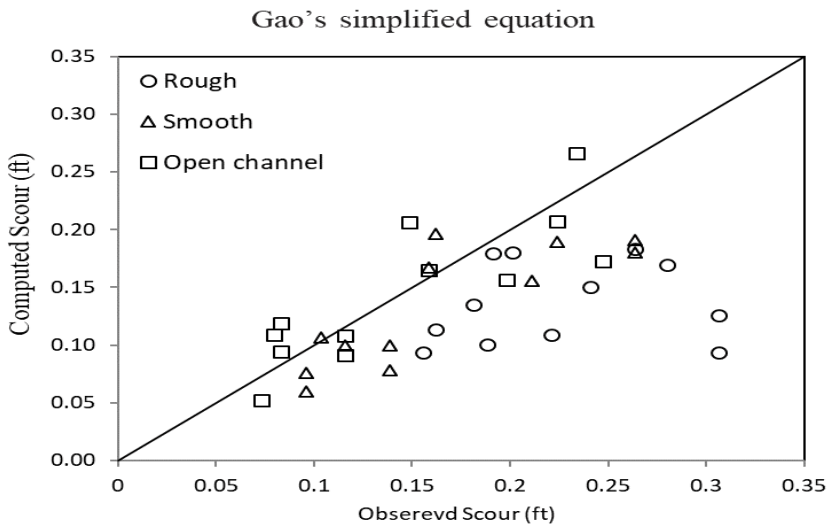

Figure AI-11c: Comparison of calculated scour depths to the measured scour depth for Gao's simplified equation under open, smooth and rough flow condition

Summary and conclusions

Three pier-scour equations, namely the Froehlich design equation, the HEC-18/Jones equation and Gao's simplified equation, were evaluated against the data from 36 flume experimental runs obtained for open channel, rough and smooth ice-covered flow under uniform bed sediment type. The most important result that can be obtained from the comparison of these three equations is that under nearly the same flow depth and approach flow velocity but different flow cover, the average calculated values from the three equations stayed nearly constant. On the other hand, in terms of ice cover, the rougher the ice surface, the more turbulent the flow and the deeper the scour depth generated. Although Gao's simplified equation was reasonably successful in prediction of pier scour depth for both the open-channel and smooth-ice conditions, it underestimated the pier-scour depth under rough ice-covered flow conditions. Therefore, it can be concluded that none of the equations adequately model scour depth under rough ice conditions and the equations are in need of another term to make them more suitable to be used for the ice-covered flow conditions.

References

Brunner, G.W. (2002). HEC-RAS, River analysis system hydraulic reference manual: U.S. Army Corps of Engineers Report CPD-69, 350 p.

Brandimarte, L., Paron, P., and Di Baldassarre, G. (2012). Bridge pier scour: A review of processes, measurements and estimates. Environmental Engineering & Management Journal (EEMJ), 11(5).

Brice J.C., Blodgett J.C. (1978), Countermeasures for hydraulic problems at bridges, Federal Highway Administration Report FHWA-RD-78-162.

Froehlich, D. C. (1989). Local scour at bridge abutments. In Proceedings of the 1989 National Conference on Hydraulic Engineering, 13-18.

FHWA, Evaluating Scour at Bridges, NH1-01-001, Federal Highway Administration, Washington, DC, USA, 4th edition, 1988.

Froehlich, D.C. (1988). Analysis of on-site measurements of scour at piers, *in* Abt, S.R., and Gessler, Johannes, eds., Hydraulic Engineering—Proceedings of the 1988 National Conference on Hydraulic Engineering: New York, American Society of Civil Engineers, 534-539.

Gao, D., Posada, G., & Nordin, C. F. (1993). Pier scour equations used in China. In Hydraulic Engineering (pp. 1031-1036). ASCE

Heza, Y. B. M., Soliman, A. M. and Saleh, S. A. (2007). Prediction of the scour hole geometry around exposed bridge circular-pile foundation. Journal of Engineering and Applied Science, 54(4), 375.

Hirshfield, F. (2015). The Impact of Ice Conditions on Local Scour Around Bridge Piers (Doctoral dissertation, University of Northern British Columbia).

Hicks, F. (2009). An overview of river ice problems: CRIPE07 guest editorial. Cold Regions Science and Technology, 55(2), 175-262.

Jain, S. C. and Fischer, E. E. (1980). Scour around bridge piers at high flow velocities. Journal of the Hydraulics Division, 106(11), 1827-1842.

Landers, M.N. and Mueller, D.S. (1996). Channel scour at bridges in the United States: U.S. Department of Transportation, Federal Highway Administration Publication FHWARD-95-184, 140 p.

Liu, H. K., Chang, F. F. and Skinner, M. M. (1961). Effect of bridge constriction on scour and backwater. Civil Engineering Section, Colorado State University.

Melville, B. W. and Sutherland, A. J. (1988). Design method for local scour at bridge piers. Journal of Hydraulic Engineering, 114(10), 1210-1226.

Melville, B. W. (1992). Local scour at bridge abutments. Journal of Hydraulic Engineering, 118(4), 615-631.

Moore, J. N. and Landrigan, E. M. (1999). Mobilization of metal-contaminated sediment by ice-jam floods. Environmental Geology, 37(1-2), 96-101.

Richardson, E.V. and Davis, S.R. (1995). Evaluating scour at bridges. U.S. Department of Transportation, Federal Highway Administration Hydraulic Engineering Circular 18, Publication FHWA-IP-90-017, 204 p.

Shen, H., Schneider, V. R. and Karaki, S. (1969). Local scour around bridge piers Journal of the Hydraulics Division, 95(6), 1919–1940.

Sui, J., Wang, J., Yun, H. E., and Faye, K. (2010). Velocity profiles and incipient motion of frazil particles under ice cover. International Journal of Sediment Research, 25(1), 39-51.

Wu, P., Balachandar, R., and Sui, J. (2015). Local Scour around Bridge Piers under Ice-Covered Conditions. Journal of Hydraulic Engineering, 142(1), 04015038.

Willmot, C. J. (1981). On the validation of models, Physical Geography, 2, 184–194.

Warren, L. P. (2011). Scour at Bridges: Stream Stability and Scour Assessment at Bridges in Massachusetts. *US Geological Survey.*

Wardhana, K. and Hadipriono, F. C. (2003). Analysis of recent bridge failures in the United States. Journal of performance of constructed facilities, 17(3), 144-150.

APPENDIX II

Table AII-1: Experimental data collected for D_{50}= 0.50 mm

Run #	Cover	D (mm)	D_{50} (mm)	ɵ (degrees)	y_0 (mm)	y_{max} (mm)	U (m/s)	Q (m^3/s)
1A	Open flow	60	0.50	10.61	200	12	0.11	0.044
2A	Open flow	60	0.50	10.33	130	16	0.16	0.042
3A	Open flow	60	0.50	11.02	230	20	0.15	0.069
4A	Open flow	90	0.50	10.61	180	19	0.13	0.045
5A	Open flow	90	0.50	10.33	90	25	0.21	0.037
6A	Open flow	90	0.50	11.02	210	29	0.18	0.075
7A	Open flow	110	0.50	11.37	195	25	0.13	0.051
8A	Open flow	110	0.50	10.78	90	30	0.23	0.041
9A	Open flow	110	0.50	10.85	230	35	0.18	0.084
10A	Open flow	170	0.50	11.37	220	15	0.11	0.048
11A	Open flow	170	0.50	10.78	110	27	0.16	0.035
12A	Open flow	170	0.50	10.85	260	55	0.14	0.075
13A	Smooth	60	0.50	10.91	240	20	0.10	0.048
14A	Smooth	60	0.50	10.97	120	25	0.16	0.038
15A	Smooth	60	0.50	11.10	260	30	0.16	0.083
16A	Smooth	90	0.50	10.91	190	26	0.13	0.049
17A	Smooth	90	0.50	10.97	100	35	0.21	0.042
18A	Smooth	90	0.50	11.10	220	36	0.18	0.077
19A	Smooth	110	0.50	10.85	120	30	0.13	0.032
20A	Smooth	110	0.50	11.13	100	42	0.17	0.035
21A	Smooth	110	0.50	10.89	260	52	0.12	0.060
22A	Smooth	170	0.50	10.85	180	26	0.07	0.026
23A	Smooth	170	0.50	11.13	120	47	0.13	0.030
24A	Smooth	170	0.50	10.89	280	45	0.15	0.087
25A	Rough	60	0.50	11.17	220	21	0.15	0.068
26A	Rough	60	0.50	11.24	110	35	0.18	0.040
27A	Rough	60	0.50	11.30	240	41	0.19	0.091
28A	Rough	90	0.50	11.17	195	41	0.13	0.050
29A	Rough	90	0.50	11.24	137	53	0.13	0.037
30A	Rough	90	0.50	11.30	229	59	0.16	0.076
31A	Rough	110	0.50	11.13	210	42.5	0.13	0.054
32A	Rough	110	0.50	10.89	120	45	0.19	0.047
33A	Rough	110	0.50	11.37	230	61	0.19	0.087
34A	Rough	170	0.50	11.13	220	21	0.12	0.053
35A	Rough	170	0.50	10.89	120	35	0.16	0.039
36A	Rough	170	0.50	11.37	240	41	0.17	0.082

Table AII-2: Experimental data collected for D_{50}=0.47 mm

Run #	Cover	D (mm)	D_{50} (mm)	ɵ (degrees)	y_0 (mm)	y_{max} (mm)	U (m/s)	Q (m^3/s)
1B	Open flow	60	0.47	11.83	250	22	0.11	0.056
2B	Open flow	60	0.47	11.62	110	35	0.18	0.040
3B	Open flow	60	0.47	11.45	280	25	0.17	0.094
4B	Open flow	90	0.47	11.83	200	35	0.13	0.054
5B	Open flow	90	0.47	11.62	90	60	0.25	0.045
6B	Open flow	90	0.47	11.45	230	68	0.20	0.093
7B	Open flow	110	0.47	11.50	242	25	0.12	0.058
8B	Open flow	110	0.47	11.83	100	71	0.28	0.056
9B	Open flow	110	0.47	11.72	253	75	0.20	0.101
10B	Open flow	170	0.47	11.50	250	24	0.12	0.059
11B	Open flow	170	0.47	11.83	100	45	0.18	0.036
12B	Open flow	170	0.47	11.72	270	48	0.16	0.084
13B	Smooth	60	0.47	11.62	250	29	0.12	0.061
14B	Smooth	60	0.47	11.59	110	35	0.17	0.037
15B	Smooth	60	0.47	11.55	260	42	0.17	0.090
16B	Smooth	90	0.47	11.62	200	31.2	0.15	0.060
17B	Smooth	90	0.47	11.59	100	64	0.23	0.046
18B	Smooth	90	0.47	11.55	240	68	0.20	0.096
19B	Smooth	110	0.47	11.59	243	42	0.10	0.048
20B	Smooth	110	0.47	11.10	90	78	0.21	0.038
21B	Smooth	110	0.47	11.57	255	85	0.20	0.102
22B	Smooth	170	0.47	11.59	260	29	0.09	0.049
23B	Smooth	170	0.47	11.10	105	48	0.15	0.032
24B	Smooth	170	0.47	11.54	250	46	0.18	0.089
25B	Rough	60	0.47	11.48	220	47	0.16	0.072
26B	Rough	60	0.47	11.45	100	55	0.17	0.034
27B	Rough	60	0.47	11.59	250	57	0.22	0.109
28B	Rough	90	0.47	11.48	220	67	0.14	0.061
29B	Rough	90	0.47	11.45	100	73	0.23	0.046
30B	Rough	90	0.47	11.59	230	85	0.20	0.090
31B	Rough	110	0.47	11.58	240	80	0.12	0.058
32B	Rough	110	0.47	11.61	90	92	0.20	0.037
33B	Rough	110	0.47	11.62	220	95	0.19	0.085
34B	Rough	170	0.47	11.58	220	49	0.12	0.053
35B	Rough	170	0.47	11.61	110	58	0.16	0.036
36B	Rough	170	0.47	11.62	280	61	0.17	0.093

Table AII-3: Experimental data collected for D_{50}=0.58 mm

Run#	Cover	D (mm)	D_{50} (mm)	ɵ (degrees)	y_0 (mm)	y_{max} (mm)	U (m/s)	Q (m^3/s)
1C	Open flow	60	0.58	11.35	210	12	0.09	0.038
2C	Open flow	60	0.58	11.25	130	12	0.16	0.042
3C	Open flow	60	0.58	11.12	240	15	0.15	0.072
4C	Open flow	90	0.58	11.35	170	18	0.11	0.037
5C	Open flow	90	0.58	11.25	90	25	0.25	0.045
6C	Open flow	90	0.58	11.12	230	38	0.20	0.093
7C	Open flow	110	0.58	11.6	200	20	0.15	0.059
8C	Open flow	110	0.58	11.69	100	24	0.28	0.056
9C	Open flow	110	0.58	11.64	220	36	0.20	0.087
10C	Open flow	170	0.58	11.6	250	17	0.12	0.059
11C	Open flow	170	0.58	11.69	100	27	0.18	0.036
12C	Open flow	170	0.58	11.64	270	27	0.16	0.084
13C	Smooth	60	0.58	11.06	200	15	0.11	0.044
14C	Smooth	60	0.58	11.07	120	19	0.15	0.036
15C	Smooth	60	0.58	11.12	220	18	0.15	0.066
16C	Smooth	90	0.58	11.06	170	20	0.13	0.044
17C	Smooth	90	0.58	11.07	100	34	0.23	0.046
18C	Smooth	90	0.58	11.12	240	43	0.20	0.096
19C	Smooth	110	0.58	11.06	210	27	0.11	0.047
20C	Smooth	110	0.58	10.74	90	32	0.21	0.038
21C	Smooth	110	0.58	10.08	230	50	0.20	0.094
22C	Smooth	170	0.58	11.06	260	18	0.09	0.049
23C	Smooth	170	0.58	10.74	105	32	0.15	0.032
24C	Smooth	170	0.58	10.08	250	37	0.18	0.089
25C	Rough	60	0.58	8.28	220	32	0.16	0.072
26C	Rough	60	0.58	8.65	100	41	0.17	0.034
27C	Rough	60	0.58	8.79	250	45	0.22	0.109
28C	Rough	90	0.58	8.28	220	38	0.14	0.061
29C	Rough	90	0.58	8.65	100	43	0.23	0.046
30C	Rough	90	0.58	8.79	230	49	0.20	0.090
31C	Rough	110	0.58	10.43	195	31	0.14	0.054
32C	Rough	110	0.58	8.39	90	33	0.20	0.037
33C	Rough	110	0.58	8.34	190	60	0.15	0.057
34C	Rough	170	0.58	10.43	200	39	0.11	0.044
35C	Rough	170	0.58	8.39	140	36	0.15	0.042
36C	Rough	170	0.58	8.34	220	37	0.13	0.057

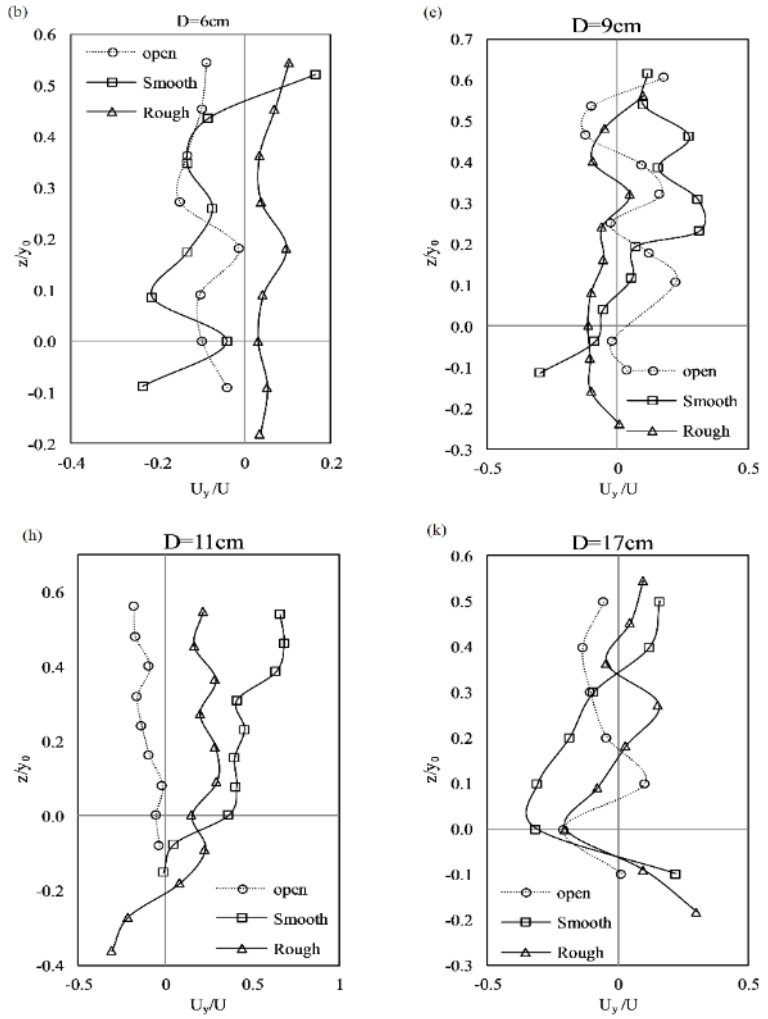

Figure AII-1: Scour hole velocity profiles for the lateral (U_y) component under open, smooth and rough ice-cover distinguished by the pier size and under D_{50}= 0.47 mm for the lowest discharge

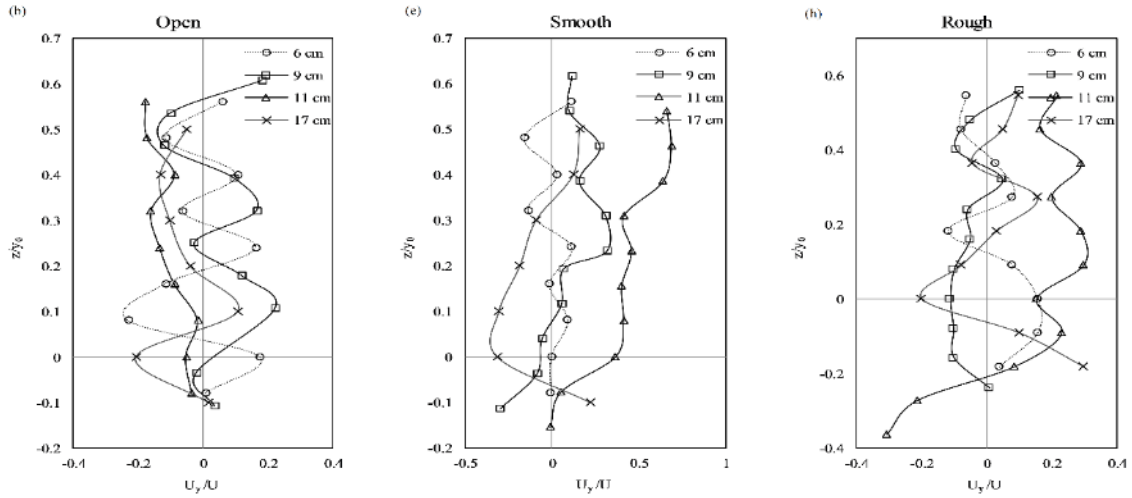

Figure AII-2: Scour hole velocity profiles for the lateral (U_y) velocity component distinguished by flow cover for all the pier size and under D_{50}= 0.47 mm for the lowest discharge